

Adesanya, Olusola (1982) *Seismic velocities of the upper crust of the Southern Uplands*. PhD thesis.

<http://theses.gla.ac.uk/4298/>

Copyright and moral rights for this thesis are retained by the author

A copy can be downloaded for personal non-commercial research or study, without prior permission or charge

This thesis cannot be reproduced or quoted extensively from without first obtaining permission in writing from the Author

The content must not be changed in any way or sold commercially in any format or medium without the formal permission of the Author

When referring to this work, full bibliographic details including the author, title, awarding institution and date of the thesis must be given

SEISMIC VELOCITIES OF THE UPPER CRUST OF THE
SOUTHERN UPLANDS

by

OLUŞOLA ADESANYA

Thesis submitted in fulfilment of the degree of
Doctor of Philosophy (by research) in the Faculty
of Science, Department of Geology, University of
Glasgow.

January, 1982.

Dedicated to the memory of my late father
And to 'Bimbo for her love and devotion at
all times.

C O N T E N T S

	<u>PAGE</u>
ACKNOWLEDGEMENTS	vii
SUMMARY	viii
CHAPTER 1 : Introduction	1
1.1 The problem	1
1.2 Regional geology and tectonics of the Southern Uplands.	2
1.3 Previous seismic work.	4
1.4 Background to the present problem (upper crustal seismic velocity structure)	5
1.5 Theoretical bases for modelling anisotropy	18
1.6 The present project.	26
CHAPTER 2 : Techniques and Instrumentations	28
2.1 Laboratory measurements	28
2.2 Laboratory treatment of rock specimens	41
2.3 Density measurements	45
2.4 Preparation of specimen for SEM examination	46
2.5 Field measurement of velocity.	47
CHAPTER 3 : Seismic Velocity Data: Presentation and Results	54
3.1 Introduction	54
3.2 Laboratory P-wave velocity results	56
3.3 Laboratory S-wave velocity results	73
3.4 In situ velocity results (hammer lines)	81
3.5 Summary and conclusions.	85

	<u>PAGE</u>
CHAPTER 4 : Modelling of Velocity Anisotropy in the Southern Uplands Rocks : Shale/Greywacke Sandwiches	90
4.1 Introduction	90
4.2 Velocity behaviour in the Southern Uplands rocks.	90
4.3 Anisotropy in a layered sequence of shale and greywacke	93
4.4 Conclusion.	100
CHAPTER 5 : Cracks, Velocities and Anisotropy in the Rocks of the Southern Uplands	101
5.1 Introduction	101
5.2 Crack-density (ϵ) and elastic moduli from self-consistent crack-theory.	102
5.3 Crack-spectra from inversion of velocity data	111
5.4 Anisotropy caused by oriented cracks in greywackes	120
5.5 Conclusion.	129
CHAPTER 6 : Distribution of Igneous Rocks in the Southern Uplands	130
6.1 Southern Uplands plutons : possible wide distribution at depth	130
6.2 Probable presence of ophiolite rocks at depth in the Southern Uplands.	135
6.3 Conclusion .	146
CHAPTER 7 : Conclusions.	147
REFERENCES	150
APPENDICES	159

LIST OF FIGURES

	<u>PAGE</u>
1-1 Geological sketch map of the South of Scotland (after Creig, 1971).	3
1-2a Map of Central Scotland showing the Broughton Array and the UKAEA Array (EKA) stations (after El Isa, 1977).	6
1-2b Map of Central Scotland showing the seven LOWNET sites (after Crampin <u>et al</u> , 1970).	7
1-3a Map of the Atlantic seaboard of Britain, showing the main physiographical units and locations of seismic surveys penetrating the Moho (after Hall, 1978).	9
1-3b Summary of P-wave velocity structure of the crust from the surveys shown in Fig. 1-3a (after Hall, 1978).	10
1-4a P-wave velocity distribution in the crust of the N.W. of Britain (after Bamford <u>et al</u> , 1978).	12
1-4b Poisson's ratio structure of the crust of N.W. Britain (after Assumpção & Bamford, 1978).	13
1-5 The UKAEA Eskdalemuir Seismological Recording Station (from El Isa, 1977).	16
1-6 Location of EKA close shots (after El Isa, 1977).	17
1-7 Velocity-depth functions at EKA (after El Isa, 1977).	19
1-8 Postma model: Elementary volume of a stratified medium (after Postma, 1955).	21
1-9 Co-ordinate system for stress-strain relationship in an anisotropic medium.	23
2-1 Specimen assembly of the East Anglia apparatus.	32
2-2 Seismic wave signal from rock sample (ref. Edinburgh).	34
2-3 Schematic diagram of the Edinburgh and Glasgow systems.	37
2-4 Three orthogonal directions of cores from rock samples.	41
2-5a Geological map of the Girvan area (from Creig, 1971).	48

/

	<u>PAGE</u>
2-5b Location of hammer lines along Whitehouse shore (Girvan).	50
2-6 Field instrument layout of the hammer line refraction.	52
3-1 P-wave velocity variation with pressure in a sample of greywacke.	55
3-2 The effect of saturation on velocity in greywackes.	57& 58
3-3 Anomalous behaviour of V_p in saturated shales (e.g. V_p dry > V_p saturated).	60& 61
3-4 P-wave velocity hysteresis in dry greywacke.	64
3-5 to 3-7 P-wave velocity hysteresis in dry shales.	65-67
3-8 & 3-9 Lack of hysteresis in saturated shales.	68-70
3-10 Saturated shale showing anomalous hysteresis effect (V_p with increasing pressure > V_p with decreasing pressure).	71
3-11 S-wave velocity variation with pressure in the greywackes.	75& 78
3-12 Whitehouse shore (Girvan) showing hammer lines and the corresponding V_p values.	84
3-13 Mean laboratory velocities versus pressure (and depth) for the Southern Uplands rocks.	89
4-1 Transversely isotropic material consisting of shale and greywacke layers.	94
4-2 Anisotropy modelling from shale/greywacke sandwiches.	99
5-1 Theoretical plot of \bar{V}_p/\bar{V}_s versus \bar{V}_s from O'Connell & Budiansky (1974).	109
5-2 \bar{V}_p/\bar{V}_s versus \bar{V}_s in the Southern Uplands greywackes.	110
5-3 Crack volume-concentration versus aspect ratio ($\text{Log } \alpha$) for (a) greywacke	114
(b) Chelmsford granite.	115
5-4 Linear compressibility versus pressure in the Southern Uplands greywackes.	124
5-5/	

	<u>PAGE</u>
5-5 (a) Anisotropy modelling of hammer line velocities due to oriented cracks in greywacke.	127
(b) Anisotropy modelling of EKA velocities due to oriented cracks in greywacke.	128
6-1 Three major plutons of the Southern Uplands (after Stephens & Halliday, 1979).	132
6-2a The Geology of Ballantrae Igneous Complex (after Church & Gayer, 1973).	136
(b) The Bay of Islands Igneous Complex (after Salisbury & Christensen, 1978).	137
(c) Stratigraphy of the Bay of Islands Complex (after Salisbury & Christensen, 1978).	138
(d) Distribution of ophiolite and metamorphic belts of New Guinea and the Appalachian - Caledonian system (after Church & Gayer, 1973).	140
6-3 Vp, Vs versus depth for the Bay of Islands Complex (after Salisbury & Christensen, 1978).	142
6-4 Comparison of the petrology and seismic velocity structure of the Bay of Islands Complex with the velocity structure of oceanic crust (after Salisbury & Christensen, 1978).	143
6-5a Stratigraphy of the Bay of Islands Complex with a top layer of Lower Palaeozoic sediments (from Salisbury & Christensen, 1978).	144
(b) Velocity versus depth for each layer of rocks shown in Fig. 6-5a, with the LISPB velocity distribution in the upper crust of the Southern Uplands.	145

LIST OF TABLES

2-1 Zero-length delays for P-and S-wave velocity measurements at Edinburgh.	38
3-1 Dry and saturated P-wave velocities in the Lower Palaeozoic rocks of the Southern Uplands.	62

	<u>PAGE</u>
3-2 P-wave velocity cycles in 'unstressed' dry greywackes and granodiorite.	74
3-3 Shear wave velocities in dry and saturated greywackes.	76
3-4 Densities and porosities of the rocks of the Southern Uplands.	79
3-5 Hammer Line velocities in shales and greywackes from Girvan.	83
3-6 Comparison of mean laboratory and in situ velocities for Southern Uplands rocks.	87
4-1 Results of mixing shale and greywacke with the corresponding composite velocities.	98
5-1 Variation of Poisson's ratio (σ) and crack-density (ξ) with pressure.	104
5-2 Crack-spectra and volume-concentration in the Southern Uplands greywackes.	113
5-3 Velocity anisotropy in the Southern Uplands greywackes due to oriented cracks.	125

LIST OF PLATES

1. Equant-shaped pores alternating with slots of material along grain-boundaries.
2. Magnification of Plates 1a & b to reveal tubular nature of cavities in the centre of the micrographs.
3. A mosaic showing the presence of elongate cracks along grain-boundaries.
4. An example of dPdT cracks in a sample of greywacke.

ACKNOWLEDGEMENTS

My primary acknowledgement is certainly to my supervisors, Drs. J. Hall and D.W. Powell for their meticulous interest and guidance in the execution of this project. Thanks to the head of department, Professor B.E. Leake, with whose permission this work was carried out. I am grateful also to Dr. A.C. McLean for making useful comments at various stages of the work.

Successful completion of this thesis would not be possible without the technical assistance of Messrs R. Morrison, G. Gordon, R.T. Cumberland, D. MacLean and R. MacDonald. I gratefully acknowledge the assistance given during the field work by Messrs. M.A. Al Azzawi and M. Ali.

Laboratory velocity measurements were initially carried out at the School of Environmental Studies, University of East Anglia, with the kind permission of Dr. P.N. Chroston, and assistance from C.J. Evans and W. Haddad. At a late stage of this work, Dr. C.J. Evans and Mr. J. Jackson were particularly helpful in the use of the modified East Anglia gear. Drs. C. Ford and C.M. Graham of the Experimental Petrology Unit of the Grant Institute of Geology, University of Edinburgh were very helpful in the use of high-pressure system at Edinburgh.

Mrs. G. Kelly receives my gratitude for her fast and efficient typing of this thesis.

I thank my mother and all members of my family for their moral support throughout the period of my study.

The financial support by the Federal Department of Water Resources, Nigeria, is well appreciated.

SUMMARY

The Southern Uplands of Scotland is a region largely composed of deformed Lower Palaeozoic rocks of Ordovician and Silurian systems. At outcrops, these rocks are mainly alternating shales and greywackes with steep dips and regional NE-SW strike which are intruded in places, by granitic plutons. The Southern Uplands Fault (SUF) which forms the northern boundary of the region is said to coincide with the subduction zone where a southerly oceanic plate was being consumed under a continent. Tectonic contrasts north and south of the SUF have been a subject of intensive geological and geophysical studies for the past decade. Field seismic refraction experiments, in particular, have shed some light about the velocity distribution in the crust of the Southern Uplands.

In investigating the upper crustal structure of the Southern Uplands, field and laboratory measurements (in cores from shale and greywacke) have been carried out. Hammer line velocities in rocks exposed at Girvan range from 2.9-4.0 km/s in the greywackes and 2.2-3.8km/s in the shales. Velocity anisotropy in the sequence of shale/greywacke reaches 19%. From a seismic refraction experiment at Eskdalemuir (EKA), V_p along geological strike is 5.3 km/s and across strike, 4.9 km/s, resulting in velocity anisotropy of about 8%. Below the middle of the Southern Uplands, the mean P-wave velocity from a pair of long-range refraction lines is about/...

about 5.9 km/s. The difference in velocity between directions that are parallel and normal to strike is about 3%.

In order to interpret the hammer line and EKA data, shale and greywacke samples were collected from Girvan and cored for laboratory measurements of seismic velocities. Three orthogonal cores from each specimen were run under confining pressures and room temperature, using the pulse-transmission technique. Results from these experiments indicate strong anisotropy in the shales (17%) at 1bar, decreasing with pressure to about 12% at 750bar pressure (\approx 2 km depth). Generally, anisotropy in the laboratory cores from greywacke is weak (\leq 2%). The mean V_p of 5.1 km/s obtained from the Eskdalemuir refraction experiment lies between the laboratory mean velocities in shale and greywacke. Thus, velocity anisotropy at Eskdalemuir could be due to shale/greywacke sandwiching. However, calculations show that the mean velocity in the greywacke would have to be greater than that observed in the laboratory cores by about 1km/s in order to reproduce the EKA data.

The hammer line data cannot be explained by the layered model of Postma because all field velocities in shale and greywacke are lower than those observed at 1bar in the laboratory experiments. Differences are generally greater than/

than 20%. In particular, the relatively strong anisotropy in the greywackes (12-15%) in situ is in complete contrast to the weak anisotropy observed in the laboratory cores. A model of aligned cracks in an isotropic greywacke was developed to explain both the hammer line and the EKA data. The modelling is done by adding or subtracting linear porosities in multiples of the isotropic linear porosity (A_{ist}) observed in the greywacke samples in the laboratory. This is to simulate different mixtures of isotropic and oriented cracks. This model explains both the hammer line and EKA data, but requires about 6% porosity in the exposed rocks in situ and about 1-2% in the rocks at 300m depth (applicable to the EKA experiment). It is concluded that strong anisotropy in the greywacke in situ (in contrast to laboratory observation) is due to bedding plane fractures. Inversion of laboratory velocity data and examination of cracks by the scanning electron microscope (SEM) indicate that cavities that cause anisotropy in the greywackes have aspect ratios that are less than 1×10^{-2} .

The mean V_p of 5.9 km/s observed at about 2 km depth (\approx 750 bar pressure) in the middle of the Southern Uplands is inconsistent with values found in greywackes and shales but is consistent with values in acid to intermediate igneous rocks. It is then likely that such rocks representing either oceanic layer 2 on which the Lower Palaeozoic sediments were deposited or part of a later intrusive batholith, are generally within 2 km of the present surface.

CHAPTER ONE

INTRODUCTION

1.1 The Problem

The Southern Uplands of Scotland form a region of strongly-deformed Lower Palaeozoic sediments, mainly greywackes and shales, which are, in places, intruded by granite plutons. In the past decade, the region has been subjected to geological and geophysical research studies concerned, inter alia, with the form and origin of the plutons, and the nature and depth of the pre-Ordovician basement (e.g., Dewey, 1971; Powell, 1970; Bamford et al, 1976, 1977 and 1978).

The present problem is an extension of the continuing investigation of the upper crustal structure in the Southern Uplands. An attempt is made to explain the seismic velocity anisotropy in the region as observed under Eskdalemuir (El Isa, 1977), in terms of the elastic properties of the rocks exposed there. This requires field and laboratory measurements of compressional and shear wave velocities in the Lower Palaeozoic shales and greywackes, and direct examination of the rocks using optical and electron microscopes. The conclusions of these analyses are used to model the observed velocity structure by various combinations of sandwiching of fractures, shales and greywackes.

1.2 /...

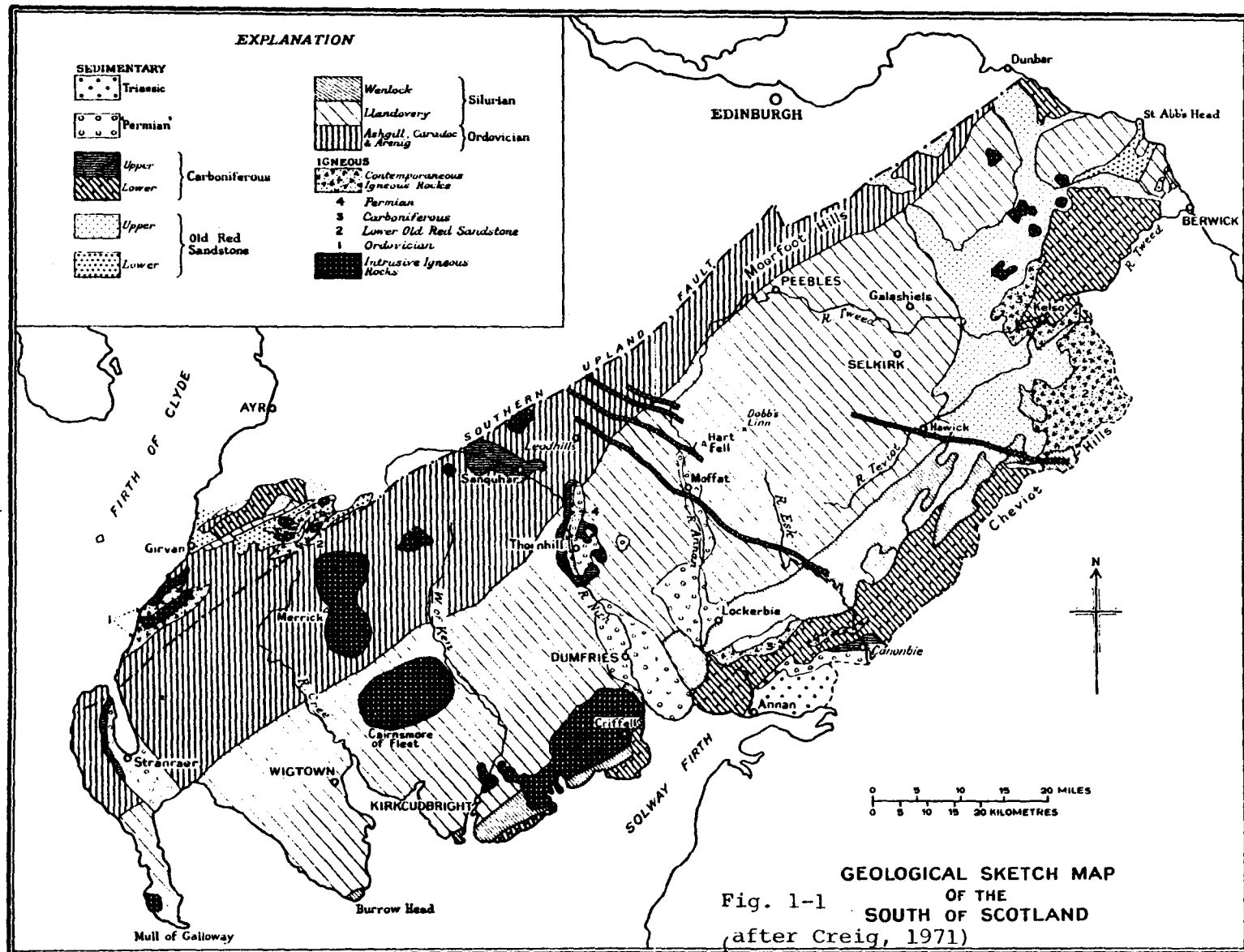
1.2 Regional geology and tectonics of the Southern Uplands.

A principal physical feature of the South of Scotland (Fig. 1-1) is the hill range of the Southern Uplands. They are formed by the Lower Palaeozoic rocks of the Ordovician and Silurian systems.

The stratigraphy of the Lower Palaeozoic rocks of the Southern Uplands was described by Lapworth in the 19th century, and later adapted and extended by Peach and Horne (1899). Lapworth's recognition that the main mass of the rocks in the Southern Uplands was unfossiliferous led him to form the opinion that the recurrence of shales with similar faunas represented repetition of the same bands of rock caused by folding. Extensive researches in different parts of the Southern Uplands in the last two decades, have invalidated Lapworth's general interpretation of the structure of the region.

The broad structural pattern now envisaged for the Southern Uplands is one of alternating zones of shales and greywackes. Widespread reversed strike-faults and subsequent wrench faults are the results of horizontal compression in NNW to SSE direction which also led, by NE-SW folding, to the repetitions of outcrop recognised by Lapworth (Creig, 1971).

Dewey (1971) and others (Weir, 1979; Longman et al, 1979; and Bluck, 1980) envisage the accumulation of sediments on the southern margin of a continent under which oceanic plate was being consumed in a northerly dipping subduction zone. Thus the collision of two plates, Laurentian and Afro-European, (Mitchell & McKerrow, 1975; Phillips et al, 1976) forms the basis of the structural evolution/...



Sample description

The greywacke samples are broadly divided into two groups; fine-grained and coarse-grained. The latter are poorly-sorted with grain-sizes ranging from less than 0.1mm to about 3mm. Large sized grains are typically y shale (and occasionally, other rock) fragments. In the fine-grained greywackes, grain-sizes average about 0.01mm-0.04mm. In all the samples, quartz is predominant and fractured. Cementing medium is typically calcite in the coarse-grained variety and clay in the fine-grained type. Clay minerals, however, constitute about 10% or less of the greywacke samples.

evolution of the Southern Uplands. Though opinions vary as to the location and number of post-Cambrian subduction zones in the north-west of Britain, Dewey has proposed one zone which ultimately determines the Southern Uplands Fault (Fig. 1-1). However, Lambert and McKerrow (1976) have proposed two zones in succession, an early Ordovician zone partly coincident with the Highland Boundary Fault, succeeded by a mid-Ordovician establishment of the Southern Uplands trough as an oceanic trench. The southeastern zone is less certain but is considered to have subducted south-eastwards to give rise to volcanics from the Lake Districts to North Wales (Fitton and Hughes, 1970) and south-westwards into Dingle Bay, south-west Ireland (Howard, 1975).

McKerrow et al (1977) proposed the operation of an accretionary prism mechanism which invokes initiation of subduction along a Glen App Benioff zone not later than Caradoc times. Pre-Cambrian foundation of the Laurentian continental crust which is said to floor the Midland Valley (Kennedy, 1958) could extend as far south-east as the Southern Uplands Fault (Upton et al, 1976). Seismic evidence (Bamford et al, 1977) on the possible existence of such foundation under the Southern Uplands is not conclusive, hence further seismic work is currently going on in and around the region.

The petrography of the greywacke is summarised in the insert (page 4a).

1.3 Previous seismic work

In the past two decades, considerable efforts have been made/...

made by seismologists to explain the structure of the continental crust around Britain on the basis of seismic velocity distribution. These efforts constitute a response to the development of multisensor techniques for continuous teleseismic recordings. Such techniques involve the utilization of seismic arrays which were later used for detecting nuclear tests (Wilson, 1967; Borg & Bath, 1971). Promising results from arrays earlier built by the United Kingdom Atomic Energy Authority (UKAEA) in the U.S.A. in 1961, led to the establishment of large and fully instrumental arrays at Eskdalemuir (EKA) which became operational in 1962 (Truscott, 1964-65). Other seismic array stations sited in the Central and Southern Scotland are LOWNET (Crampin et al, 1970), which is a network of radio-linked short-period seismometers, and Broughton (see Fig. 1-2). Since its establishment, EKA has been utilized in the studies of the lower crust and mantle, some of which are presented below.

Agger and Carpenter (1964-65), in their crustal studies in the vicinity of EKA, analysed records of shots fired in the Irish Sea, and which were received at Eskdalemuir. They obtained Pn velocities at ranges of $110 \leq \Delta \leq 130$ km, the mean of which was 7.90 ± 0.11 km/s (14 observations); and Pg velocities (mainly first arrivals from $\Delta < 130$ km) the mean of which was 6.09 ± 0.06 km/s (15 observations). The nature of the experiment excludes details about the shallow structure.

Blundell and Parks (1969) have reviewed the seismic explosion studies for the crustal structure around the British Isles. The main goal of their experiment, designed to use the time-term approach/...

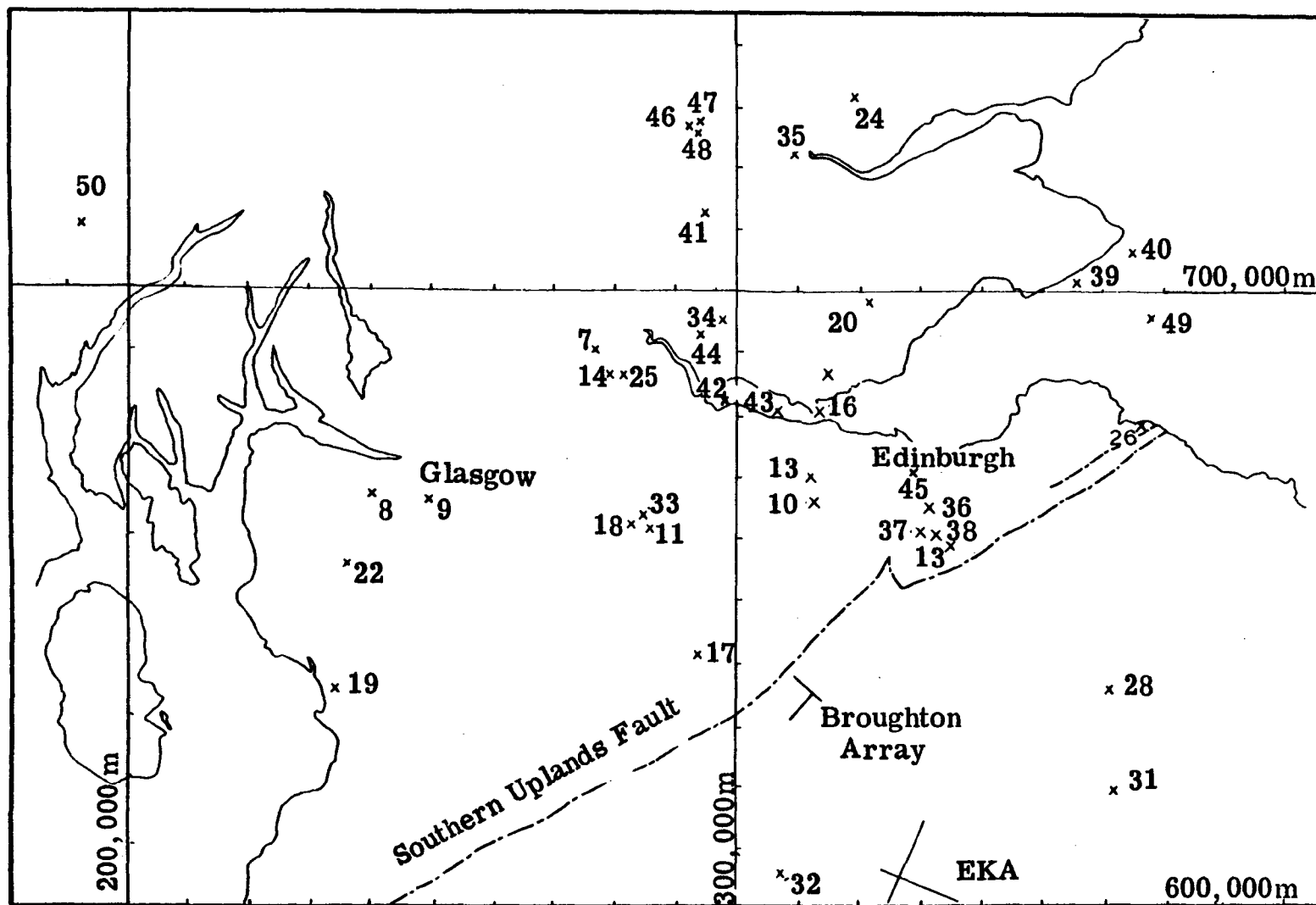


Fig.1-2a Map of Central Scotland showing the Broughton Array and the UKAEA Array (EKA) stations (after El Isa, 1977).

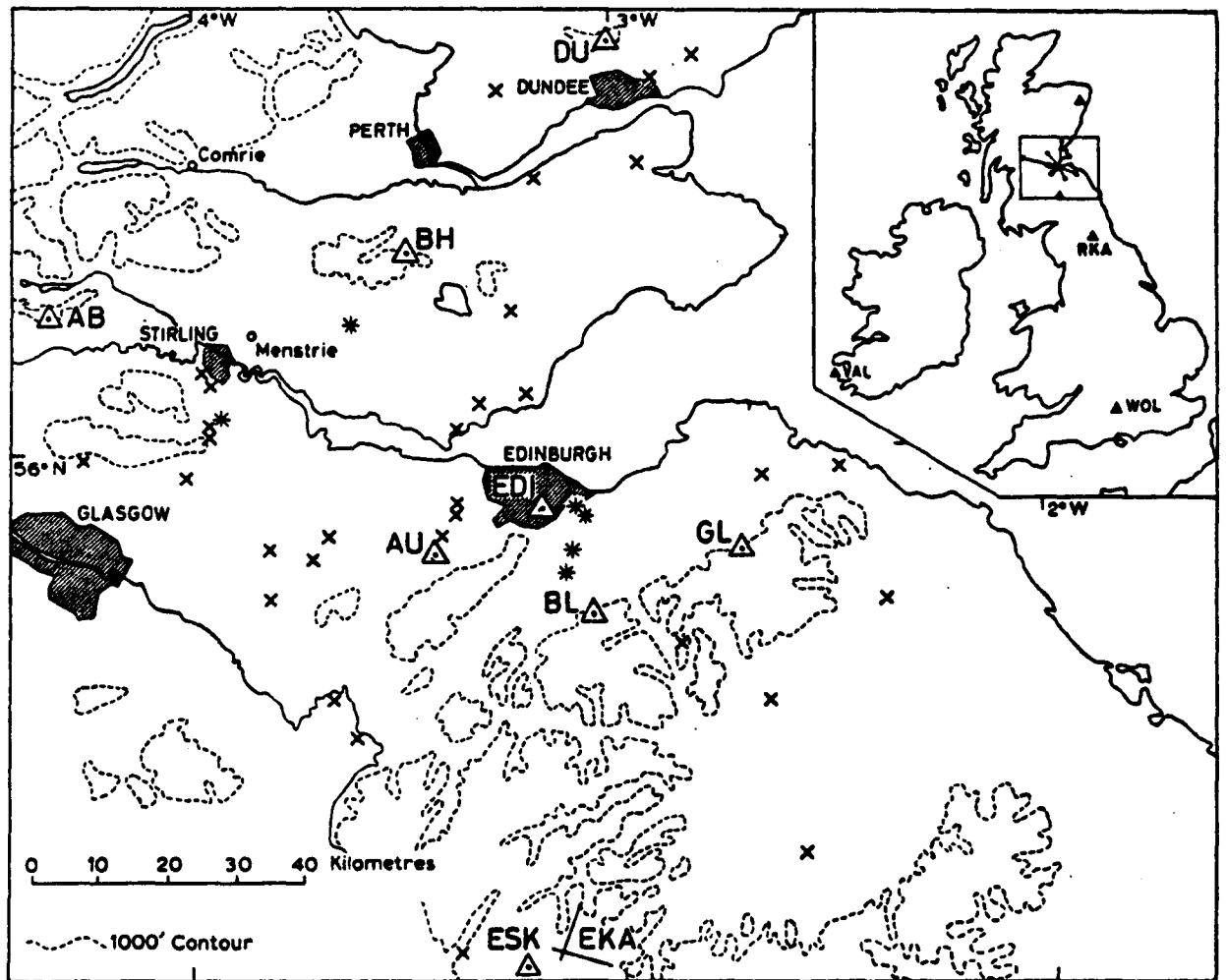


Fig. 1-2b Map of Central Scotland showing the seven LOWNET sites. Stars are well-recorded natural events, and crosses are active quarries. Other seismic stations are Eskdalemuir UKAEA array (EKA), Eskdalemuir WWSS (ESK), Rookhope (RKA), Tilliecorthie, Valentia WWSS (VAL) and Wolverton (WOL). (after Crampin, 1978)

approach for the data interpretation, was to study the crustal structure in the Irish Sea area. Pn was observable only at EKA and Rookhope. The control on velocity was poor and uncertainties in determining the time-terms were large. Consequently the authors placed no great confidence on the value of 30 km proposed for the base of the crust. Summary of the P-wave velocity structure of the crust beneath and around the British Isles, to-date has been made available by Hall (1978) [see Fig. 1-3a, b].

Jacob (1969) analysed 71 local events recorded at Eskdalemuir. Most of the events were quarry blasts. The analysis indicated a gradual increase in velocity from 5.54 km/s at the surface to 5.94 km/s at 12 km at which depth the velocity jumps to 6.4 km/s.

In a review of seismic studies around the British Isles, Willmore (1973) concluded that the main features of the work are,

- (1) The Moho shallows towards the west.
- (2) Pn increases with range.
- (3) Lower crustal velocities ranging from 6.9 - 7.3 km/s have been found in some parts of the area.

More recent publications on the crustal structure underneath northern Britain can be found in Bamford et al (1976). The authors described, comprehensively, the Lithospheric Seismic Profile in Britain (LISPB) and gave some preliminary results. The experiment was completed in summer 1974. Further interpretation given/...

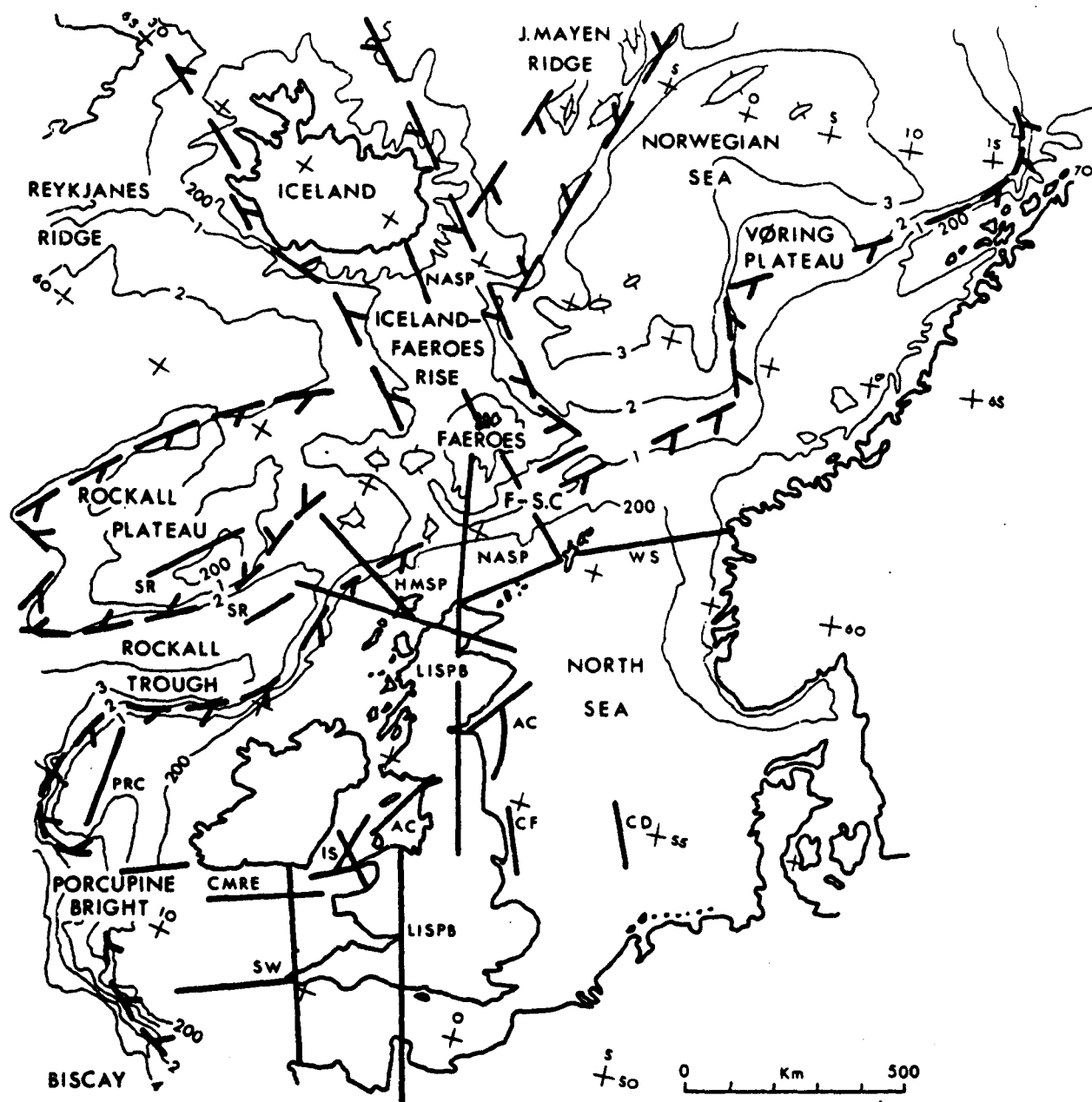


Fig. 1-3a Map of the Atlantic seaboard of Britain, showing the main physiographical units and locations of seismic surveys penetrating to the Moho. Bathymetric contours are at 200 m, 1 km, 2 km, 3 km, 4 km. F-SC = Faeroe-Shetland channel. Seismic surveys are referenced as follows: AC = Agger and Carpenter (1964); CD, CF = Collette *et al.* (1970); CMRE = Bamford (1971, 1972), Bamford and Blundell (1970); HMSP = University of Durham (1975, pers. comm.); IS = Blundell and Parks (1969); LISPb = Bamford *et al.* (1976); NASP = Bott *et al.* (1974, 1976), Smith and Bott (1975); PRC = Whitmarsh *et al.* (1974); SR = Scrutton (1970, 1972), Scrutton and Roberts (1971); SW = Bott *et al.* (1970); WS = Willmore (1973), see also Sellevoll (1973). Results of many surveys of the adjacent oceanic areas are summarised in Bott and Watts (1971). (after Hall, 1978)

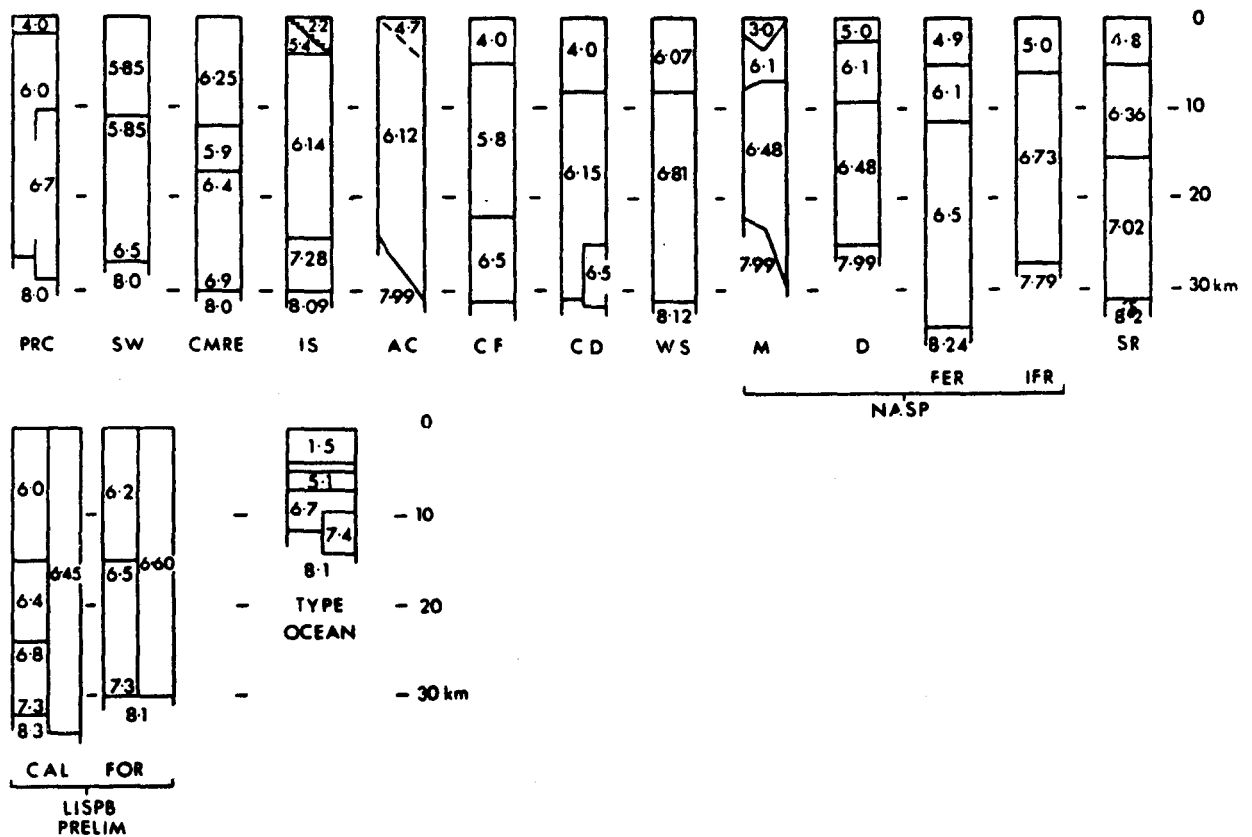


Fig. 1-3b Summary of P-wave velocity structure of the crust from the surveys shown in Figure 1. Layer velocities are in km/s; alternative interpretations are blocked together. Section WS pertains to the Shetlands; SR to the Rockall plateau; in N.A.S.P., M refers to the Moray Firth, D to the Cape Wrath-Shetlands, FER to the Faeroes and IFR to the Iceland-Faeroes rise; in L.I.S.P.B., FOR refers to the Caledonian foreland north of Cape Wrath, CAL to the Grampian Highlands.
(after Hall, 1978)

given by Bamford et al (1977) indicates the following model of the Southern Uplands (Fig. 1-4a).

- (i) A top superficial layer (< 2.5 km thickness) of 5.0 km/s.
- (ii) An upper crustal sequence (with velocity that is dependent on area of study) contains material of $5.8 - 6.0$ km/s to depths greater than 10 km.
- (iii) Mid-crustal rocks with $V_p \approx 6.3$ km/s to an undefined depth.

A layer of $V_p = 6.48 \pm 0.06$ km/s recognised by Smith and Bott (1975) and identified by them as granulite facies Lewisian basement rocks, extends from Caledonian foreland into the Midland Valley but appears to terminate at the Southern Uplands Fault. Therefore contrary to Jacob's interpretation of EKA data, a 6.4 km/s layer is not recognised under the Southern Uplands (Fig. 1-4a).

In order to add to the understanding of the physical properties and structure of the crust and upper mantle in Northern Britain, Assumpção and Bamford (1978) presented data on the distribution of Poisson's ratio (σ) in the region (including Southern Uplands) (See Fig. 1-4b). LISPB Poisson's ratios are generally close to the conventional 0.25 except for layer 1 in the Southern Uplands ($\sigma = 0.231$) and layer 2 under the Midland Valley ($\sigma = 0.224$). These low values of σ were said, by the authors, to indicate some anomalous properties of the layers, possibly as a result of tectonic activity close to the Southern Uplands Fault.

A/...

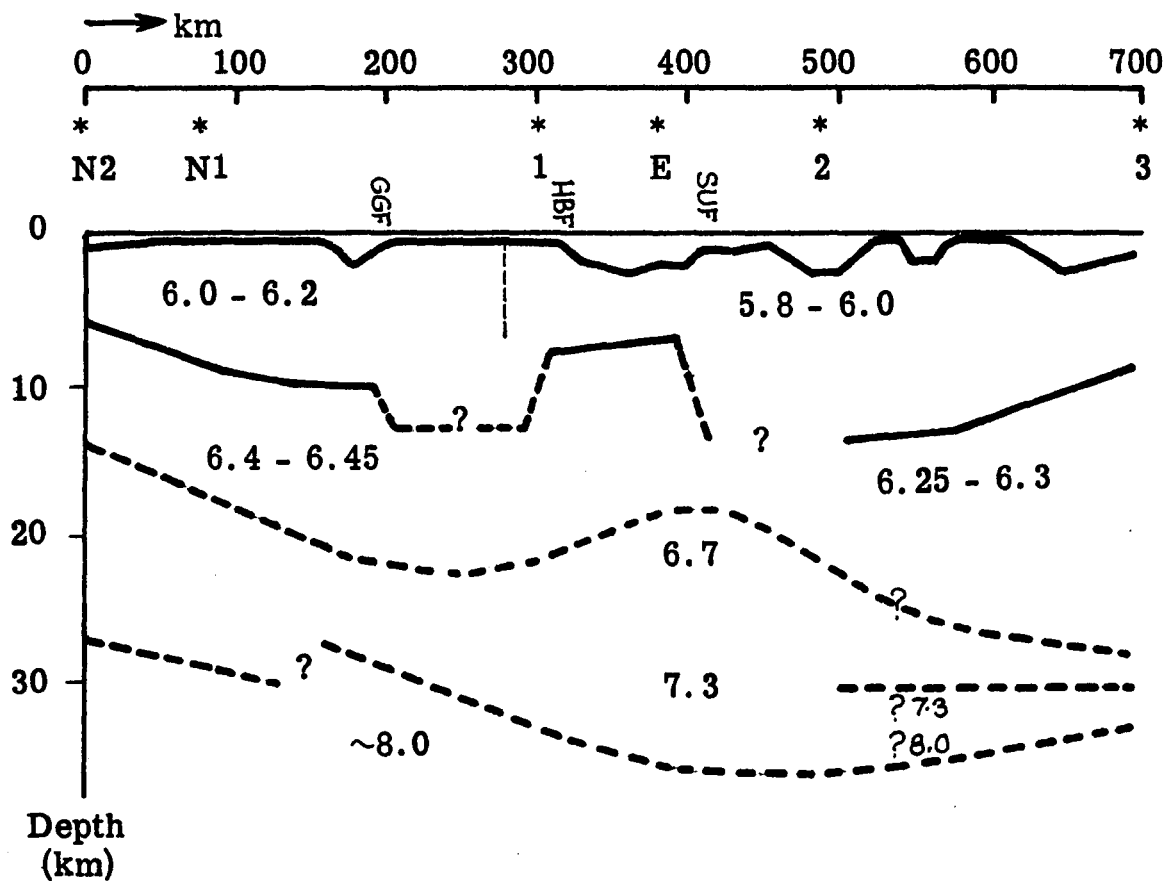


Fig. 1-4a P-wave velocity distribution in the crust of the N.W. of Britain (after Bamford et al, 1978)

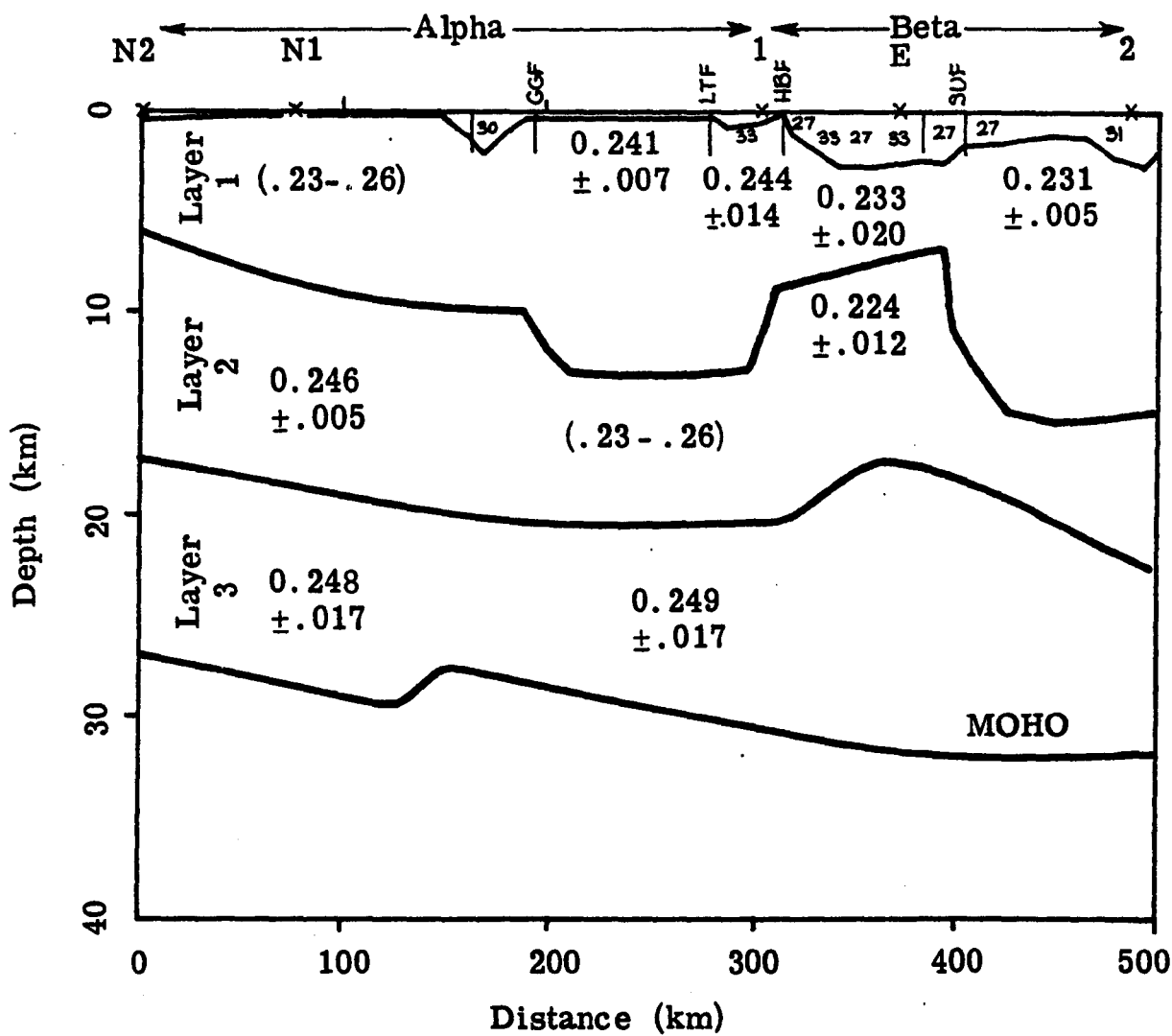


Fig. 1-4b Poisson's ratio structure of the crust of N.W. Britain (after Assumpção & Bamford, 1978).

A team of workers (from Edinburgh University and the Global Seismology Unit, IGS) are currently shooting a seismic refraction line approximately perpendicular to LISPB in the Southern Uplands i.e. an along-strike profile. Preliminary results for the main upper crustal layer (Warner, 1981; personal communication) indicate average $V_p = 6.0 \pm 0.05$ km/s

$$V_s = 3.45 \pm 0.05 \text{ km/s}$$

$$\sigma = 0.253 \pm 0.01$$

(LISPB results indicate: $V_p = 5.84 \pm 0.02$ km/s

$$\sigma = 0.231 \pm 0.005).$$

These results suggest V_p and σ are higher along strike than normal to strike. Laboratory data will be compared with the field values later in this thesis.

1.4 Upper crustal seismic velocity structure (Background to the present problem.)

An explosion experiment was mounted at Eskdalemuir (El Isa, 1977) to examine the shallow velocity structure within the Lower Palaeozoic rocks. A directional variation of P-wave velocity in the rocks of Southern Uplands was revealed. Explanation of the observed anisotropy constitutes the background to the present problem. The aim of the explosion experiment was to: identify any lateral inhomogeneity such as dipping refractors and also to reveal possible anisotropic effects on the P-wave velocities in the Lower/...

Lower Palaeozoic rocks of the Southern Uplands.

Shot-pattern of the explosion experiment at EKA.

All seismometers at EKA are positioned on steeply dipping Lower Palaeozoic bedrock (mainly shale and greywacke) and no change of lithology is expected within the first kilometer of depth.

The Eskdalemuir array (EKA) consists of two perpendicular arms (blue and red) [Fig. 1-5] with seismometers located at intervals of 1 km. Four reversed in-line shots were fired into the two array arms [Fig. 1-6] and two shots in-between. Charge sizes average about 4 kg/shot, divided into separate units of about 0.2, 0.4 or 0.6 kg, depending on shot-hole depth. These separate units were fired simultaneously. Shot-holes were drilled by hand-percussion through peat or other superficial deposits to a depth of 1-2m or rockhead if the latter is found to be shallower than 2m. Details of the array are set out in El Isa's thesis (1977, unpublished). Some of his conclusions from which the present project emerged are outlined below.

- (i) Variation in P-wave velocity with direction was recognised in the Southern Uplands rocks—5.3 km/s under the Blue arm which is aligned at 20° to the geological strike and 4.9 km/s under the Red arm, at about 70° inclined to geological strike [Figures 1-5 & 1-6].
- (ii) Velocity appears to increase with depth at a rate of/...

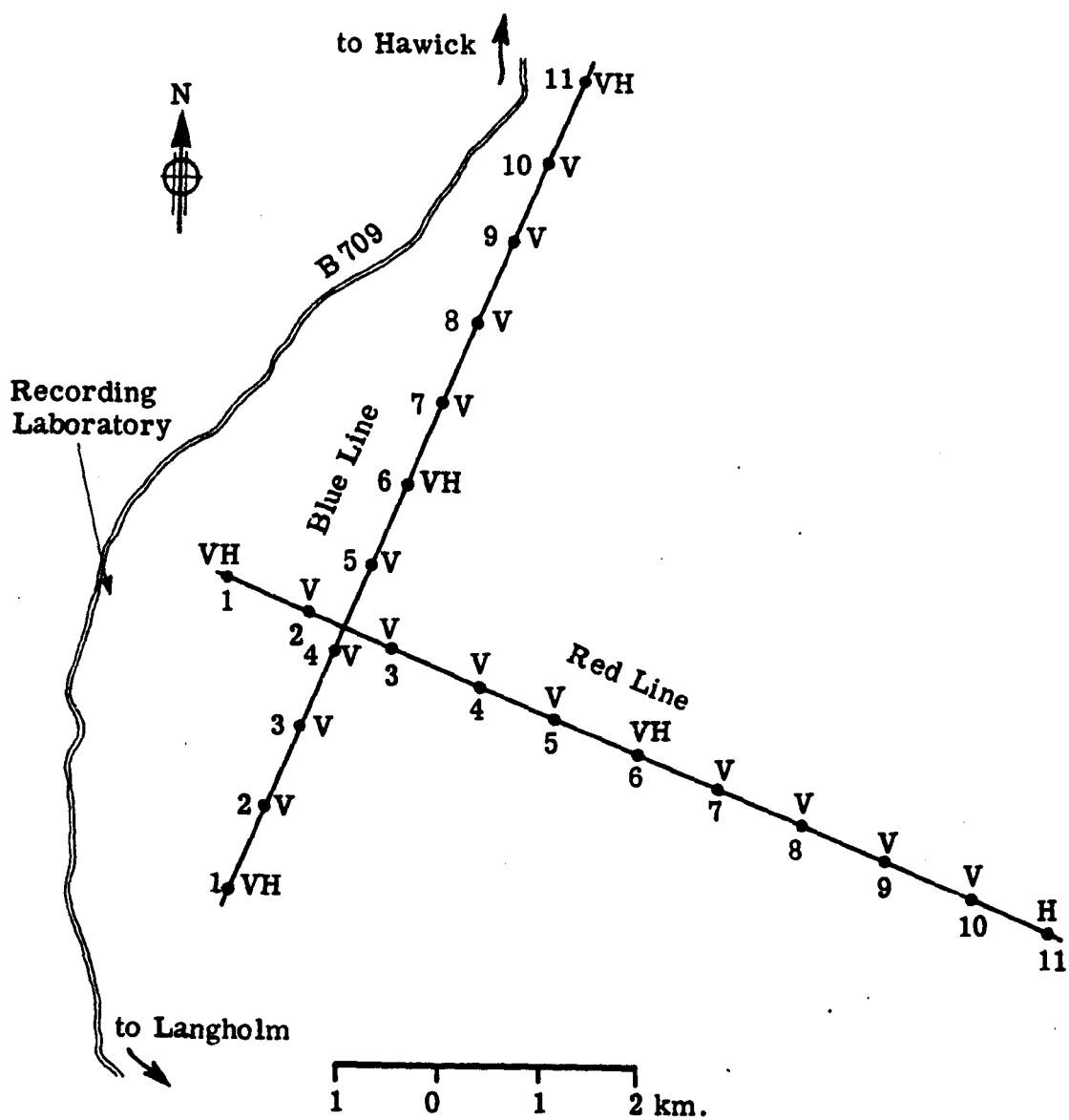


Fig. 1-5 The UKAEA Eskdalemuir Seismological Recording Station (from El Isa, 1977).

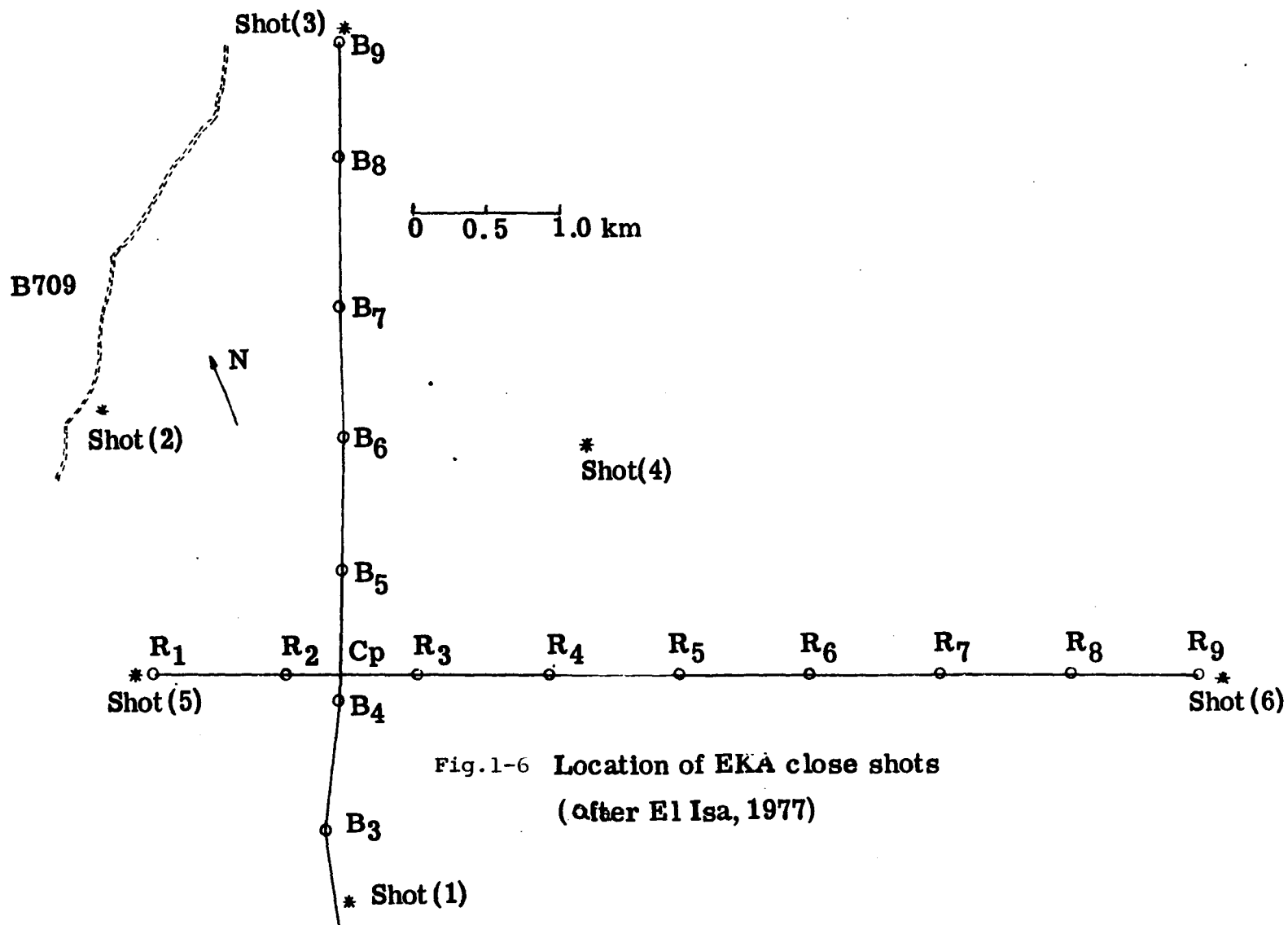


Fig.1-6 Location of EKA close shots
(after El Isa, 1977)

of 1.3 to 1.4 km/s/km to a depth of 0.7 to 0.9 km, thereafter reducing to a rate of 0.3 km/s/km near the limit of depth penetration (0.8 to 1.0 km) [Fig. 1-7].

Velocity-increase from 5.54 km/s to 6.4 km/s at a decreasing rate over a depth range of 0-12 km has been observed at EKA by Jacob (1969). The increase of velocity with depth is considered to be due to the closure of cracks under pressure. This effect was first noticed and interpreted in this way by Adams & Williamson (1923), and has been noted and similarly interpreted by subsequent workers (Birch, 1960, 1961; and Hall & Al Haddad, 1979). The latter workers worked on Lewisian rocks of the northwest of Scotland.

El Isa concluded that P-wave velocities within the Lower Palaeozoic rocks of Scotland around EKA not only increase with depth but also vary with azimuth. Since similar rocks occur throughout the Southern Uplands, similar anisotropy, dependent upon the attitude of the bedding in the rocks, is to be expected. Further investigation as to its cause would allow the definition of the variation of anisotropy with depth and rock fabric orientation.

Throughout this thesis, velocity anisotropy is defined as

$$\frac{V_{\max} - V_{\min}}{V_{\text{mean}}}$$

1.5 Theoretical bases of anisotropy

Two bases for modelling anisotropy in rocks are used.

(A) The first case is that of a laminated medium consisting of two kinds of isotropic layers which alternate forming a periodic structure/...

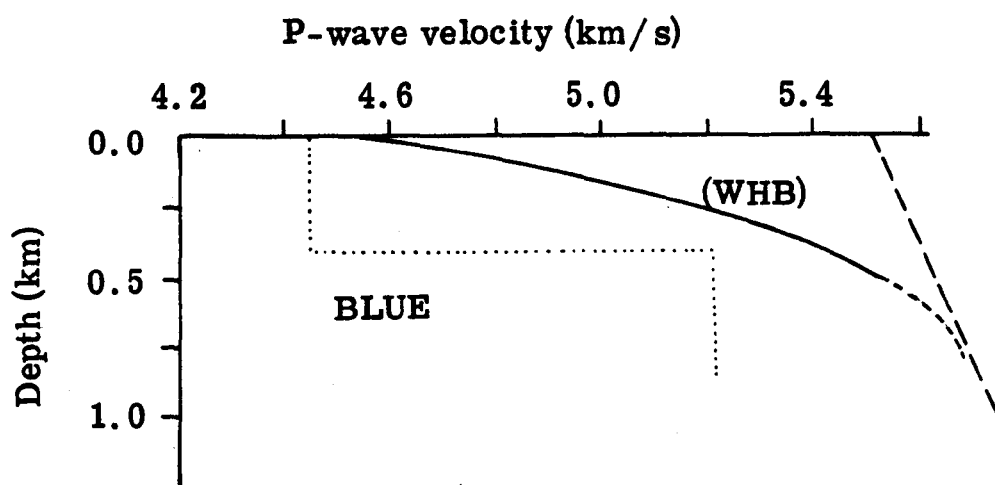
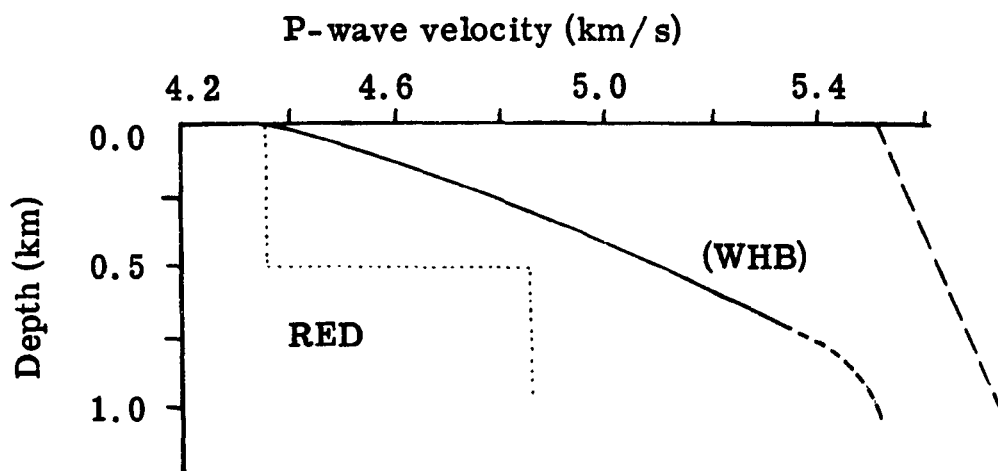


Fig. 1-7. Velocity depth functions at EKA (after El Isa, 1977).

The dashed line (from Jacob, 1969) and the curve marked (WHB) (from El Isa, 1977) illustrate velocity-depth functions under EKA in a medium where velocity increases continuously with depth. The dotted lines (El Isa, 1977) illustrate a two-layer model of the upper crust under the Eskdalemuir Array.

structure [Fig. 1-8]. (B) The second case assumes an isotropic medium containing 'flat' cracks with a preferred orientation. The overall elastic symmetry of the composite material in both cases is axial or transversely isotropic. Both cases are reasonable for rocks of the Southern Uplands since the succession consists of alternations of shale and greywacke, affected by fracturing including cleavage which may have regionally-consistent orientation.

(A) Anisotropy due to stratification.

Of the structural patterns envisaged for the Southern Uplands, one is that of alternating beds of greywacke and shale that are steeply dipping and becoming younger to the northwest. Such a layered structure is regarded as an anisotropic medium consisting of alternating plane parallel layers of materials which are themselves isotropic. This case of a laminated medium has been examined by workers such as Hagedoorn (1954), Cholet and Richard (1954), Postma (1955), White and Angona (1955), Crampin (1977), and Levin (1980). In theory, such laminated transversely isotropic solids are considered to have one axis of symmetry, "vertical", and are characterised by five independent elastic constants (C_{11} , C_{12} , C_{13} , C_{33} , C_{44} , using Postma's notations) compared to two in an isotropic medium, where, $C_{11} = C_{33} = \lambda + 2\mu$; $C_{12} = C_{13} = \lambda$; $C_{44} = \mu$.

λ is Lamé's constant

μ is modulus of rigidity.

$C_{ij} = C_{ji}$ ($i, j = 1, 2, \dots, 6$) is coefficient of elasticity.
In/...

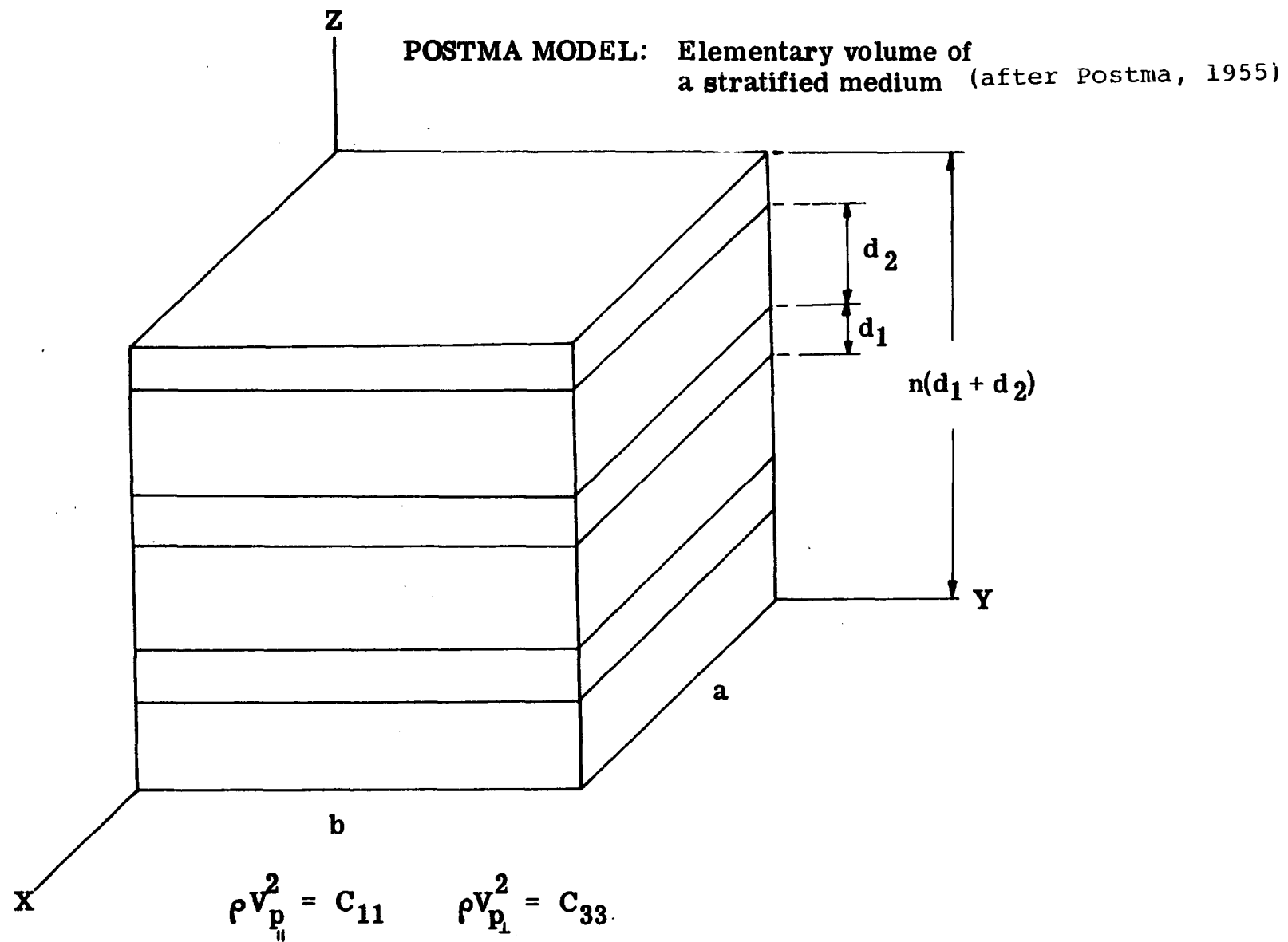


Fig. 1-8

In explaining the subscripts (ij), it is usual to choose axes of reference in directions that are related to the symmetry of the substance under consideration such that all six stress components (σ_{ij}) are expressed as linear functions of strain (ϵ_{ij}) such as,

$$\sigma_x = c_{11}\epsilon_x + c_{12}\epsilon_y + c_{13}\epsilon_z + c_{14}\gamma_{yz} + c_{15}\gamma_{zx} + c_{16}\gamma_{xy} \quad (1)$$

$$\sigma_y = c_{21}\epsilon_x + c_{22}\epsilon_y + c_{23}\epsilon_z + c_{24}\gamma_{yz} + c_{25}\gamma_{zx} + c_{26}\gamma_{xy} \quad (2)$$

$$\sigma_z = c_{31}\epsilon_x + c_{32}\epsilon_y + c_{33}\epsilon_z + c_{34}\gamma_{yz} + c_{35}\gamma_{zx} + c_{36}\gamma_{xy} \quad (3)$$

$$\tau_{yz} = c_{41}\epsilon_x + c_{42}\epsilon_y + c_{43}\epsilon_z + c_{44}\gamma_{yz} + c_{45}\gamma_{zx} + c_{46}\gamma_{xy} \quad (4)$$

$$\tau_{zx} = c_{51}\epsilon_x + c_{52}\epsilon_y + c_{53}\epsilon_z + c_{54}\gamma_{yz} + c_{55}\gamma_{zx} + c_{56}\gamma_{xy} \quad (5)$$

$$\tau_{xy} = c_{61}\epsilon_x + c_{62}\epsilon_y + c_{63}\epsilon_z + c_{64}\gamma_{yz} + c_{65}\gamma_{zx} + c_{66}\gamma_{xy} \quad (6)$$

where the 36 constants c_{ij} are known as the elastic coefficients. Since $c_{ij} = c_{ji}$ (7) (Postma, 1955; Jaeger, 1974), the above relations reduce to 21 independent coefficients. A further reduction of the number of coefficients follows from the symmetry of the material in question as considered below.

(i) For a solid with three mutually perpendicular planes of symmetry, the stress-strain relations reduce to,

$$\sigma_x = c_{11}\epsilon_x + c_{12}\epsilon_y + c_{13}\epsilon_z, \dots\dots\dots (9)$$

$$\sigma_y = c_{12}\epsilon_x + c_{22}\epsilon_y + c_{23}\epsilon_z, \dots\dots\dots (10)$$

$$\sigma_z = c_{13}\epsilon_x + c_{23}\epsilon_y + c_{33}\epsilon_z, \dots\dots\dots (11)$$

$$\tau_{yz} = c_{44}\gamma_{yz}, \tau_{zx} = c_{55}\gamma_{zx}, \tau_{xy} = c_{66}\gamma_{xy} \dots\dots\dots (12)$$

which give nine independent coefficients.

(ii) If the Z-axis is taken as the axis of symmetry [Fig. 1-9] such that the properties of the material are the same in all directions at right angles to it, the elastic coefficients (c_{ij}) in the relations between the components of stress and strain are/...

are invariant with respect to rotations (through θ) of the coordinate system around the Z-axis. This is a case of transverse isotropy, and the equations relating stress to strain are further reduced to,

$$\sigma_X = C_{11}\epsilon_X + (C_{11} - 2C_{66})\epsilon_Y + C_{13}\epsilon_Z \dots\dots\dots (13)$$

$$\sigma_Y = (C_{11} - 2C_{66})\epsilon_X + C_{11}\epsilon_Y + C_{13}\epsilon_Z \dots\dots\dots (14)$$

$$\sigma_Z = C_{13}\epsilon_X + C_{13}\epsilon_Y + C_{33}\epsilon_Z \dots\dots\dots (15)$$

$$\tau_{YZ} = C_{44}\gamma_{YZ}, \tau_{ZX} = C_{44}\gamma_{ZX}, \tau_{XY} = C_{66}\gamma_{XY} \dots (16)$$

$C_{11} = C_{22}$, $C_{13} = C_{23}$, $C_{44} = C_{55}$ and $C_{12} = C_{11} - 2C_{66}$, involving five independent coefficients. The derivation of stress-strain relations for other types of crystal symmetry can be found in Jaeger (1974).

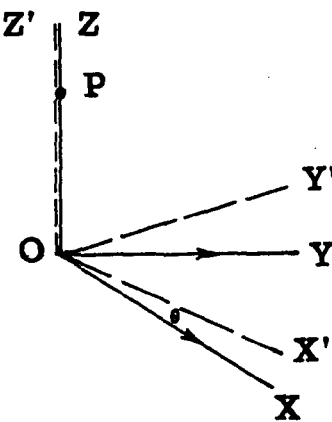


Fig. 1-9 Co-ordinate system for stress-strain relationship in an anisotropic medium.

The five elastic constants resulting from transverse isotropy, can be expressed in terms of the elastic properties and densities of the individual layers. For propagation in the plane of symmetry, the velocities are given by,

/...

$$\rho v_p^2 = C_{11}$$

$$\rho v_{SH}^2 = C_{66} \text{ where } C_{66} = (C_{11} - C_{12})/2$$

$$\rho v_{SV}^2 = C_{44}$$

where v_p is compressional wave velocity

v_{SH} is S-wave velocity with polarization
in the plane of symmetry

v_{SV} is S-wave velocity with polarization along Z-axis

ρ is density of the medium

In sedimentary rocks such as in the Southern Uplands, the plane of circular symmetry is the bedding plane and the Z-axis is normal to bedding. For propagation along Z-axis, the velocities are given by,

$$\rho v_{p\perp}^2 = C_{33}$$

$$\rho v_{SH}^2 = C_{44} \text{ where, in this case,}$$

v_{SH} is independent of polarization direction.

Crampin (1977) has derived an equation relating the velocities of the composite anisotropic medium with the elastic moduli of the individual layers and direction of propagation. The relations are,

$$\rho v_p^2 = A \pm B \cos 2\theta \pm C \cos 4\theta \dots\dots\dots (17)$$

$$\rho v_{SH}^2 = D \pm E \cos 4\theta \dots\dots\dots (18)$$

$$\rho v_{SV}^2 = F \pm G \cos 2\theta \dots\dots\dots (19)$$

where $C = -E$

θ is azimuth measured by rotating the elastic tensor

about the axis of symmetry (Z in this case). An element

in the new coordinate system after a rotation of θ can be expressed

in terms of the original elements and multiples of θ as in (17), (18)

and (19).

/...

Mixing of layers of shales and greywackes alone in terms of laboratory velocity data did not account for the observed anisotropy at EKA. A second theoretical model based on cracks was therefore considered.

(B) Anisotropy due to crack orientation

The physical properties of rocks are dependent on cracks. Velocity anisotropy results when the cracks in a rock have a preferred orientation (Crampin, 1978; Bamford & Nunn, 1979).

In recent years, theoretical techniques have been advanced to model the effect of cracks on the elastic properties of (cracked) solids. Many of the techniques are derived from Eshelby (1957) who determined elastic constants directly by analysis of the strain around an ellipsoidal inclusion. Nur (1971) used this method to estimate the elastic constants of a system of dry cracks and Anderson et al (1974), also have used Eshelby's results to calculate the overall elastic constants of an isotropic matrix containing oriented ellipsoidal inhomogeneities. Most other works (O'Connell & Budiansky, 1974, 1977; Budiansky & O'Connell, 1976; Walsh, 1965; Mavko & Nur, 1978; Toksoz et al 1976; Cheng & Toksoz, 1979; and Siegfried & Simmons 1978) assume random orientation of cracks in the rock or solid medium. Of all the above formulations, only O'Connell & Budiansky (1974, 1977) and Budiansky & O'Connell, (1976) addressed themselves to the interaction of cracks by use of a self-consistent approach which is valid for strong concentration of cracks

The observed anisotropy in-situ (El Isa, 1977) in the Southern Uplands rocks may be attributed to the presence of cracks along bedding planes, as the latter are preferred sites for the development/...

development of joints and cracks. A concentration of such aligned cracks displaying velocity anisotropy must have its effective elastic constants arranged in a form of anisotropic symmetry (Crampin, 1977). The author showed that if θ is measured from an axis of symmetry, velocities vary as the reduced equations (17), (18) and (19) in Section (A) above.

O'Connell and Budiansky, (1974) found that the effects of thin elliptical cracks were almost identical to those of circular cracks in a randomly orientated system (formulations in appendix 2). However, the overall symmetry of a material containing parallel penny-shaped cracks is axial or transversely isotropic, and a system of aligned elliptical cracks will certainly modify the effects of an aligned circular crack-system. These effects are considered in later chapters when the self-consistent technique is used to calculate the crack parameters in greywackes of the Southern Uplands from observed P- and S-wave velocities measured in the laboratory. SEM examination of the rock samples is used to study the crack system in the rocks.

1.6 The present project

An explanation of the observed velocity anisotropy in the Southern Uplands requires some velocity information on shale and greywacke which are the principal rocktypes of the Southern Uplands. The present work therefore comprises two parts, (i) Near-surface measurement/

measurement of velocity by hammer line experiment at Whitehouse shore, Girvan. This provides velocities in individual units of shale and greywacke, and samples for further laboratory work.

- (ii) The second part is the laboratory measurement of seismic velocities in cores of shales and greywackes sampled from Girvan.

Using the pulse-transmission technique of Birch (1960), P- and S-wave velocities were measured with increasing and decreasing confining pressure up to 0.5 GPa (5 kbar). Where possible, three orthogonal cores from each sample of rock were run, to be able to investigate directional variation of the physical properties of the rocks. The increase of confining pressure during velocity measurement simulates conditions in-situ where pressure is known to increase with depth. Velocity information obtained is used to model anisotropy in Southern Uplands rocks, using some theoretical crack models such as O'Connell & Budiansky (1974, 1977), Toksoz et al (1976), and Cheng & Toksoz (1979).

Direct examination of the rocks using scanning electron microscope (SEM) helps in the study of the system of cracks present in the rocks.

2.1 Laboratory measurements

Introduction

As mentioned in Chapter 1, seismological studies previously carried out in the Southern Uplands have yielded information on the crustal velocity distributions. The variability in structure as suggested by the previously measured in situ velocities (e.g. LISPB III, IV, V; and El Isa, 1977), calls for independent and more comprehensive study of seismic velocities in the Southern Uplands rocks. Laboratory measurement of velocities in suites of greywacke and shale offers the invaluable opportunity of increasing our knowledge about the physical properties of the dominant Lower Palaeozoic rocktypes of the region and how those properties might vary with depth.

Three basic methods are now employed for velocity measurements in the laboratory. Of these, the pulse-transmission technique (Birch, 1960, 1961) has been found to be the best compromise for natural rock specimens (Anderson & Liebermann, 1968). The method has been successfully used by subsequent investigators such as Simmons (1964); Christensen (1965); Peselnick & Stewart (1975); and Hall & Simmons (1979).

Measurement of velocity consists of the determination of travel time of a compressional or shear pulse through cylindrical rock specimens of known length and diameter. A high-voltage pulse is applied to a piezoelectric disc (see next section) which covers one end/...

end of the specimen. The acoustic pulse generated is transmitted to a second transducer which detects the acoustic pulse as an electric signal which is displayed on a dual-trace oscilloscope. Travel time is measured precisely by comparison with that through a variable length mercury delay line or by using a time marker to pick the first arrival.

Transducer materials used

It is pertinent to mention that different transducer materials were used for P-and S-wave velocity measurements in this work. Piezoelectric ceramic disc was used for P-wave velocity while AC-cut quartz crystal was employed for the S-wave velocity experiments.

Virtually all transducers currently in use in electro-acoustic experiments are piezoelectric. The property of such materials being utilized is their ability to develop electrical potential when they undergo physical deformation or conversely, physical deformation of the material results when subjected to an electric field. Comprehensive review of the properties of piezoelectric transducer materials has been made by Jaffe & Berlincourt (1965).

While there have been few problems in the generation and detection of P-waves, great difficulty has been encountered by earlier workers in the generation of S-waves without significant P-wave energy/

energy. Hughes et al (1949) showed that compressional and shear wave velocities could be obtained from a single input compressional pulse. This method was unsatisfactory for the determination of S-wave velocity in rocks (Hughes & Maurette, 1956). For the same reason that the presence of P-wave energy always preceded S-wave, the method of critical reflection of P-to S-wave described by Jamieson & Hoskins (1963) has been rejected for the present work. Use was made by Hughes & Maurette (1956), of Y-cut quartz crystal to generate S-waves. Again compressional waves accompanying the S-wave precluded any accuracy in determining the arrival of the first shear wave. Thus AC-cut quartz transducers, used by Peselnick (1962) to generate shear waves were utilized in the present S-wave experiments. They are known to give unambiguous S-wave arrival (Simmons, 1964), hence an improvement over previous techniques of generating S-waves. It should be added, however, that for quartz transducers, compared with ceramics, higher voltages are needed for the generation of observable S-wave energy.

P-wave velocity measurement at East Anglia

The first set of runs was carried out in 1979 at the School of Environmental Sciences, University of East Anglia.

/...

Experimental details

Each of the right circular cylindrical cores of approximately 2.54 cm. mean diameter, was placed between a pair of 1 MHz barium titanate longitudinal transducers which were held inside steel holders. A P.T.F.E. tube was slipped over the transducer-rock assembly and the assembly placed inside a steel pressure chamber (Fig. 2-1). Pore-pressure was presumably maintained at atmospheric pressure (about 1 bar) through a pore-fluid vent in one of the transducer assemblies. This allows flow of liquid out of the samples as cracks close under confining pressure. A maximum working pressure of 3.0 kbar was attainable inside the vessel. The pressure medium was a mixture of petroleum ether and kerosene.

A pulse generator, "Farnell PG 5222" produced a pulse of 100V which was impressed on the transmitting transducer, propagated through the rock core as elastic waves and received by the second transducer. The received signal was amplified and displayed on an oscilloscope. Pulse transit time was measured by the delay of an oscilloscope marker pulse from input to output. Back-to-back delays through transducers and steel holders were measured and made available for P-wave velocity calculations by Evans (1979 ; personal communication). Overall accuracy of the time and velocity measurements is approximately 2%.

All measurements were made at room temperature (18°-29°C) as displayed on a "Cormack digital thermometer 5000". A "Hewlett-Packard 5328A" universal counter indicated the transit time of pulses through/

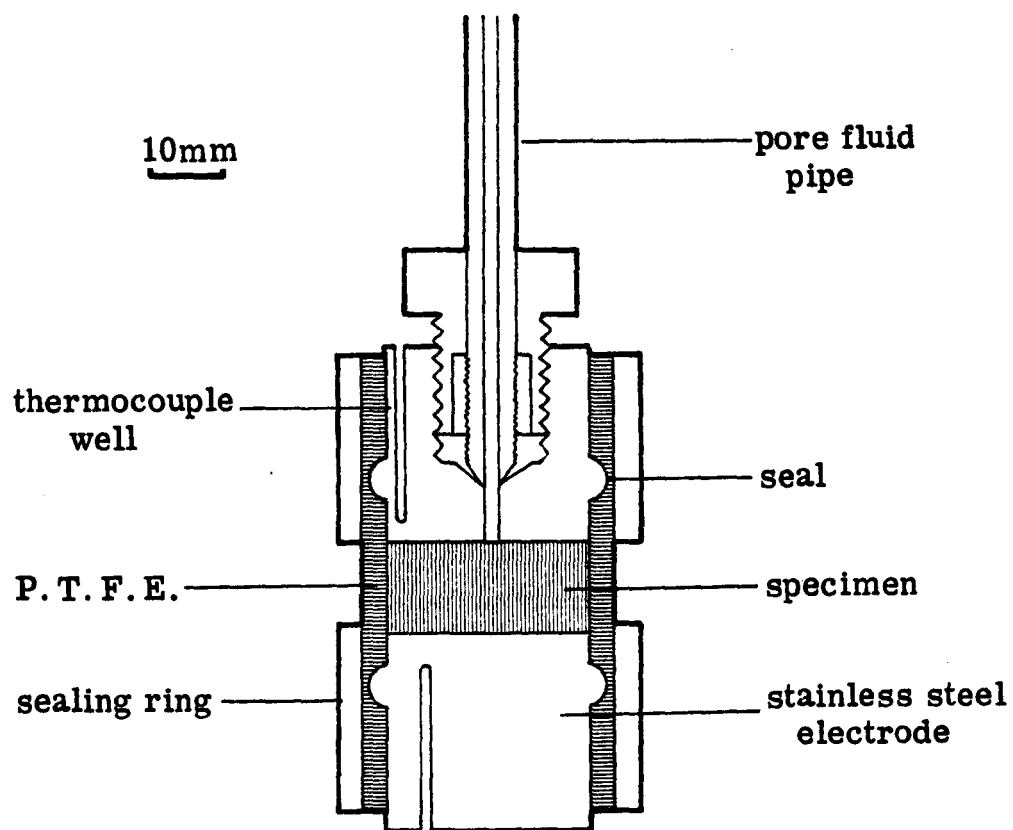


Fig. 2-1 Specimen Assembly of the East Anglia apparatus.

through rock cores as soon as the oscilloscope marker pulse was made to coincide with the first arrival of the displayed wave train. The electronic gear used is similar to that described by Al Haddad (1977). Further description of the East Anglia gear could be found also in Evans et al (1978).

Where possible, two or three specimens cored at right angles from the same hand specimen were run in order to reveal anisotropy.

Further velocity runs on the same suites of rocks and on additional specimens also from Girvan were made at the Experimental Petrology Unit, University of Edinburgh on account of the latter's proximity to Glasgow and the acquisition of electronic gear by this department. Adaptation of the newly-acquired gear to use with the pressure system at Edinburgh commenced in September, 1979. Problems of system-generated noise which completely obscured the required signal, and other experimental difficulties did not subside until early 1980. The problems are highlighted briefly in the next section where construction of a suitable end-plug for use in pressure vessel is discussed.

Sample assembly and pressure vessel (Edinburgh)

Use of the pressure vessels of the Experimental Petrology Unit of Edinburgh University, required that a new sample assembly, different from that of East Anglia, be designed for our acoustic experiments/

experiments. A steel end-plug was connected to a transducer-rock assembly which was jacketed inside a plastic tube, and the whole set-up slipped inside a brass-tube (internal diameter 4.11 cm. and length is 24.13 cm). The brass tube was machined in the department to fit the bore inside the pressure vessel at Edinburgh.

Originally, two pairs of electrical leads were used to connect transducers to pulse generator and oscilloscope. The problem of noise, which always preceded the actual signal obscuring the latter, necessitated the use of coaxial leads. Apart from simplicity of the set-up, there was improvement in the quality of signal received. Noisy onset of the signal was further improved by shortening the coaxial cables. High frequency (9MHZ) noise, though still preceding the actual signal, was greatly compressed leaving a 'quiet' delay (Fig. 2-2) before the onset of the P-wave arrival.

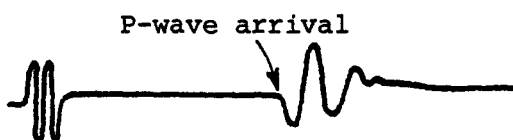


Fig. 2-2 Seismic wave signal from rock sample.
(ref. Edinburgh)

Application of a voltage of about 300V produced a good signal with signal-to-noise ratio (S/N) of more than 20dB. As mentioned earlier, time-measurement was by a mercury delay line which must be calibrated prior to any experimental work on velocity.

/

Calibration of the mercury delay line

In the pulse transmission technique, the elapsed time between generated and recorded electronic pulse is greater than the transit-time of an elastic wave through the specimen. Lengthening of the pulse transit-time arises from electronic and transducer delays. Therefore the zero-setting of the delay line was determined by finding the settings that would correspond to the first arrivals through steel samples of lengths ranging from 25.2 mm to 50.9 mm and extrapolating to zero-length (Birch, 1960; and Simmons, 1965).

In the past, mercury delay lines were reported by Birch to have been used by McSkimmin (1950) and Laughton (1957). They always give a transmitted signal with a continuously variable delay. One transducer is fixed at the base of the mercury column, and the other, mounted on a slide, is moved in a vertical plane with a screw. The position of the slide is read with a dial gauge which is controlled within 0.005 mm - a distance that corresponds to 0.003 μ s delay in mercury. The velocity of the mercury in the column was measured separately (by Hall, 1979) and found to be 1.453 ± 0.001 mm/ μ s.

Accuracy of the measurement of transit-time through specimens depends on the quality of the signal and the calibration of the mercury line. The principal limitation on the accuracy of velocity measurement, however, is the gradual onset of the first motion. This results from the gradual build-up of the mechanical response of transducers and relative attenuation of high frequencies in the rocks.

/...

rocks. In the present work, uncertainties were reduced by increasing input voltage to about 200-300V for P-waves and 500-600V for S-waves. The signal through the mercury line has a similar shape to that through the steel or rock sample (Fig. 2-3). Matching of the two signals together helped to enhance precision of setting which would have been less if a vertical time marker were used to pick the first arrival (Ref. East Anglia).

The different lengths of mild steel used for the calibration experiment, were cut from the same bar of approximately 25.4 mm diameter. On the dial gauge of the mercury line, settings corresponding to the first arrivals through each steel length were obtained at various pressures to 5.0 kbar. Sets of readings for P- and S-wave velocities are shown in table 2-1.

/...

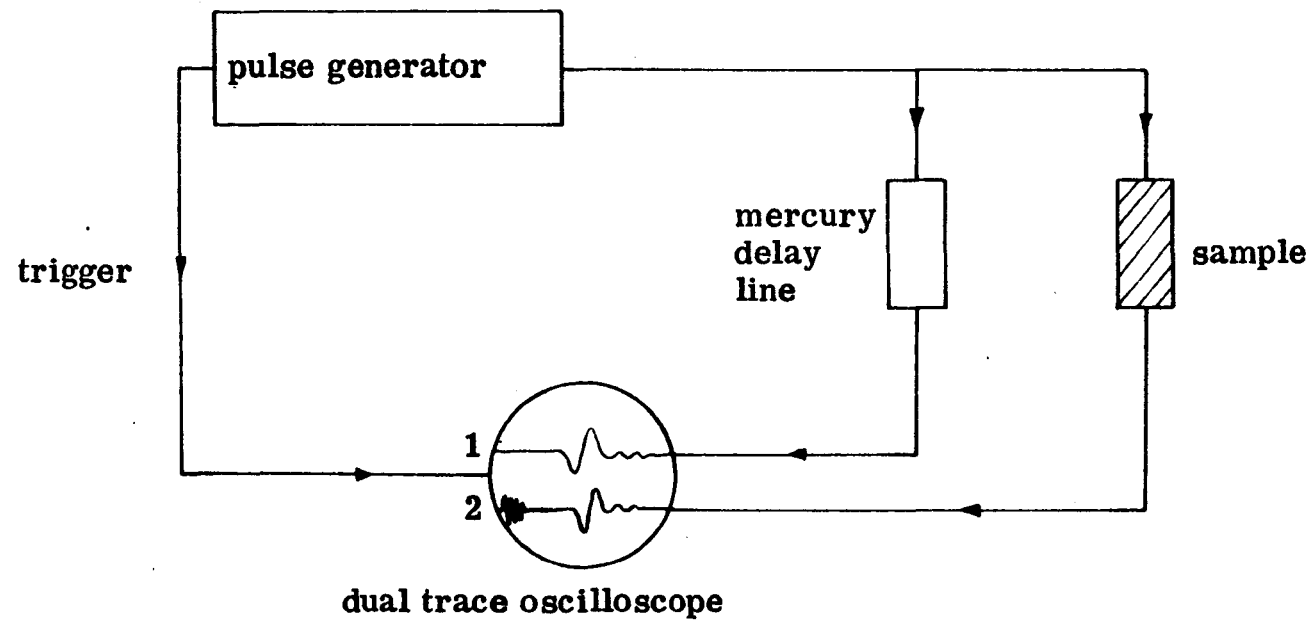


Fig. 2-3 **Schematic diagram of Edinburgh and Glasgow systems**

Table 2-1: Zero-length delays for P- & S-wave velocity measurements.

Confining Pressure (kbar)	ZERO-LENGTH DELAYS (mm Hg) IN TRANSDUCERS		
	Set 01	Set 02	Set 05
	P-wave (x-1mm Hg)	S-wave (x-1mm Hg)	P-wave (x-1mm Hg)
0.001	2.620	0.947	2.876
0.10	2.664	0.989	2.937
0.25	2.725	0.989	3.017
0.50	2.824	1.025	3.105
0.75	2.893	1.057	3.159
1.00	2.945	1.086	3.203
1.50	3.006	1.134	3.269
2.00	3.024	1.159	3.309
2.50	3.040	1.168	3.350
3.00	3.050	1.173	3.382
3.50	3.060	1.174	3.407
4.00	3.071	1.175	3.433
4.50	3.081	1.177	3.458
5.00	3.092	1.179	3.485

Velocity measurements at confining pressures to 5.0 kbar (Edinburgh)

Using the rock-transducer assembly and the pressure chamber described earlier, compressional and shear-wave velocities in Lower Palaeozoic rocks of the Southern Uplands were measured at confining pressures to 5.0 kbar. Method of measurement is similar to that described for East Anglia but for some modification by the apparatus. Here pulses were generated by a "Velonex 345" pulse generator which requires no external amplifier. Improved signal-to-noise ratio was achieved by varying the pulse width. For 1MHz transducer in use, this should be close to 1 μ s or a little less. Very short pulse width was found to reduce the strength of the signal.

Pulse transit times were measured with a mercury delay line (described earlier) by matching the signals from both the rock and mercury on the dual-trace oscilloscope. Pressure was measured by the change in resistance of a calibrated manganin wire gauge. The pressure medium was a mixture of nitrogen and argon. All measurements were made at room temperature. A limitation of this system was the difficulty in maintaining a steady state of pressure inside the vessel. Enough time (i.e. > 10 minutes) could not be spared between readings for the pressure conditions to equilibrate. Results of the p-and S-wave velocity measurements are discussed in Chapter 3.

Pore pressure was maintained at 1bar by wrapping water-saturated samples inside a 40 mesh copper gauze to provide space for water/

water expelled from cracks during pressure increases. Acoustic coupling between rock face and steel holder of the transducers was achieved by use of silicon grease (P-wave) and high viscosity Dow-resin (S-wave). Thin film of these coupling materials helped fill any imperfections on the faces of the rock and steel holders.

Velocity measurement at low pressures (0-200bar) Glasgow.

The initial difficulty encountered in measuring velocities at pressures below 250 bars, at both East Anglia and Edinburgh, and the need to correlate field and laboratory measured velocities prompted the idea of low-pressure experiment. With the aid of a steel chamber obtained from Civil Engineering Department, P-wave velocity in 24 cores of greywacke and shale was measured. The large volume of the vessel was reduced by filling the inner space with rock waste while hydraulic oil, the pressure medium, took the rest of the space.

Pressure was applied by a hand pump and measured with a Bourdon gauge mounted above the hand pump. Once raised, pressure is maintained by a piston balance. A maximum confining pressure of 200 bars was attainable inside the vessel. Because a new P-wave transducer set (003) was in use, calibration of the mercury delay line was repeated using the same steel lengths used earlier at Edinburgh.

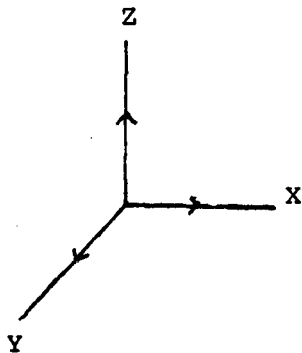
/...

2.2. Laboratory treatment of rock specimens

Shape of specimens

In line with the recommendation of Birch (1960) the most convenient shape of the specimens for velocity measurement is a right circular cylinder in which length to diameter (L:D) ratio should not exceed 5 (Anderson & Liebermann, 1968). For $L:D > 5$, P-waves often recede into noise level as boundary reflections interfere with the direct wave. At large L/D, the first arrival travels with the bar velocity, $(E/\rho)^{1/2}$ where E is Young's modulus and ρ is the bulk density of the specimen.

From each of six samples of greywackes, three orthogonal cores (Fig. 2.4) were obtained using a 2.5 cm. diameter diamond corer.



In the present work,

$Z \equiv N$, core normal to bedding
or rock fabric.

$Y \equiv V$, $X \equiv H$, cores parallel to
bedding or rock fabric.

Fig. 2.4 Three orthogonal directions of cores from rock samples.

Due to the fissility of shale, samples collected from the field did not furnish 3 mutually perpendicular cores from any one specimen of shale. Measurements were therefore made on incomplete sets of cores from shale samples.

/...

In the course of coring and grinding, many shale samples were lost, and a considerable length of time was spent on trying to obtain cores from these samples with limited success.

Special treatment of shale.

Attempts to check the loss of shale specimens through coring and grinding include,

- (i) cutting of shale samples into cubes prior to drilling was abandoned;
- (ii) instead, irregularly-shaped lumps of shale were plastered and cast into rectangles to keep them together while coring. Both plaster and rock often disintegrated under the vibratory motion of the drilling machine.
- (iii) the steel clamp of the drilling machine was then replaced with a wooden platform over which specimens were stuck using nails to keep the rock stationary during drilling.

Even in response to (iii) above, many of the cores came out in bits. The latter were then glued together with polyester resin. To further enhance cohesion in the shale specimens the entire curved surface of the core was thinly coated with plastic padding, left to dry for about 2 hours and smoothed with an abrasive. It is assumed that the resultant porosity of the cores after the above treatment, is probably not much different from the actual porosity of/...

of rock in situ since some cracks induced by sampling, transportation, and coring might have been sealed when resin was used to glue bits of the rock cores together.

It is apposite to mention that Jones & Wang (1981) in order to facilitate coring of their shale specimens set pieces of rock in paraffin blocks, and dry-cored with an air-cooled fine diamond bit at a speed of 2580 r.p.m. Even this technique failed to furnish a complete set of 3 orthogonal cores from one sample of shale.

Grinding

Using a 1/4 inch-wide grinder in the department, cores from greywacke and shale were ground to right-circular cylinders with flat, parallel faces. Instrument marks, in form of very minute ridges and hollows on the ground faces could result in lack of good contact between rock and transducer. Later a "Buehler Isomet" variable, low speed saw was used. The saw cuts the core ends directly to the required flatness and parallelism.

Cutting is done with a diamond wafering blade with high or low concentration diamond edge. The cutting fluid used was water instead of the manufacturers' liquid. This was to prevent any possible reaction between the fluid and rock constituents; and since saturation was always done with water, it was considered safe to use the latter as the cutting fluid. It must be mentioned that the /...

micrometer arm of the low-speed saw, which allows the movement of the clamp and specimen in a horizontal plane, helps to ensure cutting of cores with parallel faces.

Lengths of specimens range from 26mm to 39mm with standard deviations of about 0.003 to 0.06, except for one specimen with 0.21. The length and standard deviations were obtained from 5 readings taken with a micrometer screw gauge.

Saturation of samples

Inclusion of fluid in the pores of rocks under test is one of the environmental factors being investigated in the present work. Therefore it was necessary to run samples both saturated and dry.

Saturation was effected by vacuum pumping on samples immersed in water. Using a water jet pump, vacuum of about 20mm Hg could be achieved.

At a late stage in the work, incomplete saturation was suspected and another saturation technique was devised. Samples were placed in a vacuum chamber and air was evaporated using a vacuum pump which was left running overnight. Water was then introduced into the container to saturate the samples.

/...

2.3 Density measurements

Measurements of density are useful in this work for three reasons;

- (i) Seismic velocity is dependent on density;
- (ii) density is a rough guide to composition; and
- (iii) porosity can be estimated as a by-product of density determination.

Samples were first oven-dried at 110°C for 24 hrs. after which dry weights were measured. After saturation, weights of saturated specimens in air and in water were also taken. Readings on the hydrostatic balance can be taken to 0.001g ($\approx 0.1\%$). Porosity and bulk densities were then calculated from all weight measurements. Care was taken to work only on unweathered rocks. Alteration (if any) was not observable in hand specimen. Any adherent air-bubbles on the surface of the specimens were carefully brushed off. Calculations of densities and porosity were made for individual cores. The formulae used are set out in Appendix 1.

Apart from specimen preparation for velocity measurements in the laboratory, rocks were also sectioned for optical and scanning electron microscopy (SEM). Below is the outline of preparation of specimens for examination under the SEM.

/...

2.4 Preparation of specimen for SEM examination

- (1) Slices approximately 1cm x 1cm were obtained from each velocity sample of greywacke using the "Isomet" low-speed saw. The speed used for cutting was about 200 r.p.m., slow enough to minimise introduction of new cracks.
- (2) The rock slices were mounted on a steel stub with epoxy and then successively handlapped on carborundum papers with grades 180, 400 and 600 and a 1/4 grade grit paper. Only gentle pressures were applied, and handlapping of each rock slice was done for at least 20 mins. on each grade of carborundum papers.
- (3) Aluminium oxide powder (size 0.05 μ) was then used to further grind the specimens, again spending at least 20 mins. or more with slight pressures applied by the fingers.
- (4) Next, an electrically-worked diamond polisher of different grades was used with Hyprez liquid as lubricant, polishing each slice of rock for 20 mins.
- (5) The last stage of the preparation of crack-sections involved handlapping of rock-slices using Hyprez "five star" diamond compound as the lubricant of grade "1/4 - FS - 475". A time lap of 20 mins. was spent on each specimen. After grinding and polishing, the specimens were immersed in acetone to dissolve and dry out water and other chemicals that might have penetrated the cracks present in the rocks.
- (6) The specimens were ready for SEM examination after being gold-plated inside a vacuum chamber.

/...

During preparation of a section, new cracks and other surface damage may form. This renders accurate observation of microporosity rather difficult. This was why only gentle pressure was applied during long periods of grinding and polishing. Brace et al (1972) took a step further by subjecting their specimens to ion-thinning to remove surface damage left by grinding.

Briefly, the procedure consists of placing the specimen, after grinding, inside an ion-milling instrument. An ionized argon beam (6 KV) was used to bombard the sample at an angle of 15° to 17°. The beam is supposed to knock off individual atoms at a maximum intensity of 50 $\mu\text{a}/\text{mm}^2$. 10 to 50 μm of material was removed from the ground surface by bombardment, resulting in an uneven surface because thinning rates vary significantly from mineral to mineral.

The only locally-available ion-beam thinner had an inappropriately-small target area, so attempts at using this technique in this study were abandoned.

2.5 Field measurement of velocity

Introduction to the area of hammer lines (Girvan)

The Girvan coast was picked as the site for hammer lines on account of easy access to large exposures of similar rocks to those under EKA. The map (Fig. 2.5a) shows the main elements of the/...

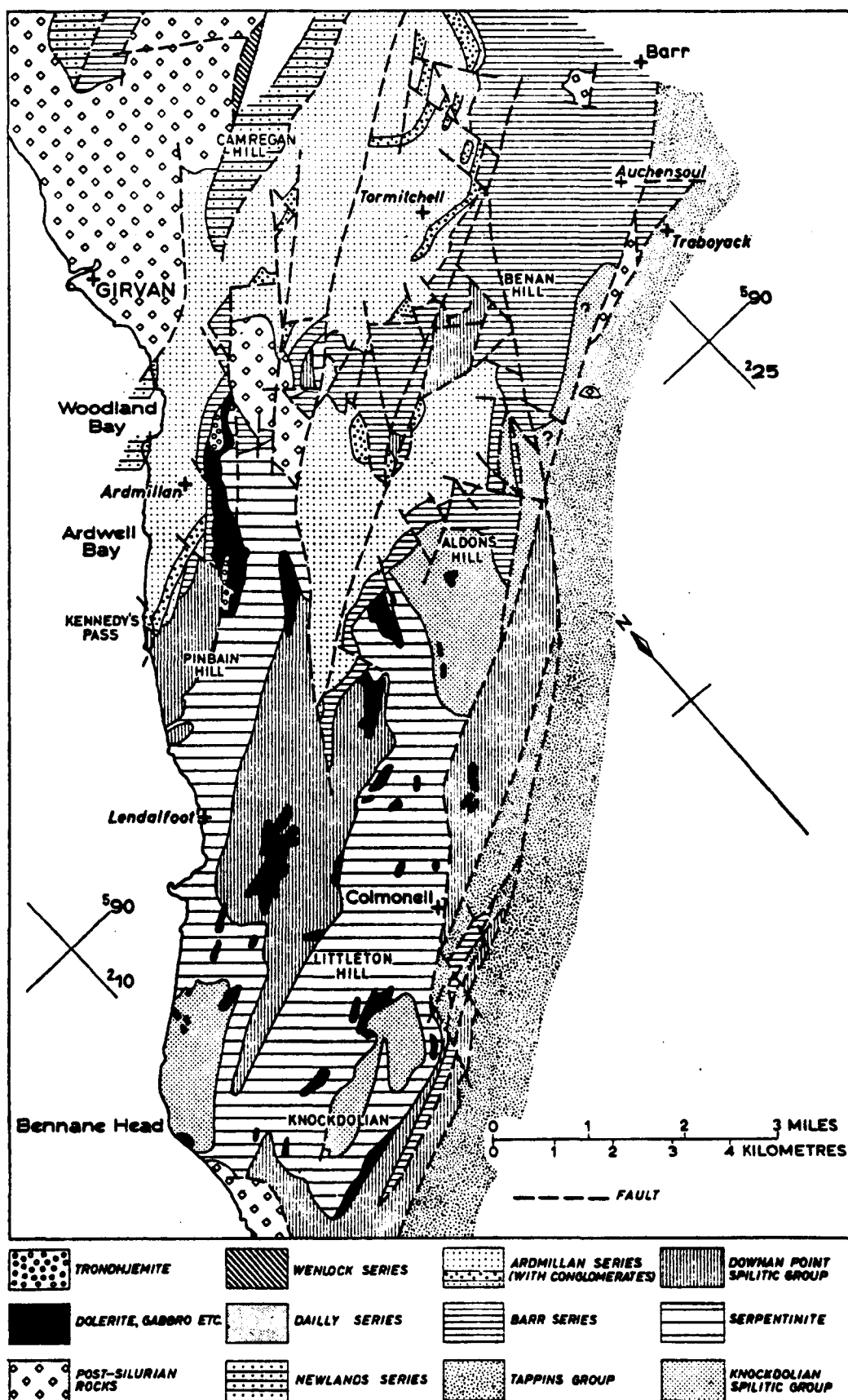


Fig. 2-5a *Geological map of the Girvan area* (from Greig, 1971)

(Based on work of the Institute of Geological Sciences, Bailey and McCallien 1957 and Williams 1962)

the geology of the area, based on the work of the Institute of Geological Sciences (IGS), Bailey & McCallien (1957) and Williams (1962). In Fig. 2.5b, positions of hammer lines are indicated. The area of study extends for approximately 1.5 km from Port Cardloch in the north to Ardwell Bay in the south.

Along the shore, the alternating ribs of vertical beds of hard greywacke and more-easily eroded shale are well exposed. This rhythmic pattern is attributed to alternation of periods of turbidity current-flow with periods of quiescence when sand accumulates. It is generally observable that thick beds of shale (red and greyish) are predominant in the northern part of the shore while outcrops along Ardwell Bay (South) are composed predominantly of greywacke. In the central part, alternations of thin beds of greywacke and shale are well defined. Sole markings on the beds indicate they were transported from the northeast (Lawson & Lawson, 1976).

The Lower Palaeozoic rocks along the Girvan coast are structurally complex. It is evident that the rocks have been subjected to various tectonic activities in the past. The beds are subvertical and shifted in places by minor wrench faults. Most of the exposures are under water for several hours either side of the tide level. Access is, however, gained to considerable length of rocks at low tide, and the rocks are obviously saturated except for larger cracks.

Results from previous seismic work in the Southern Uplands lack data on surface distribution of velocities. Some hammer refraction lines on exposed rocks at Girvan would therefore offer a good control on near-surface velocity distribution in the/...

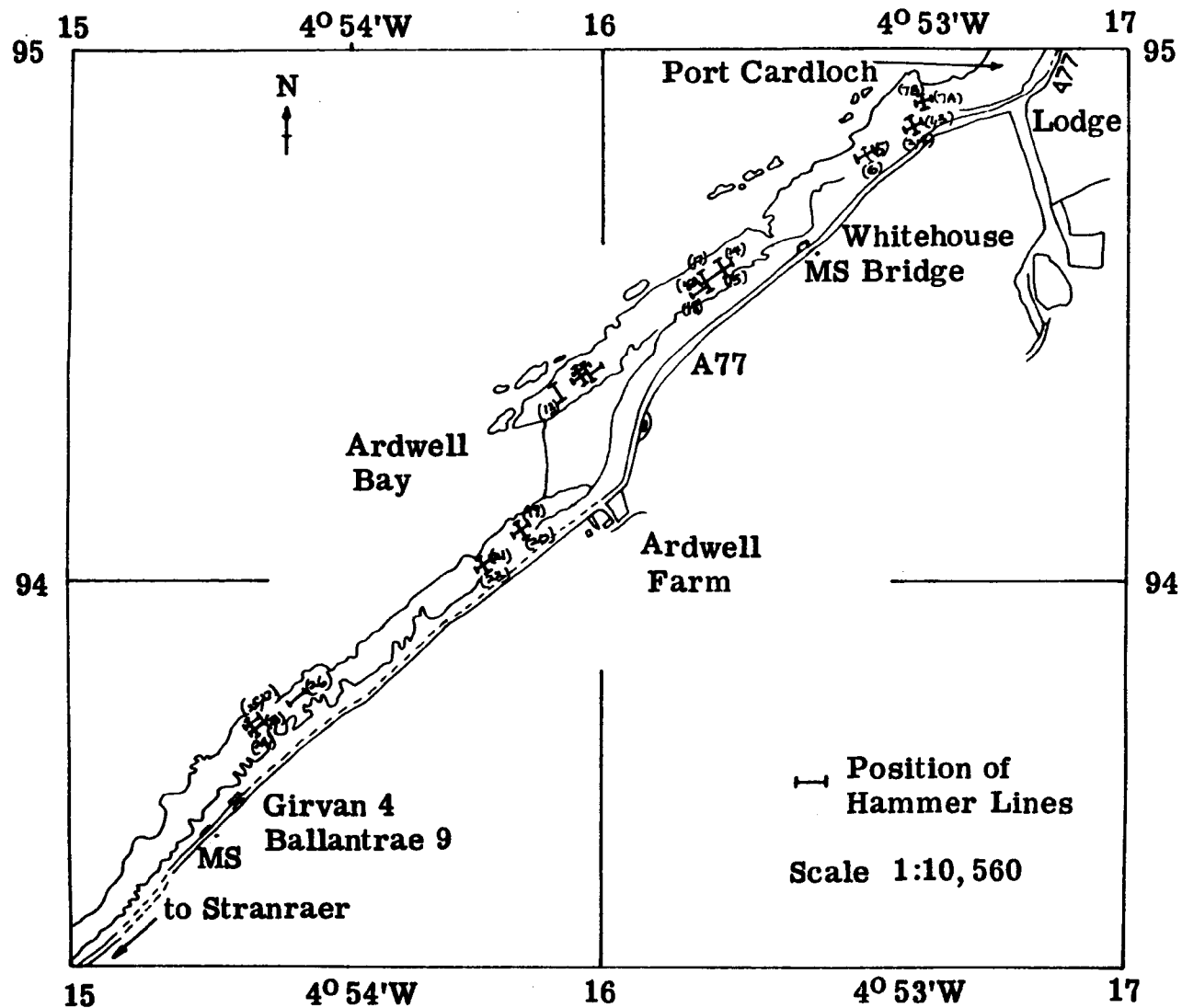


Fig. 2-5b Location of hammer lines along Whitehouse shore (Girvan).

the Lower Palaeozoic shale and greywacke and also aid in understanding both anisotropic and layering effects on velocities.

The hammer seismic surveys.

Velocities have been measured on individual beds of shale and greywacke and also where the two rocks form an alternating sequence.

The Bison Model 1550, a single-channel signal enhancement seismograph, provided the means of measuring travel times of seismic waves through the rocks, from the sledge hammer to the geophone. Field layout of the instruments is shown in Fig 2.6.

The geophone was planted on solid rock with a flat, circular metal base. Sometimes the metal base was replaced with a spike for good coupling to rock. On such occasion, the geophone was tilted (about 10° from vertical) away from the direction of wave-generated source (the hammer) to optimise the P-wave arrival (Hall, 1971). As localities were quite close to the sea (in the west) and bounded in the east by the busy trunk road A77 (to Stranraer), seismic signals were often immersed in a background of noise. Several hammer impacts at the same point, especially at distances beyond 10m, were required to enhance the Signal/Noise ratio.

Hammer impacts were spaced at approximately 2m intervals over/...

over a range of 30m for lines along geological strike. This range was, in some cases, reduced to, as low as 14m, for lines normal to bedding. Orientation of the lines normal to one another was to investigate the effect of anisotropy on the surface velocity of the rocks.



Fig.2.6 Hammer seismic instrument layout

Most of the lines were reversed, thus providing a check on the precision or repeatability of arrival times. Using 50ms. sweep time, first arrivals could be picked to within 0.1ms. The rocks in the area of hammer surveys are low-lying, thus distortions in velocity determination were not expected from topographic variations.

Field apparatus

An electromagnetic geophone was in direct contact with the earth; it converts the motion of the earth which results from hammer shots into electric signals. The latter constitute the input into the instrumental system (Fig. 2.6). The geophone consists of a coil and a magnet; one of these elements is fixed (in this case the magnet) rigidly to the case of the geophone which moves with the earth in response to the seismic source. Relative motion between the two elements produces an/...

an e.m.f. The voltage of this e.m.f. is proportional to the velocity of the motion.

The Bison model 1550 signal enhancement seismograph provided a means of amplifying, displaying, and enhancing the seismic ground motion picked up by the geophone from the remote hammer impacts. The hammer, which in this case is the seismic source, incorporates a switch which triggers a timer when the hammer strikes. Closure of the switch starts a recording process in which the geophone response to earth motion is amplified, digitized, stored and continually displayed on the oscilloscope. To pick the first-arriving signal in the wave train, a marker pulse is moved to coincide with the very first part of the seismic signal. The time corresponding to the marker location, as displayed digitally, represents the interval between hammer impacts and geophone position.

3.1 Introduction

Laboratory measurement of seismic velocities in Lower Palaeozoic shales and greywackes of the Southern Uplands is needed to explain both the directional and depth variations of velocity observed at EKA. Velocities were measured in cores of shale and greywacke from about 200 bars to 5kbar at Edinburgh and East Anglia. Lack of velocity data below 200 bar pressure was offset by low-pressure (0-200 bars) measurements made in Glasgow. Changes in velocities with pressure (and therefore with depth) are illustrated in the various velocity-pressure curves for the cores that were successfully run (e.g. Fig. 3-1).

Despite the vast abundance of shales in sedimentary basins such as the Southern Uplands, there have been very few laboratory measurements of velocities in these rocks. This is probably due to the extreme difficulty in obtaining cohesive samples. Many samples of the highly fragile shales yielded incomplete sets of data. In fact, friability actually prevented running most shale cores more than once, as they were often cracked beyond recovery at the end of each pressure run.

Data and results from all measurements are presented in the following sections.

3.2/

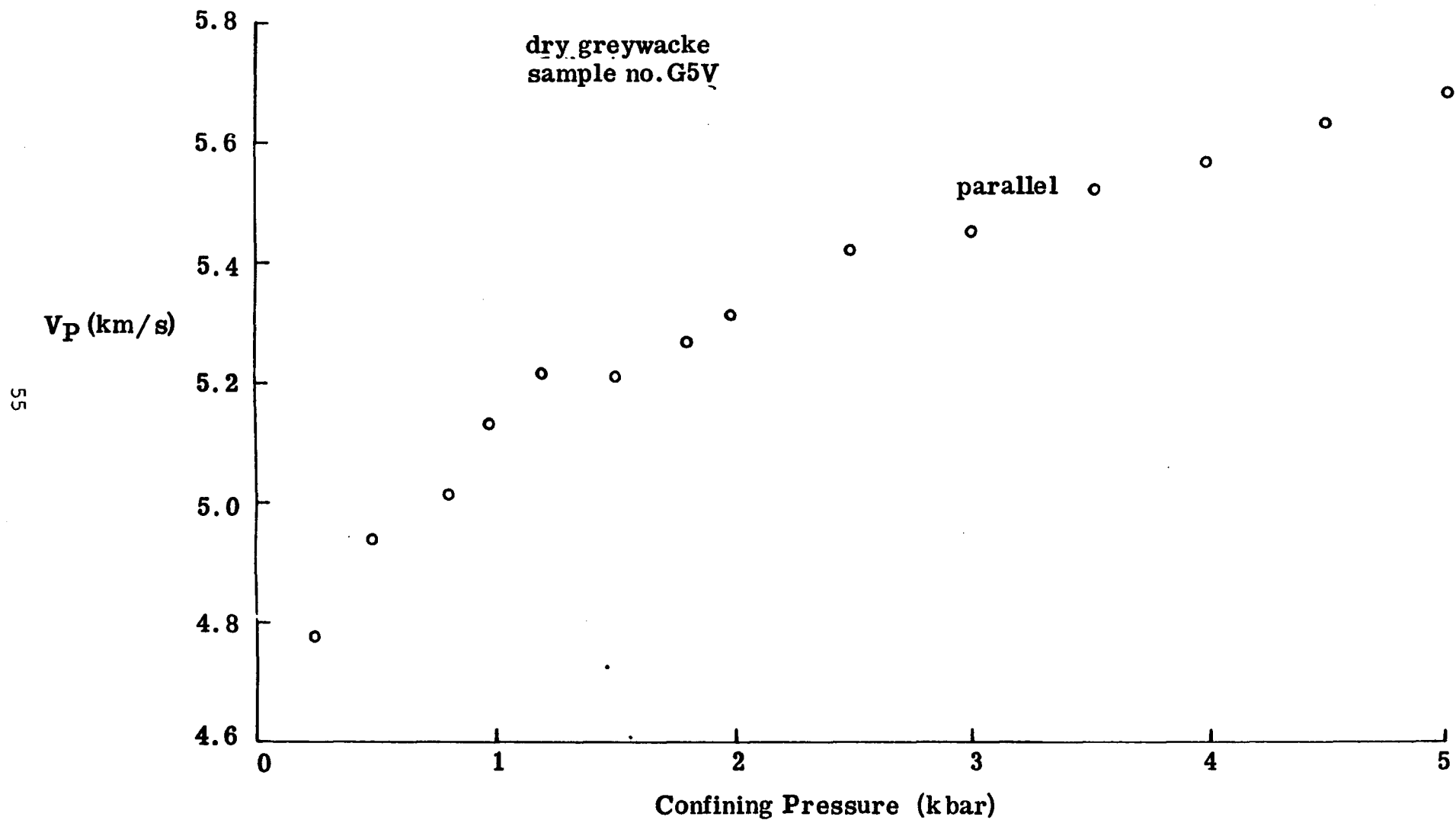


Fig. 3-1 P-wave velocity variation with pressure in a sample of greywacke.

3.2 Laboratory P-wave velocity

Results from laboratory measurement of P-wave velocity are presented in Table 3-1 for confining pressures to 5.0kbar.

Fig 3-1 illustrates a typical velocity-pressure relationship. V_p in the greywacke is observed to increase at about 0.3-0.4 km/s per kbar for the first 1kbar, reducing to about 0.1 km/s per kbar in shale and generally less than 0.05 km/s per kbar in greywacke at about 4.0-5.0kbar pressure. Hall & Al Haddad (1979) working with Lewisian metamorphic rocks, observed the rate of increase of V_p with pressure for closed-crack rocks tends to lie in the range 0.01-0.03 km/s per kbar. A rapid initial rate of increase of V_p with depth has been inferred at EKA (El Isa, 1977). This phenomenon has always been attributed (Adams & Williamson, 1923) to the closure of cracks under confining pressure (in laboratory experiments) or overburden pressure (in situ). It could be observed that even at high pressures (Fig. 3-1) velocity tends to increase, especially in shale. As the influence of porosity must have diminished above 1kbar pressure, the high-pressure increase of V_p , although slow, can be attributed to some intrinsic property of the solid rock such as compressibility or effect of 'round' cracks. The latter do not deform like flat cracks but decrease in volume as pressure is increased.

V_p is known to be sensitive to saturation (King, 1966; Hughes & Jones, 1950; and Nur & Simmons, 1969), thus in the present work, it is expected to increase on saturation (e.g. Fig. 3-2). However/...

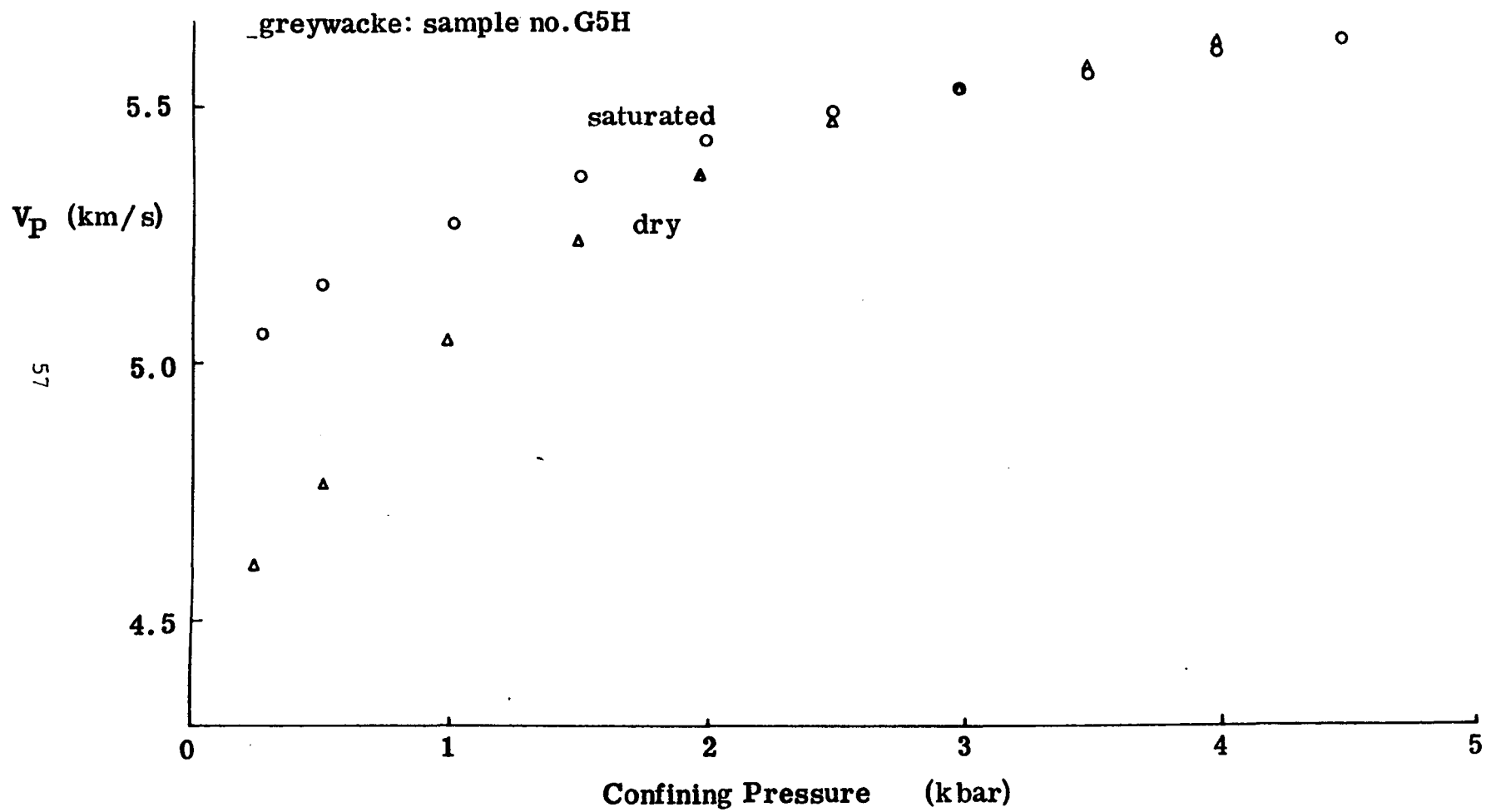


Fig. 3-2a The effect of saturation on velocity in greywackes

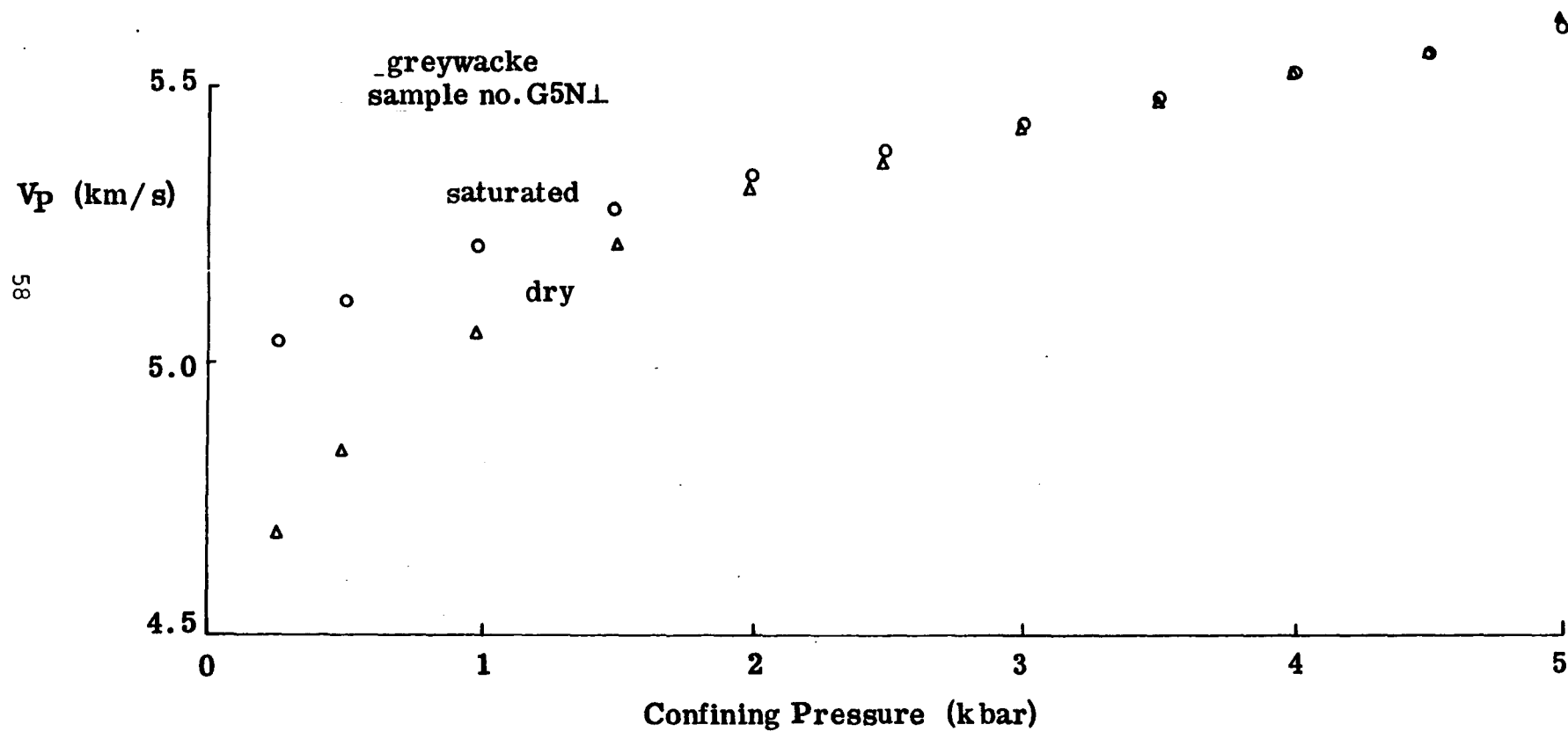


Fig. 3-2b The effect of saturation on velocity in greywackes

However Figures 3-3a and 3-3b for some samples show higher P-wave velocity in dry cores than in saturated cores. Differences are in the order of 0-5% in greywacke and up to 27% in shale. This anomalous behaviour is observed only in some Edinburgh data which are more complete than the set of data from East Anglia. It is considered that pore-pressure build-up in the cracks (Wyllie et al, 1958) may be responsible. Partial saturation in the samples is also a possible factor. Wyllie et al (1958) proposed that the presence of three phases; air, water and solid, results in large acoustic impedance differential between the different phases. This leads to reduction in the strength of wave energy being transmitted, hence low P-wave velocity is observed in the saturated rock. Toksoz et al (1976) consider that for cavities of aspect ratio, 1 or 0.1, i.e. spherical pores, P-wave velocity is higher in the dry rock than in the saturated. Partial saturation and abundance of spherical pores are further investigated in Chapter 5 where the influence of crack shape and size on velocity behaviour in the greywackes is discussed.

In virtually all the shale samples run, dry P-wave velocity is higher than saturated V_p (Table 3-1). It has been revealed from differential thermal analysis (D.T.A.) that some of the shales and greywackes from the Southern Uplands contain clay minerals such as montmorillonite which can easily acquire and lose water. Therefore the effect of clay-water interaction cannot be ignored in the cases where V_p is higher in dry samples.

In/...

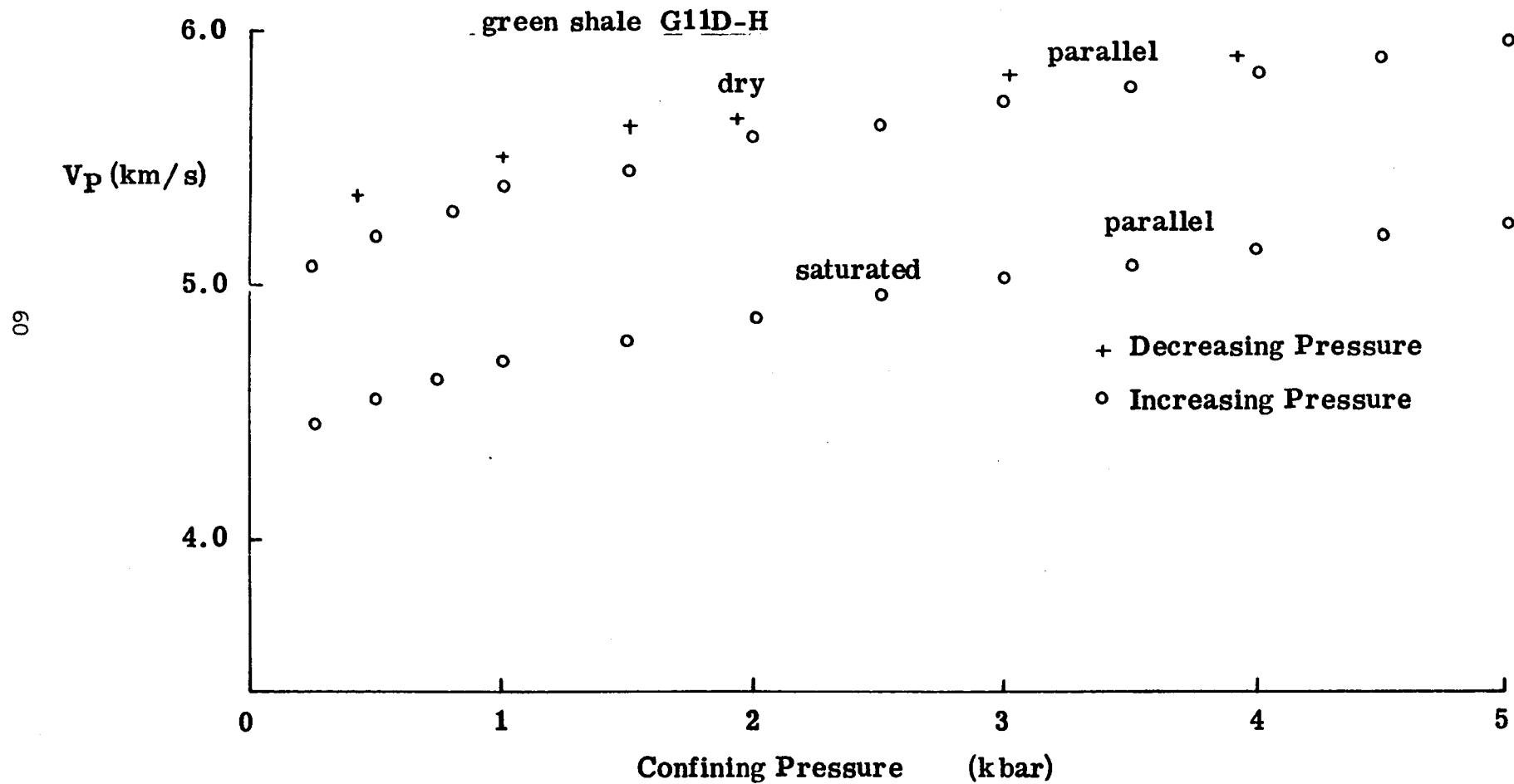


Fig. 3-3a Anomalous behaviour of V_p in saturated shale (e.g. V_p dry > V_p saturated)

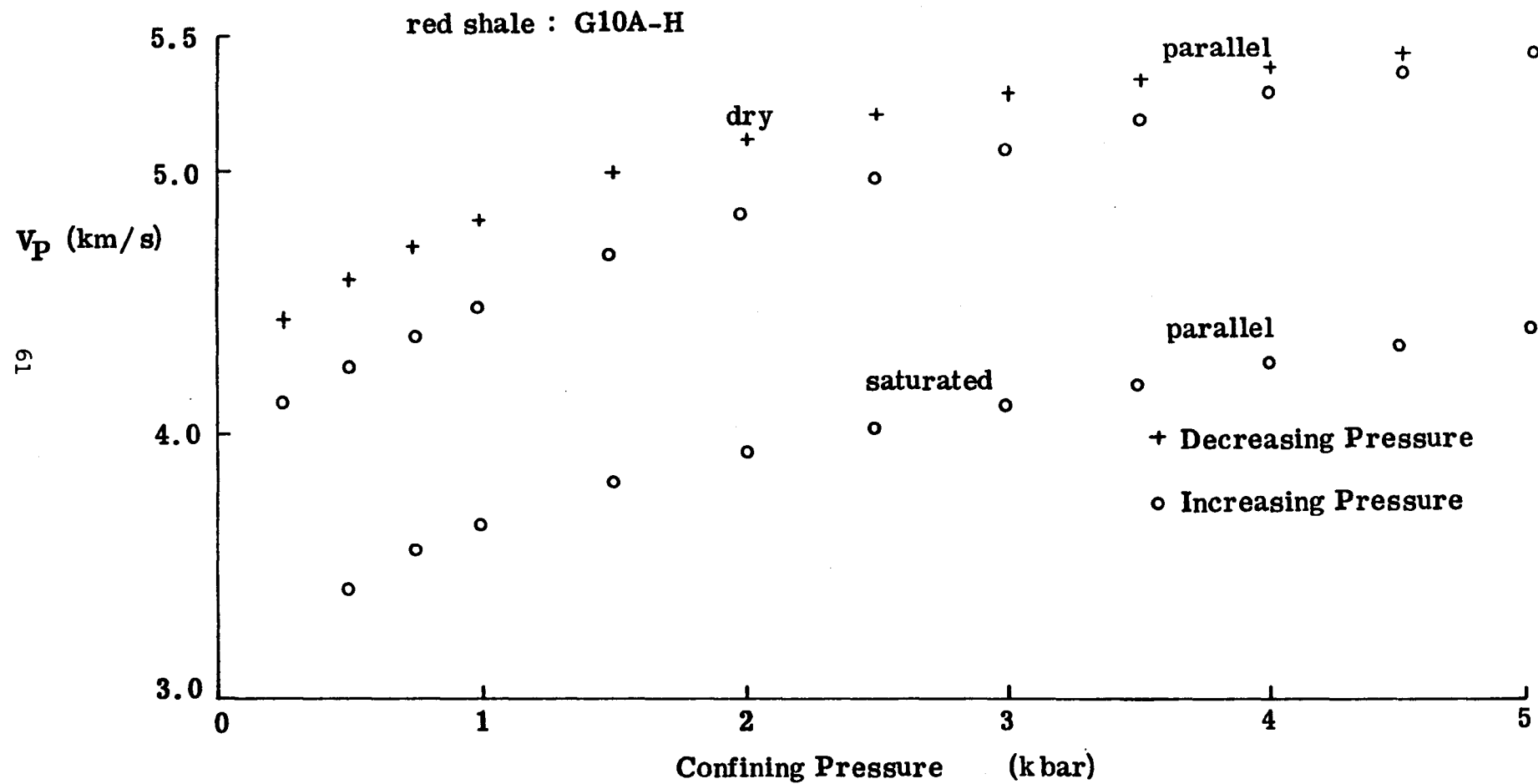


Fig. 3-3b Anomalous behaviour of V_p in saturated shale (e.g. .
 $(V_{p \text{ dry}} > V_{p \text{ saturated}})$

Table 3-1 Dry and saturated P-wave velocities in the Lower Palaeozoic rocks of the Southern Uplands.

Core No.	lithology	core orientation to bedding	density Mg/m ³	porosity %	Vp Km/s	confining pressure (kbar)						
						0.25	0.50	1.00	2.00	3.00	4.00	5.00
G4N⊥	greywacke	normal	2.689 2.683	0.6	Sat. dry	5.37 5.29	5.48 5.38	5.64 5.50	5.78 5.62	5.87 5.74	5.94 5.86	6.01 5.98
G4H	"	parallel	2.680 2.671	0.9	Sat. dry	5.42 5.30	5.57 5.45	5.77 5.65	5.95 5.84	6.04 5.95	6.11 6.06	6.16 6.15
G4V	"	"	2.689 2.684	0.5	Sat. dry	5.12 4.85	5.26 5.00	5.46 5.22	5.66 5.47	5.78 5.61	5.86 5.74	5.90 5.85
G5N⊥	"	normal	2.671 2.652	1.9	Sat. dry	5.04 4.69	5.11 4.84	5.21 5.06	5.34 5.32	5.44 5.45	5.53 5.54	5.60 5.62
G5H	"	parallel	2.665 2.653	1.2	Sat. dry	5.06 4.62	5.15 4.77	5.27 5.05	5.43 5.38	5.53 5.53	5.61 5.63	5.66 5.72
G5V	"	"	2.670 2.655	1.5	Sat. dry	5.02 4.79	5.13 4.94	5.27 5.12	5.42 5.33	5.53 5.46	5.59 5.58	5.63 5.68
G6N⊥	"	normal	2.660 2.640	2.0	Sat. dry	- 5.14	- 5.27	5.39 5.44	5.65 5.66	5.75 5.79	5.83 5.88	5.88 5.92
G6H	"	parallel	2.650 2.625	2.5	Sat. dry	5.32 5.01	5.35 5.20	5.40 5.40	5.47 5.58	5.52 5.70	5.57 5.81	5.60 5.89
G6V	"	"	2.639 2.607	3.2	Sat. dry	5.18 5.23	5.26 5.39	5.39 5.58	5.57 5.77	5.68 5.86	5.75 5.93	5.78 5.99
G7N⊥	"	normal	2.678 2.668	1.0	Sat. dry	5.18 5.04	5.25 5.17	5.37 5.33	5.54 5.50	5.66 5.61	5.73 5.71	5.76 5.77
G7H	"	parallel	2.690 2.683	0.7	Sat. dry	5.30 5.32	5.38 5.37	5.46 5.47	5.58 5.61	5.67 5.70	5.75 5.79	5.80 5.85
G7V	"	"	2.686 2.678	0.8	Sat. dry	5.28 5.13	5.34 5.22	5.41 5.34	5.52 5.48	5.61 5.57	5.68 5.65	5.74 5.72
G8N⊥	"	normal	2.750 2.741	0.9	Sat. dry	5.57 5.11	5.65 5.22	5.73 5.40	5.82 5.64	5.89 5.79	5.95 5.89	6.00 5.96
G8H	"	parallel	2.765 2.751	1.4	Sat. dry	- 5.41	- 5.51	5.93 5.67	6.00 5.87	6.06 6.00	6.11 6.07	6.13 6.11
G8V	"	"	2.760 2.752	0.8	Sat. dry	- 5.47	- 5.55	5.88 5.68	5.96 5.85	6.04 5.97	6.10 6.07	6.16 6.14
G9N⊥	"	normal	2.704 2.695	0.9	Sat. dry	5.50 5.23	5.61 5.43	5.70 5.64	5.80 5.83	5.87 5.93	5.93 5.99	5.98 6.01
G9H	"	parallel	2.706 2.692	1.4	Sat. dry	5.16 5.42	5.27 5.55	5.43 5.72	5.63 5.90	5.77 6.01	5.85 6.07	5.90 6.10
G9V	"	"	2.708 2.694	1.4	Sat. dry	- 5.38	- 5.50	5.79 5.67	5.91 5.88	6.00 6.00	6.08 6.06	6.14 6.10
G10A-H	red shale	"	2.460 2.345	11.5	Sat. dry	3.20 4.28	3.41 4.42	3.66 4.54	3.93 4.65	4.11 4.97	4.27 5.18	4.40 5.44
G11D-N⊥	green shale	normal	-	-	Sat. dry	3.84 3.70	3.99 3.90	4.12 4.23	4.19 4.60	4.43 4.84	4.62 5.00	4.89 5.10
G11D-H	"	parallel	2.650 1.588	6.2	Sat. dry	4.44 5.07	4.54 5.20	4.70 5.37	4.88 5.57	5.03 5.72	5.15 5.75	5.26 5.27
G13N⊥	red shale	normal	-	-	dry	3.30	3.55	3.91	4.35	4.60	4.73	4.90
G13V	"	parallel	-	-	dry	-	4.21	4.48	4.82	5.02	5.16	5.25
G14A-H	"	"	-	-	Sat.	3.69	3.75	3.85	4.03	4.19	4.33	4.44
G14B-N⊥	"	normal	2.540	7.7	Sat.	3.28	3.34	3.43	3.59	3.74	3.88	4.01
G14C-N⊥	"	"	-	-	Sat.	2.69	2.87	3.11	3.40	3.58	3.73	3.85

Note: "G" denotes all samples are from Girvan. The symbols N(⊥) indicates core is normal to bedding, and H & V indicate cores are parallel to bedding.

The above Table shows velocities measured at Edinburgh.

In Fig. 3-4, velocity hysteresis is quite observable suggesting that velocity measured at a given pressure is a function of the path followed to reach the pressure (Stewart & Peselnick, 1977). In the dry greywacke sample illustrated in Fig. 3-4, the difference between P-wave velocity for increasing pressure cycle and that for decreasing pressures is about 3%. A similar amount of hysteresis in shale is illustrated in Figures 3-5, 3-6, & 3-7. For most saturated samples, hysteresis is not apparent (Figures 3-8 & 3-9). Where it occurs in a saturated sample, V_p along increasing pressure-run is often higher than V_p along decreasing cycle of pressure (Fig. 3-10). It is suspected that the relatively lower V_p observed when pressure is being decreased is a result of the failure of the cracks to get re-saturated. This is rather speculative as the mechanism of hysteresis in rocks still needs further investigation.

The restricted number of shale specimens precludes elaborate presentation of results on velocity behaviour in the shales of the Southern Uplands. However, for saturated red shales, P-wave velocity anisotropy ranges from 17% at low pressures (0-200 bars) to 10% at pressures above 1.5kbar. Anisotropy in the greywackes decreases with saturation - for instance, in samples nos. G7 and G9, velocity anisotropy is approximately 3% at 5.0kbar. For sample no. G4, anisotropy in the saturated rock is about 5-6% at low pressure and 8% when the same rock is dry. These values reduce to 4% and 6% respectively at 5.0kbar pressure.

The/...

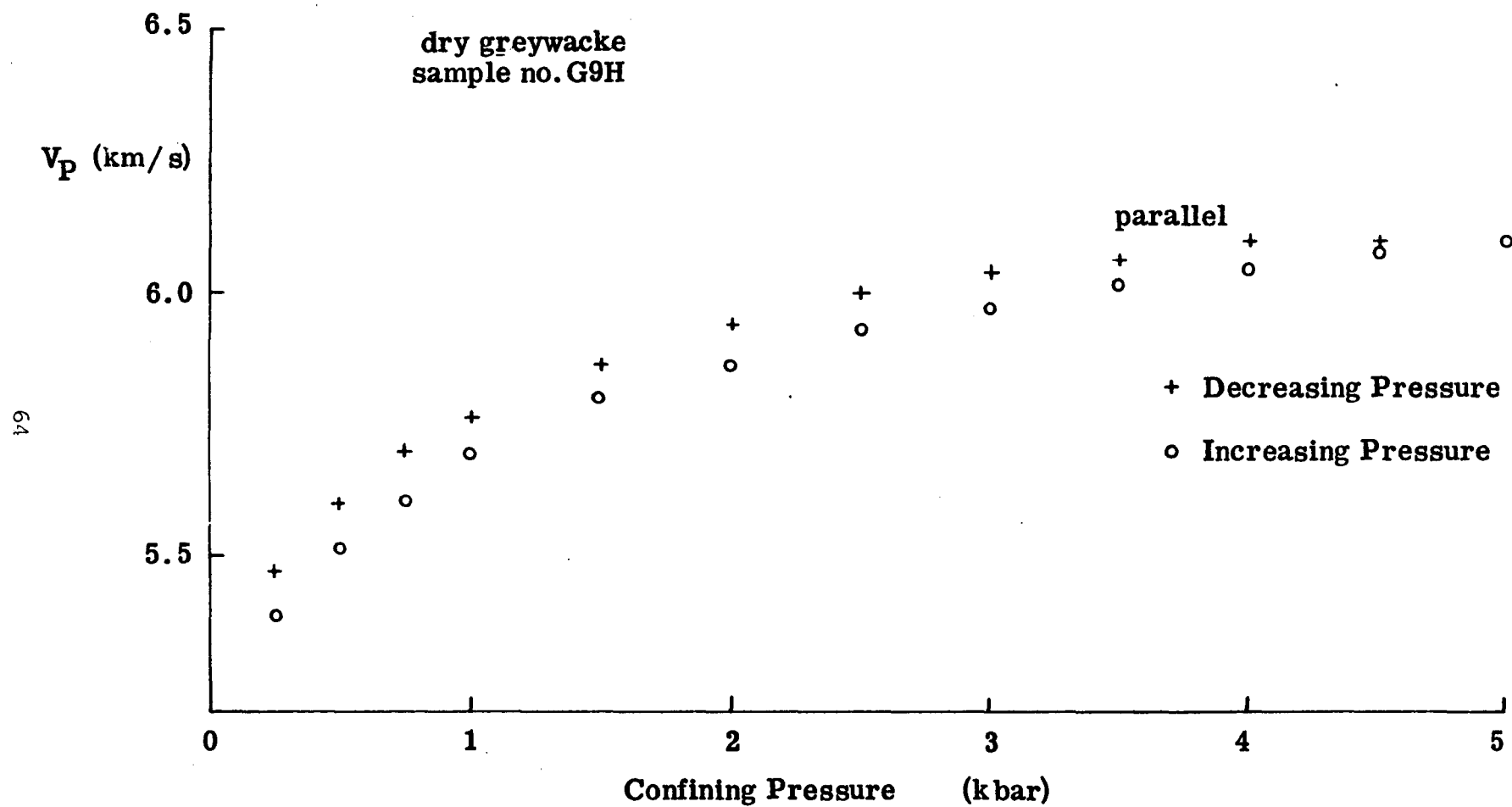


Fig. 3-4 P-wave velocity hysteresis in dry greywacke

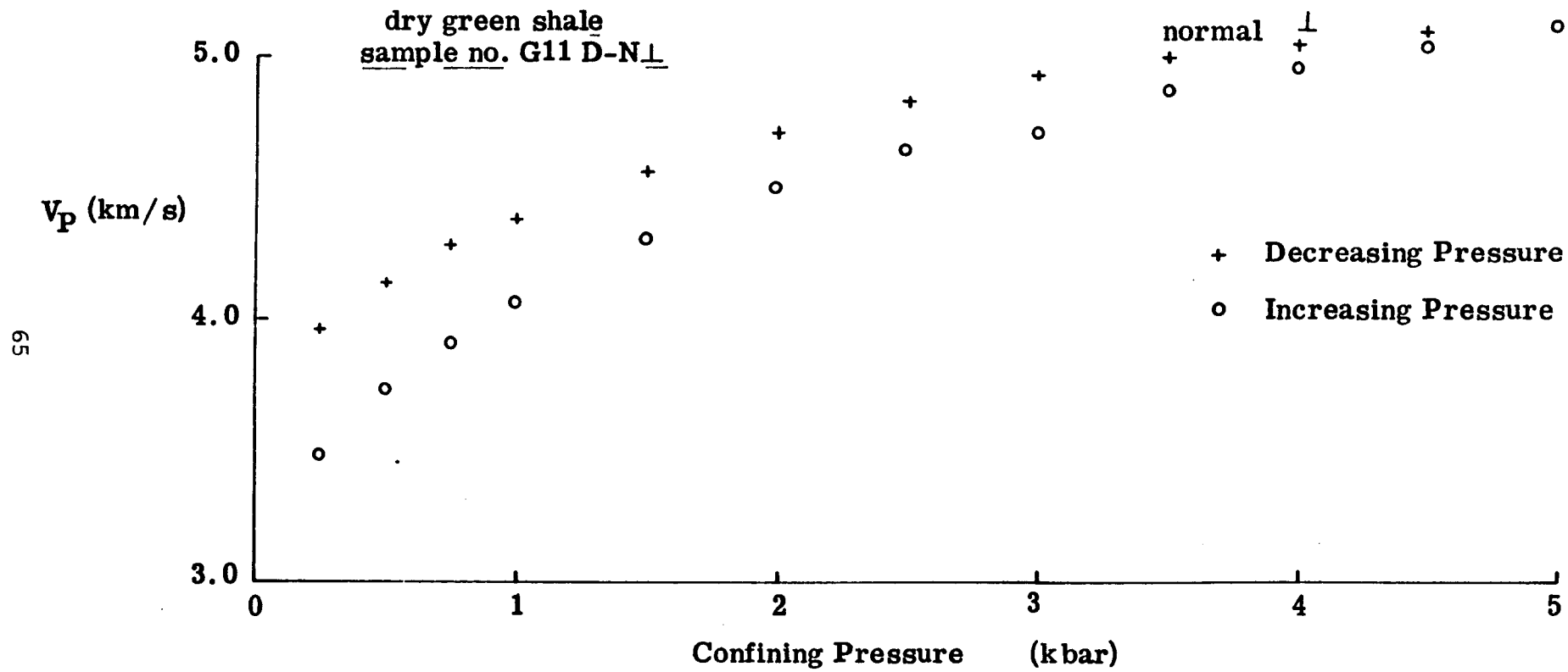


Fig. 3-5 P-wave velocity hysteresis in dry shale .

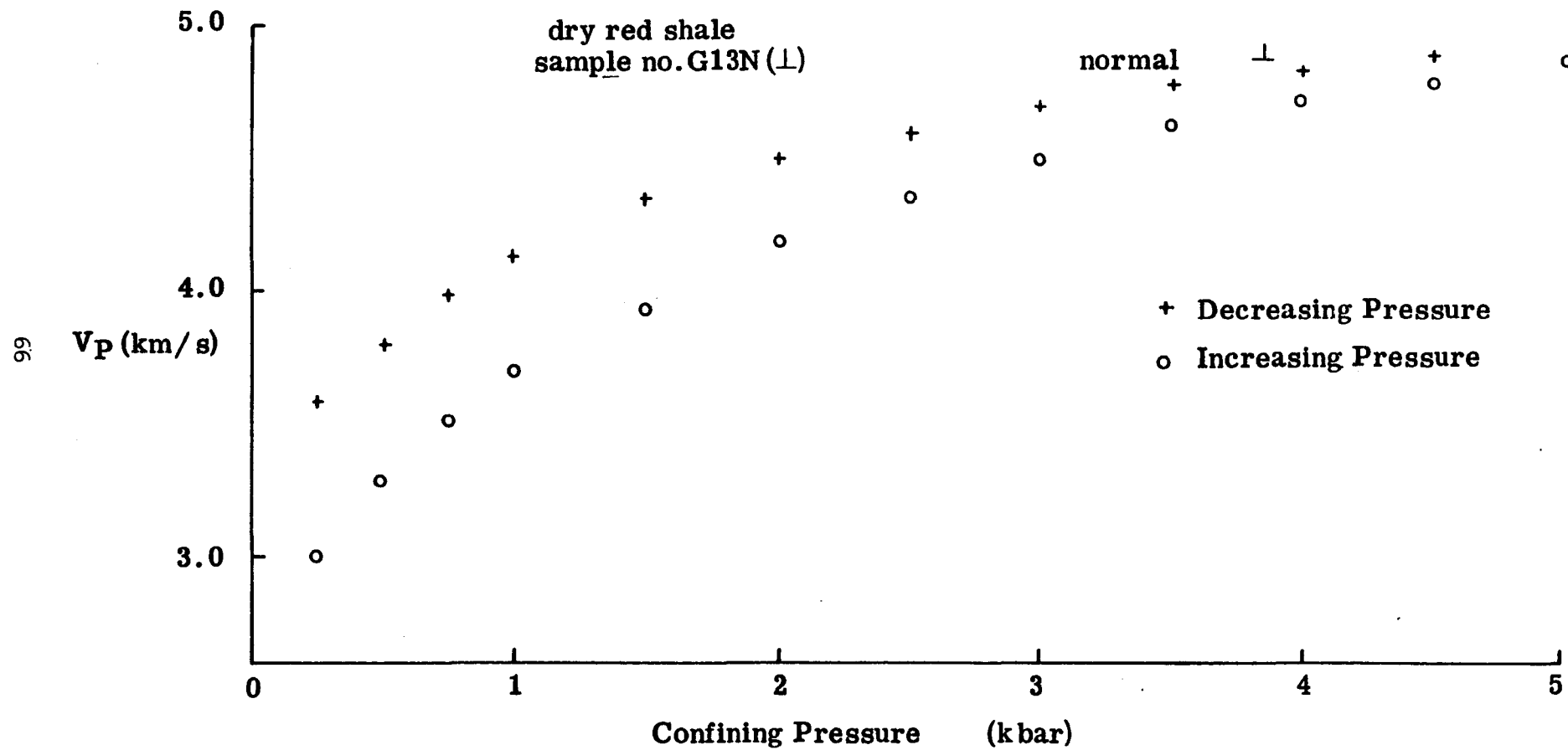


Fig. 3-6 P-wave velocity hysteresis in dry shale .

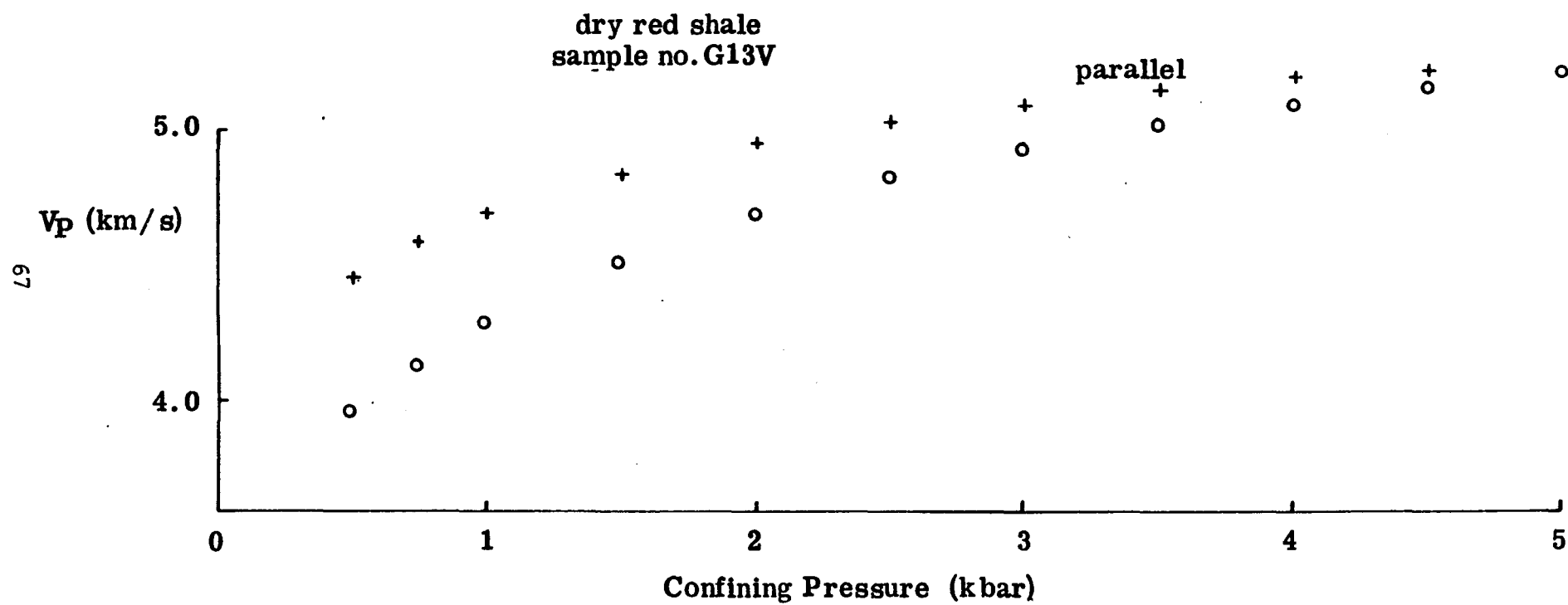


Fig. 3-7 P-wave velocity hysteresis in dry shale .

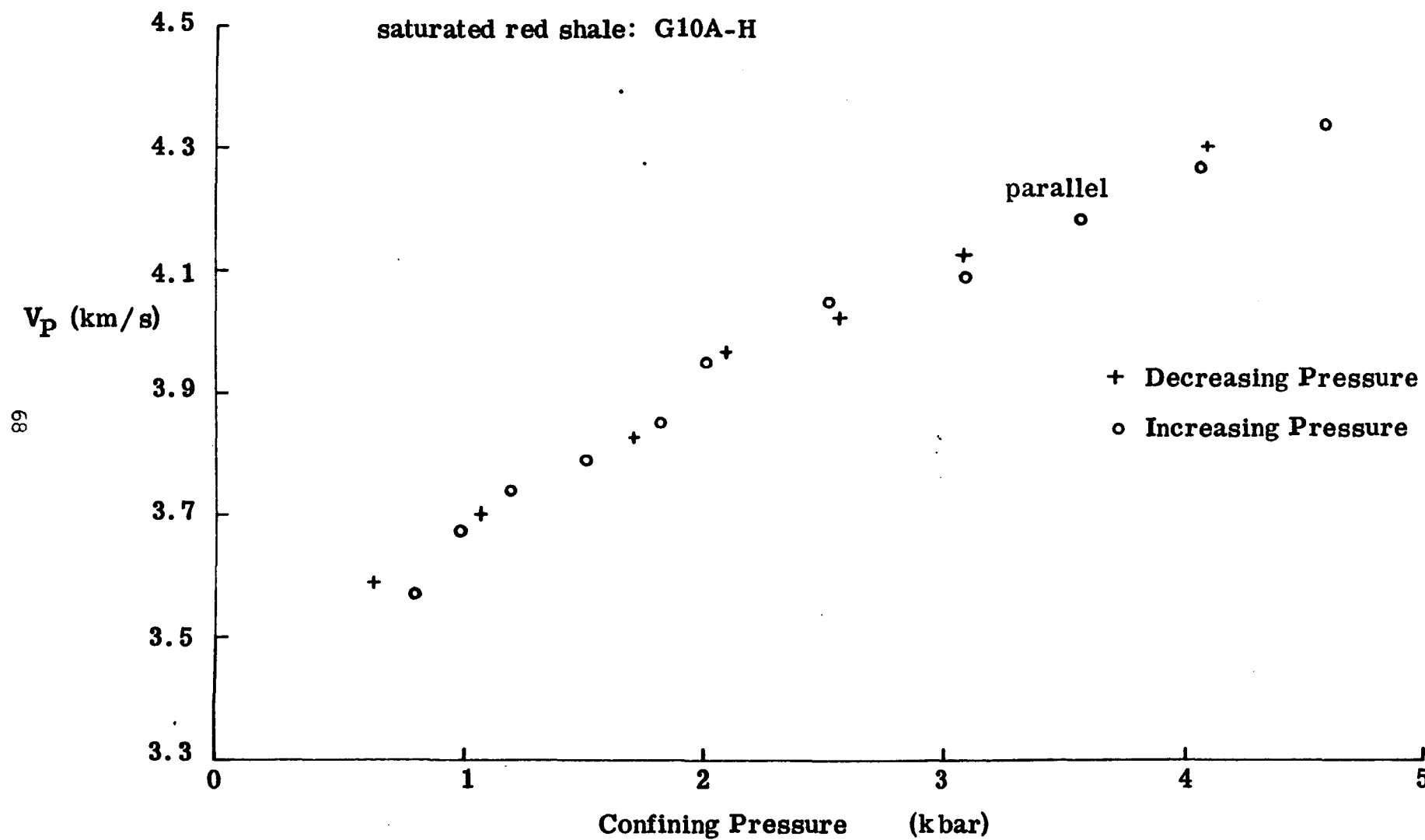


Fig. 3-8 Lack of hysteresis in saturated shale .

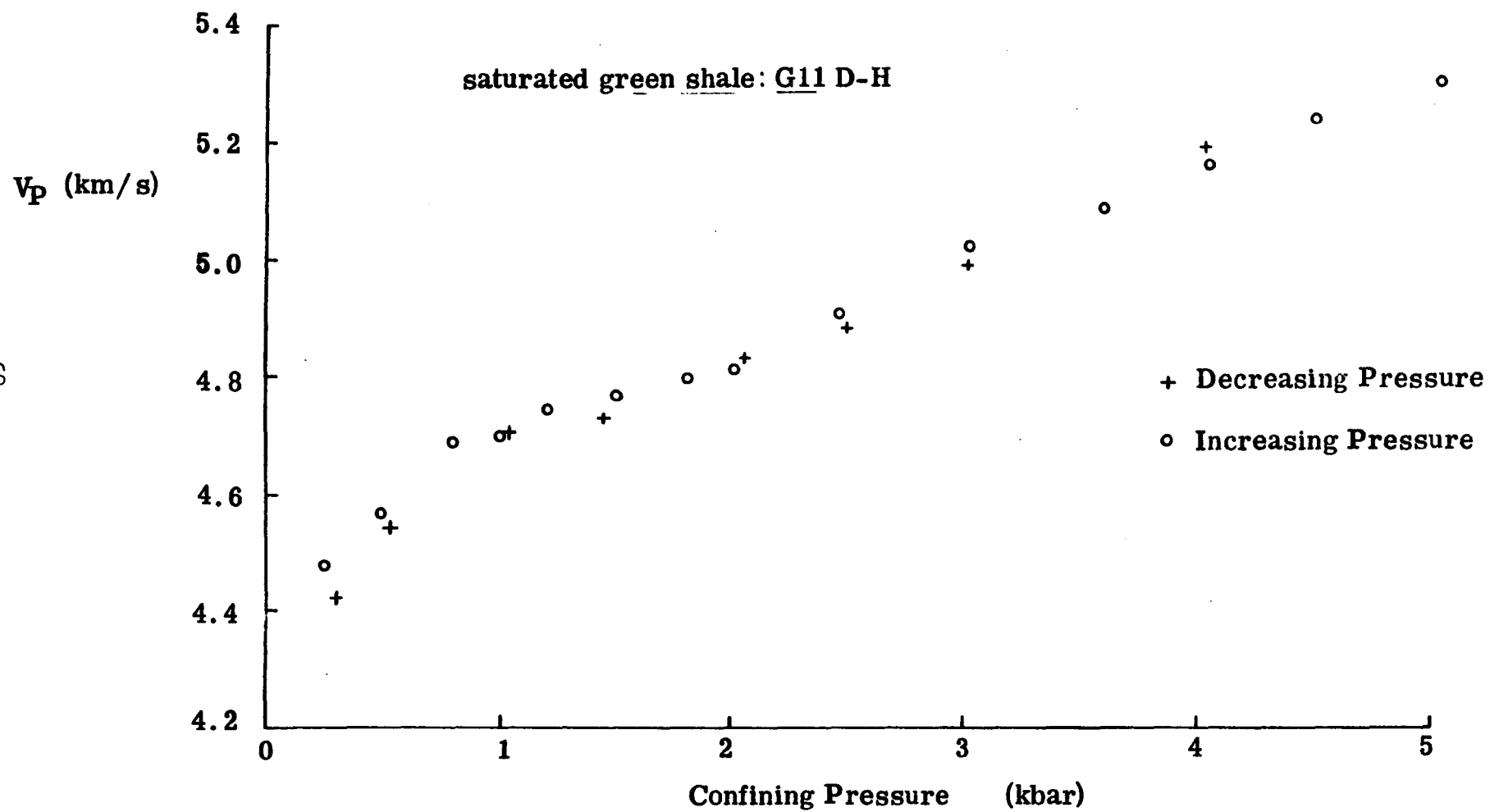


Fig. 3-9a Lack of hysteresis in saturated shale .

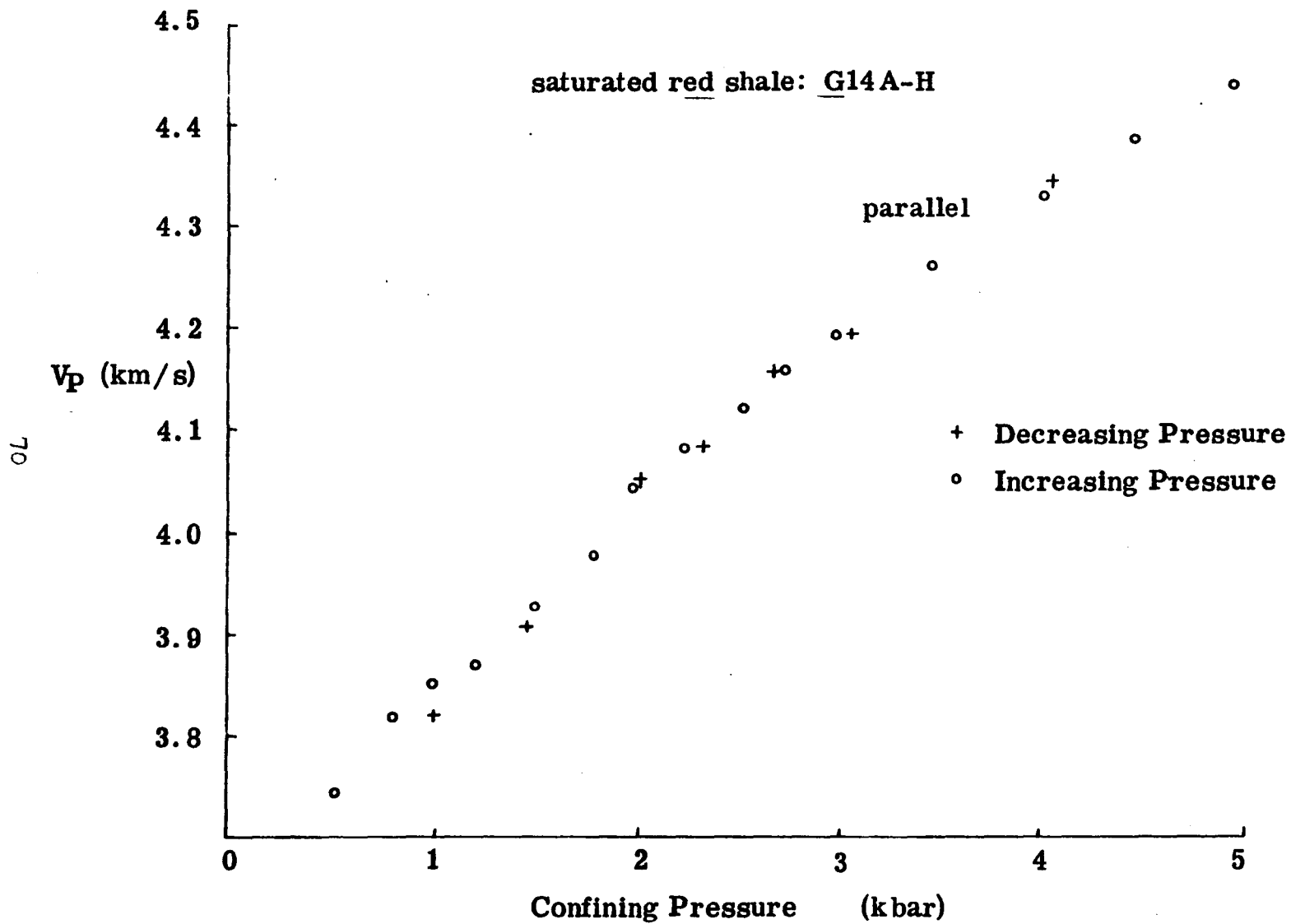


Fig. 3-9b Lack of hysteresis in saturated shale .

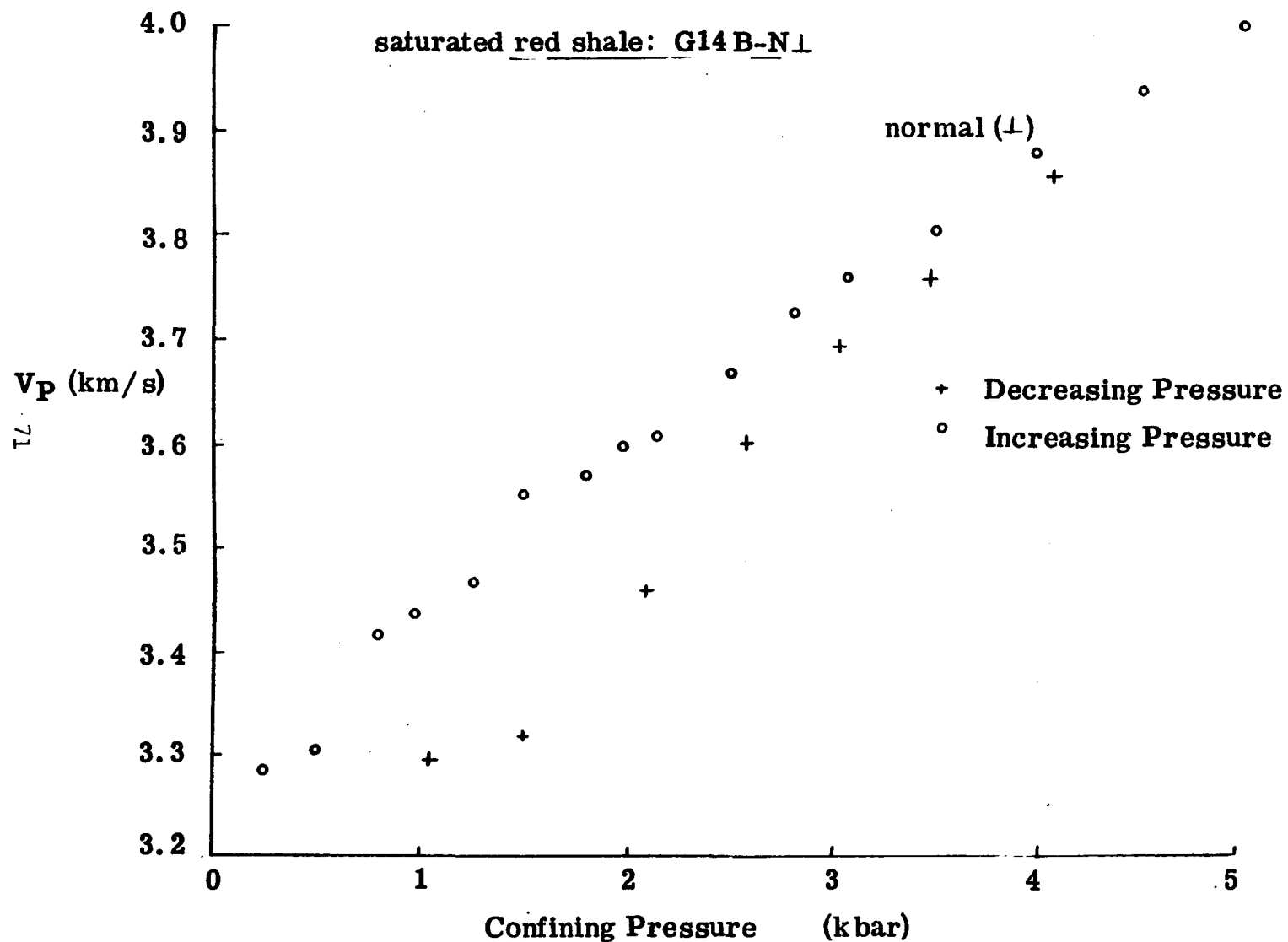


Fig. 3.10 Saturated shale showing anomalous hysteresis effect
(V_p with increasing pressure > V_p with decreasing pressure)

The strong anisotropy in shale samples is considered to be related to the mineral fabric. This laboratory-observed velocity anisotropy in shale is complemented by a similar amount of anisotropy from hammer line refraction surveys (see Section 3.5) where V_p normal to bedding is less than V_p parallel to bedding. Anisotropy in the greywackes in situ is stronger than in the laboratory samples. This could be related to the size of the latter which may not be representative of the rock in place.

Changes in velocities in the Southern Uplands rocks with pressure (and hence with depth) are summarised in a later section.

Initially in the present work, only seven shear-wave runs were successfully carried out at Edinburgh, i.e. 4 saturated runs on cores nos. G5N , H & V, and G6V; and 3 dry runs on G5N , H & V. As it became necessary at a late stage of the present work to obtain more S-wave velocity data, some of the greywacke cores were run also for P-wave velocity at East Anglia. The new values of V_p were found to be higher than the previous values obtained at Edinburgh. Differences up to 0.4-0.6 km/s are common; the author was therefore compelled to run fresh samples of greywacke (G4') at Edinburgh. Each core of greywacke was taken through four cycles of up and down pressure runs so as to investigate the effect of re-cycling the rocks. Results are presented in Table 3-2. There was no systematic rise in P-wave velocity from first to fourth cycles. Differences are generally less/...

less than 0.1 km/s. This suggested that the higher P-wave velocities obtained from East Anglia were not due to the effect of recycling. Since the recycling experiments at Edinburgh were made with new transducers, freshly calibrated, and the data repeated earlier Edinburgh runs, it is suspected that the East Anglia transducer delay corrections used in these latest UEA measurements may be wrong. East Anglia velocity data were therefore adjusted in proportion to their differences from Edinburgh data.

From a sample of Spango granodiorite, three orthogonal cores were obtained and run at Edinburgh. The orientations of cores X, Y, and Z (Table 3-2) are rather arbitrary as there is no obvious preferred orientation of minerals in hand specimen. Results from the velocity runs suggest that the rock is isotropic. The experiment was carried out to demonstrate the possibility of the existence of igneous rocks in some areas where refraction work has been done in the Southern Uplands (e.g. LISPB, & Southern Uplands Profile, 1981) and which tend to show higher P-wave velocity than has been observed from laboratory measurement in the Lower Palaeozoic greywackes.

3.3 Laboratory Vs results

In Fig. 3-11, the behaviour of shear-wave velocity in a sample of greywacke is illustrated. In Table 3-3 the shear-wave velocities for both dry and saturated greywackes are shown.

Like/...

Table 3.2 P-wave velocity in 'unstressed' dry greywacke.

Confining Pressure (bars)											
cycle	250	500	1000	1500	2000	2500	3000	3500	4000	4500	5000
<u>Sample G4N1</u>											
1st	5.311	5.342	5.441	5.505	5.552	5.606	5.637	5.652	5.669	5.699	5.716
2nd	5.311	5.371	5.442	5.522	5.577	5.613	5.651	5.683	5.690	5.693	5.734
3rd	5.290	5.350	5.493	5.545	5.588	5.612	5.625	5.646	5.671	5.692	5.692
4th	5.300	5.343	5.486	5.526	5.600	5.625	5.638	5.670	5.689	5.700	5.705
<u>Sample G4H</u>											
1st	5.083	5.188	5.401	5.483	5.519	5.564	5.588	5.633	5.652	5.662	5.679
2nd	5.091	5.202	5.400	5.463	5.537	5.572	5.608	5.634	5.674	5.690	5.702
3rd	-	5.117	5.301	5.425	5.487	5.569	5.612	5.640	5.661	5.669	5.703
4th	-	5.160	5.293	5.408	5.471	5.549	5.591	5.619	5.654	5.678	5.682
<u>Sample G4V</u>											
1st	5.055	5.203	5.346	5.440	5.478	5.518	5.555	5.570	5.593	5.619	5.629
2nd	5.029	5.195	5.347	5.456	5.525	5.569	5.588	5.593	5.621	5.635	5.650
3rd	5.041	5.180	5.329	5.430	5.527	5.590	5.601	5.623	5.634	5.657	5.657
4th	5.096	5.214	5.378	5.464	5.528	5.591	5.604	5.652	5.664	5.673	5.670
* ΔV_p											
km/s	.041	.011	.032	.024	.050	0.073	0.049	0.082	0.071	0.054	0.041
<u>GRANODIORITE SAMPLE SOL 1</u>											
X	5.679	5.825	5.883	5.958	5.980	5.971	5.987	6.016	6.024	6.036	6.031
Y	5.621	5.794	5.894	5.948	5.959	5.972	5.989	6.005	6.032	6.047	6.048
Z \perp	5.655	5.768	5.873	5.875	5.892	5.929	5.930	5.950	5.948	5.954	5.972
<u>LAVA SAMPLE SOL 2Y</u>											
"Parallel"	5.319	5.423	5.486	5.520	5.547	5.569	5.597	5.625	5.646	5.668	5.683

* ΔV_p = difference between velocities of the 1st and 4th cycles in G4'V.

"Orientation of cores from the sample of granodiorite is with reference to joint direction as observed in-situ. X & Y are parallel to the joint direction while Z is normal to it. There is no obvious preferred orientation of constituent minerals.

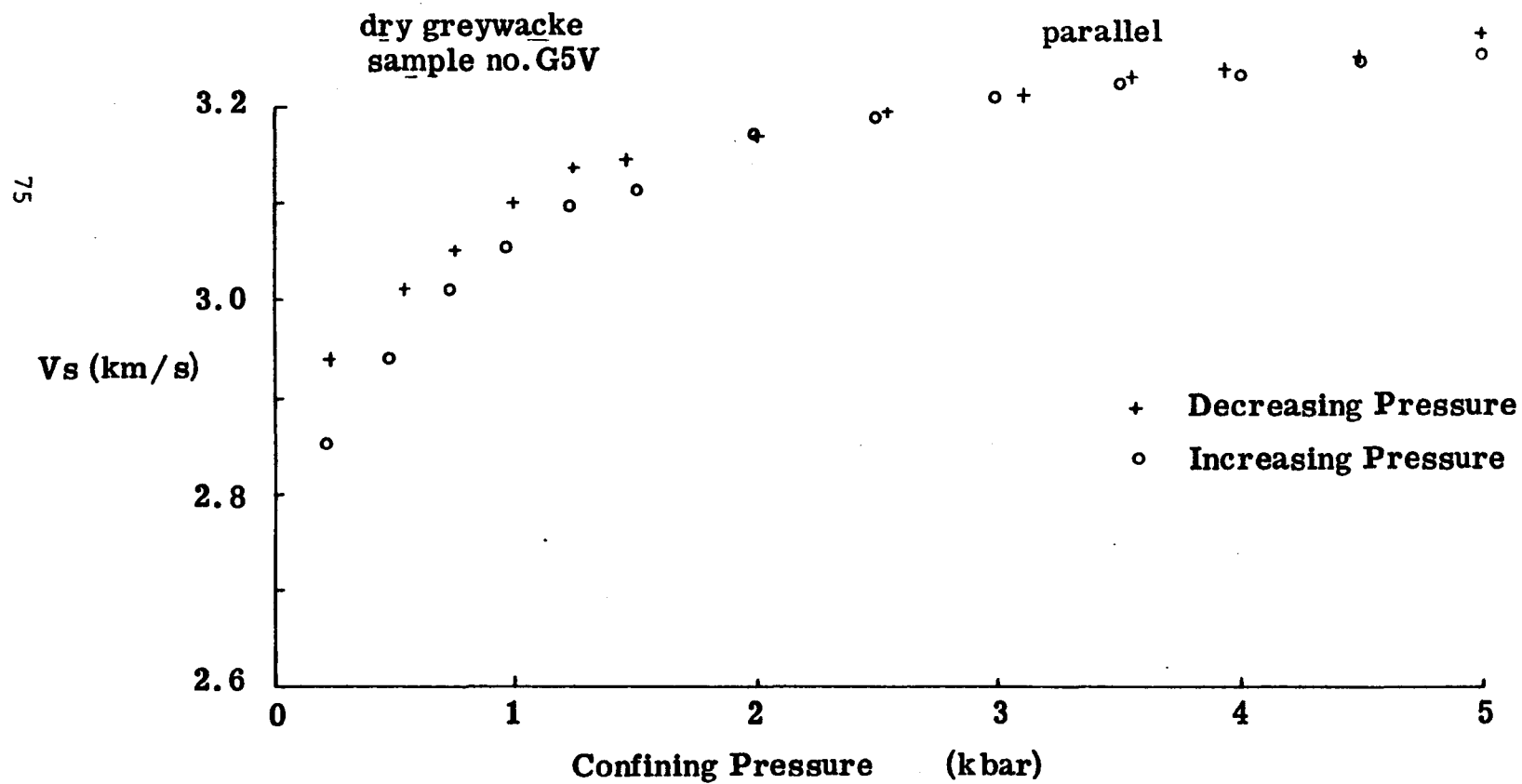


Fig. 3-11a S-wave velocity variation with pressure in the greywackes.

Table 3-3 : SHEAR WAVE VELOCITIES IN DRY AND SATURATED GREYWACKE

EDINBURGH

Core No.	Core Orientation	250	500	1000	1500	2000	2500	3000	3500	4000	4500	5000
G5N ^L	Sat	2.90	2.94	2.99	3.02	3.05	3.07	3.08	3.10	3.12	3.14	3.15
	Dry	2.97	3.04	3.15	3.21	3.25	3.27	3.30	3.32	3.34	3.36	3.37
G5H	Sat	2.89	2.94	3.01	3.05	3.09	3.12	3.14	3.16	3.18	3.20	3.22
	Dry	3.03	3.10	3.19	3.25	3.30	3.32	3.35	3.37	3.39	3.40	3.41
G5V	Sat	2.56	2.71	2.87	2.92	2.95	2.99	3.01	3.03	3.05	3.07	3.09
	Dry	2.90	3.02	3.08	3.14	3.18	3.19	3.21	3.23	3.24	3.25	3.27
G6V	Sat	3.04	3.08	3.15	3.19	3.21	3.24	3.26	3.28	3.30	3.32	3.34
<u>EAST ANGLIA</u>												
Core No.												
G4N ^L	Sat	3.02	3.09	3.18	3.24	3.29	3.32	3.35	3.37	3.39	3.41	
	Dry	3.00	3.04	3.15	3.21	3.26	3.30	3.33	3.35	3.37	3.38	
G4H	Sat	3.17	3.32	3.46	3.54	3.58	3.62	3.64	3.65	3.67	3.68	
	Dry	3.10	3.23	3.36	3.44	3.50	3.54	3.56	3.59	3.61	3.63	
G4V	Sat	3.15	3.26	3.38	3.44	3.48	3.50	3.52	3.54	3.55	3.56	
	Dry	3.02	3.15	3.28	3.37	3.42	3.46	3.48	3.49	3.50	3.50	
G6N ^L	Sat	2.91	2.97	3.04	3.10	3.14	3.18	3.22	3.25	3.28	3.31	
	Dry	2.94	3.02	3.10	3.16	3.19	3.21	3.23	3.24	3.25	3.26	
G6H	Sat	2.82	3.00	3.17	3.26	3.32	3.35	3.36	3.38	3.38	3.39	
	Dry	2.82	3.00	3.17	3.26	3.32	3.35	3.36	3.38	3.38	3.39	
G6V	Sat	2.95	3.04	3.14	3.18	3.22	3.25	3.28	3.31	3.33	3.36	
	Dry	3.00	3.10	3.26	3.36	3.44	3.51	3.57	3.62	3.66	3.69	
G8N ^L	Sat	3.11	3.15	3.20	3.23	3.24	3.27	3.28	3.30	3.30	3.31	
G8H	Sat	3.10	3.14	3.18	3.21	3.23	3.26	3.27	3.29	3.30	3.31	
G8V	Sat	3.17	3.21	3.25	3.28	3.31	3.32	3.33	3.34	3.35	3.36	

Vibration directions of shear waves in cores are not identified because P-wave velocities in the rocks show they are near-isotropic.

Like V_p , S-wave velocity also could be observed to increase with pressure. It is worth noting that in the present work, S-wave velocity in dry cores shows normal hysteresis in that V_s along decreasing pressure cycle is higher than for increasing cycle of pressure. Hysteresis is rather weak in saturated greywacke except in core no. G5H (Fig. 3-11b). In this specimen, V_s is lower along decreasing path of pressure than along increasing path. This may be due to initial partial saturation in the cracks. Saturation increases when the cracks close under pressure. Failure of the cracks to relax completely when pressure is decreased keeps them saturated, hence depressing V_s . O'Connell & Budiansky (1977) suggest that when the cracks are interconnected, V_s is independent of the degree of saturation. It seems likely that the cracks in core no. G5H may be isolated and partially-saturated. Biot (1956a, b) and Gregory (1976) have shown theoretically and experimentally, respectively, that saturation reduces shear-wave velocity.

As mentioned in the previous section, further measurements of velocities at East Anglia revealed a repeatability problem in velocities from East Anglia and Edinburgh experiments. Since core no. G6V was run (saturated) at both places, it provided an adjustment criterion for the high V_s data from East Anglia. Differences between the two sets of V_s data (for G6V) were found to range from 0.20 km/s to 0.33 km/s, giving a mean of 0.29 km/s which was subtracted from the rest of the East Anglia data. This brings V_s (Edinburgh) and V_s (East Anglia) to within 1.5% of each other.

/...

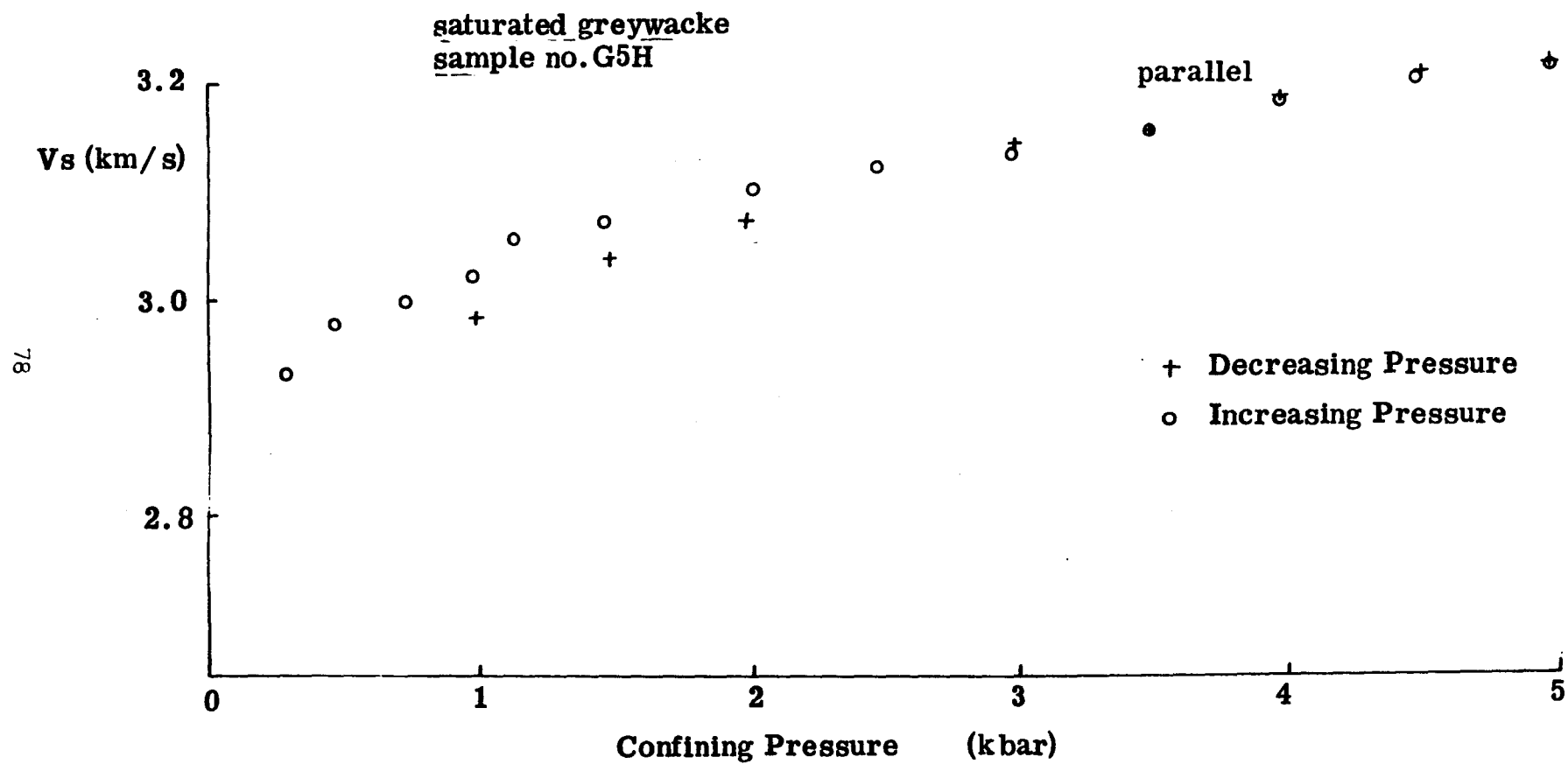


Fig. 3-11b S-wave velocity variation with pressure in the greywackes.
(V_s with increasing pressure > V_s with decreasing pressure)

3.4 Densities and porosities of shale and greywacke

Direct measurements on cores from shale and greywacke have produced average saturated bulk density in greywacke of 2.69 ± 0.04 (s.d) Mg/m^3 and in the red shales, 2.45 ± 0.07 (s.d) Mg/m^3 . Details of the various bulk and grain densities are shown in Table 3-4.

Core No.	Lithology	Wet bulk density Mg/m^3	Grain density Mg/m^3	Porosity %
G4N \perp	Greywacke	2.689	2.695	0.55
V	"	2.689	2.698	0.53
H	"	2.680	2.695	0.88
G5N \perp	"	2.671	2.702	1.85
V	"	2.670	2.695	1.50
H	"	2.675	2.686	1.24
G6N \perp	"	2.660	2.693	2.00
V	"	2.639	2.693	3.22
H	"	2.650	2.693	2.53
G7N \perp	"	2.678	2.695	1.03
V	"	2.673	2.686	0.79
H	"	2.690	2.702	0.74
G8N \perp	"	2.750	2.766	0.94
V	"	2.760	2.773	0.78
H	"	2.765	2.729	1.05
G9N \perp	"	2.704	2.720	0.92
V	"	2.708	2.732	1.39
H	"	2.706	2.729	1.36
G10A-H	Red Shale	2.462	2.652	11.50
G11D-H	Green Shale	2.652	2.762	6.23
G14B-N \perp	Red Shale	2.540	2.668	7.70
G14D-H	"	2.457	2.650	11.70
G14C-N \perp	"	2.331	2.540	13.54
G4' N \perp	Greywacke	2.683	2.698	0.9
V	"	2.683	2.695	0.7
H	"	2.685	2.694	0.5
SOL 1 X	Granodiorite	2.680	2.691	0.6
Y	"	2.680	2.690	0.6
Z \perp	"	2.677	2.689	0.7
SOL2Y	Lava.	2.698	2.722	1.4

G4' cores were obtained from the same hand specimen which produced the original G4 cores.

The above table clearly shows the variability in the density values for the Lower Palaeozoic rocks. A saturated bulk density of about 2.7 Mg/m^3 appears reasonable for greywacke when compared with previously measured values on similar rocktypes but the density values for red shale are at variance with previous works. McLean (1961) obtained a mean of 2.75 ± 0.05 for the Lower Palaeozoic greywackes of Ayrshire. Table 1 (below) of Bott and Masson - Smith (1960) shows the density values for the Southern Uplands shales and greywackes.

Age & Lithology	Place	Number of Specimens	Saturated density ($10^3 \times \text{kg/m}^3$)	Grain density ($10^3 \times \text{kg/m}^3$)
Silurian shale	5 localities in Southern Uplands	27	2.714 ± 0.049	2.759 ± 0.043
Silurian greywacke	7 localities in Southern Uplands	63	2.706 ± 0.055	2.732 ± 0.036

Powell (1956) obtained $2.68\text{--}2.83 \text{ Mg/m}^3$ with a mean of $2.77 \pm 0.05 \text{ Mg/m}^3$ for Ordovician shales, sandstones and slates from Wales. The author also obtained $2.60\text{--}2.78 \text{ Mg/m}^3$ with a mean of $2.70 \pm 0.05 \text{ Mg/m}^3$ for Silurian shales and sandstones. The values agree with the density value obtained for green shale of the present work. The present density results for red shales show relatively low values. McLean (1961) however mentioned the swelling of argillaceous rocks after saturation. If/...

If this were true for the present red shales, then 'swelling' must have increased the bulk volume, hence reducing the bulk-density. It should be mentioned that some of the red-shale samples were lost on saturation, and the few samples shown in Table 3-4 barely managed to survive after being coated in thin films of plastic padding.

It seems clear from the above that the difference between the densities of green shale and red shale is, at least, partially responsible for the lower P-wave velocity in red shale both in the laboratory and in situ (see Section 3.5). The tendency for velocity to increase with density has been demonstrated by previous workers (Adams & Williamson, 1923; Birch & Bancroft, 1938, 1940; Hughes & Maurette, 1956; and Birch, 1961).

3.5 In situ velocity results

The hammer lines

On continuous outcrops of steeply dipping shale and greywacke, hammer lines were spread to a maximum distance of 30m mostly along the general geological strike. No change of velocity with range was observable on the time-distance (T-X) plots (see Appendix 5).

P-wave velocity in shale and greywacke and in a sequence of both lithologies, was determined by picking the first/...

first arriving P-waves. Using a 50ms sweep time, first arrivals could be picked to within 0.1 ms. Travel times were measured at approximately 2m intervals over a range of 14m (normal to bedding) to 30m (parallel to bedding). Of the 28 successful lines surveyed, 25 were reversed. The reversed profiles helped to check on the internal consistency of the time readings, e.g. the reciprocal time for most lines was repeatable to less than 0.2 ms. Reversal of the lines also helped in evaluating the actual velocity of shale and greywacke by the plus-minus method (Hagedoorn, 1959).

Results

Results from the refraction line surveys are summarised in Table 3-5 and Fig. 3-12. Velocity in the green shale is about 3.61 ± 0.14 (s.e.) Km/s, and in red shale, the best estimate from two pairs of reversed lines 7A & 7B, is 2.18 ± 0.06 km/s. The difference of about 40% between these two mean velocities for green and red shales is significant, and is attributed, in part, to the difference in densities of the two shales. From lines 3 & 4 on green and red shales, anisotropy of about 10% is obtained, whereas from lines 7A & 7B, it appears red shale is isotropic.

In the sequence of beds of shale and greywacke, lines 14-18 produced velocity anisotropy of about 19%, and the relatively low velocity observed here is considered to be due to the presence and frequency of joints and fractures along the bedding planes. When these fractures are filled by loose and/

Table 3-5: Hammer Line velocities at GIRVAN.

* Apparent velocity from single profile only.

Hammer Line No.	Length of Spread(m)	Along/ Normal to strike	Locality	Lithology	Vp from minus times (km/s) ($t_A - t_B$) \pm s.e.
* 1	24m	Parallel	Whitehouse Shore	Green shale	3.49 \pm 0.09*
* 2	23m	"	Opposite Ardmillan	"	3.66 \pm 0.18*
3	30m	Normal	House	Red/green shale	3.44 \pm 0.15
4	"	Parallel	"	Green shale	3.80 \pm 0.18
5	"	"	50m south of above lines 1-4	"	3.59 \pm 0.10
* 6	17m	Normal		"	3.50 \pm 0.20*
7A	30	Parallel	Whitehouse	Red shale	2.18 \pm 0.06
7B	20	Normal	Shore	"	2.17 \pm 0.07
8	26	Parallel	Southern end of	Weathered	2.84 \pm 0.03
9	30	"	Whitehouse shore	shale/grey wacke	2.64 \pm 0.05
10	30	"	"	"	2.56 \pm 0.04
11	20	Normal	"	"	2.43 \pm 0.13
12	18m	"	"	"	2.16 \pm 0.04
13	18m	"	"	"	2.43 \pm 0.25
14	30m	Parallel		greywacke/shale	3.83 \pm 0.01
15	22m	Normal	fresh grey-wacke/shale beds	"	2.95 \pm 0.03
16	30m	Parallel	"	"	3.24 \pm 0.16
17	26m	Normal	"	"	2.77 \pm 0.02
18	30m	Parallel	"	"	3.47 \pm 0.03
19	24m	Parallel	Ardwell Bay		3.50 \pm 0.06
20	18m	Normal	"	greywacke	3.23 \pm 0.04
21	30m	Parallel	"	"	3.48 \pm 0.06
22	22m	Normal	"	"	2.93 \pm 0.11
23	30m	Parallel	"	"	4.00 \pm 0.10
24	14m	Normal	"	"	3.36 \pm 0.10
25	28m	Parallel	"	"	3.82 \pm 0.02
26	28m	"	Gullies have broken rock into units	"	3.20 \pm 0.02
27	30m	"	Ardwell Bay (nearer Kennedy's Pass)	"	3.98 \pm 0.03

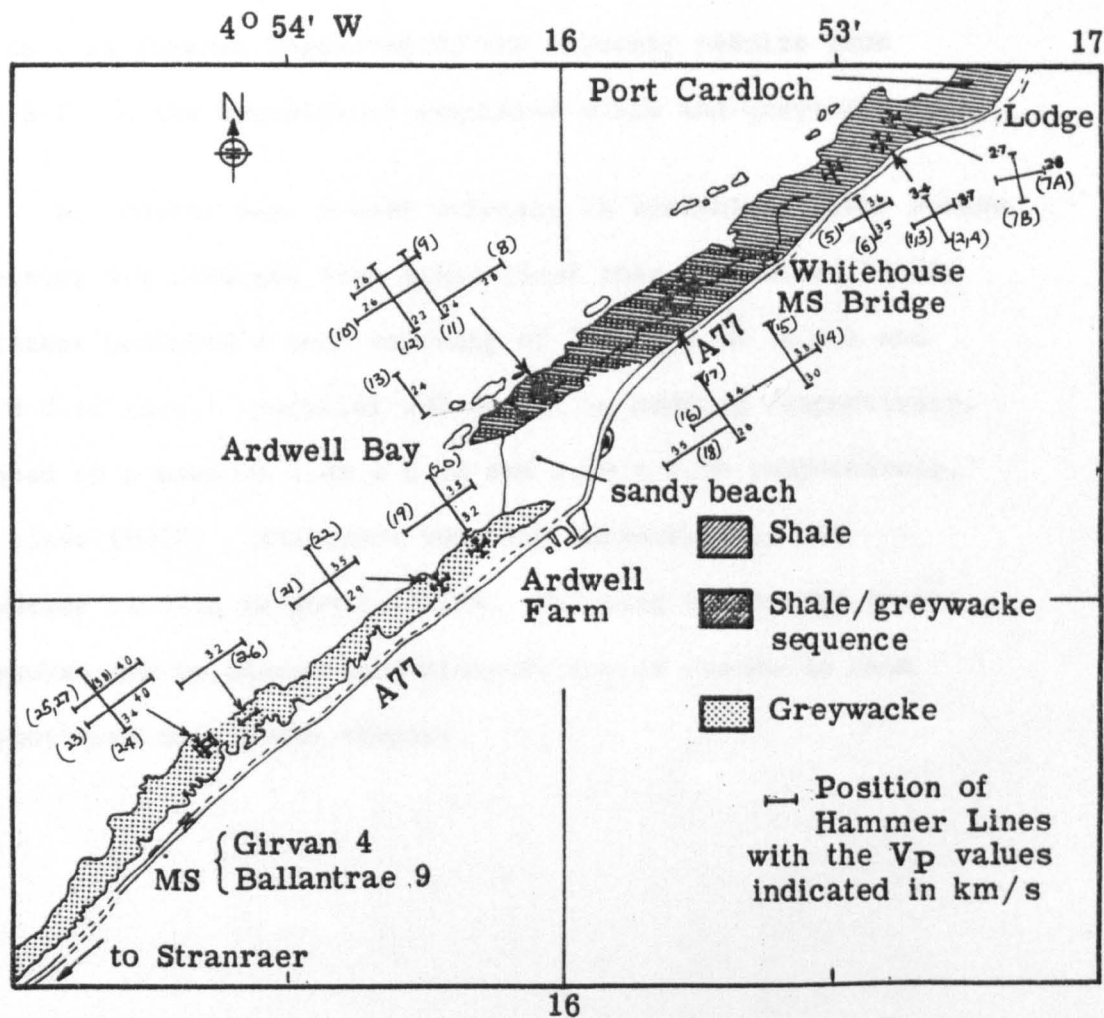


Fig. 3-12. Whitehouse shore (Girvan) showing hammer lines and the corresponding V_p values. Lines that are parallel to strike yield higher P-wave velocities.

and unconsolidated sediments (Hall, 1970), velocity is reduced. This fact is further supported by the velocity results from lines 8-13 on the sequence of weathered shale and greywacke beds.

At Ardwell Bay, P-wave velocity is variable. Lower P-wave velocities are obtained from lines 19-22 than from lines 23-27. The latter produced a mean velocity of 3.93 ± 0.14 (s.e.) and 3.36 ± 0.10 (s.e.) parallel and normal to bedding respectively, compared to a mean of 3.49 ± 0.06 and 3.08 ± 0.08 respectively, from lines 19-22. Therefore velocity anisotropy in the greywackes in situ is about 12-15%. Velocity anisotropy in the greywackes due to anisotropic distribution of cracks in them is considered in a later chapter.

3.5 Summary and conclusions

Table 3-6 shows the summary of laboratory and in situ velocities in the Southern Uplands rocks. In Fig. 3-13, the laboratory data are illustrated as expectation curves of velocity versus pressure and depth by calculating the mean velocity (\pm s.d.) at each pressure and depth, for the different rocktypes of the present work.

It is clear that laboratory-measured velocities are consistently higher than in situ values obtained from hammer lines./....

lines. Laboratory Vp at 1bar in greywackes is higher by about 20% and in shale by about 30% than hammer line velocities. The discrepancy between laboratory and hammer line velocities is considered to be due to differences in the size of rock volumes sampled. The joints and fractures in the rocks in situ are too large to be sampled in the small dimensions of laboratory cores. Therefore the effects of such structures on velocity are absent in the laboratory experiments.

At 100bar pressure, laboratory P-wave velocity of greywacke is close to EKA data (Fig. 3-13). Beyond the 300m depth at EKA, laboratory values in greywacke are not compatible with in situ values. The close agreement of laboratory Vp in granodiorite and LISPB (Bamford et al, 1977, 1978) and Warner's values of 5.8 km/s and 6.0 km/s respectively, suggests the possible existence of granitic rocks at depth under the Southern Uplands. This is considered further in Chapter 6.

Anisotropy in shale and greywacke measured in the laboratory at 1bar reaches 11%, greater than at high pressure where typical values at 5kbar are $\leq 4\%$ and 7-9% for greywacke and shale respectively. From hammer lines, anisotropy in the sequence of shale and greywacke is about 19%. Anisotropy at EKA is 8% at 300m depth and less than 3% at about 2-2.5 Km depth according to LISPB and Warner's experiments.

The laboratory observed velocities in shale and greywacke are used to model EKA observed velocity anisotropy by various mixtures of shale and greywacke in Chapter 4.

/...

Table 3-6: Comparisons of laboratory and in situ velocities for Southern Uplands rocks.

SATURATED GREYWACKE

Pressure (bars)	Approximate depth (m)	Lab. Vp \pm s.d. (km/s)	In situ Vp (km/s) \pm s.e.
1	3	5.25 \pm 0.21	3.50 \pm 0.05 (hammer line) (5.10 \pm 0.01)EKA (El Isa, 1977)
10	30	5.28 \pm 0.21	
20	60	5.30 \pm 0.20	
50	150	5.34 \pm 0.19	
80	240	5.37 \pm 0.20	
100	300	5.38 \pm 0.20	
140	420	5.40 \pm 0.20	
160	480	5.41 \pm 0.21	
200	600	5.43 \pm 0.21	

SATURATED GREEN SHALE

1	3	4.50	3.61 \pm 0.15 (from hammer line)
10	30	4.54	
20	60	4.56	
50	150	4.61	
80	240	4.63	
100	300	4.65	
140	420	4.66	
160	480	4.67	
200	600	4.68	

SATURATED RED SHALE

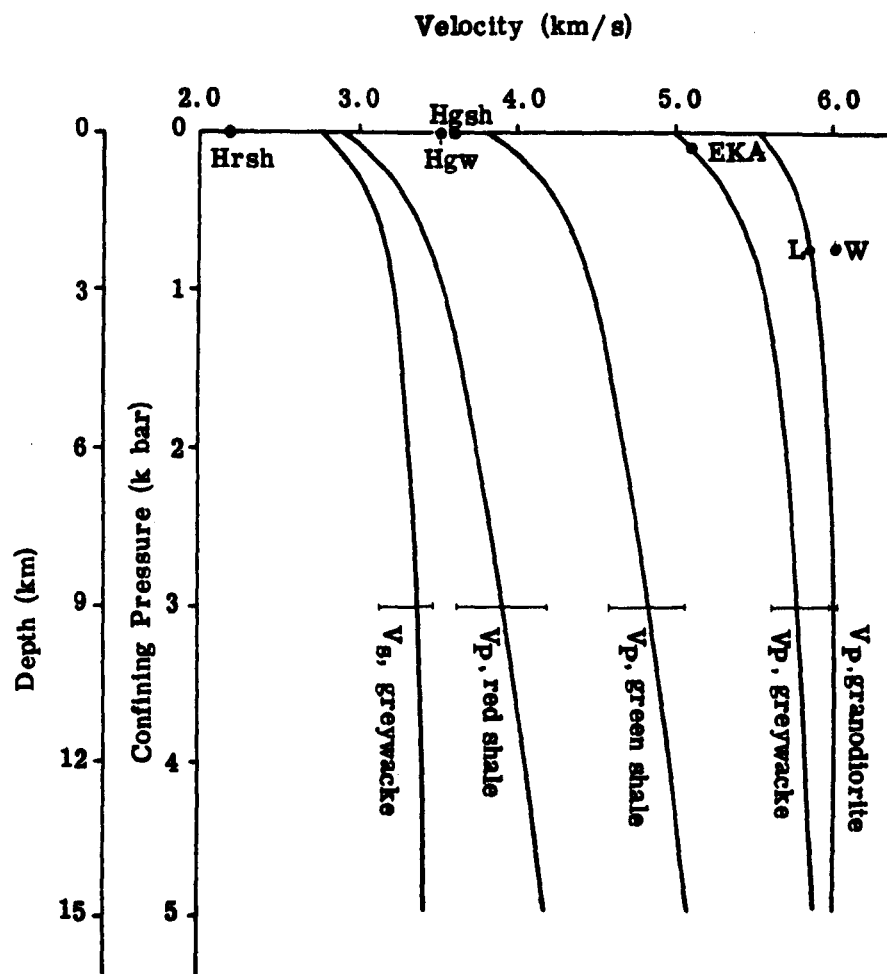
1	3	3.36 \pm 0.23	2.18 \pm 0.06 (from hammer line)
10	30	3.39 \pm 0.23	
20	60	3.42 \pm 0.23	
50	150	3.47 \pm 0.23	
80	240	3.49 \pm 0.23	
100	300	3.50 \pm 0.23	
140	420	3.52 \pm 0.23	
160	480	3.52 \pm 0.23	
200	600	3.53 \pm 0.23	

Table 3-6 (cont'd)

Pressure (kbar)	Approximate depth (km)	Lab. Vp in sat. greywacke (km/s) \pm s.d.	Lab. Vp in dry granodiorite (km/s) \pm s.d.	In situ Vp (km/s)
0.25	0.75	5.25 ± 0.17	5.70 ± 0.05	$(5.8 \pm 0.02 \text{ (LISPB)})$ $(6.0 \pm 0.05 \text{ (WARNER)})$
0.50	1.50	5.34 ± 0.17	5.80 ± 0.03	
0.75	2.25	5.50 ± 0.18	5.85 ± 0.03	
1.00	3.00	5.53 ± 0.21	5.88 ± 0.01	
2.00	6.00	5.67 ± 0.20	5.94 ± 0.03	
3.00	9.00	5.76 ± 0.19	5.96 ± 0.03	
4.00	12.00	5.83 ± 0.19	6.00 ± 0.04	
5.00	15.00	5.88 ± 0.19	6.02 ± 0.03	

Pressure (kbar)	Approximate depth (km)	Lab. Vs in sat. greywacke (km/s) \pm s.d.	In situ Vs (km/s)
0.25	0.75	3.05 ± 0.17	3.45 ± 0.05 (WARNER)
0.50	1.50	3.13 ± 0.16	
0.75	2.25	3.10 ± 0.16	
1.00	3.00	3.22 ± 0.16	
2.00	6.00	3.31 ± 0.17	
3.00	9.00	3.36 ± 0.17	
4.00	12.00	3.39 ± 0.17	
5.00	15.00	3.42 ± 0.17	

Pressure (kbar)	Approximate depth (km)	Vp sat. green shale (km/s) \pm s.d.	Vp sat. red shale (km/s) \pm s.d.
0.25	0.75	4.14 ± 0.30	3.22 ± 0.35
0.50	1.50	4.27 ± 0.28	3.34 ± 0.31
0.75	2.25	4.38 ± 0.27	3.44 ± 0.29
1.00	3.00	4.45 ± 0.26	3.51 ± 0.28
2.00	6.00	4.66 ± 0.23	3.74 ± 0.25
3.00	9.00	4.83 ± 0.21	3.91 ± 0.22
4.00	12.00	4.96 ± 0.19	4.05 ± 0.25
5.00	15.00	5.08 ± 0.19	4.18 ± 0.22



$H_{rsh} = V_p$ from hammer line on red shale, $L = V_p$ from LISPB
 $H_{gsh} = V_p$ from hammer line on green shale, $W = V_p$ from Southern Uplands Profile
 $H_{gw} = V_p$ from hammer line on greywacke, $EKA = V_p$ from EKA explosion experiment

Fig. 3-13. Mean laboratory velocities versus pressure (and depth) for the Southern Uplands rocks.

CHAPTER FOUR MODELLING OF VELOCITY ANISOTROPY IN THE SOUTHERN
UPLANDS ROCKS: SHALE/GREYWACKE SANDWICHES.

4.1 Introduction

Compressional and shear wave velocities in Lower Palaeozoic shales and greywackes have been measured in an attempt to account for the anisotropy observed at Eskdalemuir Array (EKA) from shots at ranges up to 10km. At a depth of about 300m,

$$V_{p_{\max}} = 5.3 \text{ km/s (parallel to bedding)}$$

$$V_{p_{\min}} = 4.9 \text{ km/s (normal to bedding).}$$

Mixing of layers of shale and greywacke accounts more readily for the EKA data than does the intrinsic anisotropy of either lithology, though the velocity-contrast between the components may need to be higher than that observed in the rocks cored for this study. It remains possible that the EKA data could be explained by a model of parallel joints along bedding in a greywacke lithology. This is discussed in Chapter 5, but first to be briefly discussed here are some factors that have been observed to influence seismic velocities in the laboratory cores.

4.2 Velocity behaviour in the Southern Uplands rocks.

Pressure

V_p and V_s in all laboratory samples show an initial rapid rate/...

rate of increase of velocity (typically 0.4 km/s per kbar) with pressure, reducing to 0.1km/s per kbar or less at high pressures. This rapid increase of velocities at low pressures is thought to be caused primarily by the closing of fine cracks. In situ, a similar increase of velocity with depth was inferred from T-X data at Eskdalemuir where it is proposed that V_p increases initially at 1.3-1.4 km/s per km over the first 0.8 km. This rate decreases to about 0.3 km/s per km beyond 1 km depth.

Saturation

The difference between dry and saturated P-wave velocities in the Southern Uplands greywackes ranges from less than 1% at 5.0 kbar to about 9% at pressures below 250 bars. Saturation causes V_p to rise. Anomalous increase of V_p in dry over saturated shale cores could be related to microcracks in the rocks (Gregory, 1976), and also to chemical interaction between water and the solid material around grain contacts (Toksoz et al, 1976). As discussed later in Chapter 5, incomplete saturation of cracks could result in anomalous velocity behaviour of saturated rocks, and possibly, build-up of pore-pressure in the sample (Biot, 1956; Wyllie et al, 1958; and Todd & Simmons, 1972). If incomplete saturation occurs, then acoustic wave energy is likely to be more attenuated because of the large impedance differentials between the three phases in the composite (Wyllie et al, 1958). It is proposed therefore that the effect of the mixture of fluids in the rock is to diminish the amplitude of/...

of the first arrival to such an extent that a low and anomalous velocity is observed. In the case of saturated shale specimens, observed low velocities may therefore be, in part apparent, but also in part real, on account of partial loss of cohesion of material due to water-clay interaction.

Anisotropy

Velocities in the Southern Uplands rocks may depend upon orientation with respect to bedding. This effect is readily observable in laboratory cores from shale (see also, Jones & Wang, 1981) but not as obvious in the laboratory samples of greywacke. In situ from hammer lines, anisotropy of about 19% is inferred in shale/greywacke sequence. At EKA, this reduces to about 8% at 300m depth. Elsewhere in the Southern Uplands, LISPB & Warner's refraction lines have shown a difference of 0.2km/s which could correspond to 3% 'anisotropy' at about 2.0 km depth (≈ 0.7 Kbar).

Two models are considered: (i) anisotropy due to layering and (ii) anisotropy due to oriented cracks. The first model due to Postma (1955) requires that $V_{p_{\text{shale}}} < \bar{V}_p < V_{p_{\text{greywacke}}}$ where \bar{V}_p is the field mean velocity in the composite. Table 3-6 and Fig. 3-13 show that only EKA observed mean \bar{V}_p (= 5.1 km/s) barely satisfies this condition, thus the Postma model of greywacke/shale mixing need only be considered further as a possible explanation of EKA data.

/...

For the crack effect, $\bar{V}_p < V_p$ greywacke since greywacke is chosen as the host rock to cracks which are aligned along bedding. This is discussed further in Chapter 5.

At Eskdalemuir, seismometers were placed on the shale/greywacke sequence (Truscott, 1964-65). Anisotropy there would be a combination of the effects of oriented fractures and of mixing of layers of greywacke and shale. The possible effects of mixing are considered first.

4.3 Anisotropy in a layered sequence (Postma, 1955)

A layered structure consisting of alternating shale and greywacke is illustrated in Fig. 4-1. The individual beds are regarded as isotropic and the composite material is homogeneous (on a scale large compared with bed-thickness) and anisotropic. The theory (see Chapter 1) which leads to transverse isotropy requires that an elementary volume of the layered medium contains a large number of plane parallel isotropic layers. The five elastic constants of the equivalent transversely isotropic medium (Postma, 1955; Levin, 1980) are expressed in terms of the proportion of the individual isotropic layers and their elastic properties. The elastic properties of the individual layers can in turn be derived from measured P- and S-wave velocities and densities.

The interest here is to determine the maximum anisotropy in the composite medium from mixtures (X) of shale and greywacke. The/...

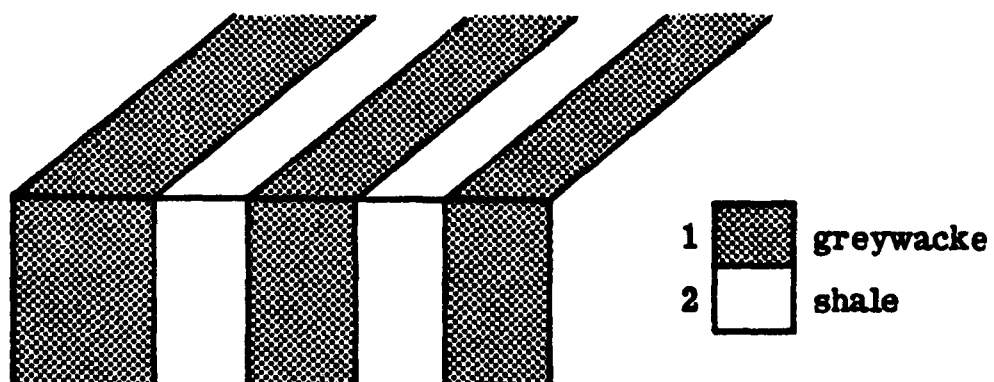


Fig. 4-1. A periodic structure containing alternating layers of shale and greywacke.

Periodicity of beds < 0.5 km.

The starting point is the specification of V_p , V_s in shale and greywacke. In the present work V_s in shale has not been measured, hence must be assumed. Calculation is first made on the assumption that $\sigma_{\text{shale}} = \sigma_{\text{greywacke}}$, where σ is Poisson's ratio. Calculations for a few cases in which it is assumed $0.3 \geq \sigma_{\text{shale}} > \sigma_{\text{greywacke}} (=0.26)$ give similar results.

$V_{p_{//}}$ is P-wave velocity parallel to layered structure.

V_{\perp} is P-wave velocity normal to layered structure.

$V_{p_{1,2}}$, $V_{s_{1,2}}$ are velocities in greywacke and shale respectively.

X is the proportion of medium 1 to medium 2.

$$P_1 = \rho_1 V_{p_1}^2, P_2 = \rho_2 V_{p_2}^2; S_1 = \rho_1 V_{s_1}^2, S_2 = \rho_2 V_{s_2}^2$$

$$\Delta P = P_1 - P_2 \text{ and } \Delta S = S_1 - S_2$$

In the case of the Southern Uplands greywackes and shale

$$\rho_1 = \rho_2 = \rho (= 2.70 \text{ Mg/m}^3).$$

V_{p_1} , V_{s_1} for greywacke and V_{p_2} for shale are determined from cores, V_{s_2} is estimated by assuming that $\sigma_1 = \sigma_2 = \sigma (=0.26)$

A rearrangement of the equations describing the model (Postma, 1955) leads to $\rho(V_{p_{//}}^2 - V_{\perp}^2) = \frac{4 \cdot X \cdot \Delta S (\Delta P - \Delta S)}{(X + 1) (P_1 + X P_2)} \dots\dots\dots (1)$

If $\sigma_1 = \sigma_2$,

$$\text{then } S_1 = f \cdot P_1, S_2 = f \cdot P_2 \text{ and } \Delta S = f \cdot \Delta P$$

$$\text{It can be shown that } f = \frac{V_{s_1}^2}{V_{p_1}^2} = \frac{(0.5 - \sigma)}{(1 - \sigma)}$$

Substituting f in (1),

/...

$$\rho (v_{p_{//}}^2 - v_{p_{\perp}}^2) = \frac{4 \cdot X \Delta P^2 f (1 - f)}{(X + 1) (P_1 + X P_2)}$$

$$= \left[\frac{(0.5 - \sigma)}{(1 - \sigma)^2} \right] \frac{2 \cdot X \cdot \Delta P^2}{(X + 1) (P_1 + X \cdot P_2)} \dots\dots\dots (2a)$$

For a choice of v_{p_1} & v_{p_2} with $\sigma_1 = \sigma_2$, which gives the maximum difference $D = \rho (v_{p_{//}}^2 - v_{p_{\perp}}^2)$ from mixing proportions of medium 1 & medium 2,

$$\frac{\delta(D)}{\delta X} = \frac{2(0.5 - \sigma)}{(1 - \sigma)^2} \Delta P^2 \cdot \left[\frac{(X + 1) (P_1 + X \cdot P_2) - X \cdot (P_1 + 2 \cdot X \cdot P_2) - X \cdot P_2}{(X + 1)^2 (P_1 + X \cdot P_2)} \right] \dots\dots (2b)$$

$$= \frac{(P_1 - X^2 P_2)}{(1 - \sigma)^2} \dots \text{where } v^2 \text{ is the denominator in equation (2b) .}$$

$$\frac{\delta(D)}{\delta X} = 0 \text{ when } P_1 - X^2 P_2 = 0$$

$$\therefore X = \left(\frac{P_1}{P_2} \right)^{\frac{1}{2}} = \pm \frac{v_{p_1}}{v_{p_2}}$$

Thus, for maximum anisotropy for a choice of v_{p_1} , v_{p_2} , the proportion of mixing $(X) = v_{p_1}/v_{p_2}$.

substituting for X in (2)

$$(v_{p_{//}}^2 - v_{p_{\perp}}^2) = \frac{2(0.5 - \sigma)}{(1 - \sigma)^2} \left[\frac{\frac{v_{p_1}}{v_{p_2}}}{\left(\frac{v_{p_1}}{v_{p_2}} + 1 \right)} \cdot \frac{\rho^2 (v_{p_1}^2 - v_{p_2}^2)^2}{\left(\rho v_{p_1}^2 + \frac{v_{p_1}}{v_{p_2}} \cdot \rho v_{p_2}^2 \right)} \right]$$

which reduces to,

$$v_{p_{//}}^2 - v_{p_{\perp}}^2 = \left(\frac{2(0.5 - \sigma)}{(1 - \sigma)^2} \right) (v_{p_1} - v_{p_2})^2 \dots\dots\dots (3)$$

Specification of v_{p_1} , v_{p_2} and the ratio of mixture also fixes/...

fixes $V_{p_{\perp}}$ of the composite, therefore $V_{p_{//}}$ can be determined.

Also from Postma (1955),

$$V_{p_{\perp}}^2 = \frac{V_{p_1}^2 \cdot V_{p_2}^2 (X + 1)}{V_{p_1}^2 + V_{p_2}^2} \quad (\text{See also, White \& Angona, 1955}).$$

Since $X = V_{p_1}/V_{p_2}$.

it can be shown that,

$$V_{p_{\perp}}^2 = V_{p_1} \cdot V_{p_2}$$

Table 4-1 and Fig. 4-2 show the results of mixing greywacke and shale for each choice of laboratory measured V_{p_1} in greywacke and V_{p_2} in shale. Fig. 4-2 has been obtained by plotting a pair of values ($\bar{V}_p, \Delta V_p$) for every combination of V_{p_1} and V_{p_2} . \bar{V}_p is the mean V_p of the composite and $\Delta V_p = V_{p_1} - V_{p_2}$. Anisotropy at such points is defined by,

$$\frac{\Delta V_p}{\bar{V}_p} \times 100\%$$

The dashed lines are contours of equal mean \bar{V}_p and the continuous lines are contours of equal ΔV_p . The observed velocity anisotropy at EKA is indicated by the shaded triangle marked 'EKA'. Anisotropy produced by combinations of the mean $V_{p_1,2}$ in greywacke and shale at 300m depth is shown by the shaded triangle marked 'LAB'. It is clear that a greater velocity contrast is needed between shale and greywacke in order to explain the EKA observed anisotropy by Postma's layered model.

/....

Table 4--1 Anisotropy from mixing of shale and greywacke.

V_{P_1} (km/s)	V_{P_2} (km/s)	$X = V_{P_1}/V_{P_2}$	$V_{P_{ij}}$ (km/s)	$V_{P_{\perp}}$ (km/s)	\bar{V}_P (km/s)	ΔV_P (km/s)
5.40	3.25	1.66	4.65	4.19	4.42	0.46
5.40	3.50	1.54	4.70	4.35	4.53	0.35
5.40	3.75	1.44	4.76	4.50	4.63	0.26
5.40	4.00	1.35	4.83	4.65	4.74	0.18
5.55	3.25	1.71	4.76	4.25	4.51	0.51
5.55	3.50	1.59	4.81	4.41	4.61	0.40
5.55	3.75	1.48	4.86	4.56	4.71	0.30
5.55	4.00	1.39	4.93	4.71	4.82	0.22
5.60	3.25	1.72	4.80	4.27	4.54	0.53
5.60	3.50	1.60	4.85	4.43	4.64	0.42
5.60	3.75	1.49	4.90	4.58	4.74	0.32
5.60	4.00	1.40	4.96	4.73	4.85	0.23
5.70	3.25	1.75	4.88	4.30	4.59	0.58
5.70	3.50	1.63	4.92	4.47	4.70	0.45
5.70	3.75	1.52	4.97	4.62	4.80	0.35
5.70	4.00	1.43	5.04	4.78	4.91	0.26
5.80	3.25	1.79	4.96	4.34	4.65	0.62
5.80	3.50	1.66	4.99	4.51	4.75	0.48
5.80	3.75	1.55	5.04	4.66	4.85	0.38
5.80	4.00	1.45	5.10	4.82	4.96	0.28
5.90	3.25	1.82	5.03	4.38	4.71	0.65
5.90	3.50	1.69	5.07	4.54	4.81	0.53
5.90	3.75	1.57	5.12	4.70	4.91	0.42
5.90	4.00	1.48	5.17	4.86	5.02	0.31
6.00	3.25	1.85	5.11	4.42	4.77	0.69
6.00	3.50	1.71	5.15	4.58	4.79	0.56
6.00	3.75	1.60	5.19	4.74	4.97	0.45
6.00	4.00	1.50	5.26	4.90	5.08	0.36

$$\text{Anisotropy} = (\Delta V_P / \bar{V}_P) \times 100\%$$

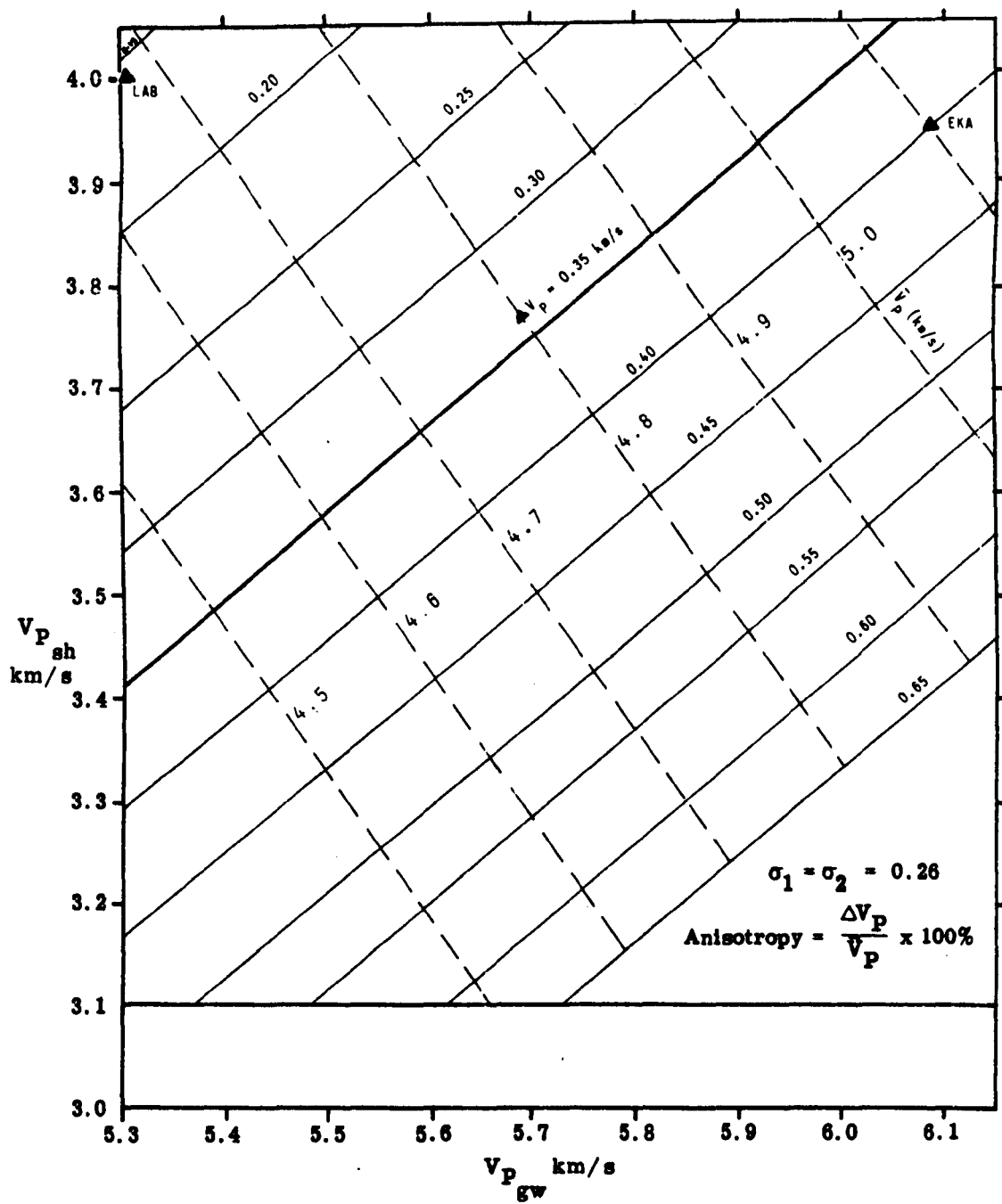


Fig. 4-2. Anisotropy from the mixing of shale/greywacke layers.

4-4 Conclusion

It can be concluded from Table 4-1 and Fig. 4-2 that velocity anisotropy at EKA cannot be attributed entirely to mixing of shale and greywacke unless there is greater velocity contrast than has been observed in the laboratory cores from the two lithologies. In particular, V_p in the greywacke component would have to be greater than the mean V_p obtained from laboratory experiments.

The inadequacy of the Postma model to explain the observed anisotropy at EKA leads to consideration of an alternative model. In the new model, the Southern Uplands greywacke is assumed to be permeated by partly oriented cracks. Anisotropy resulting from such parallel cracks is discussed in Chapter 5.

CHAPTER FIVE. CRACKS, VELOCITIES AND ANISOTROPY IN THE ROCKS
OF THE SOUTHERN UPLANDS

5.1 Introduction

In Chapter 4 attempt has been made to model anisotropy in the Southern Uplands rocks in terms of mixtures of shale and greywacke layers. Though this model is possible, it is probable that a greater velocity-contrast is required than exists between the two lithologies. In view of the fact that the EKA observed velocity is close to the mean velocity obtained from laboratory measurements in greywacke, an alternative model with greywacke as the host rock to cracks is considered in this Chapter. A physical model in which the laboratory greywacke is permeated by additional partly-oriented cracks is assumed. Cracks are introduced into the greywacke in volumes that are multiples of the isotropic linear porosity 'Aist' (see also Bamford & Nunn, 1979; Anderson et al, 1974).

Formulations are derived to express the linear compressibilities in X, Y, and Z (L) directions in terms of the elastic constants of the cracked, anisotropic composite. A cross-plot (Fig. 5-5) between the two resulting velocities (// & L) defines the anisotropy of the composite. The results of this exercise suggest that anisotropy in rocks in situ in the Southern Uplands can be caused by oriented joints and fractures along bedding planes. The size and nature of such flaws can be determined from the theoretical models/...

models of O'Connell & Budiansky (1974, 1977) and Toksoz et al (1976). Some other well known works in this regard are due to, Eshelby (1957); Walsh (1965, 1969); Wu (1966); Anderson et al (1974); O'Connell & Budiansky (1974, 1977); Budiansky & O'Connell (1976); Toksoz et al (1976); Mavko & Nur (1978); Walsh & Grosenbaugh (1979); and Cheng & Toksoz (1979). The mathematical formulations used in the present work are presented in Appendix 2. Here, the crack models from self-consistent approximation and non-interactive techniques are first discussed.

5.2 Crack-density parameter (ϵ) and elastic moduli from self-consistent crack theory (O'Connell & Budiansky (1974)).

O'Connell & Budiansky (1974) (referred to as OB) proposed a model for the effect of cracks on the macroscopic elastic properties of solids based on a self-consistent approximation. The effect of interaction between cracks is included by assuming that each crack behaves as though it were embedded in a material having the elastic properties of the cracked body. Their formulations are used to produce changes in crack-density (ϵ) and Poisson's ratio (σ) with pressure in the greywackes. Results for dry and saturated samples are shown in Table 5-1. The elastic moduli shown on the Table are normalised. The normalised moduli are calculated from laboratory measured velocities in greywacke, using equations (28) of O'Connell & Budiansky (1974) as follows,

/...

$$\frac{\bar{V}_S}{V_S} = \left(\frac{\bar{G}}{G} \right)^{\frac{1}{2}} \dots\dots\dots (i)$$

$$\frac{\bar{V}_P}{V_P} = \left[\frac{(1 - \bar{\sigma})(1 + \sigma)}{(1 + \bar{\sigma})(1 - \sigma)} \times \frac{\bar{K}}{K} \right]^{\frac{1}{2}} \dots\dots\dots (ii)$$

$$\frac{\bar{V}_P/\bar{V}_S}{V_P/V_S} = \left[\frac{(1 - \bar{\sigma})(1 - 2\sigma)}{(1 - 2\bar{\sigma})(1 - \sigma)} \right]^{\frac{1}{2}} \dots\dots\dots (iii)$$

Where, $\bar{\sigma}$, σ are effective and matrix Poisson's ratios respectively, \bar{V}_S , V_S are the effective and matrix S-wave velocities respectively, \bar{V}_P , V_P are the effective and matrix P-wave velocities respectively, \bar{K} , K are the effective and matrix bulk moduli respectively, \bar{G} , G are the effective and matrix shear moduli respectively.

Therefore, in terms of P-and S-wave velocities measured in the laboratory, the crack-densities of cracked greywacke can be estimated for dry and saturated conditions as follows,

(i) dry cracks,

$$\epsilon_{dry} = \frac{9}{16} \cdot \left(1 - \frac{\bar{K}}{K}\right) \cdot \left(\frac{1 - 2\bar{\sigma}}{1 - \sigma}\right) \dots \text{derived from equation (5) OB (1974)}$$

(ii) saturated cracks,

$$\epsilon_{sat.} = \frac{2 - \bar{\sigma}}{1 - \bar{\sigma}} \left[\left(\frac{15}{32} \cdot \left(1 - \frac{\bar{G}}{G}\right) - \frac{3}{16} \cdot \left(1 - \frac{\bar{K}}{K}\right) \cdot \left(\frac{1 - 2\bar{\sigma}}{1 + \bar{\sigma}}\right) \right] \dots \text{derived from equations (17) of OB (1974).}$$

Details of the derivations of these formulations are presented in Appendix 2. OB stated that the formulations hold for any crack/...

Table 5-1: Poisson's ratio (σ) and crack-density (ϵ) versus Pressure.

G4N ¹										
Pressure (kbar)	Sat	Dry	Sat	Dry	Sat	Dry	Sat	Dry	Sat	Dry
	\bar{V}_p/\bar{V}_s Vp/Vs	\bar{V}_p/\bar{V}_s Vp/Vs	Poisson's ratio, σ	σ	Bulk Modulus \bar{K}/K	Bulk Modulus \bar{K}/K	Shear Modulus $\bar{\mu}/\mu$	Shear Modulus $\bar{\mu}/\mu$	Crack Density ϵ	Crack Density ϵ
0.001	1.033	0.938	0.274	0.207	0.799	0.586	0.713	0.745	0.290	0.143
0.250	1.017	0.965	0.269	0.232	0.831	0.693	0.784	0.788	0.212	0.098
0.500	1.014	0.984	0.267	0.248	0.862	0.765	0.821	0.809	0.176	0.071
1.000	1.014	0.990	0.267	0.252	0.913	0.837	0.870	0.869	0.130	0.048
1.500	1.009	0.994	0.264	0.255	0.932	0.884	0.903	0.902	0.096	0.034
2.000	1.004	0.997	0.260	0.257	0.945	0.919	0.951	0.930	0.067	0.024
2.500	1.004	0.998	0.260	0.258	0.961	0.948	0.948	0.953	0.051	0.015
3.00	1.002	1.000	0.258	0.259	0.971	0.969	0.965	0.971	0.033	0.009
3.500	1.003	1.000	0.259	0.260	0.985	0.984	0.977	0.982	0.023	0.005
4.000	1.002	1.000	0.258	0.259	0.994	0.993	0.988	0.994	0.012	0.002
4.500	1.000	1.000	0.257	0.259	1.000	1.000	1.000	1.000	0.000	0.000

G4H										
0.001	1.080	1.030	0.278	0.250	0.808	0.712	0.612	0.638	0.403	0.086
0.240	1.025	1.017	0.240	0.240	0.813	0.778	0.742	0.729	0.246	0.069
0.500	1.006	1.004	0.224	0.229	0.831	0.804	0.814	0.792	0.167	0.063
1.000	0.999	1.001	0.219	0.226	0.882	0.859	0.884	0.857	0.101	0.046
1.500	0.996	0.995	0.216	0.211	0.910	0.880	0.925	0.898	0.062	0.040
2.000	0.996	0.993	0.216	0.220	0.932	0.905	0.946	0.930	0.004	0.032
2.500	0.993	0.992	0.214	0.219	0.943	0.922	0.968	0.951	0.023	0.026
3.000	0.995	0.995	0.215	0.221	0.958	0.942	0.978	0.962	0.015	0.019
3.500	0.998	0.995	0.218	0.221	0.978	0.958	0.984	0.978	0.013	0.014
4.000	0.998	0.999	0.218	0.225	0.968	0.985	0.995	0.989	0.003	0.005
4.500	1.000	1.000	0.220	0.226	1.000	1.000	1.000	1.000	0.000	0.000

G4V										
0.001	0.996	0.946	0.212	0.151	0.688	0.530	0.698	0.668	0.258	0.189
0.250	0.989	0.978	0.205	0.188	0.749	0.681	0.783	0.745	0.178	0.116
0.500	0.972	0.990	0.188	0.199	0.749	0.681	0.839	0.810	0.114	0.078
1.000	0.971	1.002	0.187	0.211	0.803	0.886	0.901	0.878	0.060	0.039
1.500	0.977	1.001	0.193	0.210	0.852	0.930	0.934	0.927	0.038	0.024
2.000	0.983	1.000	0.200	0.209	0.894	0.956	0.956	0.955	0.024	0.015
2.500	0.990	0.998	0.206	0.207	0.928	0.968	0.967	0.977	0.020	0.011
3.000	0.993	0.997	0.208	0.206	0.950	0.977	0.978	0.989	0.013	0.008
3.500	0.994	0.998	0.210	0.207	0.965	0.985	0.989	0.994	0.005	0.005
4.000	0.998	0.997	0.213	0.206	0.986	0.986	0.994	1.000	0.003	0.005
4.500	1.000	1.000	0.215	0.209	1.000	1.000	1.000	1.000	0.000	0.000

Table 5-1 (Cont'd)

G5N⁺

	Sat	Dry	Sat	Dry	Sat	Dry	Sat	Dry	Sat	Dry
Pressure (kbar)	\bar{V}_p/\bar{V}_s V_p/V_s	\bar{V}_p/\bar{V}_s V_p/V_s	Poisson's ratio, σ	σ	Bulk Modulus \bar{K}/K	\bar{K}/K	Shear Modulus $\bar{\mu}/\mu$	$\bar{\mu}/\mu$	Crack Density ϵ	ϵ
0.001	0.966	0.933	0.243	0.143	0.750	0.555	0.847	0.739	0.122	0.183
0.250	0.978	0.951	0.252	0.164	0.793	0.638	0.857	0.785	0.121	0.140
0.500	0.980	0.958	0.253	0.173	0.817	0.691	0.878	0.823	0.103	0.117
1.000	0.983	0.969	0.255	0.185	0.853	0.775	0.907	0.879	0.077	0.083
1.500	0.975	0.981	0.257	0.197	0.880	0.846	0.927	0.913	0.060	0.055
2.000	0.988	0.987	0.259	0.204	0.904	0.890	0.943	0.936	0.046	0.038
2.500	0.990	0.992	0.261	0.208	2.925	0.922	0.956	0.952	0.036	0.027
3.000	0.994	0.996	0.263	0.212	0.947	0.950	0.967	0.965	0.028	0.017
3.500	0.996	0.997	0.265	0.212	0.966	0.965	0.978	0.978	0.018	0.012
4.000	0.999	0.998	0.267	0.214	0.984	0.982	0.989	0.989	0.009	0.006
4.500	1.000	1.000	0.268	0.215	1.000	1.000	1.000	1.000	0.000	0.000

G5H

0.001	0.994	0.902	0.257	0.105	0.770	0.484	0.788	0.754	0.194	0.232
0.250	0.995	0.914	0.258	0.123	0.802	0.544	0.816	0.795	0.169	0.196
0.500	0.996	0.924	0.258	0.136	0.831	0.596	0.844	0.830	0.143	0.168
1.000	0.997	0.949	0.259	0.168	0.872	0.712	0.882	0.881	0.109	0.111
1.500	1.000	0.967	0.261	0.188	0.908	0.803	0.908	0.916	0.086	0.072
2.000	1.000	0.977	0.262	0.198	0.931	0.857	0.929	0.940	0.066	0.050
2.500	1.001	0.987	0.262	0.208	0.950	0.907	0.948	0.956	0.050	0.032
3.000	1.002	0.992	0.262	0.213	0.968	0.940	0.963	0.970	0.036	0.020
3.500	1.002	0.995	0.263	0.215	0.982	0.962	0.975	0.982	0.024	0.013
4.000	1.001	0.997	0.262	0.217	0.993	0.980	0.989	0.992	0.011	0.007
4.500	1.000	1.000	0.261	0.220	1.000	1.000	1.000	1.000	0.000	0.000

G5V

0.001	1.108	0.938	0.339	0.194	0.842	0.588	0.611	0.749	0.440	0.147
0.250	1.071	0.955	0.324	0.211	0.867	0.667	0.698	0.794	0.335	0.113
0.500	1.036	0.944	0.307	0.201	0.871	0.695	0.777	0.863	0.238	0.107
1.000	1.004	0.962	0.289	0.218	0.886	0.774	0.873	0.893	0.127	0.075
1.500	1.003	0.967	0.288	0.222	0.913	0.822	0.905	0.929	0.095	0.059
2.000	1.004	0.970	0.289	0.225	0.937	0.851	0.926	0.952	0.074	0.048
2.500	1.004	0.977	0.289	0.231	0.958	0.885	0.947	0.963	0.054	0.037
3.000	1.006	0.985	0.290	0.237	0.977	0.920	0.958	0.974	0.044	0.025
3.500	1.004	0.990	0.289	0.242	0.987	0.949	0.974	0.984	0.027	0.016
4.000	1.003	0.995	0.288	0.245	0.996	0.975	0.987	0.992	0.014	0.008
4.500	1.000	1.000	0.287	0.249	1.000	1.000	1.000	1.000	0.000	0.000

Table 5-1 (Cont'd).

G6N

Pressure (kbar)	Sat	Dry	Sat	Dry	Sat	Dry	Sat	Dry	Sat	Dry
	\bar{V}_p/\bar{V}_s V_p/V_s	\bar{V}_p/\bar{V}_s V_p/V_s	Poisson's ratio σ	σ	Bulk Modulus (\bar{K}/K)	\bar{K}/K	Shear Modulus $\bar{\mu}/\mu$	$\bar{\mu}/\mu$	Crack Density ϵ	ϵ
0.001	0.989	0.884	0.259	0.164	0.688	0.473	0.716	0.759	0.261	0.205
0.250	0.988	0.947	0.259	0.231	0.742	0.669	0.773	0.813	0.206	0.106
0.500	0.997	0.959	0.265	0.241	0.796	0.739	0.805	0.858	0.182	0.081
1.000	1.003	0.952	0.269	0.251	0.854	0.819	0.844	0.904	0.150	0.054
1.500	1.004	0.977	0.270	0.255	0.890	0.865	0.877	0.940	0.119	0.040
2.000	1.006	0.982	0.271	0.259	0.918	0.897	0.900	0.958	0.098	0.030
2.500	1.007	0.988	0.272	0.263	0.946	0.929	0.923	0.970	0.077	0.020
3.000	1.007	0.990	0.272	0.265	0.969	0.949	0.946	0.982	0.055	0.015
3.500	1.008	0.996	0.272	0.269	0.991	0.974	0.964	0.986	0.039	0.007
4.000	1.004	0.998	0.270	0.270	0.996	0.987	0.982	0.994	0.019	0.004
4.500	1.000	1.000	0.267	0.271	1.000	1.000	1.000	1.000	0.000	0.000

G6H

0.001	1.095	1.063	0.283	0.282	0.797	0.701	0.575	0.566	0.446	0.079
0.250	1.069	1.038	0.267	0.267	0.882	0.791	0.692	0.692	0.322	0.059
0.500	1.045	1.015	0.251	0.251	0.922	0.826	0.783	0.783	0.224	0.052
1.000	1.029	0.996	0.239	0.236	0.973	0.860	0.874	0.874	0.131	0.044
1.500	1.020	0.995	0.232	0.235	0.999	0.908	0.925	0.925	0.081	0.029
2.000	1.011	0.996	0.224	0.236	1.001	0.946	0.959	0.959	0.044	0.017
2.500	1.006	0.998	0.220	0.238	0.998	0.969	0.977	0.977	0.025	0.010
3.000	1.004	1.002	0.219	0.241	0.999	0.989	0.982	0.982	0.019	0.003
3.500	1.000	0.999	0.215	0.239	0.995	0.992	0.994	0.994	0.005	0.002
4.000	1.001	1.001	0.215	0.240	0.999	0.999	0.997	0.994	0.003	0.000
4.500	1.000	1.000	0.215	0.239	1.000	1.000	1.000	1.000	0.000	0.000

G6V

0.001	1.004	1.049	0.238	0.231	0.725	0.719	0.714	0.697	0.259	0.090
0.250	1.025	1.063	0.254	0.242	0.844	0.836	0.771	0.661	0.225	0.051
0.500	1.028	1.064	0.256	0.243	0.904	0.898	0.819	0.706	0.183	0.031
1.000	1.025	1.054	0.254	0.235	0.956	0.958	0.873	0.781	0.131	0.013
1.500	1.027	1.048	0.256	0.231	0.987	0.998	0.896	0.829	0.112	0.001
2.000	1.023	1.040	0.253	0.224	0.999	1.015	0.918	0.869	0.089	-0.005
2.500	1.019	1.032	0.250	0.217	1.004	1.025	0.936	0.905	0.071	-0.008
3.000	1.015	1.023	0.247	0.210	1.008	1.026	0.953	0.936	0.053	-0.009
3.500	1.010	1.011	0.243	0.198	1.006	1.005	0.970	0.962	0.003	-0.002
4.000	1.005	1.005	0.240	0.192	1.002	1.003	0.982	0.984	0.020	-0.001
4.500	1.000	1.000	0.235	0.188	1.000	1.000	1.000	1.000	0.000	0.000

Table 5-1 (Cont'd)

G8N1

	Sat		Sat		Sat		Sat		Sat
Pressure (kbar)	\bar{V}_p/\bar{V}_s V_p/V_s		Poisson's Ratio σ		Bulk Modulus (\bar{K}/K)		Shear Modulus $\bar{\mu}/\mu$		Crack density ϵ
0.001	0.965		0.241		0.732		0.832		0.133
0.250	0.973		0.248		0.801		0.883		0.093
0.500	0.986		0.257		0.860		0.906		0.080
1.000	0.998		0.266		0.929		0.935		0.061
1.500	1.003		0.269		0.962		0.952		0.047
2.000	1.007		0.272		0.981		0.958		0.044
2.500	1.001		0.268		0.979		0.976		0.023
3.000	1.003		0.270		0.993		0.982		0.019
3.500	1.000		0.268		0.996		0.994		0.006
4.000	1.001		0.268		0.999		0.997		0.003
4.500	1.000		0.267		1.000		1.000		0.000

G8H

0.001	0.966		0.262		0.749		0.844		0.131
0.250	0.990		0.278		0.847		0.877		0.114
0.500	0.995		0.281		0.884		0.900		0.094
1.000	1.001		0.285		0.927		0.923		0.076
1.500	1.002		0.286		0.947		0.940		0.059
2.000	1.004		0.287		0.966		0.952		0.049
2.500	1.000		0.284		0.971		0.970		0.029
3.000	1.002		0.286		0.983		0.976		0.024
3.500	0.999		0.284		0.986		0.988		0.011
4.000	1.001		0.285		0.999		0.994		0.007
4.500	1.000		0.284		1.000		1.000		0.000

G8V

0.001	0.964		0.257		0.748		0.850		0.122
0.250	0.970		0.262		0.804		0.892		0.086
0.500	0.979		0.268		0.850		0.915		0.070
1.000	0.987		0.273		0.897		0.938		0.053
1.500	0.991		0.276		0.927		0.955		0.039
2.000	0.991		0.276		0.942		0.973		0.021
2.500	0.996		0.279		0.965		0.979		0.019
3.000	0.998		0.281		0.978		0.985		0.014
3.500	0.998		0.281		0.984		0.990		0.008
4.000	0.999		0.281		0.991		0.996		0.003
4.500	1.000		0.282		1.000		1.000		0.000

crack of any convex shape as long as ϵ is defined in terms of area (A) and perimeter (P) such as, $\epsilon = (2N/\pi) (A^2/P)$ where N is the no. of cracks per unit volume.

Table 5-1 indicates that crack-density generally decreases with pressure and appears to be higher in saturated samples than in dry cores. This could be a consequence of saturation by vacuum-pumping, a process which sucks water into cracks and may widen or lengthen the existing cracks. Similar observation was noted and illustrated in Fig. 5 of Hadley (1976). Generally, crack-density ≥ 0.2 implies that the rocks are densely cracked (OB, 1974). In a later section, the calculated crack-density will be compared with that estimated from an SEM micrograph of one of the samples.

One anomalous behaviour of velocities in some saturated rocks (ref. Ch. 3) is reflected in the increase of Poisson's ratio with pressure. From Table 5-1, this increase can be correlated with increase in the normalised ratio \bar{V}_p/\bar{V}_s with pressure. It is suspected that partial saturation may be responsible. For such interpretation of measured velocities, OB (1974) proposed a plot of \bar{V}_p/\bar{V}_s versus \bar{V}_s , Fig. 5-1 is such a plot reproduced from the authors' publication of 1974. Similar plots from the present laboratory measurements are shown in Fig. 5-2. Superposing the latter on the cross plots of OB in Fig. 5-1, it can be observed that samples nos. G5N₁ and G5H appear to be less than 50% saturated, while G5V for which σ decreases with pressure follows/...

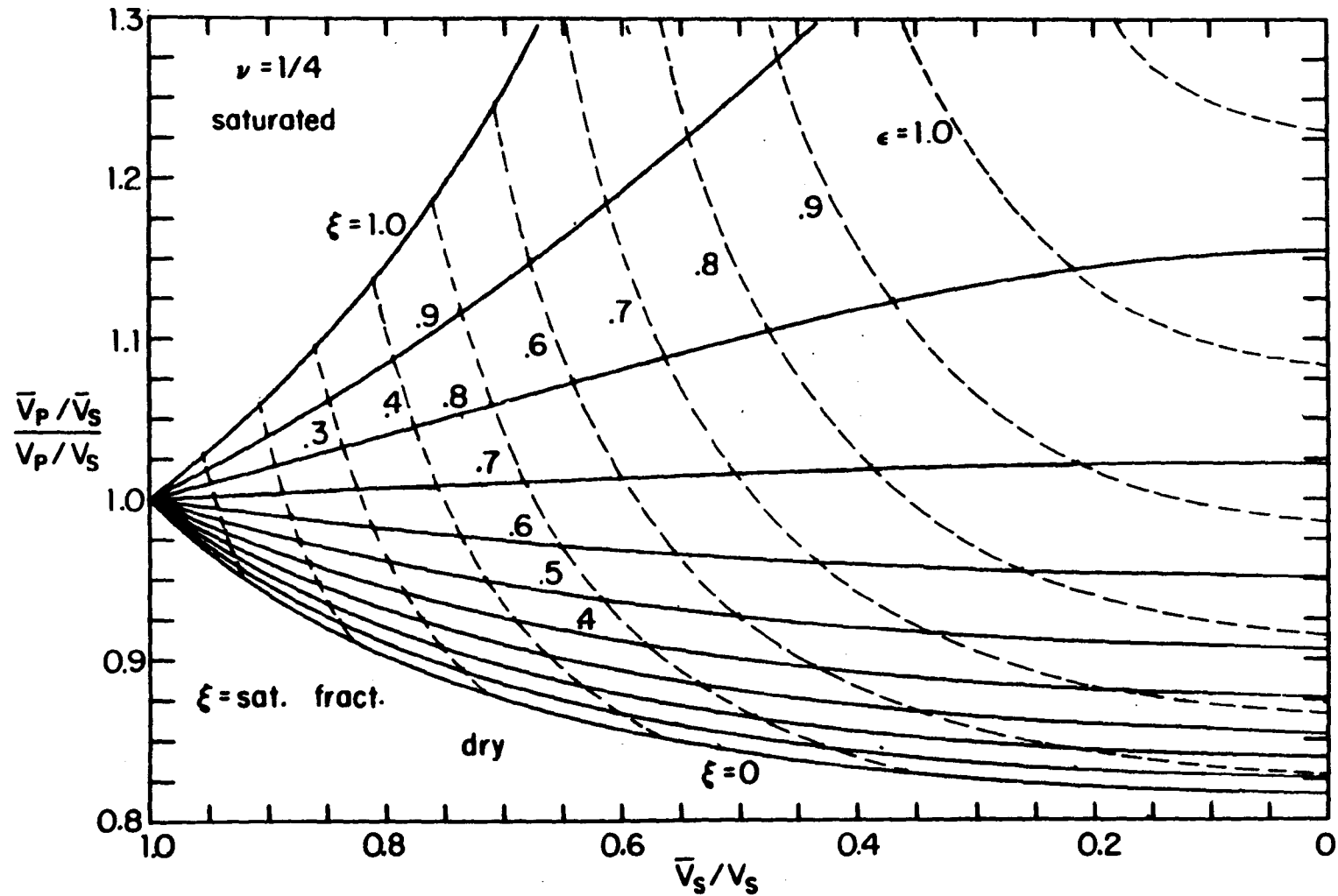


Fig. 5-1. The velocity ratio $(\bar{V}_P/\bar{V}_S)/(V_P/V_S)$ versus shear wave velocity \bar{V}_S/V_S for a partially saturated cracked solid for several values of the saturated fraction ξ . Contours of constant crack density $\epsilon = N(a^3)$ are shown as dashed lines. Measurement of \bar{V}_P/\bar{V}_P and \bar{V}_S/V_S for a real material specifies a point on this diagram from which both the crack density and degree of saturation may be determined. (after O'Connell & Budiansky, 1974).

WATER - SATURATED GREYWACKE

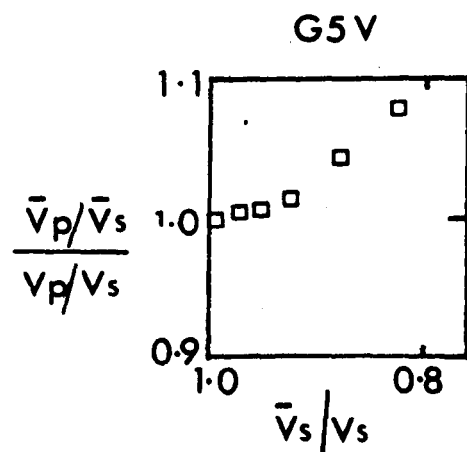
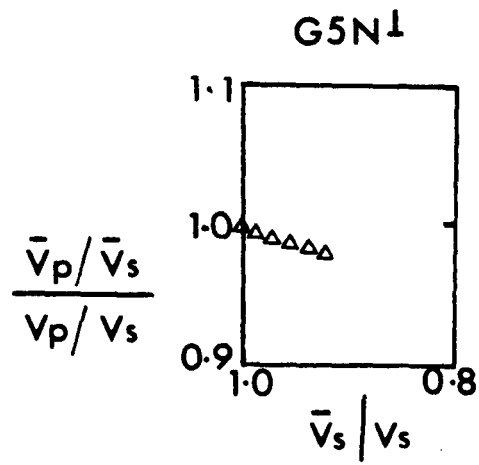
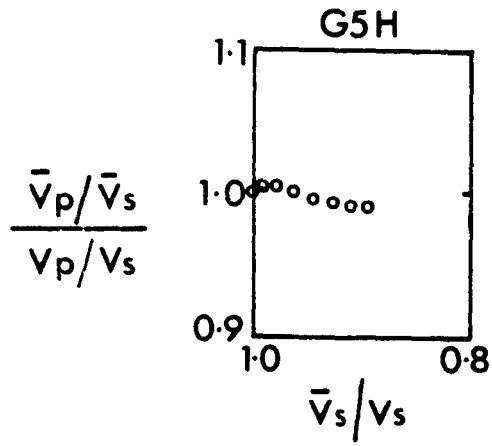


Fig. 5-2. \bar{V}_p/\bar{V}_s versus \bar{V}_s in the Southern Uplands greywackes

follows the contour of about 90% saturation.

It is recalled from Chapter 3 that partial saturation was suspected to be one of the causes of higher V_p in dry cores over saturated cores. Toksoz et al (1976), however, suggest that V_p and V_s depend on the aspect ratio (α) of the pores, that for spherical pores, the velocities are higher in gas-saturated rocks. The authors attribute this to rapid decrease of density than the elastic moduli upon gas saturation, resulting in higher velocities. [ref. $V_p = \left(\frac{K + 4/3\mu}{\rho} \right)^{1/2}$, where ρ is density]. This tends to indicate that higher V_p in dry shales and in some greywackes is also due to the presence of cavities of high aspect-ratio ($\alpha = 1.0, 0.1$). This is investigated in the next section using the theoretical formulations of Toksoz et al (1976) to determine the spectrum of cracks and their volume-concentration from the laboratory-measured velocities in the Southern Uplands greywackes.

5.3 Crack spectra from inversion of velocity data

The problem here is to find the crack/pore concentration versus aspect ratio spectrum of the Southern Uplands greywackes. Since the actual pore geometries in the rocks are unknown, the first step is to specify the aspect ratios of the cracks and pores in regular logarithmic intervals ($\alpha = 1 \times 10^{-4}$ to 1.3×10^{-2}). Then use is made of the formulation of Toksoz et al (1976) to determine the closure pressure/...

pressure (P_c) of each set of cracks of aspect ratio (α),

$$P_c = K.3\pi\alpha \frac{(1 - 2\sigma)}{4(1 - \sigma^2)}$$

(cf. $P_c = E\pi\alpha / 4 (1 - \sigma^2)$, Walsh (1965), where all terms above are defined in Appendix 2. Volume concentration is related to the effective moduli of the rock (Kuster & Toksoz, 1974), as presented also in Appendix 2. Results shown on Table 5-2 and Fig. 5-3a generally indicate a trend towards the abundance of equant-shaped cavities ($\alpha \geq 1 \times 10^{-2}$) in the greywackes. The reliability of this technique was tested by inverting the velocity data from a sample of Chelmsford granite to obtain its crack-spectrum and the corresponding volume concentrations. Low-aspect ratio cracks are observed to be more abundant (Fig. 5-3b) in the granite. The different trends observed for the greywacke and granite are consistent with their different origins (sedimentary and igneous respectively).

It should be noted that the aspect ratios obtained and specified above are useful parameters with which to describe the physical properties of the rock, and do not necessarily represent the actual crack-shape distribution. This is so because the mathematical models available usually deal with cracks that are simplified in shape or non-interacting. Thus predictions based on generalised crack models can be expected to have limitations. It follows then that the inversion from elastic property measurements to crack-shape distribution is not unique (Mavko & Nur, 1978).

/.....

Table 5-2 : Crack aspect ratio spectrum versus volume concentration
[V(α)] in Southern Uplands greywackes.

Aspect ratio α	G4N _L		G4H		G4V	
	V(α) $\times 10^{-3}$		V(α) $\times 10^{-3}$		V(α) $\times 10^{-3}$	
	Saturated	Dry	Saturated	Dry	Saturated	Dry
1 $\times 10^{-4}$	-0.0551	-2.200	-0.0543	1.330	-0.0252	-4.600
2 $\times 10^{-4}$	0.111	4.240	-0.0605	0.878	0.0111	7.060
4 $\times 10^{-4}$	-0.00356	0.934	0.0411	0.0396	0.0408	0.0459
8 $\times 10^{-4}$	0.0858	0.599	0.0538	0.334	0.00815	1.17
16 $\times 10^{-4}$	0.307	0.531	0.168	0.946	0.124	1.080
32 $\times 10^{-4}$	0.180	0.771	0.698	0.243	0.543	0.361
64 $\times 10^{-4}$	0.477	0.690	0.883	1.390	0.990	0.492
128 $\times 10^{-4}$	0.0580	0.0513	0.0614	0.266	0.0633	0.0989
	G5N _L		G5H		G6V	
1 $\times 10^{-4}$	-0.0852	-0.930	0.170		-0.176	0.697
2 $\times 10^{-4}$	0.194	0.736	0.640		1.33	-0.959
4 $\times 10^{-4}$	0.806	1.80	-0.780		-3.23	-0.135
8 $\times 10^{-4}$	1.38	-0.690	1.63		2.03	1.490
16 $\times 10^{-4}$	2.10	0.219	2.74		0.190	0.286
32 $\times 10^{-4}$	0.828	3.78	4.01		2.17	0.00590
64 $\times 10^{-4}$	5.48	1.92	4.69		3.80	2.03
128 $\times 10^{-4}$	12.10	3.22	6.42		3.67	3.54
	G6N _L		G6H		G6V	
1 $\times 10^{-4}$	0.00958	-1.61	-5.32	0.105	0.662	0.247
2 $\times 10^{-4}$	-0.00547	9.77	5.87	0.675	1.155	0.673
4 $\times 10^{-4}$	0.170	3.25	0.742	1.970	0.389	1.13
8 $\times 10^{-4}$	0.572	3.43	1.08	-0.00521	2.40	3.61
16 $\times 10^{-4}$	1.04	2.41	1.99	0.330	2.09	0.391
32 $\times 10^{-4}$	1.60	1.77	1.10	3.00	2.49	2.02
64 $\times 10^{-4}$	2.52	2.66	0.00792	2.17	0.0444	0.0048
128 $\times 10^{-4}$	2.15	0.793	0.0368	0.227	0.113	2.05
	G8N _L		G8H		G8V	
1 $\times 10^{-4}$	0.00733		-0.00684		-0.00787	
2 $\times 10^{-4}$	0.0816		0.370		0.0412	
4 $\times 10^{-4}$	0.241		0.492		0.126	
8 $\times 10^{-4}$	0.428		0.461		0.198	
16 $\times 10^{-4}$	0.685		0.506		0.298	
32 $\times 10^{-4}$	0.542		0.614		0.481	
64 $\times 10^{-4}$	0.334		0.596		0.546	
128 $\times 10^{-4}$	0.000686		0.0587		0.0249	

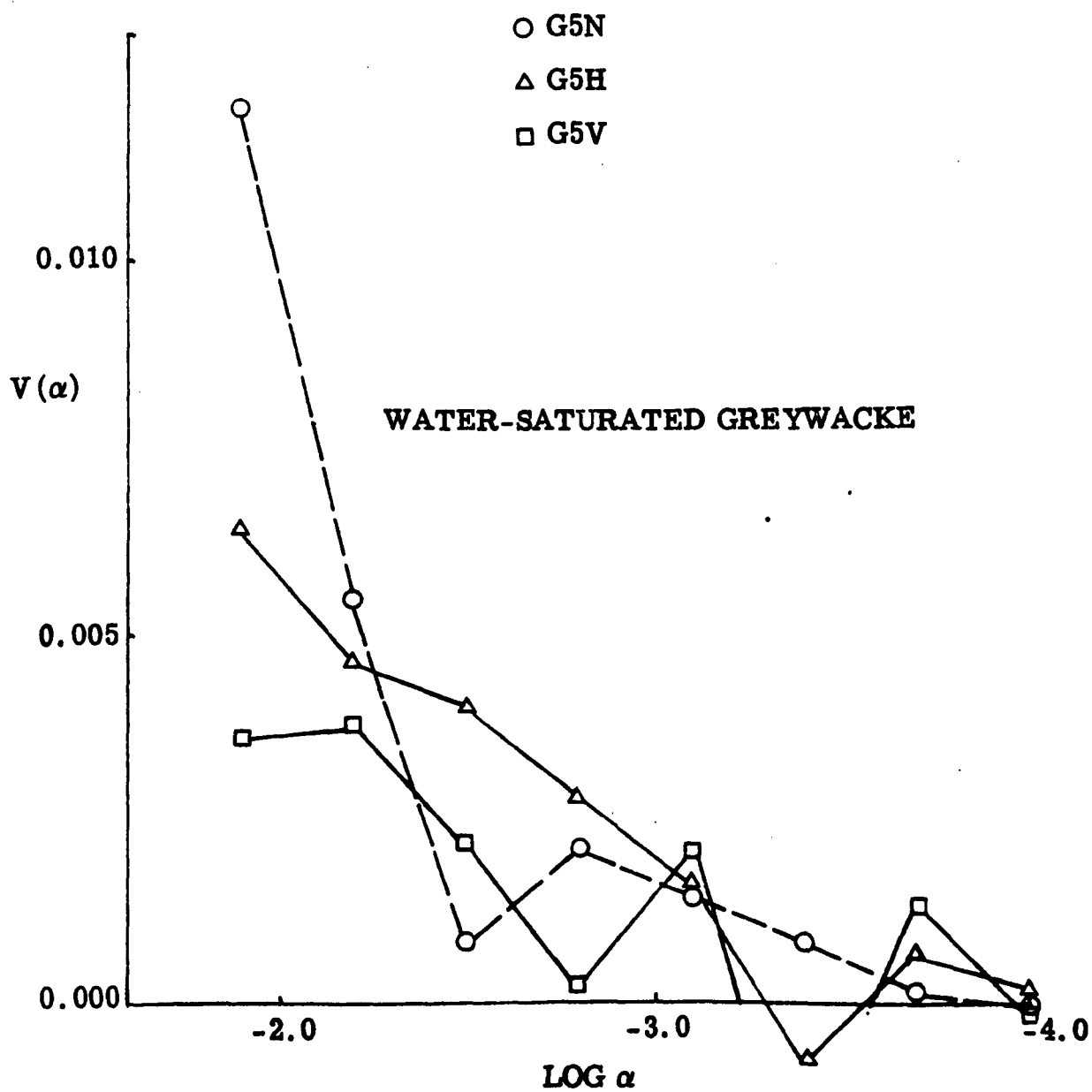
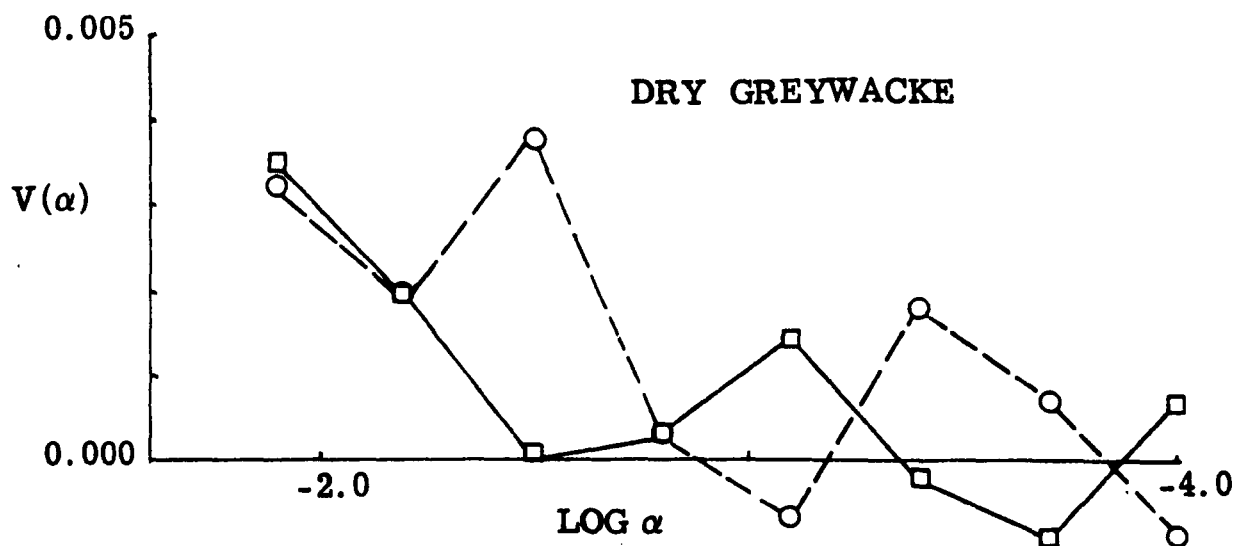
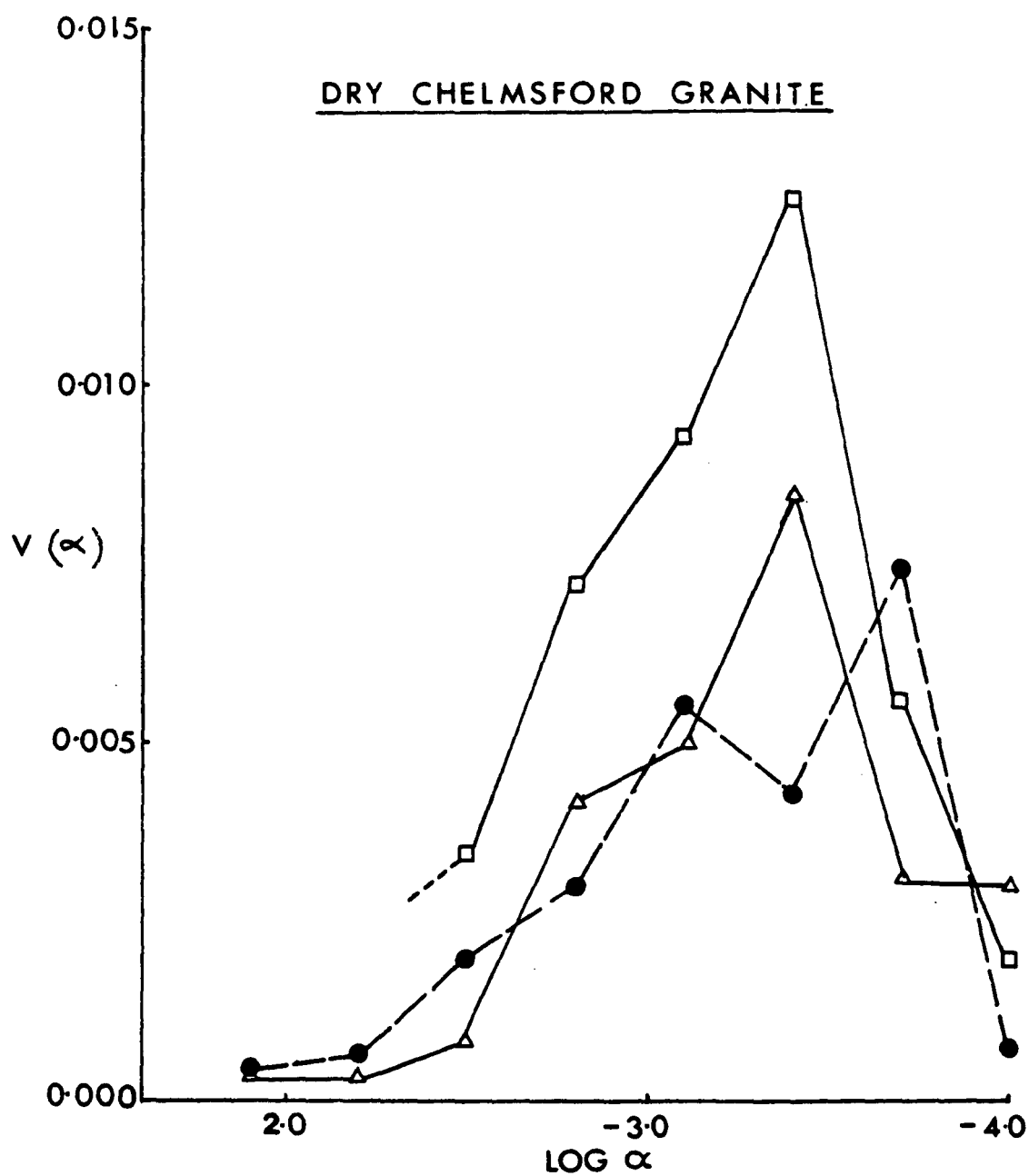


Fig. 5-3a

Crack volume-concentration versus aspect ratio ($\text{Log } \alpha$) for greywacke.



● Sample N^o. 16X

△ " " 16Y

□ " " 16Z¹

$V(\alpha)$ = Volume Concentration.

Fig. 5-3b. Crack volume-concentration versus aspect ratio (Log α) for Chelmsford granite.

The foregoing techniques are indirect methods of characterising cracks in rocks. It is possible to check on the information obtained by direct examination of the cracks through the scanning electron microscope (SEM). Crack density and pore-aspect ratios can be determined from SEM micrographs of rocks, but first a brief description of the cracks under the SEM follows.

SEM examination of the Southern Uplands greywackes

Direct information on the nature of cracks can be obtained by means of the scanning electron microscope (SEM) [e.g. Brace et al, 1972; Sprunt & Brace, 1974; Simmons & Richter, 1976; Richter & Simmons, 1977; Batzle et al, 1980; and Atkinson, 1981]. Different cracks seen in the present greywackes are shown in Plates 1 - 4.

Grain boundaries are preferred sites for crack-like flaws, but in the present greywackes, cavities whose cross-sections are equant are abundant along grain-boundaries, sometimes alternating with slots of materials (Plot 1). It is not known whether these equant-shaped cavities are tubular or more spherical, but Plates 2a & b suggest that the cavities extend into the mineral grains. In Plate 2a the longest dimension [AB] of the cavity = 17μ
the widest path [CD] = 14μ
the aspect ratio (α_{\max}) is about 0.8
the shortest path [EF] = 1.7μ
. . the minimum aspect ratio (α_{\min}) = 0.1.

/...

Similar calculation for Plate 2b gives $\alpha_{\max} = 0.6$ and $\alpha_{\min} = 0.1$. This supports the findings from velocity inversion of the abundance of cavities with near spherical cross-sections. However, some cracks are elongate in section. In Plates 3 and 4, the boundaries between a quartz grain and the surrounding feldspar grains are marked by flat cracks. In Plate 3, the grain-boundary crack (GBC) on the left-hand side appears to be sealed while the one to the right remains open at the lower portion. As done for cavities in Plates 2 a and b, the lengths and widths of these flat cracks in Plate 3 were measured, and the aspect ratio (α) was calculated to be about 6×10^{-3} . These values of α could be less if the mosaic in Plate 3 had been complete. When such flat cracks (perhaps with smaller aspect ratios) are oriented along bedding planes in situ, velocities measured normal to the plane of the cracks are less than velocities measured parallel to the plane. This hypothesis is investigated in section 5-4 where cracks are oriented to produce anisotropy in the greywackes. First, Plate 4 is used to estimate crack-density which is compared with that calculated from the self-consistent theory (O'Connell & Budiansky, 1974).

Estimation of crack-density (ϵ) from SEM micrograph.

In the present work, cracks have been noted to affect the behaviour of velocities in the Southern Uplands rocks. The/...

The variation of seismic velocities with pressure are due to variation in crack-density with pressure. Crack-densities in the greywackes have been estimated by the self-consistent approximation. The reliability of such estimation is to be tested by comparison with ϵ estimated from the SEM micrograph in Plate 4.

The crack density of a rock can be defined as,

$$\epsilon = (2N/\pi) (A^2/P) \text{ (O'Connell \& Budiansky, 1974)}$$

where A is the area defined by πab , P is perimeter of the crack, given by $4aE(K)$, where E(K) is an elliptic integral (OB, 1974) defined in the Appendix and N is the no. of cracks per unit volume.

Generally, there is no information on the 3rd dimension of the cracks, thus the above formulation cannot be used to estimate ϵ .

However, Hadley (1976) has derived two statistical formulations by which ϵ can be determined from two-dimensional micrographs.

Equation (5) of Hadley (1976) is here used to estimate ϵ from Plate 4. For cracks of various sizes and shapes, with $\alpha < 0.1$,

$$\epsilon = 3M\langle a^2 \rangle / (4\pi)$$

where α is aspect ratio (i.e. ratio of crack width to crack-length)

$\langle a^2 \rangle$ is the average of the squares of the crack lengths, and,

M is the no. of crack traces per unit area.

A single crack, as defined by Hadley, is any open flaw of aspect ratio < 1 , which does not change orientation by more/...

more than 20° over any significant portion of its length, and which is either continuously open or bridged by material of exposed thickness not greater than 3 crack-widths or one-tenth of the total crack-length, whichever is less. Results of the calculations are presented below,

No of cracks traced = 22

Total area of micrograph covered = 21870.0 μ^2

Number of crack traces per unit area (M) = $10.06 \times 10^{-4} \mu^2$

(Any visible crack [as defined above] is taken to be a trace.

The total no. of cracks is divided by the total area to obtain M).

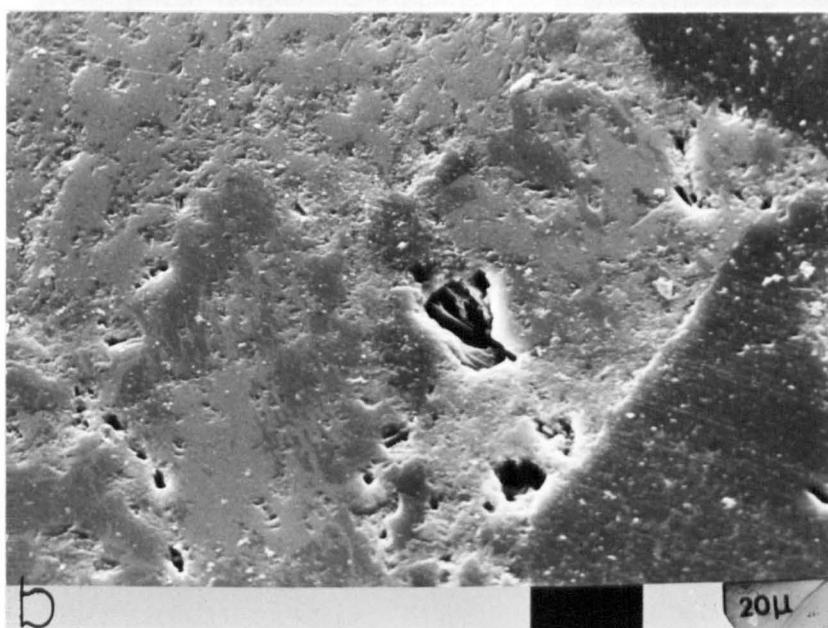
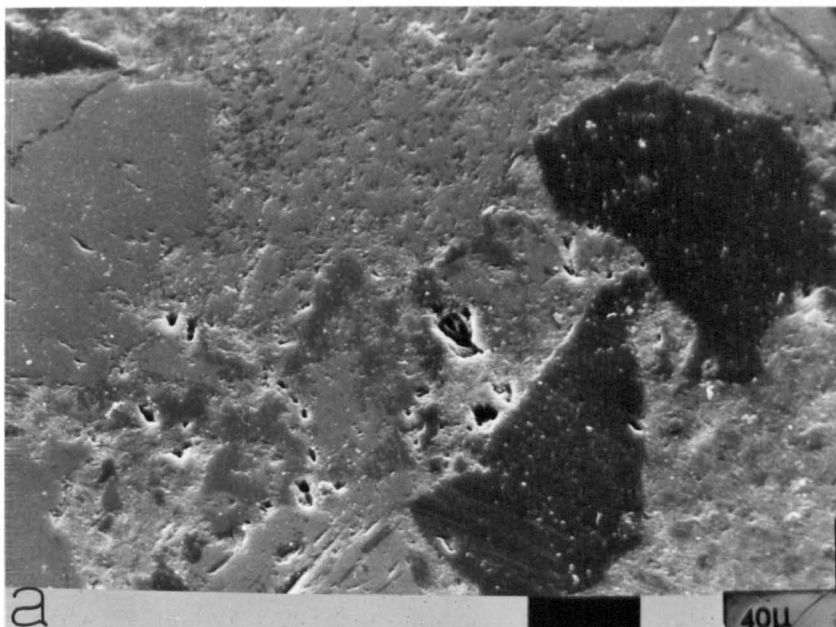
Mean of the squares of crack-lengths $\langle a^2 \rangle = 1367.55 \mu^2$

Estimated crack-density (ϵ) = 0.33

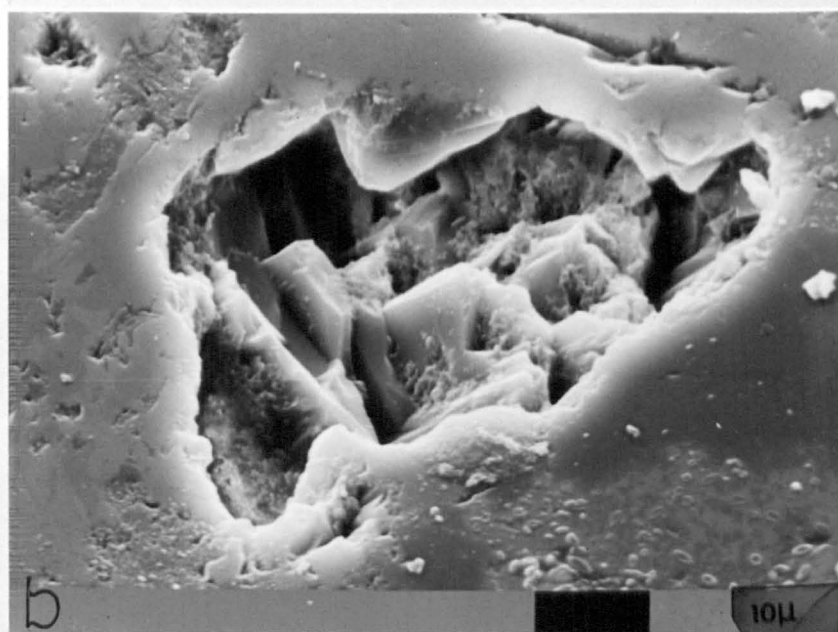
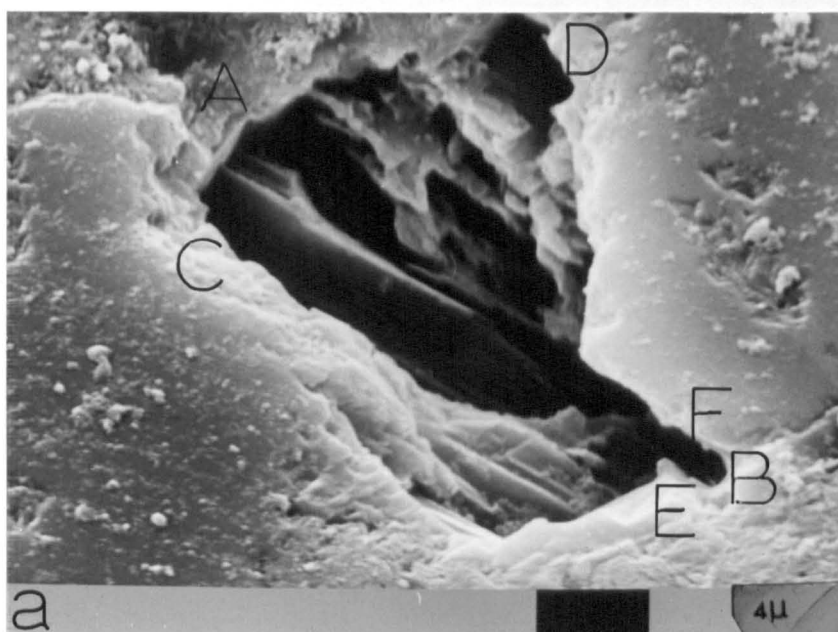
Since the crack-section of the greywackes were viewed at zero-pressure under the SEM, the estimated crack-density (ϵ) is considered to be that at atmospheric pressure. From the self-consistent approximation, 0.22 and 0.23 are obtained for the same sample G5H in dry and saturated conditions. The difference of about 0.1 between SEM-estimated ϵ and that calculated from velocity data may not be significant in view of the large uncertainties involved in low-pressure measurements.

In the next section, flat cracks which are considered to cause directional variation of velocities in situ, are re-oriented to produce velocity anisotropy in an otherwise isotropic greywacke.

/...



Plates 1a, b : Equant-shaped pores alternating with slots of material along grain-boundaries - an example of healed cracks.



Plates 2a & b : Plate 2a is a magnification of Plates 1a & b to reveal the internal structure of the cavity in the centre of micrographs. The cavities appear to be tubular. 2b shows another cavity which contains other pores that extend into the mineral.

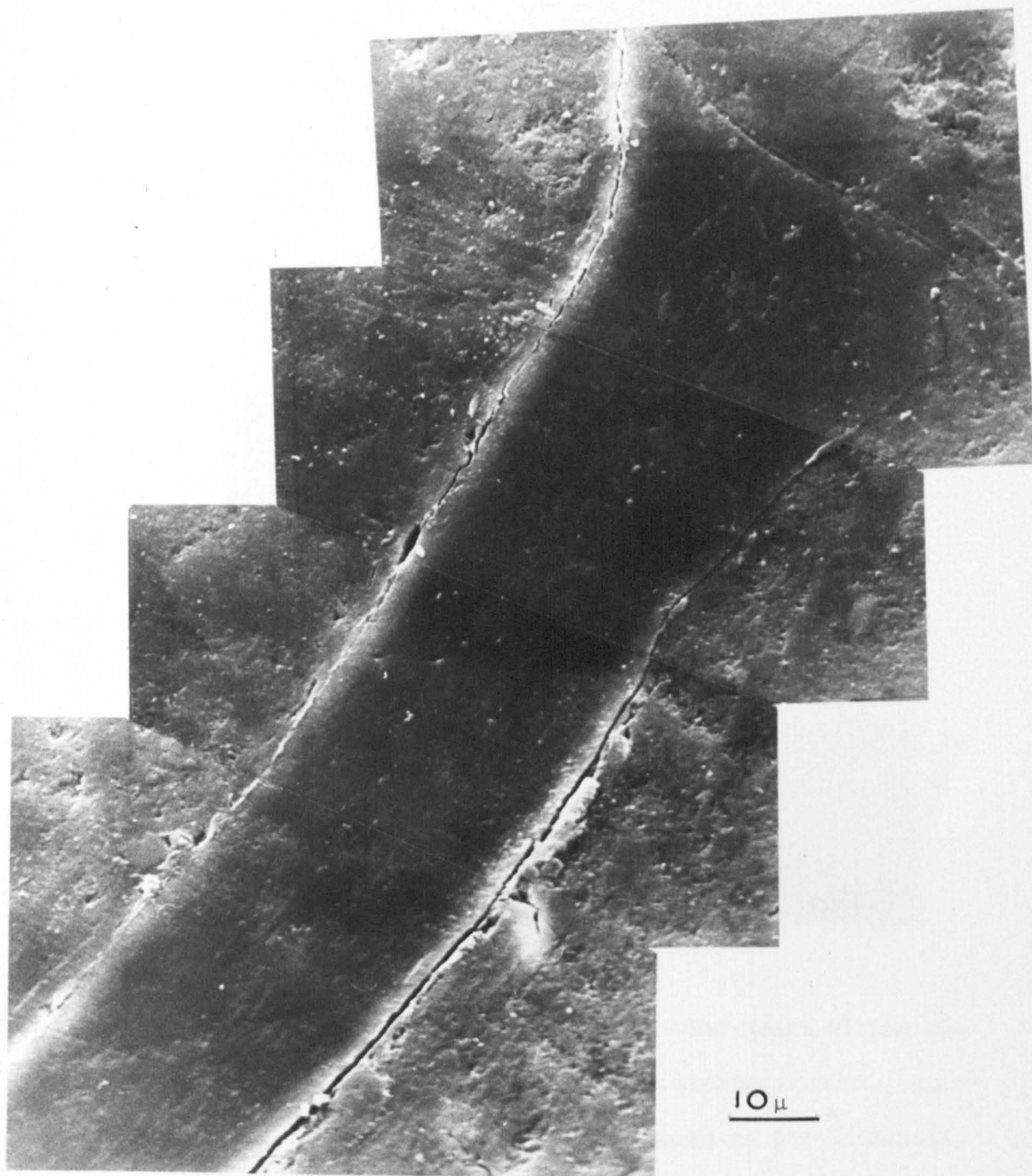



Plate 3  : The mosaic shows that not all cracks in the Southern Uplands greywackes are equant-shaped. Some are elongate in X-section. The long grain-boundary crack (GBC) to the right of the micrograph₃ is considered to have aspect ratio of about 6×10^{-3} to 9×10^{-3}

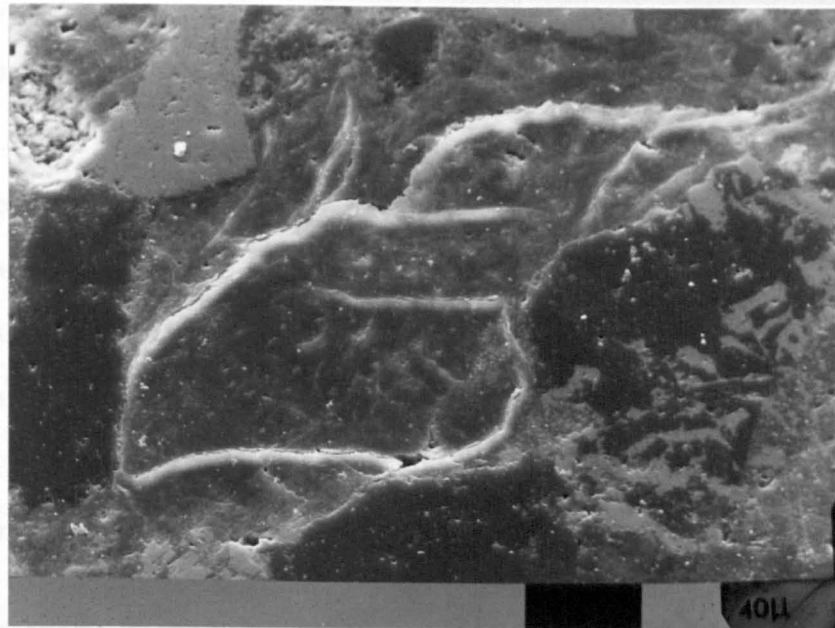


Plate 4: Illustrated here, is a cracked grain within non-cracked grain (Simmons and Richter, 1976). The cracks are termed dPdT caused by the different crystallographic orientations of the two grains with respect to the common grain-boundary. The crack-density from this micrograph is estimated (Hadley, 1976) to be 0.33.

5.4 Anisotropy from oriented cracks in the greywackes.

Most of the theoretical works available to date assume random orientations of cracks and grains in a rock, i.e. isotropy. Real rocks can be expected to be anisotropic due to preferred orientation of cracks. The overall elastic symmetry of a material containing parallel flat cracks is transversely isotropic (Postma, 1955; see also Chapter 1) and only five elastic constants are independent.

In this examination of greywackes in the laboratory, preferred orientations of minerals and cracks are not obvious because no systematic anisotropy is observed in laboratory measurements of velocities. This is in contrast to the velocity anisotropy observed at EKA and Girvan (from hammer lines). Attempt is made here to explain the EKA data and hammer line observations using the laboratory measured velocities in a greywacke that is permeated by additional oriented cracks.

In order to model anisotropy due to oriented cracks, the elastic equations for a transversely isotropic medium are restated and re-expressed as linear compressibilities in X, Y(//) and Z (\perp) directions. The new expressions of linear compressibility are then used to estimate $V_{p_{x,y}}$ and V_{p_z} (\perp) which define anisotropy.

The modelling is done by calculating from velocity measurements/...

measurements, the three equal linear compressibilities and the equivalent linear porosities (Aist) for the isotropic 'laboratory' greywacke; then additional linear porosities are added or subtracted in multiples of 'Aist' to simulate different mixtures of isotropic and oriented cracks. The velocities are then recalculated. Cross-plots of velocities parallel and normal to bedding, plotted as functions of linear porosities are then used to model field observations. The derivation of the relevant equations is presented below,

The elastic equations for a material with circular symmetry are, (Jaeger, 1974),

$$\begin{aligned}\sigma_x &= C_{11} \epsilon_x + (C_{11} - 2C_{66})\epsilon_y + C_{13} \epsilon_z \\ \sigma_y &= (C_{11} - 2C_{66}) \epsilon_x + C_{11} \epsilon_y + C_{13} \epsilon_z \\ \sigma_z &= C_{13} \epsilon_x + C_{13} \epsilon_y + C_{33} \epsilon_z\end{aligned}$$

Suppose $\sigma_x = \sigma_y = \sigma_z = P$, it follows then the

$$\epsilon_x = \epsilon_y (= \epsilon)$$

$$\text{Since } (C_{11} - 2C_{66}) = C_{12},$$

$$P = (C_{11} + C_{12}) \epsilon + C_{13} \epsilon_z \dots \dots \dots (1)$$

$$P = 2 C_{13} \epsilon + C_{33} \epsilon_z \dots \dots \dots (2)$$

(1) and (2) can be solved simultaneously to give,

A. Linear compressibility in x, y direction as,

$$\frac{\epsilon}{P} = \frac{C_{33} - C_{13}}{C_{33} (C_{11} + C_{12}) - 2C_{13}^2} \dots \dots \dots (3)$$

B./...

B. Linear compressibility in Z direction as,

$$\frac{\epsilon_z}{P} = \frac{2C_{13} - (C_{11} + C_{12})}{C_{33} (C_{11} + C_{12}) - 2C_{13}^2} \dots\dots\dots (4)$$

(3) and (4) are similar to equations (10) and (11) of Rundle & Schuler (1981).

Assuming $C_{12} = PR C_{11}$ (where PR is Poisson's ratio)

$$C_{13} = \frac{PR}{2} (C_{33} + C_{11})$$

and substituting in (3) and (4) above,

$$\frac{\epsilon}{P} = \frac{C_{33} - \frac{PR}{2} (C_{33} + C_{11})}{C_{11} C_{33} (1 + PR) - \frac{PR^2}{2} (C_{33} + C_{11})^2} \dots\dots\dots (5)$$

$$\frac{\epsilon_z}{P} = \frac{C_{11} - PR C_{33}}{C_{11} C_{33} (1 + PR) - \frac{PR^2}{2} (C_{33} + C_{11})^2} \dots\dots\dots (6)$$

when $C_{11} = C_{33}$, the medium is isotropic, and

$\frac{\epsilon}{P} = \frac{\epsilon_z}{P}$. Thus linear compressibility in any direction X,Y,Z can be expressed as,

$$\frac{\epsilon}{P} = \frac{(1 - PR)}{C_{11} (1 + PR - 2PR^2)}$$

where $C_{11} = C_{33}$

and PR is Poisson's ratio.

With substitution of real values for $\frac{\epsilon}{P}$, $\frac{\epsilon_z}{P}$ from the laboratory velocity data, $V_{P_{x,y}}$ and V_{P_z} can now be estimated. First, isotropic linear compressibilities (β_{ist}) calculated from the mean velocities in the laboratory, are plotted/...

plotted against pressure (Fig. 5-4). β_f is the high-pressure compressibility when the cracks are closed. The area under curve 1 gives the linear porosity (A_{ist}) at 1 bar. Volume porosity is assumed to be $3 \times A_{ist}$. By orienting the cracks normal to the unique axis Z (\perp), the area under curve 2 also must be $3 \times A_{ist}$. Thus compressibility in Z direction is,

$$\beta_{\perp} = \beta_f + 3 (\beta_{ist} - \beta_f) \dots\dots\dots (7)$$

[where $A_{ist} = (\beta_{ist} - \beta_f)$]

Starting with this model in which all cracks are oriented in one direction, equations (5) and (6) are used to estimate the elastic constants C_{11} and C_{33} .

$$C_{11} = \rho V_{p_{//}}^2 \quad (\text{Postma, 1955; Levin, 1980})$$

$$C_{33} = \rho V_{p_{\perp}}^2$$

where ρ is density = 2.7 Mg/m^3

and $V_{p_{//}}$, $V_{p_{\perp}}$ are respectively $V_{p_{xy}}$, V_{p_z} .

PR in this case is taken as 0.26 ± 0.03 (s.d.).

The results are summarised in Table 5-3 and Fig. 5-5a & b: Figures 5-5a & b have been produced by plotting each pair of composite velocities ($V_{p_{//}}$, $V_{p_{\perp}}$) obtained from a combination of linear porosities in X, Y ($//$), and Z (\perp) directions. Points of equal velocities are then contoured to give the thick curves ($V_{p_{//}}$) and the dashed curves ($V_{p_{\perp}}$). Field values from hammer line and EKA experiments are indicated by the shaded triangles. The triangles in Fig. 5-5a indicate the hammer line velocities of $[3.93(//), 3.36(\perp)]$ and/...

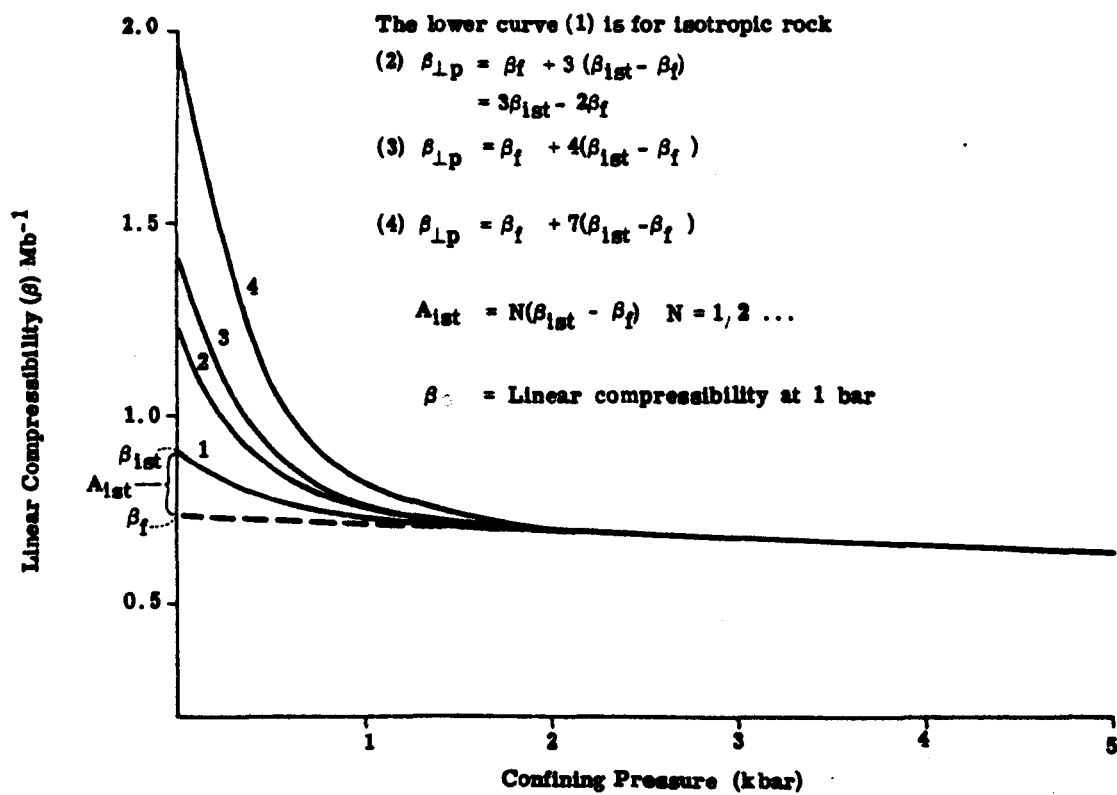


Fig. 5-4. Linear compressibility versus pressure in the Southern Uplands greywackes.

Table 5-3: Velocity anisotropy in the Southern Uplands greywackes with oriented cracks.

A = isotropic linear porosity $[(\beta_{ist} - \beta_f)]$, see Fig. 5-4]

and $\beta_{x,y}$ or $\beta_z = \beta_f + N(\beta_{ist} - \beta_f)$, $N = 0, 1, 2, \dots$

(A) The hammer line data

Linear porosity in X, Y direction	Linear porosity in Z direction	$v_{p_{x,y}}(//)$ km/s	$v_{p_z}(\perp)$ km/s	In-situ v_p km/s
—	3A	5.57	4.66	(i) $v_{p_{//}} = 3.93$ ± 0.14
—	4A	5.51	4.41	
—	7A	5.33	3.87	
A	3A	5.10	4.58	$v_{p_{\perp}} = 3.36$ ± 0.10
A	4A	5.05	4.34	
A	7A	4.91	3.81	
2A	4A	4.85	4.41	(ii) $v_{p_{//}} = 3.49$ ± 0.06
2A	8A	4.50	3.57	
2A	12A	4.37	3.16	
2A	16A	4.25	2.86	$v_{p_{\perp}} = 3.08$ ± 0.08
4A	8A	3.99	3.49	
4A	11A	3.92	3.18	
4A	12A	3.90	3.10	
4A	16A	3.81	2.82	
5A	16A	3.64	2.79	
6A	8A	3.63	3.42	
6A	10A	3.59	3.21	
6A	13A	3.54	2.97	
6A	14A	3.53	2.90	
6A	15A	3.51	2.84	
7A	14A	3.39	2.87	
A	A	5.17	5.17	
2A	2A	4.73	4.73	
3A	3A	4.38	4.38	
4A	4A	4.10	4.10	
5A	5A	3.87	3.87	
6A	6A	3.67	3.67	
7A	7A	3.50	3.50	
8A	8A	3.35	3.35	

Table 5-3 (cont'd)

(B) Eskdalemuir (EKA) data

Linear porosity X,Y direction	Linear porosity in Z direction	$V_{p_{xy}}$ (//) km/s	V_{p_z} (\perp) km/s
-	2.5A	5.64	4.92
-	3A	5.61	4.83
-	4A	5.56	4.55
-	6A	5.45	4.18
A	2A	5.24	4.97
A	3A	5.21	4.75
A	4A	5.17	4.55
A	5A	5.10	4.29
A	6A	5.06	4.12
2A	3A	4.85	4.64
2A	6A	4.74	4.07
3A	4A	4.53	4.35
3A	5A	4.50	4.18
3A	6A	4.47	4.02
A	A	5.28	5.28
2A	2A	4.89	4.89
3A	3A	4.57	4.57
4A	4A	4.30	4.30

Field velocities $V_{p_{//}} = 5.3$ km/s $V_{p_{\perp}} = 4.9$ km/s

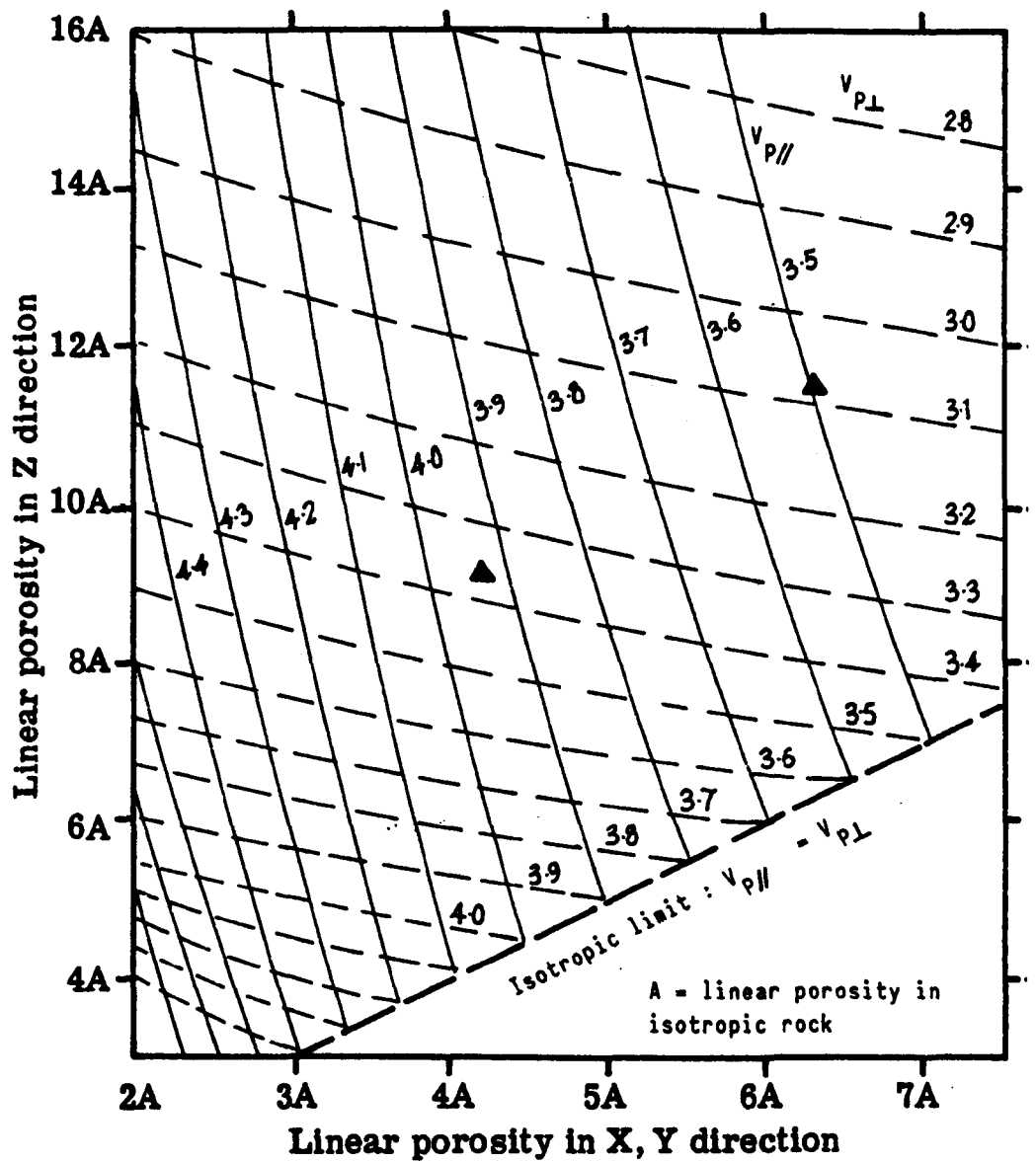


Fig. 5-5a Anisotropy modelling of hammer line data from oriented cracks in greywacke. Dashed curves correspond to contours of constant $V_{p\perp}$ normal to bedding. Continuous curves show contours of constant $V_{p\parallel}$ parallel to bedding. In-situ hammer line data are indicated by shaded triangles. The corresponding values are indicated in Table 5-3.

The dashed base line is the locus of points corresponding to isotropic velocities in the greywacke ($V_{p\parallel} = V_{p\perp}$)

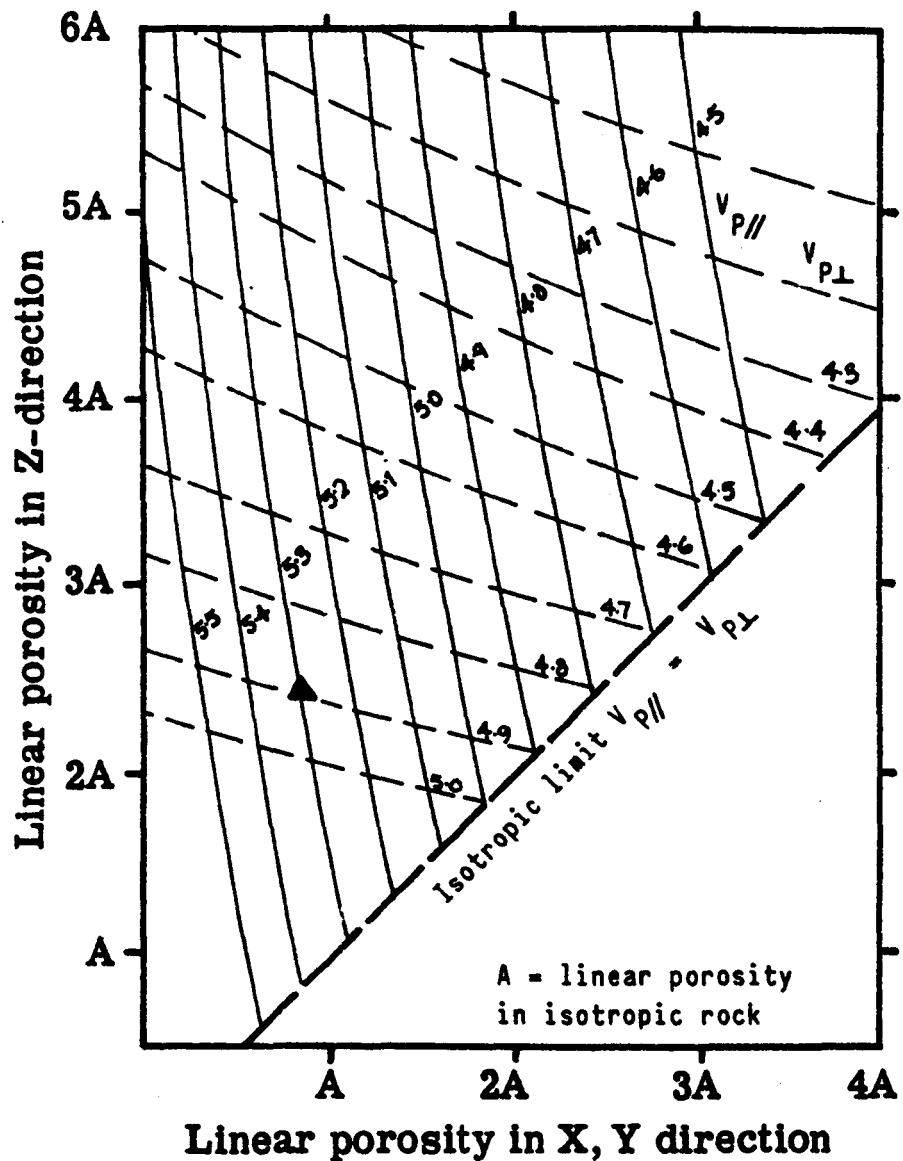


Fig. 5-5b. Modelling of EKA observed anisotropy from oriented cracks in greywacke. The contours are as described in Fig. 5-5a. The observed $V_{p//}$ and $V_{p\perp}$ at EKA correspond to the position of the shaded triangle. This suggests that more than twice the linear porosity in X,Y direction is required along Z direction in order to account for EKA data from laboratory measured velocities in greywacke. [c.f. Fig. 5-5a, linear porosity in both X,Y and Z (\perp) directions have decreased considerably from the surface, to the depth corresponding to EKA data].

and [3.49(//), 3.08 (L)] in the greywackes. In Fig. 5-5b EKA velocities are indicated by the triangle with coordinates [5.3(//), 4.9(L)]. The linear porosities corresponding to the hammer line data suggest that the Southern Uplands greywacke at the surface is densely cracked and most of the cracks are parallel to bedding. Down to a depth of 300m (at EKA), though more cracks still lie along bedding, porosity is reduced (due to overburden pressure) as indicated by the position of the triangle in Fig. 5-5b.

In comparison to laboratory velocities in greywacke, the relatively low V_p and large anisotropy observed in situ can be attributed to large fractures which lie mostly along the bedding planes of the rocks in situ.

5.5 Conclusions

The Southern Uplands greywackes can be considered anisotropic due to the preferred orientation of flat cracks in rocks in situ. The results from inversion of laboratory velocity data and SEM examination suggest that the size of such flat flaws is less than 1×10^{-2} .

Anisotropy modelling to depths greater than 300m is not considered here because field velocities (ref. LISP & Warner) are higher than laboratory values in greywacke. This may be due to change in lithology and so possible existence of igneous rocks at depth is discussed in the next chapter.

CHAPTER SIX DISTRIBUTION OF IGNEOUS ROCKS IN THE SOUTHERN
UPLANDS.

The mean greywacke velocity obtained from the laboratory is tolerably close to that of EKA at 300m depth. Beyond this depth, field observed values (e.g. LISPB, Warner's experiments) are consistently higher than laboratory values. It is then considered likely that deeper refraction lines in the Southern Uplands such as LISPB (Bamford et al 1976, 1977, 1978) and Southern Uplands Profile (Warner, 1981, pers comm.) are indicating Vp from igneous rather than sedimentary rocks. The following two sections deal with this consideration in detail.

6.1 Southern Uplands plutons : possible wide distribution at depth.

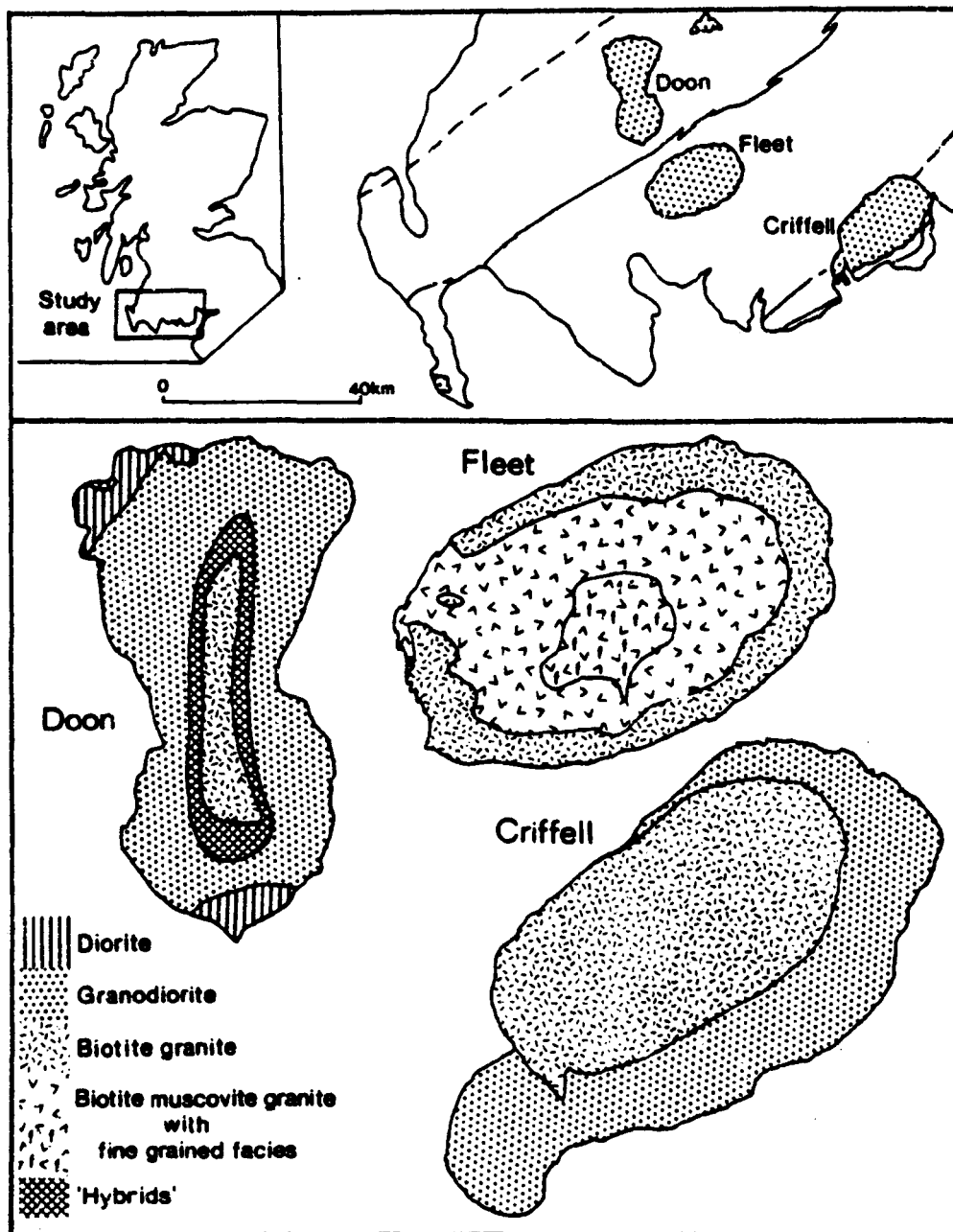
Three cores from a sample of Spango granodiorite yielded P-wave velocities that are higher than those in the Lower Palaeozoic greywackes, but are comparable to the mean in situ values obtained from LISPB and the current Southern Uplands profile. Granodiorite was chosen on account of its similarity in density to the greywackes. Thus its higher P-wave velocity was used as a diagnostic feature about the distribution of rocktypes with depth in the Southern Uplands. The extent of the distribution of the plutons at depth is hard to predict from the scope of the velocity data, but the prospect of their presence below the sediments is noted/...

noted also by Lagios & Hipkin (1979) who postulated from gravity studies that the whole of the Southern Uplands is underlain by a granite batholith.

The hand specimen of the granodiorite appears isotropic. This is supported by laboratory measured velocities in the orthogonal cores (ref. Chapter 3 Fig. 3-13 Table 3-1). The relatively lower P-wave velocity of 5.8 km/s (LISPB) approximately normal to strike could therefore be attributed to some strike parallel fractures in situ (as in the greywackes). It remains possible however that the velocity could change laterally due to lithologic changes or compositional variation within the same rock unit.

The Spango granitic mass is reported (Walker, 1928) to comprise mainly basic hornblende-biotite-granodiorite or quartz diorite in which andesine is usually thrice more abundant than orthoclase. The author's normative analysis of the rocks was compared to the norm of Deer (1935) on the igneous complex of the Cairnsmore of Carsphairn, (Fig. 6-1). The mineral group "5", corresponding to tonalite was considered closest to the mineral composition of Spango granodiorite. Deer provided the model analyses of various mineral groups some of which are reproduced below,

/...



Location and petrology of the three main Galloway plutons. Note that the three petrological maps are not on exactly the same scales. (Map of Doon area from Gardiner and Reynolds, 1932; map of Criffell-Dalbeattie complex from Phillips, 1956 – both reproduced by courtesy of the Geological Society of London. Map of Fleet area from Parslow, 1968 – reproduced by courtesy of Scottish Academic Press)

Fig. 6-1. (after Stephens & Halliday, 1979)

Modal groups of Cairnsmore Igneous Complex (Deer, 1935)

Mineral Constituent	3	5	7	9	Single crystal Vp (km/s)	Source*
Quartz	24.93	9.82	13.53	10.69	6.05	VRH
Orthoclase	26.70	15.44	13.30	13.19	6.02	VRH
Plagioclase	30.26	48.90	53.60	58.53	6.70	VRH
Biotite	14.57	16.44	11.81	12.34	5.26	VRH
Hornblende & pyroxane	3.54	9.40	8.26	5.32	6.93	VRH
Specific Gravity	2.71	2.75	2.71	2.66	* Taken mainly from Christensen (1965)	
Aggregate Vp km/s	6.14	6.31	6.34	6.38		

3 = Acid hybrid

5 = Tonalite

7 = Pyroxene-biotite hybrid

9 = Hornblende hybrid, green amphibolite stage.

From the % proportion of each mineral, an aggregate Vp was calculated for the crack-free rock using crack-free P-wave velocities (of each mineral) selected mainly from Christensen (1965). The averaging scheme used is,

$$V_p = (W_j/V_j)^{-1} \text{ (Birch, 1961; Hall \& Al Haddad, 1979)}$$

where Vp is the velocity of the aggregate in terms of the component minerals, Wj is fractional volume of rock occupied by the jth mineral of which velocity is Vj.

The/...

The above table shows that Vp varies as the proportions of the component minerals are varied from almost pure granite to more basic hornblende hybrid. Similar variation in the rocks in situ may be expected in the Southern Uplands. It is noted that the calculated aggregate velocities are higher than the laboratory measured Vp (≈ 6.0 km/s at 5.0kbar). This is so because laboratory cores are not crack-free even at high pressures, and furthermore, the laboratory cores were run dry which may have reduced the measured velocities. However, the closeness of the measured Vp to the values from LISPB-Warner's field experiments tends to suggest the possible existence of the granitic plutons below the Lower Palaeozoic sediments. Parslow (1968) postulated a gravity model which depicts the plutons as an intrusive top of a large batholith (see also Lagios & Hipkin, 1979). Furthermore, Stephens & Halliday (1979) consider that the diorites and granodiorites of the Southern Uplands were derived from a basaltic part of the lower crust. It is therefore considered that the Lower Palaeozoic sediments are intruded and underlain by the 'thick' a0 layer (Bamford et al, 1977, 1978) which consists, in part, of granitic rocks. The lower level of the a0 layer is not indicated on LISPB, although Jacob (1969) observed a 6.4 km/s layer at a depth of 12 km. This is further considered in the next section where the plutons are considered to top a crust similar in rock composition to ophiolite rocks.

/...

6-2 Probable presence of ophiolite rocks at depth in the Southern Uplands.

A notable example of the Southern Uplands igneous rocks is the Ballantrae Igneous Complex (Fig. 6-2a; see also Chapter 2, Fig. 2-5b). All main components of a typical ophiolite are recognizable, but due to poor exposure and intensity of post-emplacement Caledonian deformation (Church & Gayer, 1973), it is difficult to find a continuous ophiolite sequence within the Ballantrae Complex. However, comparison with the Bay of Islands ophiolites which are considered as typical examples of Lower Palaeozoic ophiolites (Church & Gayer, 1973) revealed similarity in rock composition to Ballantrae igneous rocks. The authors suggested that the high temperature nature of the Ballantrae ophiolite is in accord with the interpretation that it originated as a small ocean basin.

There is lithological similarity of the Ballantrae to the Bay of Islands ophiolite sequences (Fig. 6-2a, b, c). The following units of rocks are found at Ballantrae:

- (i) Pillow lavas
- (ii) Fragments of volcanic and diabasic rocks
- (iii) Sheeted diabase
- (iv) Gabbro, and
- (v) other cumulate rocks.

The lithological similarity and the fact that the Ballantrae/...

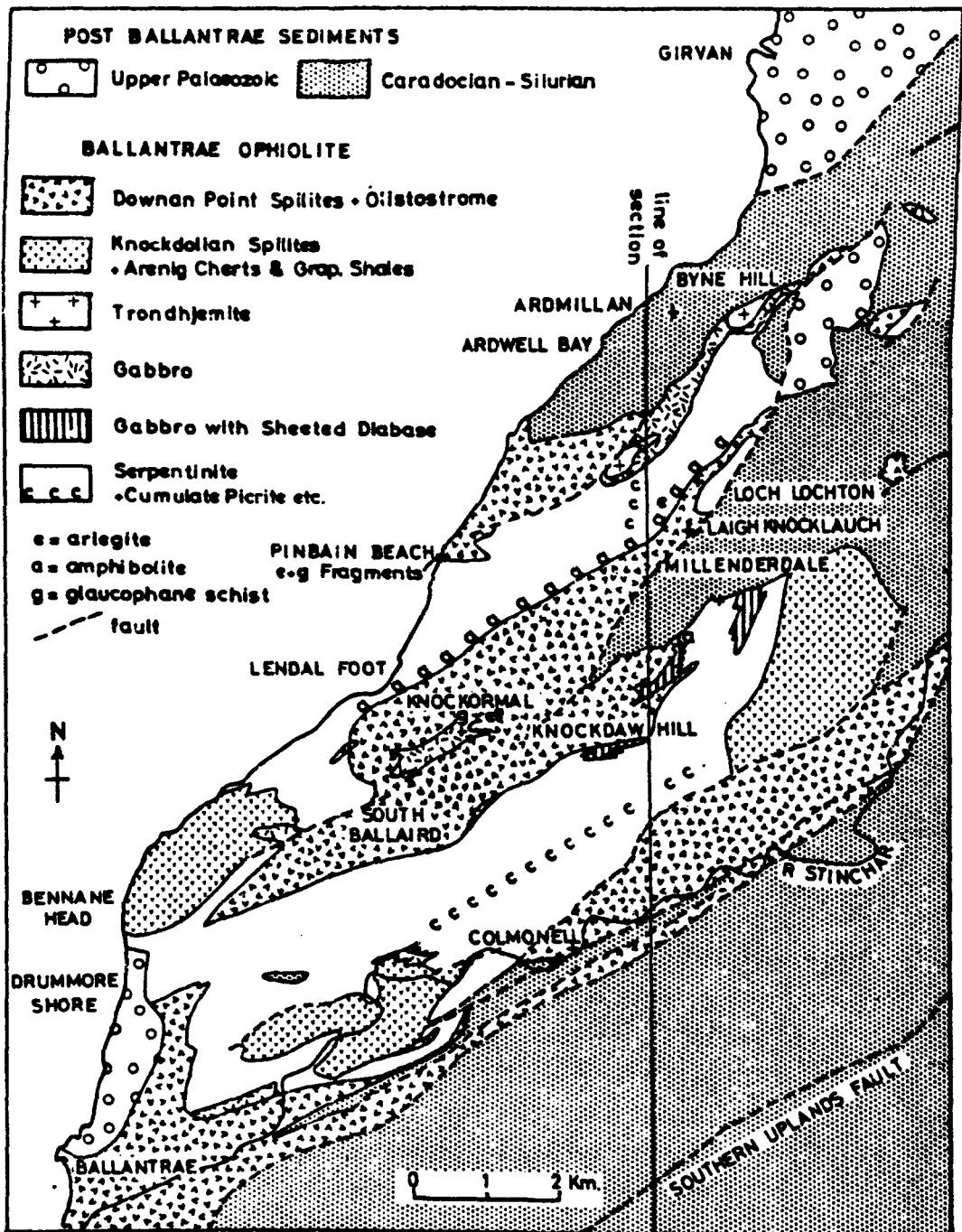


Fig. 6-2a . Geologic sketch map of the Ballantrae region, modified from Fig. 2. Bailey & McCallien (1957).
(after Church & Gayer, 1973)

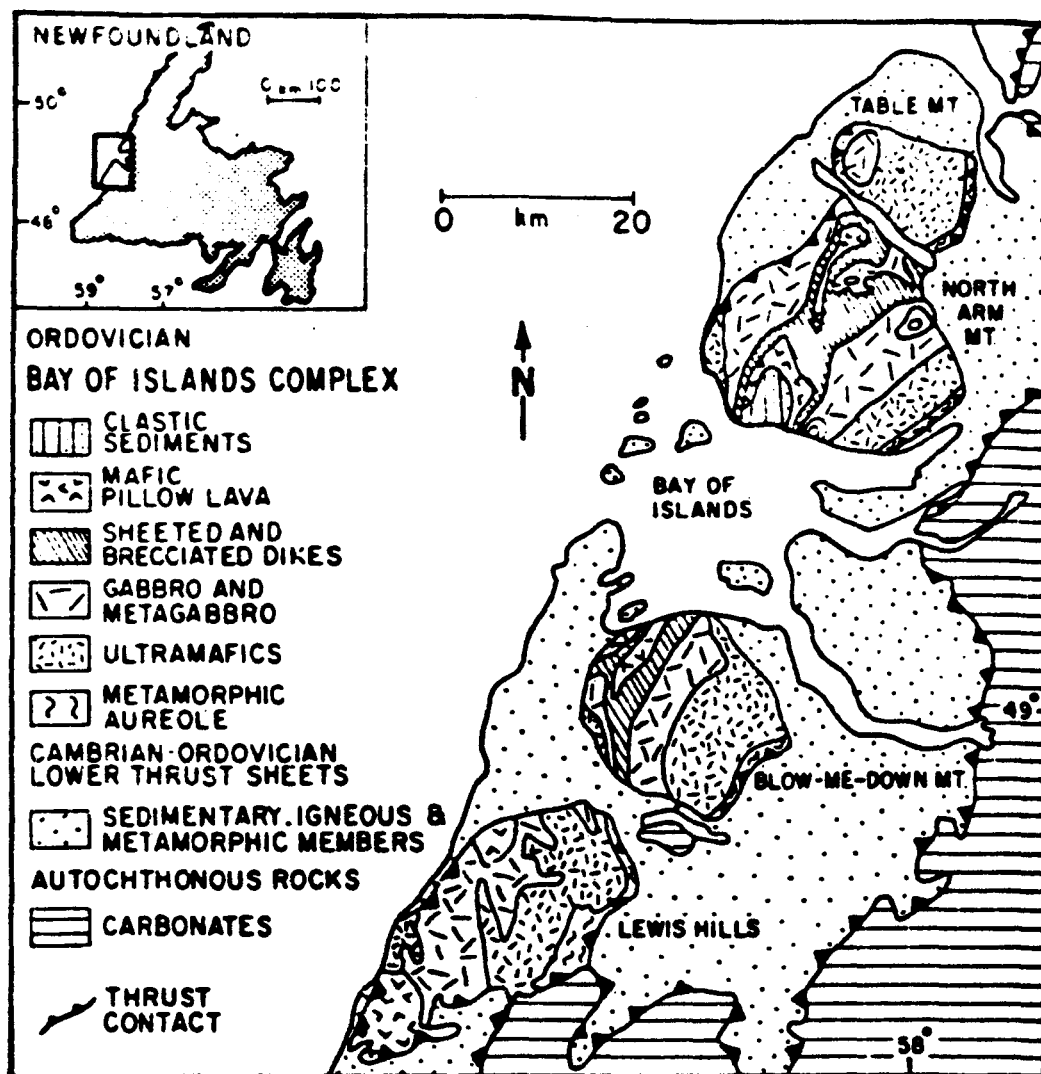


Fig. 6-2b Geology of the Bay of Islands complex, Newfoundland [after Williams, 1971].
(from Salisbury and Christensen, 1978)

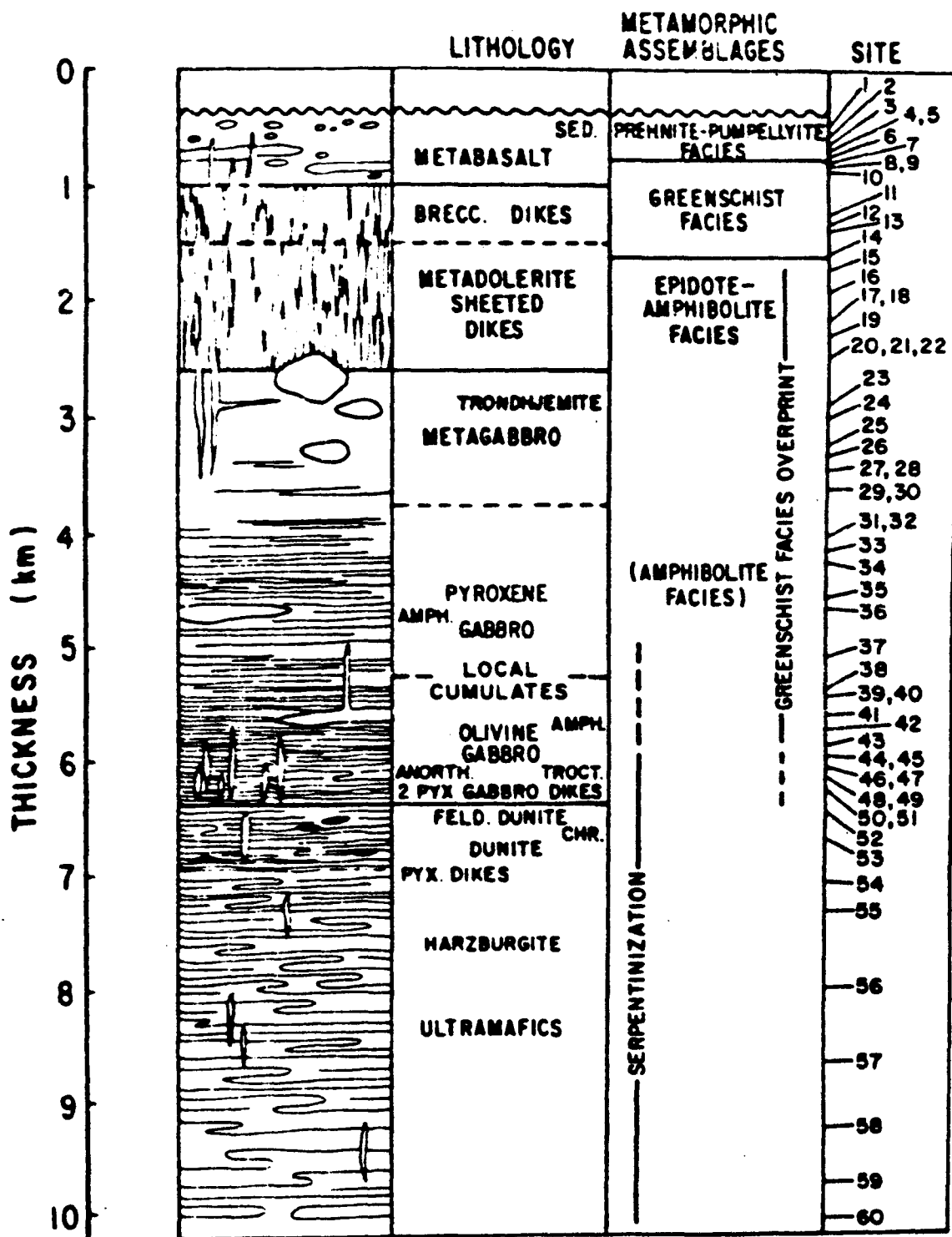


Fig. 6-2c. Stratigraphy of the Blow-Me-Down massif, Bay of Islands complex.
(after Salisbury and Christensen, 1978).

Ballantrae complex is assumed to be the easterly equivalent of the Betts Cove-Nippers Harbour ophiolite of Newfoundland (Fig. 6-2d), makes it plausible to predict the velocities of the Ballantrae ophiolite (or related rocks) at depth in terms of the velocity distribution in the Bay of Islands rocks. Such reconstruction of the ophiolite structure (hence oceanic crust) has been done by Salisbury & Christensen (1978) in terms of laboratory-measured P- and S-wave velocities on ophiolite rocks, notably from the Bay of Islands complex. Other workers (Birch, 1960, 1961; Christensen, 1965; and Simmons, 1964) have reported seismic velocities at high pressures for many rocks similar to those found in ophiolites. More recently, Christensen (1978); Christensen & Salisbury (1979) and Christensen & Smewing (1981) have reported field and laboratory velocities in rocks from various complexes including Oman and the Bay of Islands. The velocity values are used to define oceanic crustal structure and infer that in the localities mentioned, and on the basis of geophysical evidence, the ophiolites are segments of oceanic crust emplaced on land. Because of the similarity between Ballantrae and the Bay of Islands complexes, (Church & Gayer, 1973), it is tempting to advocate an investigation into the existence of these rocks under the Southern Uplands. Assuming such possibility, the works of Christensen & Salisbury quoted above provide the basis for predicting the velocities of ophiolite rocks at depth in the Southern Uplands.

/...

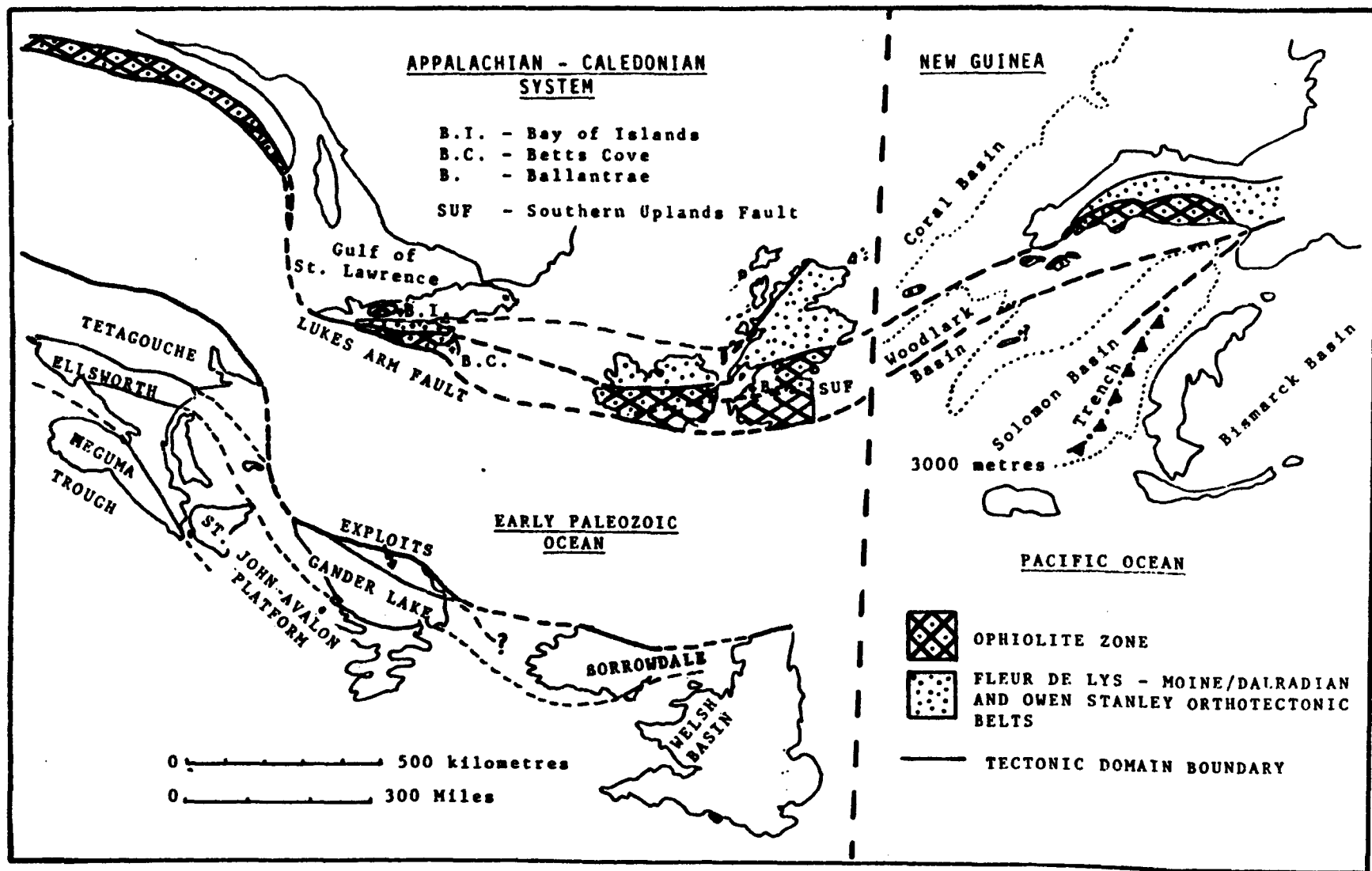


Fig. 6-2d Map illustrating the distribution of the ophiolite and orthotectonic metamorphic belts of New Guinea and the Appalachian-Caledonian system.
(after Church & Gayer, 1973)

Salisbury & Christensen (1978) plotted laboratory measured V_p and V_s as a function of depth (Fig. 6-3) for the Blow-Me-Down (BMD) massif [Bay of Islands complex]. Thus they were able to construct the seismic velocity structure of the complex and compare it with the oceanic crustal structure obtained from sonobuoy data of Christensen & Salisbury (1975). The seismic layering is illustrated in Fig. 6-4.

In Fig. 6-5a, the stratigraphic layering (Salisbury & Christensen, 1978) of the Bay of Islands ophiolite is shown but with altered depths. This is so because 5km depth of water (\approx 0.5 kbar pressure) has been added to the top of the sea-bed to transform the oceanic crustal layering to the continental equivalent; (on land, 0.5kbar \approx 1.5 km depth). Therefore, the metabasalt layer (Fig. 6-4) is topped by about 1.5km thick layer of sedimentary rocks. The authors' data shown in Fig. 6-4 are then supplemented by laboratory core velocities [from Birch (1960) and Hyndman (1977), in DSDP Vol. 37] in the lithologies shown in Fig. 6-5a. Thus it is possible to draw V_p -depth curve for each layer (Fig. 6-5b). The shaded portion indicates the LISP interpretation. Fig. 6-5b shows that metabasalts and brecciated dykes could occupy most of the 6.0 km/s upper crustal layer; the other oceanic crustal components could only be minority constituents. Granites also could explain the 6.0 km/s velocity.

A lower crustal layer with velocities in the range 6.3-7.0-km/s may contain a substantial amount of remnants of deeper oceanic crust. Lack of definition of mid-and lower-...

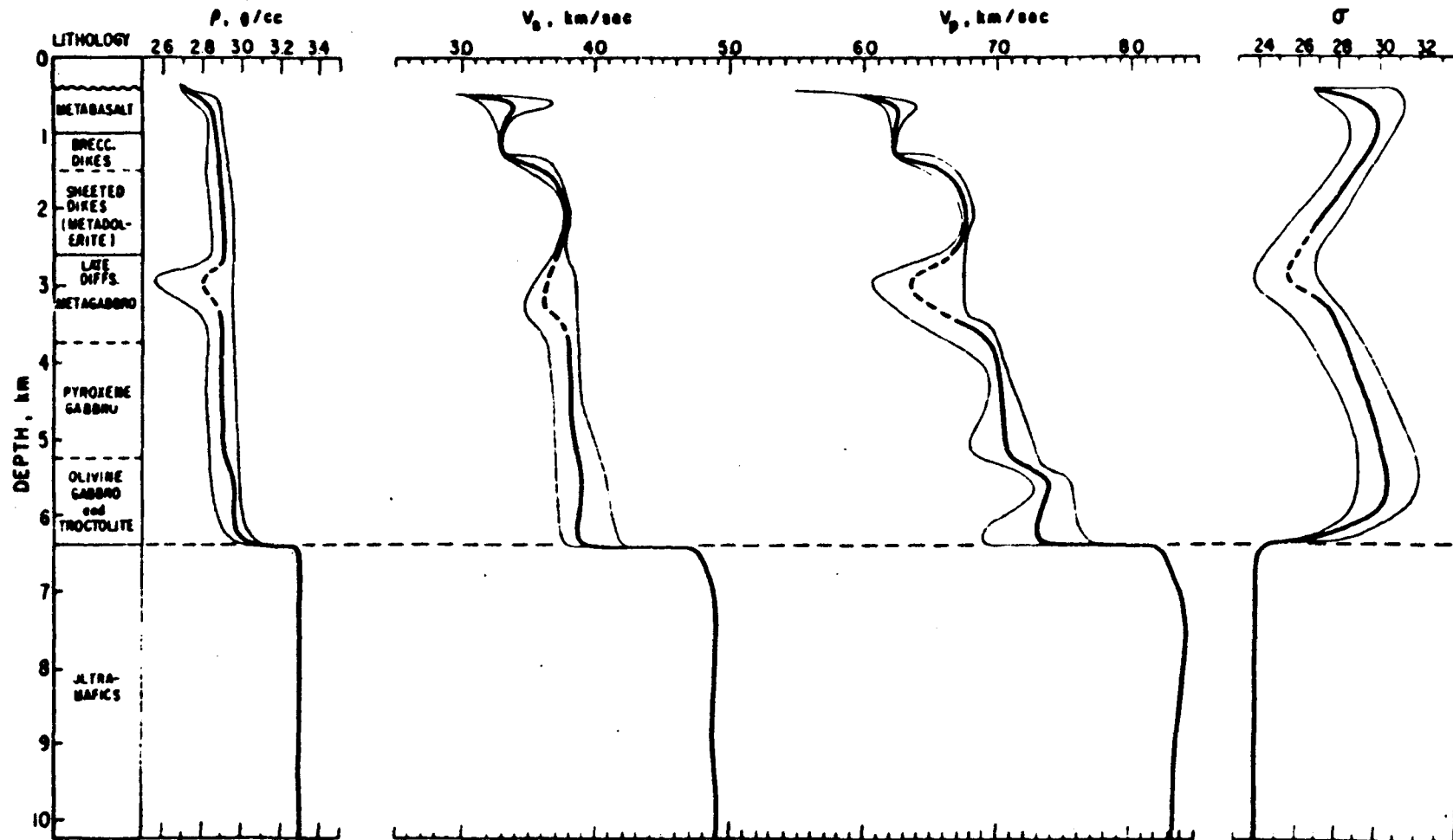


Fig. 6-3. Envelopes of compressional (V_p) and shear (V_s) wave velocity, density (ρ), and Poisson's ratio (σ) versus depth for the Blow-Me-Down massif. Heavy curves represent best fit to data. Dashed lines between 2.6 and 3.8 km indicate discontinuous velocity inversions. Velocities shown at depths less than 1.3 km represent maximum velocities.

(after Salisbury and Christensen, 1978)

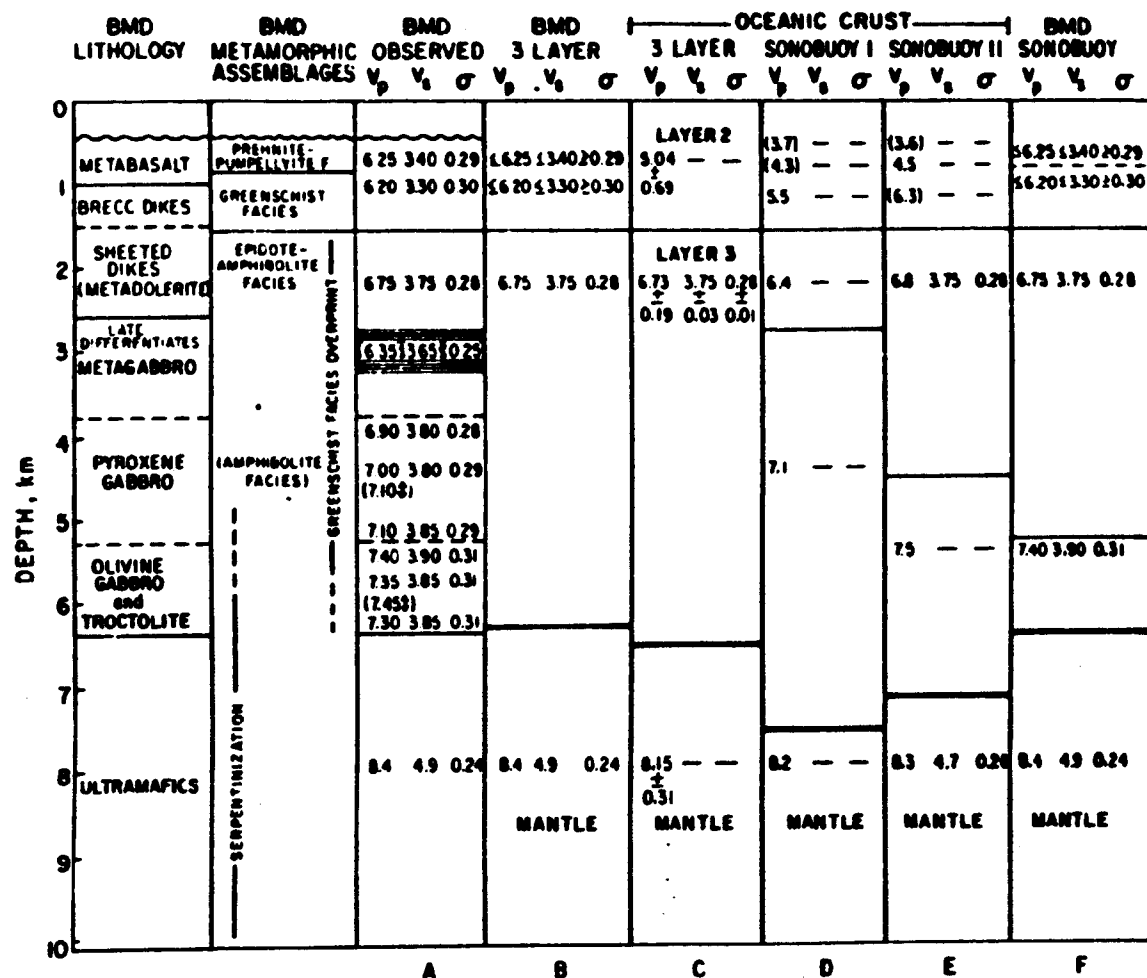


Fig. 6-4 Comparison of the petrology and seismic velocity structure of the Blow-Me-Down (BMD) massif with the velocity structure of the oceanic crust. Column A is the seismic velocity structure of the Blow-Me-Down massif as reconstructed in the laboratory; column B, as seen by classical refraction techniques; and column F, as seen by sonobuoy techniques. Column C is the oceanic seismic velocity structure [after *Christensen and Salisbury, 1975*] as seen by classical refraction; and columns D and E, as seen by sonobuoy techniques. The arrows after values indicate propagation velocity for vertical direction. The heavy line indicates the Mohorovičić discontinuity.

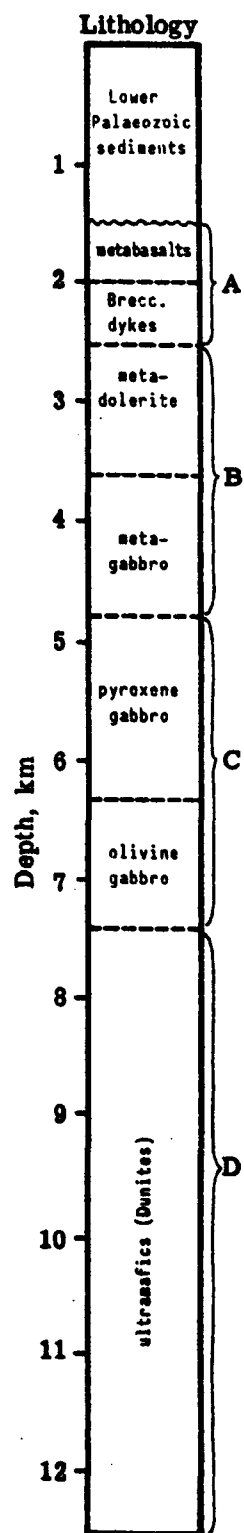


Fig. 6-5a. Stratigraphy of the Bay of Islands Complex with a top layer of Lower Palaeozoic sediments. (from Salisbury & Christensen, 1978).

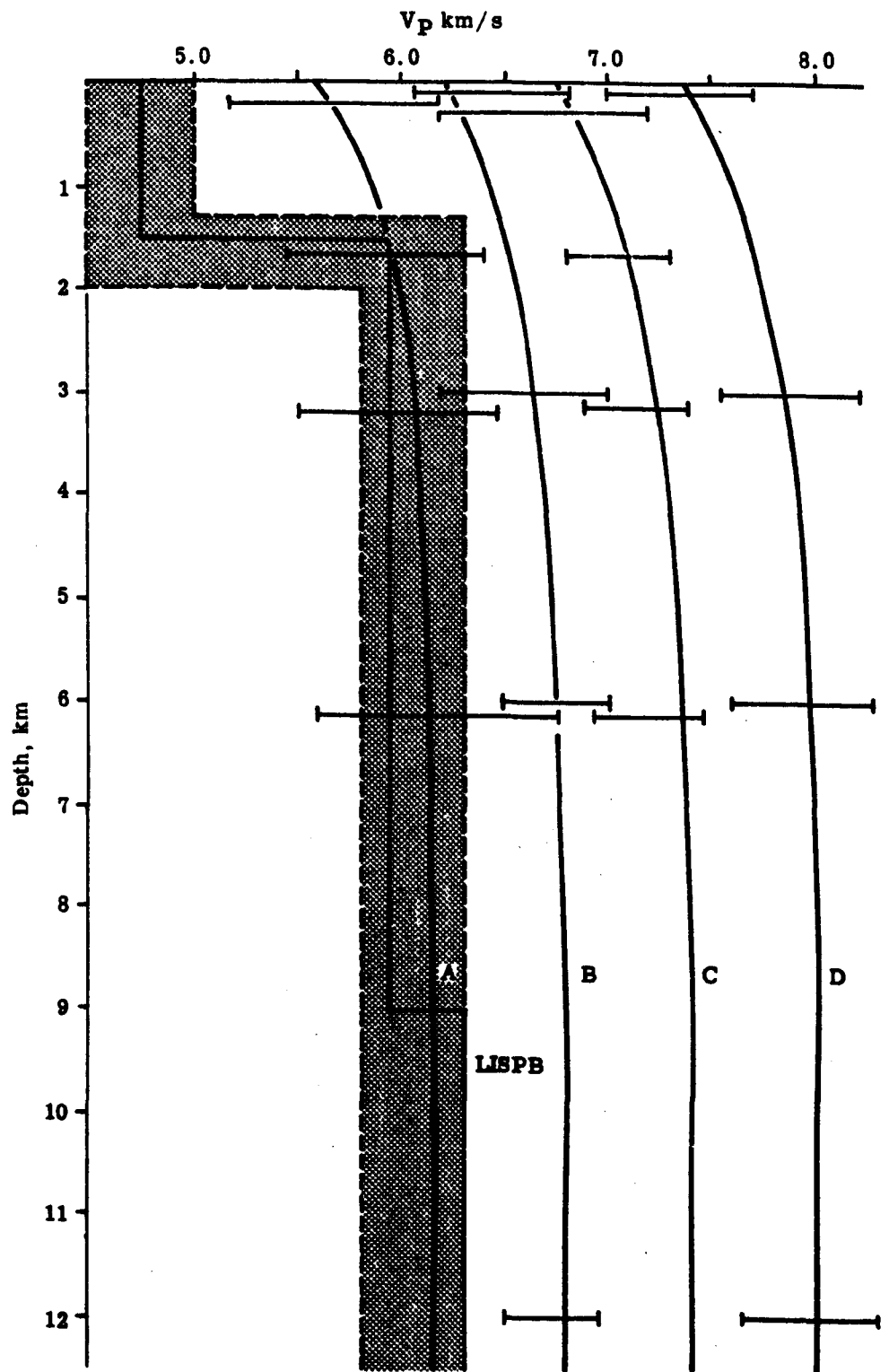


Fig. 6-5b. Velocity versus depth for each layer of rocks shown in Fig. 6-5a, with the LISPB velocity distribution in the upper crust of the Southern Uplands.

lower-crustal velocities in the Southern Uplands from LISPB precludes further discussion at this stage.

6.3 Conclusion

The overall picture of the upper crust that can be inferred from the present study is one consisting of a top sedimentary sequence, floored by granitic rocks (varying in composition from granite to diorite) and/or by basalts. Other rocktypes found in oceanic crust may constitute the lower crust. Limited data in this regard precludes elaborate treatment of the latter supposition, but attention given to it in the literature (see previous section) tends to stress its probable validity.

1. The upper crustal seismic velocity distribution in the Southern Uplands may be summarised as follows,
 - (a) Outcrop velocities lie in the range 2.9-4.0 km/s in greywackes (anisotropy up to 15%), and 2.2-3.8 km/s in shales (anisotropy up to 10%).
 - (b) At about 300m below Eskdalemuir, the mean velocity is 5.1 km/s and the anisotropy is 8% (El Isa, 1977).
 - (c) At about 2 km depth below the middle of the Southern Uplands, the mean velocity is 5.9 km/s with anisotropy roughly 3% (LISPB & Warner's lines).
 - (d) Maximum velocities are always in the direction of the strike of the rocks.

Laboratory measurements of seismic velocities in cores from shale and greywacke samples were made in order to interpret the field observations in terms of possible rock-distribution in situ.

2. In the laboratory at 1bar, core velocities measured parallel (//) and normal (\perp) to rock fabric in shale are 4.31 and 3.63 km/s respectively with anisotropy of 17%. In the greywackes, $V_{p//} = 5.15$ km/s and $V_{p\perp} = 5.04$ km/s.

At 100bar pressure, $V_{p//} = 4.37$ km/s and $V_{p\perp} = 3.72$ km/s in shale giving anisotropy of about 16%. In the greywackes, $V_{p//} = 5.27$ km/s and $V_{p\perp} = 5.17$ km/s.

/...

At 750bar pressure, corresponding to about 2 km depth, shale velocities are 4.63 (//) and 4.10 km/s (\perp) (anisotropy reaches 12%) $V_{p//}$ and $V_{p\perp}$ in the greywackes are respectively 5.50 km/s and 5.40 km/s.

Anisotropy is rather weak ($\leq 2\%$) in the greywackes while the shales consistently show strong anisotropy.

3. The velocities observed in the laboratory cores suggest that neither greywacke nor shale (as sampled) could explain the field data. Therefore two other models are considered: (i) anisotropy due to layering (Postma, 1955)
(ii) anisotropy due to oriented cracks not present in small cores.
4. Since only the mean velocity at Eskdalemuir lies within the range of the component velocities, only EKA data are treated in the layered model of Postma. However, the layered model is inadequate because the velocity-contrast between shale and greywacke is not high enough. In particular V_p in the greywackes would have to be greater than that observed in the laboratory by about 1 km/s.
5. The second model, of oriented cracks in the greywackes, explains all field data except for velocities below 300m depth (c.f. LISP & Warner's experiments). The model requires that crack porosities be as high as 6% in the exposed rocks in situ, and/...

and about 1-2% in rocks at 300m depth. (c.f. Cracks in the laboratory samples of greywacke appear to consist of a spectrum of shapes defined by aspect ratios between 1×10^{-4} and 1. Equant-shaped cavities are more abundant than flat cracks. This helps to explain some of the anomalous behaviours of V_p/V_s (σ) noted from laboratory measurements.

6. Velocities in the rocks as observed in LISPB and Warner's experiments below 2.0 km depth cannot be interpreted as indicative of greywackes and shales. It is likely that the rocks at these depths are crystalline. Granitic and extrusive basic rocks (e.g. those typical of the oceanic layer 2) could be major constituents of the main upper crustal layer beneath the Southern Uplands.

Suggestions for further work

1. Future laboratory experiments, as far as they are directed towards explaining the velocities inferred from field work applicable to depths > 2 km under the Southern Uplands, should cover crystalline rocks. In the Southern Uplands, these may be either basic rocks (e.g. Ballantrae ophiolite) or the granitic plutons.
2. More refraction lines are necessary in the Southern Uplands with particular reference to depths > 2 km. Combination of these with a comprehensive laboratory work on a variety of Southern Uplands rocks would help to elucidate, better, the crustal structure in the region.

REFERENCES

- ADAMS, L.H. and WILLIAMSON, E.D. 1923. On the compressibility of minerals and rocks at high pressures. J. Franklin Inst. 195, 475-529.
- AGGER, H.E. and CARPENTER, E.W. 1964-65. A crustal study in the vicinity of the Eskdalemuir Seismological Array Station. Geophys. J.R. Astron. Soc. 9, 69-83.
- AL HADDAD, F.M. 1977. Seismic studies of Pre-Cambrian Lewisian metamorphic complex, N.W. Britain. Univ. Glasgow Ph.D. thesis (unpubl.)
- ANDERSON, D.L., MINSTER, B. and COLE, D. 1974. The effect of oriented cracks on seismic velocities. J. Geophys. Res. 79, 4011-4015.
- ANDERSON, O.L. and LIEBERMANN, R.C. 1968. Sound velocities in rocks and minerals: experimental methods, extrapolations to very high pressures, and results. In Mason, W.P. (ed.) Physical Acoustics IVB, New York, 329-472.
- ASSUMPCAO, M. and BAMFORD, D. 1978. LISPB-V. Studies of crustal shear waves. Geophys. J.R. Astron. Soc. 54, 61-73.
- ATKINSON, B. 1981. Cracks in rocks under stress. Nature 390, 632.
- BAMFORD, D., FABER, S., JACOB, B., KAMINSKI, W., NUNN, K., PRODEHL, C., FUCHS, K., KING, R. and WILLMORE, P. 1976. A Lithospheric Seismic Profile in Britain - 1, Preliminary Results. Geophys. J.R. Astron. Soc. 44, 145-160.
- BAMFORD, D. and NUNN, K.R. 1979. In situ seismic measurements of crack anisotropy in the Carboniferous limestone of Northwest England. Geophys. Prospect. 27, 322-338.
- BAMFORD, D., NUNN, K., PRODEHL, C. and JACOB, B. 1977. LISPB-111. Upper crustal structure of Northern Britain, J. Geol. Soc. 133, 481-488.
- BAMFORD, D., NUNN, K., PRODEHL, C. and JACOB, B. 1978. LISPB-IV. Crustal structure of Northern Britain. Geophys. J.R. Astron. Soc. 54, 43-60.

/...

- BATZLE, M.L., SIMMONS, G. and SIEGFRIED, R.W. 1980. Micro-crack closure in rocks: Direct observation. J. Geophys. Res. 85, 7072-7090.
- BIOT, M.A. 1956. Theory of propagation of elastic waves in a fluid-saturated porous solid: 1. Low-frequency range, 2. Higher-frequency range. J. Acoust. Soc. Am. 28, 168-191.
- BIRCH, F. 1960. The velocity of compressional waves in rocks to 10kbar, 1. J. Geophys. Res. 65, 1083-1102.
- BIRCH, F. 1961. The velocity of compressional waves in rocks to 10kbar, 2. J. Geophys. Res. 66, 2199-2224.
- BIRCH, F. and BANCROFT, D. 1938. The effect of pressure on the rigidity of rocks. J. Geol. 46, 59-87 and 113-141.
- BIRCH, F. and BANCROFT, D. 1940. New measurements of the rigidity of rocks at high pressures. J. Geol. 48, 752-766.
- BLUCK, B.J., HALLIDAY, A.W., AFTALION, M. and MACINTYRE, R.M. 1980. Age and origin of Ballantrae ophiolite and its significance to the Caledonian orogeny and Ordovician time scale. Geology 8, 492-495.
- BLUNDELL, D.J. and PARKS, R. 1969. A study of the crustal structure beneath the Irish Sea. Geophys. J.R. Astron. Soc. 17, 45-62.
- BORG, H. and BATH, M. 1971. The Uppsala Seismograph Array Station. Pure Appl. Geophys. 89, 19-31.
- BOTT, M.H.P. and ~~MASSON~~-SMITH, D. 1960. A gravity Survey of the Criffell granodiorite and New Red sandstone deposits near Dumfries. Proc. Yorks. Geol. Soc. 32, 317-332.
- BRACE, W.F., SILVER, E., HADLEY, K. and GOETZE, C. 1972. Cracks and pores: A closer look. Science 178, 162-164.
- BUDIANSKY, B. and O'CONNELL, R.J. 1976. Elastic moduli of a cracked solid. Int. J. Solids Structures 12, 81-97.
- CHENG, C.H. and TOKSOZ, M.N. 1979. Inversion of seismic velocities for the pore aspect ratio spectrum of a rock. J. Geophys. Res. 84, 7533-7543.

/...

- CHOLET, J. and RICHARD, H. 1954. A test on elastic anisotropy measurements at Berriane. Geophys. Prospect. 2, 232-246.
- CHRISTENSEN, N.I. 1965. Compressional wave velocities in metamorphic rocks at pressures to 10kbars. J. Geophys. Res. 70, 6147-6164.
- CHRISTENSEN, N.I. 1978. Ophiolites, seismic velocities and oceanic crustal structure. Tectonophysics 47, 131-157.
- CHRISTENSEN, N.I. and SALISBURY, M.H. 1975. Structure and constitution of the lower oceanic crust. Rev. Geophys. Space Phys. 13, 57-86.
- CHRISTENSEN, N.I. and SALISBURY, M.H. 1979. Seismic anisotropy in the oceanic upper mantle: Evidence from the Bay of Islands ophiolite complex. J. Geophys. Res. 84, 4601-4610.
- CHRISTENSEN, N.I. and SME WING, J.D. 1981. Geology and seismic structure of the northern section of the Oman ophiolite. J. Geophys. Res. 86, 2545-2555.
- CHURCH, W.R. and GAYER, R.A. 1973. The Ballantrae ophiolite. Geol. Mag. 110, 497-510.
- CRAMPIN, S. 1977. A review of the effect of anisotropic layering on the propagation of seismic waves. Geophys. J.R. Astron. Soc. 49, 9-27.
- CRAMPIN, S. 1978. Seismic wave propagation through a cracked solid: polarization as a possible dilatancy diagnostic. Geophys. J.R. Astron. Soc. 54, 467-496.
- CRAMPIN, S., JACOB, A.W.B., MILLER, A. and NEILSON, G. 1970. The LOWNET radio-linked seismometer network in Scotland. Geophys. J.R. Astron. Soc. 21, 207-216.
- CREIG, D.C., 1971. The South of Scotland. In British Regional Geology. 3rd Edition, Edinburgh.
- DEER, W.A. 1935. The Cairnsmore of Carsphairn Igneous Complex. Q.J. Geol. Soc. Lond. 91, 47-76.
- DEWEY, J.F. 1971. A model for the Lower Palaeozoic evolution of the southern margin of the early Caledonides of Scotland and Ireland. Scott, J. Geol. 7, 219-240.
- EL ISA, Z.H.M. 1977. Seismic studies of local events received at three arrays in Southern Central Scotland. Univ. Glasgow Ph.D. thesis(unpubl) /...

- ESHELBY, J.D. 1957. The determination of the field of an ellipsoidal inclusion and related problems. Proc. R. Soc. Lond. Ser. A 241, 376-396.
- EVANS, C., LEE, C.J. and CHROSTON, P.N. 1978. Transient effects in laboratory measurements of compressional wave velocity and electrical conductivity. Nature 276, 485-487.
- FITTON, J.G. and HUGHES, D.J. 1970. Volcanism and plate tectonics in the British Ordovician. Earth Planet. Sci. Lett. 8, 223-228.
- GREGORY, A.R. 1976. Fluid saturation effect on dynamic elastic properties of sedimentary rocks. Geophysics 41, 895-921.
- HADLEY, K. 1976. Comparison of calculated and observed crack densities and seismic velocities in Westerly granite. J. Geophys. Res. 81, 3484-3494.
- HAGEDOORN, J.G. 1954. A practical example of an anisotropic velocity layer. Geophys. Prospect. 2, 52-60.
- HAGEDOORN, J.G., 1959. The Plus-Minus method of interpreting seismic refraction sections. Geophys. Prospect. 7, 158-162.
- HALL, J. 1970. The correlation of seismic velocities with Formations in the southwest of Scotland. Geophys. Prospect. 18, 134-148.
- HALL, J. 1971. Seismic studies in the Region of the Firth of Clyde. Univ. Glasgow Ph.D. thesis (unpubl.)
- HALL, J. 1978. Crustal structure of the Northeast Atlantic seaboard. In Bowes, D.R. and Leake, B.E. (eds.) Geological evolution of N.W. Britain and environs. Spec. Issue. Geol. J. 10, 23-38.
- HALL, J. 1979. Laboratory book on physical properties of rocks. (unpubl.)
- HALL, J. and AL HADDAD, F.M. 1979. Variation of effective seismic velocities of minerals with pressure and its use in velocity prediction. Geophys. J.R. Astron. Soc. 57, 107-118.
- HALL, J. and SIMMONS, G. 1979. Seismic velocities of Lewisian metamorphic rocks at pressures to 8 kbar: relationship to crustal layering in North Britain. Geophys. J.R. Astron. Soc. 58, 337-347.
- HOLMES, A. 1930. Petrographic methods and calculations.

/...

- HOWARD, D.W. 1975. Deep-seated igneous intrusions in Co. Kerry. Proc. R. Ir. Acad. Ser. B. 75, 173-183.
- HUGHES, D.S. and JONES, H.J. 1950. Variations of elastic moduli of igneous rocks with pressure and temperature. Bull. Geol. Soc. Am. 61, 843-856.
- HUGHES, D.S. and MALRETTE, C. 1956. Elastic wave velocities in granite. Geophysics 21, 277-284.
- HUGHES, D.S. PONDROM, W.L. and MIRNS, R.L. 1949. Transmission of elastic pulses in metal rods. Phys. Rev. 75, 1552-1556.
- HYNDMAN, R.D. 1977. Seismic velocity measurements of basement rocks from DSDP Leg 37. In Robinson, P.T. (Sci. ed.) Initial Reports of the Deep Sea Drilling Project 37, 373-387.
- JACOB, A.W.B. 1969. Crustal phase velocities observed at the Eskdalemuir Seismic Array. Geophys. J.R. Astron. Soc. 18, 189-197.
- JAEGER, J.C. 1974. Elasticity, Fracture and Flow, with Engineering and Geological Applications. New York.
- JAFFE, H. and BERLIN COURT, D.A. 1965. Piezoelectric transducer materials. Proc. IEEE 53, 1372-1386.
- JAMIESON, J.C. and HOSKINS, H. 1963. The measurement of shear wave velocities in solids using axially polarised ceramic transducers. Geophysics. 28, 87-90.
- JONES, L.E.A. and WANG, H.F. 1981. Ultrasonic velocities in Cretaceous shales from the Williston basin. Geophysics 46, 288-297.
- KENNEDY, W.Q. 1958. The tectonic evolution of the Midland Valley of Scotland. Trans. Geol. Soc. Glasg. 23, 106-133.
- KING, M.S. 1966. Wave velocities in rocks as a function of changes in overburden pressure and pore fluid saturants. Geophysics 31, 50-73.
- KUSTER, G.T. and TOKSOZ, M.N. 1974. Velocity and attenuation of seismic waves in two-phase media, Part 1 - Theoretical formulations. Geophysics 39, 587-606.
- LAGIOS, E. and HIPKIN, R.G. 1979. The Tweedale Granite - a newly discovered batholith in the Southern Uplands. Nature 280, 672-675.
- /...

- LAMBERT, R. St.J. and MCKERROW, W.S. 1976. The Grampian Orogeny. Scott. J. Geol. 12, 271-292.
- LAPWORTH, C. 1882. The Girvan succession. Q.J. Geol. Soc. Lond. 38, 537-666.
- LAUGHTON, A.S. 1957. Sound propagation in compacted ocean sediments. Geophysics 22, 233-260.
- LAWSON, J.A. and LAWSON, J.D. 1976. Geology explained around Glasgow and southwest Scotland including Arran. London.
- LEVIN, F.K. 1980. Seismic velocities in transversely isotropic media, II. Geophysics 45, 3-17.
- LONGMAN, C.D., BLUCK, B.J. and VAN BREEMEN, O. 1979. Ordovician conglomerate and the evolution of the Midland Valley. Nature 280, 578-581.
- MAVKO, G. and NUR, A. 1978. The effect of non-elliptical cracks on the compressibility of rocks. J. Geophys. Res. 83, 4459-4468.
- MCKERROW, W.S., LEGGETT, J.K. and EALES, M.H. 1977. An imbricate thrust model for the Southern Uplands of Scotland. Nature 267, 237-239.
- MCLEAN, A.C. 1961. Density measurements of rocks in southwest Scotland. Proc. R. Soc. Edinb. 68, 103-111.
- McSKIMIN, H.J. 1950. Ultrasonic measurement techniques applicable to small solid specimens. J. Acoust. Soc. Am. 22, 413-418.
- MITCHELL, A.H.G. and MCKERROW, W.S. 1975. Analogous evolution of the Burma orogen and the Scottish Caledonides. Bull. Geol. Soc. Am. 86, 305-315.
- NUR, A. 1971. Effects of stress on velocity anisotropy in rocks with cracks. J. Geophys. Res. 76, 2022-2034.
- NUR, A.M. and SIMMONS, G. 1969. The effect of saturation on velocity in low porosity rocks. Earth Planet. Sci. Lett. 7, 183-193.
- O'CONNELL, R.J. and BUDIANSKY, B. 1974. Seismic velocities in dry and saturated cracked solids. J. Geophys. Res. 79, 5412-5426.
- O'CONNELL, R.J. and BUDIANSKY, B. 1977. Viscoelastic properties of fluid-saturated cracked solids. J. Geophys. Res. 82, 5719-5735.
- PARSLOW, G.R. 1968. The physical and structural features of the Cairnsmore of Fleet granite and its aureole. Scott. J. Geol. 4, 91-108.

/...

- PEACH, B.N. and HORNE, J. 1899. The Silurian rocks of Britain. Vol.1, Scotland. Mem. Geol. Surv. U.K.
- PESELNICK, L. 1962. Elastic constants of Solenhofen limestone and their dependence upon density and saturation. J. Geophys. Res. 67, 4441-4448.
- PESELNICK, L. and STEWART, R.M. 1975. A sample assembly for velocity measurements of rocks at elevated temperatures and pressures. J. Geophys. Res. 80, 3765-3768.
- PHILLIPS, W.E.A., STILLMAN, C.J. and MURPHY, T. 1976. A Caledonian plate tectonic model. J. Geol. Soc. 132, 579-609.
- POSTMA, G.W. 1955. Wave propagation in a stratified medium. Geophysics 20, 780-806.
- POWELL, D.W. 1956. Gravity and magnetic anomalies in North Wales. Q.J. Geol. Soc. Lond. 61, 375-397.
- POWELL, D.W. 1970. Magnetised rocks within the Lewisian of Western Scotland and under the Southern Uplands. Scott. J. Geol. 6, 253-369.
- RICHTER, D. and SIMMONS, G. 1977. Microcracks in crustal igneous rocks: Microscopy. In HEACOCK, J.G. (ed.) The Earth's Crust: Its Nature and Physical Properties. Geophys. Monogr. Ser. 20, 149-180. AGU, Washington D.C.
- RUNDLE, J.B. and SCHULER, K.W. 1981. A composite model for the anisotropic elastic moduli of lean oil shale. Geophysics 46, 163-171.
- SALISBURY, M.H. and CHRISTENSEN, N.I. 1978. The seismic velocity structure of a traverse through the Bay of Islands Ophiolite Complex, Newfoundland, an exposure of oceanic crust and upper mantle. J. Geophys. Res. 83, 805-817.
- SIEGFRIED, R. and SIMMONS, G. 1978. Characterisation of oriented cracks with differential strain analysis. J. Geophys. Res. 83, 1269-1278.
- SIMMONS, G. 1964. Velocity of shear waves in rocks to 10 kilobars, 1. J. Geophys. Res. 69, 1123-1130.

/...

- SIMMONS, G. 1965. Ultrasonics in geology. Proc. IEEE 53, 1337-1346.
- SIMMONS, G. and RICHTER, D. 1976. Microcracks in rocks. In Strens, R.G.J. (ed.) The Physics and Chemistry of Minerals and Rocks. 105-137. Interscience, New York.
- SMITH, P.J. and BOTT, M.H.P. 1975. Structure of the crust beneath the Caledonian Foreland and Caledonian Belt of the North Scottish Shelf Region. Geophys. J.R. Astron Soc. 40, 187-205.
- SPRUNT, E.S. and BRACE, W.F. 1974. Direct observations of microcavities in crystalline rocks. Int. J. Rock Mech. Min. Sci. Geomech. Abstr. 11, 139-150.
- STEPHENS, W.E. and HALLIDAY, A.N. 1979. Compositional variation in the Galloway plutons. In Atherton, M.P. and Tarney, J. (eds.) Origin of Granite Batholiths. Shiva Press.
- STEWART, R. and PESELNICK, L. 1977. Velocity of compressional waves in dry Franciscan rocks to 8 kbar and 300°C. J. Geophys. Res. 82, 2027-2039.
- TODD, T. and SIMMONS, G. 1972. Effect of pore-pressure on the velocity of compressional waves in low-porosity rocks. J. Geophys. Res. 70, 3731-3744.
- TOKSOZ, M.N., CHENG, C.B. and TIMUR, A. 1976. Velocities of seismic waves in porous rocks. Geophysics 41, 621-645.
- TRUSCOTT, J.R. 1964-65. The Eskdalemuir Seismological Station. Geophys. J.R. Astron. Soc. 9, 59-68.
- UPTON, B.G.J., ASPEN, P., GRAHAM, A. and CHAPMAN, N.A. 1976. Pre-Palaeczoic basement of the Scottish Midland Valley. Nature 260, 517-518.
- WALKER, F. 1928. The plutonic intrusions of the Southern Uplands east of the Nith Valley. Geol. Mag. 65, 153-162.
- WALSH, J.B. 1965. The effect of cracks on the compressibility of rocks. J. Geophys. Res. 70, 381-389.
- WALSH, J.B. 1969. New analysis of attenuation in partially melted rocks. J. Geophys. Res. 74, 4333-4337.

/...

- WALSH, J.B. and GROSENBAUGH, M.A. 1979. A new model for analysing the effect of fractures on compressibility. J. Geophys. Res. 84, 3532-3526.
- WEIR, J.A. 1979. Tectonic contrasts in the Southern Uplands. Scott J. Geol. 15, 169-186.
- WHITE, J.E. and ANGONA, F.A. 1955. Elastic wave velocities in laminated media. J. Acoust. Soc. Am. 27, 310-317.
- WILLMORE, P.L. 1973. Crustal studies in the region of the British Isles. Tectonophysics 20, 341-357.
- WILSON, J.T. 1967. Seismic detection of nuclear explosions. In Runcorn, S.K. (ed.) International Dictionary of Geophysics 2, 1343-1345. Oxford.
- WU, T.T. 1966. The effect of inclusion-shape on the elastic moduli of a two-phase material. Int. J. Solids and Structures 2, 1-8.
- WYLLIE, M.R.J., GREGORY, A.R. and GARDNER, G.H.F. 1958. An experimental investigation of factors affecting wave velocities in porous media. Geophysics 23, 459-493.

APPENDIX 1

Density and porosity calculations from weight measurements.

(A) "Petrographic methods and calculations" - Arthur Holmes, 1930

Weight of saturated sample in air = W_s

Weight of saturated sample in water = w_s

Weight of dry sample in air = W

$$\text{Saturated bulk density } \rho_{bw} = \frac{W_s}{W_s - w_s}$$

$$\text{Porosity } \phi = \frac{W_s - W}{W_s - w_s} \times 100\%$$

$$\text{Grain density } \rho_g = \frac{W}{W - w_s}$$

(B) From Rieke and Gillingerian, 1974

$$\phi = \frac{\rho_g - \rho_{bw}}{\rho_g - \rho_f} \quad \text{where } \rho_f \text{ is fluid density}$$

$\rho_f = 1$ when fluid is water

$$\text{Therefore } \phi = \frac{\rho_g - \rho_{bw}}{\rho_g - 1}$$

$$\text{and } \rho_g = \frac{\rho_{bw} - \phi}{1 - \phi}$$

The above relationships can be extended to calculate the dry bulk density of a rock sample viz,

$$(C) \quad \rho_{bw} = \frac{W_s}{W_s - w_s}$$

$$\text{Dry bulk density } \rho_{dry} = \frac{W}{W_s - w_s}$$

$$\rho_{bw} - \rho_{dry} = \text{fractional porosity } \phi$$

$$\therefore \phi = \rho_{bw} - \rho_{dry}$$

$$\phi = \frac{W_s - W}{W_s - w_s}$$

/...

It should be mentioned that all the above relationships have been tested with the present weight measurements; and results are the same whichever equation is used. As long as the three parameters, W_s , W and w_s are known, the porosity and densities of the sample can always be calculated.

APPENDIX 2

Two crack models mentioned in the text are the self-consistent approximation and the non-interactive techniques. O'Connell & Budiansky's model assumes that all cracks in the rock have the same shape and permits the determination of crack-density (ϵ) from the ratio of the velocity of the cracked rock to that of a crack-free equivalent. Calculations using velocities at varying pressure give a rough idea of how crack-density changes with pressure. On the other hand, the non-interactive model allows the characterisation of cracks in terms of pore aspect-ratio spectrum and the calculation of the change in pore-spectrum under pressure due to the closing of cracks. This allows the prediction of the pressure-dependence of seismic velocities. The mathematical formulations used in the calculations are described below.

A. Self-consistent approach of O'Connell & Budiansky (1974) herein referred to as OB.

O'Connell & Budiansky (1974) proposed a model for the effect of cracks on the microscopic elastic properties of solids based on a self-consistent approximation. According to the authors, the final numerical results for elliptical cracks are indistinguishable for all ' ϵ ' from those for circular cracks. Therefore, results for circular cracks may be used for the general case with negligible error as long as the density of the cracks is characterised by,

$$\epsilon = (2N/\pi) (A^2/P) \dots\dots\dots (1)$$

/...

where A , defined by πab , is the area of the crack-section in the plane normal to the shortest axis, P is the perimeter of the crack-section defining A , and is given by $4aE(k)$,

$$\text{where } E(k) = \int_0^{\pi/2} (1 - k^2 \sin^2 \theta)^{\frac{1}{2}} d\theta$$

$$\text{and } K = (1 - b^2/a^2)^{\frac{1}{2}}$$

For circular cracks, $a = b$, and equation (1) reduces to $\epsilon = N \langle a' \rangle$; N = number of cracks per unit volume, and ' a ' is the major axis of the crack.

From the measured velocities in a solid, it is possible to estimate the crack-density as follows. First, the effective elastic moduli of the cracked solid are calculated from the observed velocities. The effective elastic moduli \bar{K}/K and \bar{G}/G are obtainable from equations (28) of OB,

$$\frac{\bar{V}_s}{V_s} = \left(\frac{\bar{G}}{G} \right)^{\frac{1}{2}}$$

$$\frac{\bar{V}_p}{V_p} = \frac{[(1 - \bar{\sigma})(1 + \sigma) \cdot \bar{K}]^{\frac{1}{2}}}{[(1 + \bar{\sigma})(1 - \sigma) \cdot K]}$$

$$\frac{\bar{V}_p/\bar{V}_s}{V_p/V_s} = \frac{[(1 - \bar{\sigma})(1 - 2\sigma)]^{\frac{1}{2}}}{[(1 - 2\bar{\sigma})(1 - \sigma)]}$$

where \bar{V}_p , \bar{V}_s are the effective P-and S-wave velocities respectively, V_p , V_s are the intrinsic P-and S-wave velocities of the solid material observed at the highest pressure when all cracks are assumed closed.

In terms of observed P-and S-wave velocities therefore, the crack-density of a cracked rock under different saturation conditions can be estimated as follows,

/...

For dry circular cracks

$$\frac{\bar{K}}{K} = 1 - \frac{16}{9} \left(\frac{1 - \bar{\sigma}^2}{1 - 2\bar{\sigma}} \right) \epsilon \quad \dots\dots\dots 2a$$

where \bar{K}/K is the normalised bulk modulus,

$\sigma, \bar{\sigma}$ are the intrinsic and effective Poisson's ratios,

from (2a)

$$\epsilon = \frac{9}{16} \cdot \left(1 - \frac{\bar{K}}{K} \right) \left(\frac{1 - 2\bar{\sigma}}{1 - \bar{\sigma}^2} \right) \quad \dots\dots\dots 2b$$

Equation (2b) is used to calculate crack-density in dry rocks.

Partial saturation

Equation (17b) OB (1974) gives

$$\frac{\bar{G}}{G} = 1 - \frac{32}{45} (1 - \bar{\sigma}) \left[1 - \epsilon + \frac{3}{2 - \bar{\sigma}} \right] \epsilon \quad \dots\dots\dots (3)$$

where ϵ = fraction of saturation.

$$\text{from (3), } \left[\frac{(1 - \epsilon) + \frac{3}{2 - \bar{\sigma}}}{1} \right] \epsilon = \frac{45}{32} \left(1 - \frac{\bar{G}}{G} \right) \frac{1}{(1 - \bar{\sigma})}$$

$$\text{i.e. } (1 - \epsilon) \epsilon + \frac{3}{2 - \bar{\sigma}} \epsilon = \frac{45}{32} \left(1 - \frac{\bar{G}}{G} \right) \frac{1}{(1 - \bar{\sigma})} \quad \dots\dots\dots (4)$$

Also from (17a) OB, 1974,

$$\frac{\bar{K}}{K} = 1 - \frac{16}{9} \left(\frac{1 - \bar{\sigma}^2}{1 - 2\bar{\sigma}} \right) (1 - \epsilon) \epsilon \quad \dots\dots\dots (5)$$

$$\frac{16}{9} \left(\frac{1 - \bar{\sigma}^2}{1 - 2\bar{\sigma}} \right) (1 - \epsilon) \epsilon = 1 - \frac{\bar{K}}{K}$$

$$\therefore (1 - \epsilon) \epsilon = \frac{9}{16} \left(1 - \frac{\bar{K}}{K} \right) \left(\frac{1 - 2\bar{\sigma}}{1 - \bar{\sigma}^2} \right) \quad \dots\dots\dots (6)$$

Substituting for $(1 - \epsilon) \epsilon$ in equation (4) above,

/...

$$\frac{9}{16} (1 - \frac{\bar{K}}{K}) (\frac{1 - 2\bar{\sigma}}{1 - \bar{\sigma}^2}) + \frac{3}{2 - \bar{\sigma}} \cdot \epsilon = \frac{45}{32} (1 - \frac{\bar{G}}{G}) \cdot \frac{1}{(1 - \bar{\sigma})}$$

$$\frac{3}{2 - \bar{\sigma}} \cdot \epsilon = \frac{45}{32} (1 - \frac{\bar{G}}{G}) \cdot \frac{1}{(1 - \bar{\sigma})} - \frac{9}{16} (1 - \frac{\bar{K}}{K}) (\frac{1 - 2\bar{\sigma}}{1 - \bar{\sigma}^2})$$

$$\therefore \epsilon = \frac{2 - \bar{\sigma}}{1 - \bar{\sigma}} \left[\frac{15}{32} \cdot (1 - \frac{\bar{G}}{G}) - \frac{3}{16} (1 - \frac{\bar{K}}{K}) (\frac{1 - 2\bar{\sigma}}{1 + \bar{\sigma}}) \right] \dots\dots (7)$$

⇒ Crack-density for partial saturation,

For 100% saturation

$$\epsilon_{100\%} = \frac{45}{32} \cdot \frac{(\bar{\sigma} -) (2 - \bar{\sigma})}{(1 - \bar{\sigma}) (1 - 2\bar{\sigma})} \text{ (see equation 16 of OB)}$$

The results for partial saturation can be applied to situations in which some of the cracks are only partly-filled with water, the rest of the crack-space containing a high-compressibility gas or air.

(B) The non-interactive model of cracks (Kuster & Toksoz, 1974; Toksoz et al, 1976; Cheng & Toksoz, 1979).

The problem here is to find the volume-concentration of each set of cracks present in the rock. The first step is to specify a range of crack-shapes (as a series of aspect ratios, α_m) from near-spherical pores ($\alpha_m \geq 10^{-2}$) to flat cracks ($\alpha_m = 1 \times 10^{-4}$). The closure-pressure (P_c) of the cracks are then determined by,

$$P_c = K \cdot 3\pi\alpha \cdot \frac{(1 - 2\sigma)}{4(1 - \sigma^2)} \dots\dots\dots (1)$$

where K and σ are the intrinsic bulk modulus and Poisson's ratio, calculated from the observed P-and S-wave velocities at high pressure (when all cracks are assumed closed). Velocities at/...

at lower pressures are used to calculate the effective elastic properties of the medium as a function of pressure. In the following equations used to determine the volume-concentration of each set of cracks, unprimed quantities (K, μ, ρ) refer to the matrix (and are known from high-pressure velocities); primed quantities (K', μ', ρ') refer to the inclusions (air or water; values are obtained from standard tables); and starred quantities (K^*, μ^*, ρ^*) refer to the effective properties of the composite medium (calculated as a function of pressure as indicated above). If $V(\alpha_m)$ is the volume-concentration of cracks of aspect ratio, α_m , at 1bar, the relationship between the various quantities stated can be expressed as,

$$\frac{K^* - K}{K' - K} \cdot \frac{3K + 4\mu}{3K^* + 4\mu} = \sum_{m=1}^M \alpha_m \left[1 + \frac{dV}{V}(\alpha_m, P_c) \right] \cdot \frac{1}{3} T_1 (\alpha_m) \frac{V(\alpha_m)}{\alpha_m} \dots (2)$$

The fractional change in volume ($\frac{dV}{V}$) of a crack with aspect ratio (α at 1bar), under a confining pressure (P) is given by,

$$\frac{dV}{V} = -\frac{P}{K^*} \left[\frac{4(1 - \sigma^2)}{3\pi\alpha(1 - 2\sigma)} \right] \dots \dots \dots (3)$$

$\frac{dV}{V}$ decreases with increasing pressure until the pressure,

$P = K^* \cdot 3\pi\alpha \frac{(1 - 2\sigma)}{4(1 - \sigma^2)}$ when $\frac{dV}{V} = -1$, i.e. the crack is just closed. This pressure is called the closure-pressure, P_c . Beyond this pressure, the closed crack has no effect on velocity or its variation.

Each quantity in (2) has been defined and can be determined from laboratory-observed velocities, except $V(\alpha_m)$ and T_1 . T_1 is/...

is a scalar quantity which can be obtained from other constants defined below (ref. Toksoz et al, 1976).

$$T_1 = \frac{3F_1}{F_2}$$

where

$$F_1 = 1 + A \left[\frac{3}{2} (g + \Phi) - R \left(\frac{3}{2} g + \frac{5}{2} \Phi - \frac{4}{3} \right) \right]$$

Φ = total porosity empirically obtained, and

$$F_2 = 1 + A \left[1 + \frac{3}{2} (g + \Phi) - \frac{R}{2} (3g + 5\Phi) \right] + B(3 - 4R) +$$

$$\frac{A}{2} (A + 3B) (3 - 4R) \cdot [g + \Phi - R(g - \Phi + 2\Phi^2)].$$

$$A = \frac{\mu'}{\mu} - 1, \quad B = \frac{1}{3} \left(\frac{K'}{K} - \frac{\mu'}{\mu} \right)$$

$$R = \frac{3\mu}{3K + 3\mu}, \quad g = \frac{\alpha^2}{1 - \alpha^2} \cdot (3\Phi - 2).$$

We repeat equation (2) for the series of closure pressures, P_c , corresponding to the series of aspect ratios, α_m . We omit from the RHS, terms involving aspect ratios of cracks already closed. We thus obtain M equations, the first of which includes all α_m , the second of which has all α_m except α_1 , and so on. The last equation has α_M only.

Terms on the LHS are known from elastic constants at varying pressure, calculated from observed velocities. Thus from the last equation, we may calculate $V(\alpha_M)$, and by a series of back substitutions obtain, sequentially, all other $V(\alpha_i)$.

APPENDIX 3

- (a) Computer program for the self-consistent model.
- (b) In-put data sample.
- (c) Output sample.

Computer program: 'CRACKDEN' for the self-consistent model

```

C
C EVALUATION OF CRACK PARAMETERS FROM SELF CONSISTENT MODEL
C
C MAIN PROGRAM
C
C DIMENSION VS(20),VP(20),VSN(20),VPN(20),R1(20),SIGMA(20),R3(20)
C DIMENSION PSA(20),HMOD(20),SMOD(20),F2(20),R4(20),E(20),FE(20)
C DIMENSION NAME(20),DRYF(20)
C
C VSN IS NORMALISED SHEAR VELOCITY
C VPN IS NORMALISED COMPRESSIONAL VELOCITY
C R1 IS (VFN/VSN)/(VF/VS)
C R3 IS REVERSE R1 USING CRACK THEORY RELATION
C (POISSON'S RATIO CALCULATED FROM VELOCITY DATA)
C R4 IS SAME AS POISSON'S RATIO=0.25
C E IS EVALUATED CRACK DENSITY FROM 100% SATURATION
C F2 IS CRACK DENSITY FROM PARTIAL SATURATION
C PSA IS FRACTION OF SATURATION
C HMOD IS BULK MODULUS FROM OBSERVED VP,VS,POISSON'S RATIO
C SMOD IS SHEAR MODULUS FROM VS DATA
C DRYF IS CRACK-DENSITY IN DRY SAMPLE
C CALL PAPER(1)
C ISFT=1
57 WRITE(6,51)ISFT
51 FORMAT(30X,'DATA SET NO=',I2)
READ(5,200)(NAME(I),I=1,20)
200 FORMAT(20A4)
WRITE(6,201)(NAME(I),I=1,20)
201 FORMAT(/,20A4,/)
NOP=11
READ(5,10)(VS(I),I=1,NOP)
READ(5,10)(VF(I),I=1,NOP)
10 FORMAT(11F7.3)
V1=VS(NOP)
V2=VP(NOP)
R2=V2/V1
WRITE(6,30)V2,V1,R2
30 FORMAT(10X,'FINAL VP=',F6.3,5X,'FINAL VS=',F6.3,5X,'VP/VS=',F6.3)
WRITE(6,29)
29 FORMAT(/)
C R2 IS RATIO OF INTRINSIC VP & VS
WRITE(6,31)
31 FORMAT(6X,'VS',2X,'VP',6X,'VS*/VS',4X,'VP*/VP'/)
DO 20 I=1,NOP
VSN(I)=VS(I)/V1
VPN(I)=VP(I)/V2
R1(I)=(VP(I)/VS(I))/R2
Q=(VP(I)/VS(I))**2
SIGMA(I)=(Q/2.-1.)/(Q-1.)
20 CONTINUE
P=SIGMA(NOP)
PP=0.25
CN=9./16.

```

```

D=45./32.
C=15./32.
CC=45./16.
CP=3./16.
DO 21 I=1,NCF

C
C   TO OBTAIN (VP*/VS*)/(VP/VS) FROM OBSERVED POISSON'S RATIO
C   USING CRACK THEORY RELATION TO CONFIRM THE VALIDITY OF RELATION.
R3(I)=SQRT(((1.-SIGMA(I))*(1.-2.*P))/((1.-2.*SIGMA(I))*(1.-P)))
C   CRACK DENSITY OF SATURATED CIRCULAR CRACKS.
F(I)=D*(((SIGMA(I)-P)*(2.-SIGMA(I)))/((1.-SIGMA(I))*2*(1.-2.*P)))
C   BULK MODULUS FROM OBSERVED VP,VS,& POISSON'S RATIO DATA.
RMOD(I)=(VPM(I)**2)*(1.+SIGMA(I))*(1.-P)/((1.-SIGMA(I))*(1.+P))
C   SHEAR MODULUS FROM OBSERVED VS DATA
SMOD(I)=VSM(I)**2
C   CRACK DENSITY FROM PARTIAL SATURATION CASE.
E2(I)=C*(1.-SMOD(I))*((2.-SIGMA(I))/(1.-SIGMA(I)))-CP*(1.-RMOD(I)
3)*(1.-2.*SIGMA(I))*(2.-SIGMA(I))/(1.-SIGMA(I)**2)
C   E2 IS CRACK DENSITY IN THE CASE OF PARTIAL SATURATION
R4(I)=SQRT(((1.-SIGMA(I))*(1.-2.*PP))/((1.-2.*SIGMA(I))*(1.-PP)))
C
C   CRACK-DENSITY IN DRY SAMPLE
C
DRYE(I)=CN*(((1.-RMOD(I))*((1.-2.*SIGMA(I))/(1.-SIGMA(I)**2)))
IF(E2(I).EQ.0.)GO TO 22
ST=(CC*(P-SIGMA(I))*(1.-2.*SIGMA(I))/((1.-SIGMA(I)**2)*E2(I))+2.
4*(1.-2.*P))/((1.+3.*P)*(2.-SIGMA(I)))
GO TO 23
22 ST=0.22
23 PSA(I)=1.-ST
C   YOUNG'S MODULUS
EF(I)=1.-(((1.-SIGMA(I)**2)/CC)*(3.*(1.-PSA(I))+(4./(2.-SIGMA(I)
5))*E2(I)))
21 CONTINUE
WRITE(6,50)((VS(I),VP(I),VSM(I),VPM(I)),I=1,NCF)
50 FORMAT(4F10.3)
WRITE(6,71)
WRITE(6,72)
71 FORMAT(//)
72 FORMAT(4X,'RATIO1',5X,'RATIO3',4X,'RATIO4',4X,'POISSON',4X,'YOUNG
6',4X,'BULK',4X,'RIGIDITY',3X,'CR.DENS',3X,'PART.SAT',2X,'CR.DENS'
7,3X,'DRYE'//)
WRITE(6,59)((R1(I),R3(I),R4(I),SIGMA(I),EF(I),RMOD(I),SMOD(I),E(I
8),PSA(I),E2(I),DRYE(I)),I=1,NCF)
59 FORMAT(11F10.3)
CALL PSPACE(0.2,0.916,0.2,0.518)
CALL PSPACE(0.2,0.436,0.2,0.518)
CALL MAP(1.0,0.5,0.8,1.3)
CALL SCALES
CALL BORDER
CALL CTRMAG(10)
CALL CTRSET(2)
CALL PTPLT(VSM,R1,1,NCF,44)
CALL PSPACE(0.2,0.916,0.2,0.518)
CALL PSPACE(0.45,0.686,0.2,0.518)
CALL MAP(0.0,1.5,0.0,2.0)
CALL BORDER
CALL SCALES
CALL PTPLT(E2,R1,1,NCF,44)
CALL FRAME
CALL PSPACE(0.2,0.916,0.2,0.518)
CALL PSPACE(0.2,0.436,0.2,0.359)
CALL MAP(0.0,1.5,0.0,1.0)
CALL BORDER

```

```

CALL SCALES
CALL PTPILOT(F2,VSN,1,NOR,44)
CALL PSPACE(0.2,0.916,0.2,0.518)
CALL PSPACE(0.2,0.434,0.359,0.518)
CALL MAP(0.,1.5,0.,1.0)
CALL BORDER
CALL PTPILOT(F2,VPN,1,NOR,44)
CALL PSPACE(0.2,0.916,0.2,0.518)
CALL PSPACE(0.44,0.676,0.2,0.359)
CALL MAP(0.,1.5,0.,1.0)
CALL BORDER
CALL PTPILOT(F2,SMOD,1,NOR,44)
CALL PSPACE(0.2,0.916,0.2,0.518)
CALL PSPACE(0.44,0.676,0.359,0.518)
CALL MAP(0.,1.5,0.,1.0)
CALL BORDER
CALL PTPILOT(F2,HMOD,1,NOR,44)
CALL PSPACE(0.2,0.916,0.2,0.518)
CALL PSPACE(0.68,0.916,0.2,0.359)
CALL MAP(0.,1.5,0.,1.0)
CALL BORDER
CALL PTPILOT(F2,STGMA,1,NOR,44)
CALL PSPACE(0.2,0.916,0.2,0.518)
CALL PSPACE(0.68,0.916,0.359,0.518)
CALL MAP(0.,1.5,0.,1.0)
CALL BORDER
CALL PTPILOT(F2,EF,1,NOR,44)
CALL CTRMAG(20)
CALL CTRSET(0)
ISFT=ISFT+1
IF(ISFT.GT.3)GO TO 56
CALL FRAME
GO TO 57
56 CALL GFEND
STOP
END

```

000608 CRACKDEN 5K LISTED T34 1P34

FMAS 2980 FMAS	GALV26 ?	SCIA.
FMAS 2980 FMAS	GALV26 ?	SCIA.
FMAS 2980 FMAS	GALV26 ?	SCIA.
FMAS 2980 FMAS	GALV26 ?	SCIA.
FMAS 2980 FMAS	GALV26 ?	SCIA.
FMAS 2980 FMAS	GALV26 ?	SCIA.
FMAS 2980 FMAS	GALV26 ?	SCIA.
FMAS 2980 FMAS	GALV26 ?	SCIA.

Example of input data for 'CRACKDEN'

GHOST * GRID FILE CONTAINS 23 2036-BYTE RECORDS

SAT GREYWACKE 4N										
2.880	3.020	3.090	3.180	3.240	3.290	3.320	3.350	3.370	3.390	3.410
5.205	5.370	5.480	5.640	5.720	5.780	5.830	5.870	5.910	5.940	5.965
SAT GREYWACKE 4H										
2.880	3.170	3.320	3.460	3.540	3.580	3.620	3.640	3.650	3.670	3.680
5.190	5.420	5.570	5.770	5.880	5.950	6.000	6.040	6.080	6.110	6.140
SAT GREYWACKE 4V										
2.975	3.150	3.260	3.380	3.440	3.480	3.500	3.520	3.540	3.550	3.560
4.920	5.170	5.260	5.450	5.580	5.680	5.750	5.800	5.840	5.880	5.910
SAT GREYWACKE 6N										
2.800	2.910	2.970	3.040	3.100	3.140	3.180	3.220	3.250	3.280	3.310
4.910	5.100	5.250	5.410	5.520	5.600	5.680	5.750	5.810	5.840	5.870
SAT GREYWACKE 6H										
2.570	2.820	3.000	3.170	3.260	3.320	3.350	3.360	3.380	3.385	3.390
4.670	5.000	5.200	5.410	5.520	5.570	5.590	5.600	5.610	5.620	5.625
SAT GREYWACKE 6V										
2.840	2.950	3.040	3.140	3.180	3.220	3.250	3.280	3.310	3.330	3.360
4.345	5.140	5.310	5.470	5.550	5.600	5.630	5.660	5.680	5.690	5.710
SAT GREYWACKE 8N										
3.020	3.110	3.150	3.200	3.230	3.240	3.270	3.280	3.300	3.305	3.310
5.170	5.370	5.510	5.670	5.750	5.790	5.810	5.840	5.860	5.870	5.875
SAT GREYWACKE 8H										
3.040	3.100	3.140	3.180	3.210	3.230	3.260	3.270	3.290	3.300	3.310
5.350	5.590	5.690	5.800	5.860	5.910	5.940	5.970	5.990	6.020	6.030
SAT GREYWACKE 8V										
3.094	3.170	3.210	3.250	3.280	3.310	3.320	3.330	3.340	3.350	3.356
5.410	5.580	5.700	5.820	5.900	5.950	6.000	6.030	6.050	6.070	6.090

DATA SET NO= 1 Output from 'CRACKDEN'

SAT GREYWACKE 4N

FINAL VP= 5.965 FINAL VS= 3.410 VP/VS= 1.749

172

VS	VP	VS*/VS	VP*/VP
2.880	5.205	0.845	0.873
3.020	5.370	0.886	0.900
3.090	5.480	0.906	0.919
3.180	5.540	0.933	0.946
3.240	5.720	0.950	0.959
3.290	5.780	0.965	0.969
3.320	5.830	0.974	0.977
3.350	5.870	0.982	0.984
3.370	5.910	0.988	0.991
3.390	5.940	0.994	0.996
3.410	5.965	1.000	1.000

RATIO1	RATIO3	RATIO4	POISSON	YOUNG	BULK	RIGIDITY	CR.DENS	PART.SAT	CR.DENS
1.033	1.033	1.043	0.279	0.499	0.799	0.713	0.119	0.715	0.290
1.017	1.017	1.027	0.269	0.550	0.831	0.784	0.062	0.708	0.212
1.014	1.014	1.024	0.267	0.578	0.862	0.821	0.052	0.709	0.176
1.014	1.014	1.024	0.267	0.621	0.913	0.870	0.052	0.718	0.130
1.009	1.009	1.019	0.264	0.645	0.932	0.903	0.035	0.716	0.096
1.004	1.004	1.014	0.260	0.657	0.945	0.931	0.017	0.707	0.067
1.004	1.004	1.014	0.260	0.673	0.961	0.948	0.015	0.711	0.051
1.002	1.002	1.012	0.258	0.678	0.971	0.965	0.007	0.703	0.033
1.003	1.003	1.013	0.259	0.706	0.985	0.977	0.010	0.722	0.023
1.002	1.002	1.012	0.258	0.725	0.994	0.983	0.007	0.733	0.012
1.000	1.000	1.010	0.257	0.781	1.000	1.000	0.000	0.780	0.000

DATA SET NO= 2

APPENDIX 4

- (a) Computer program for the non-interactive model.
- (b) Input data sample.
- (c) Output sample.

000610 BTMPROG4 1K LISTED T36 1P36

```

C
C      THIS PROG CALCULATES THE CLOSURE PRESSURE OF A CRACK
C
C      MAIN PROGRAM
C
      IMPLICIT REAL*8(A-H,O-Z)
      DIMENSION ALPHA(8),P(8),NAME(20)
      PI=3.142
      NALPHA=8
      READ(5,100)NSAMP
100  FORMAT(I3)
      KOUNT=0
      READ(5,200)(ALPHA(N),N=1,NALPHA)
200  FORMAT(F11.2)
      1 READ(5,300)(NAME(I),I=1,20)
300  FORMAT(20A4)
      WRITE(6,301)(NAME(I),I=1,20)
301  FORMAT(1,20A4,/)
      WRITE(6,77)
      77 FORMAT(1,'      ALPHA(N)          P(N) KPAR    ',/)
      READ(5,400)7KAY
      READ(5,400)SIGMA
400  FORMAT(F6.3)
      DO 22 N=1,NALPHA
      P(N)=7KAY*3.*PI*ALPHA(N)*((1.-2.*SIGMA)/(4.*(1.-(SIGMA**2))
      2)*1000./
      WRITE(6,404)ALPHA(N),P(N)
404  FORMAT(1X,F11.2,7X,F6.3)
      22 CONTINUE
      KOUNT=KOUNT+1
      IF(KOUNT.EQ.NSAMP)GO TO 999
      GO TO 1
999  STOP
      END

```

000610 BTMPROG4 1K LISTED T36 1P36

FMAS 2980 FMAS GALV26 ?	SOLA.CHEMISTRY.GLASGO
FMAS 2980 FMAS GALV26 ?	SOLA.CHEMISTRY.GLASGO
FMAS 2980 FMAS GALV26 ?	SOLA.CHEMISTRY.GLASGO
FMAS 2980 FMAS GALV26 ?	SOLA.CHEMISTRY.GLASGO
FMAS 2980 FMAS GALV26 ?	SOLA.CHEMISTRY.GLASGO
FMAS 2980 FMAS GALV26 ?	SOLA.CHEMISTRY.GLASGO
FMAS 2980 FMAS GALV26 ?	SOLA.CHEMISTRY.GLASGO
FMAS 2980 FMAS GALV26 ?	SOLA.CHEMISTRY.GLASGO

Input for BIMPROG4

FILE 'BIMDATA4'

0	1.00E-4	2.00E-4	4.00E-4	8.00E-4	16.00E-4	32.00E-4	64.00E-4	128.00E-4
DRY GREYWACKE SH								
0.456								
0.224								
DRY GREYWACKF SH								
0.491								
0.237								
DRY GREYWACKF SV								
0.519								
0.264								
SAT GREYWACKF SH								
0.510								
0.273								
SAT GREYWACKF SH								
0.502								
0.262								
SAT GREYWACKF SV								
0.512								
0.279								

Output from BIMPROG4

FILE 'BINRES4'

DRY GREYWACKE 5N

ALPHA(N)	P(N) KHAR
0.100-03	0.062
0.200-03	0.125
0.400-03	0.250
0.800-03	0.500
0.160-02	0.999
0.320-02	1.998
0.640-02	3.997
0.130-01	7.994

DRY GREYWACKE 5H

ALPHA(N)	P(N) KHAR
0.100-03	0.064
0.200-03	0.129
0.400-03	0.258
0.800-03	0.516
0.160-02	1.032
0.320-02	2.063
0.640-02	4.127
0.130-01	8.254

DRY GREYWACKE 5V

ALPHA(N)	P(N) KHAR
0.100-03	0.062
0.200-03	0.124
0.400-03	0.248
0.800-03	0.496
0.160-02	0.993
0.320-02	1.986
0.640-02	3.971
0.130-01	7.943

000A09 HIMPROG 4K LISTED T36 LPR4

```

C
C   THIS PROG CALCULATES VOL CONCENTRATION OF A CRACK
C
C   DATA PROGRAM
C
      IMPLICIT REAL*8(A-H,C-Z)
      DIMENSION ALPHA(8),P(8),EMOD(8),NAME(20),GEFF(8),ELOW(8),EPOR(8),
1ETWC(8),TWON(8),F(8),D(8),DVFC(8),PR(8,8),CCFFF(8),V(8),C(8),VP(8
2),VS(8),FMI(8)
      PI=3.142
      NALPHA=8
      READ(5,10)NSAMP
10  FORMAT(T3)
      KOUNT=0
      READ(5,200)(ALPHA(M),M=1,NALPHA)
      WRITE(6,200)(ALPHA(M),M=1,NALPHA)
200  FORMAT(8F11.2)
      1 READ(5,101)(NAME(I),I=1,20)
101  FORMAT(20A4)
      WRITE(6,102)(NAME(I),I=1,20)
102  FORMAT(1,20A4,1/)
      WRITE(6,66)
      66  FORMAT(1,' P(N)      VP(N)      VS(N)      ',/)
      DO 3 N=1,8
      READ(5,56)P(N),VP(N),VS(N)
      WRITE(6,56)P(N),VP(N),VS(N)
      56  FORMAT(3(F5.3,5X))
      3  CONTINUE
C
C *** TO CALCULATE BULK AND SHEAR MODULI
C
      WRITE(6,22)
      22  FORMAT(1,' EMOD(N)      FMI(N)  ',/)
      READ(5,59)RHO,STGMA
      59  FORMAT(2(D6.3,3X))
      DO 44 N=1,8
      FMI(N)=RHO*(VS(N)**2)*1.0CF=2
      EMOD(N)=RHO*(VP(N)**2-((VS(N)**2)*4./3.))*1.0CF=2
      44  CONTINUE
      WRITE(6,57)((EMOD(N),FMI(N)),N=1,8)
      57  FORMAT(1X,2(F8.3,4X))
C
C *** THIS CALCULATES TWON AGAINST ALPHA
C
      READ(5,15)ZKAY,ZKDASH,ZMI,ZMDASH
      15  FORMAT(2(F7.3,D10.3))
      R=3.*ZMI/((3.*ZKAY)+(4.*ZMI))
      R=((ZKDASH/ZKAY)-(ZMDASH/ZMI))/3.
      A=(ZMDASH/ZMI)-1.
      READ(5,16)PMT
      16  FORMAT(F5.3)
      DO 20 N=1,NALPHA
      GEFF(N)=((ALPHA(N)**2)/(1.-(ALPHA(N)**2)))*((3.+PMT)-2.)

```

```

      FWN(M)=1.+A*(1.5*(GFF(M)+PHI))-R*((1.5*GFF(M))+(2.5*PHI)-(4./3.)
2))
      FTLC(M)=1.+A*(1.+(1.5*(GFF(M)+PHI))-R*.5*((3.*GFF(M))+(5.*PHI
3)))+R*(3.-(4.*R))+A*.5*(A+(3.*R))*(3.-(4.*R))*((GFF(M)+PHI)-R*
4(GFF(M)-PHI+(2.*PHI**2)))
      TWON(M)=3.*FLCN(M)/FTWO(M)
20 CONTINUE
C
C *** TO CALCULATE RATE OF CLOSURE OF CRACKS
C
      DO 40 N=1,8
      E(N)=(FMO(N)-7KAY)/(ZKDASH-7KAY)
      D(N)=((3.*7KAY)+(4.*ZMU))/((3.*FMO(N))+(4.*ZMU))
      DVFC(N)=E(N)*D(N)
      DO 30 M=1,NALPHA
      FPOR(M)=(-P(N)/(FMO(N)*(10.**3)))*((4.*(1.-(STGMA**2)))
7/(3.*PI*ALPHA(M)*(1.-2.*STGMA)))
      IF(1.0+FPOR(M)) 400,400,401
400 COEFF(M)=0.0
      GO TO 401
401 COEFF(M)=(1.0+FPOR(M))*(TWON(M)/3.)
      30 CONTINUE
      DO 777 N=1,8
      RR(N,M)=COEFF(M)
777 CONTINUE
      40 CONTINUE
C
C *** THIS CALCULATES VOLUME CONCENTRATION
C
      WRITE(6,39)
39 FORMAT(/,' ALPHA(K)          V(K) ',/)
      V(8)=(DVFC(8)-RR(7,8)*V(7))/RR(7,7)
      V(7)=(DVFC(7)-RR(6,7)*V(6)+RR(6,8)*V(8))/RR(6,6)
      V(6)=(DVFC(6)-RR(5,6)*V(5)+RR(5,7)*V(7)+RR(5,8)*V(8))/RR(5,
45)
      V(4)=(DVFC(4)-RR(4,5)*V(5)+RR(4,6)*V(6)+RR(4,7)*V(7)+RR(4,8)
3*V(8))/RR(4,4)
      V(3)=(DVFC(3)-RR(3,4)*V(4)+RR(3,5)*V(5)+RR(3,6)*V(6)+RR(3,7)*V(7
2)+RR(3,8)*V(8))/RR(3,3)
      V(2)=(DVFC(2)-RR(2,3)*V(3)+RR(2,4)*V(4)+RR(2,5)*V(5)+RR(2,6)*V(6
1)+RR(2,7)*V(7)+RR(2,8)*V(8))/RR(2,2)
      V(1)=(DVFC(1)-RR(1,2)*V(2)+RR(1,3)*V(3)+RR(1,4)*V(4)+RR(1,5)*V(5
3)+RR(1,6)*V(6)+RR(1,7)*V(7)+RR(1,8)*V(8))/RR(1,1)
      WRITE(6,800)((ALPHA(K),V(K)),K=1,NALPHA)
800 FORMAT(1X,F9.2,5X,F10.3)
      KOUNT=KOUNT+1
      IF(KOUNT.EQ.NSAMP)GO TO 999
      GO TO 1
999 STOP
      END

```

000609 BTMPROG 4K LISTED T36 LP36

Example of input data for 'BIMPROG'

6

1.00E-4 2.00E-4 4.00E-4 8.00E-4 16.00E-4 32.00E-4 64.00E-4 128.00E-4

DRY GREYWACKE SN

0.001	4.501	2.892
0.054	4.542	2.907
0.109	4.582	2.925
0.218	4.650	2.957
0.436	4.770	3.015
0.872	4.948	3.094
1.743	5.154	3.170
3.486	5.260	3.208

2.652 0.210

0.331 0.001E-3 0.274 0.000E-4

0.019

DRY GREYWACKE SH

0.001	4.360	2.970
0.056	4.365	3.000
0.111	4.426	3.010
0.223	4.525	3.035
0.445	4.678	3.074
0.890	4.907	3.150
1.781	5.170	3.234
3.561	5.292	3.295

2.653 0.182

0.359 0.001E-3 0.289 0.000E-4

0.012

Output for 'BIMPROG'

DRY GREYWACKE 5N

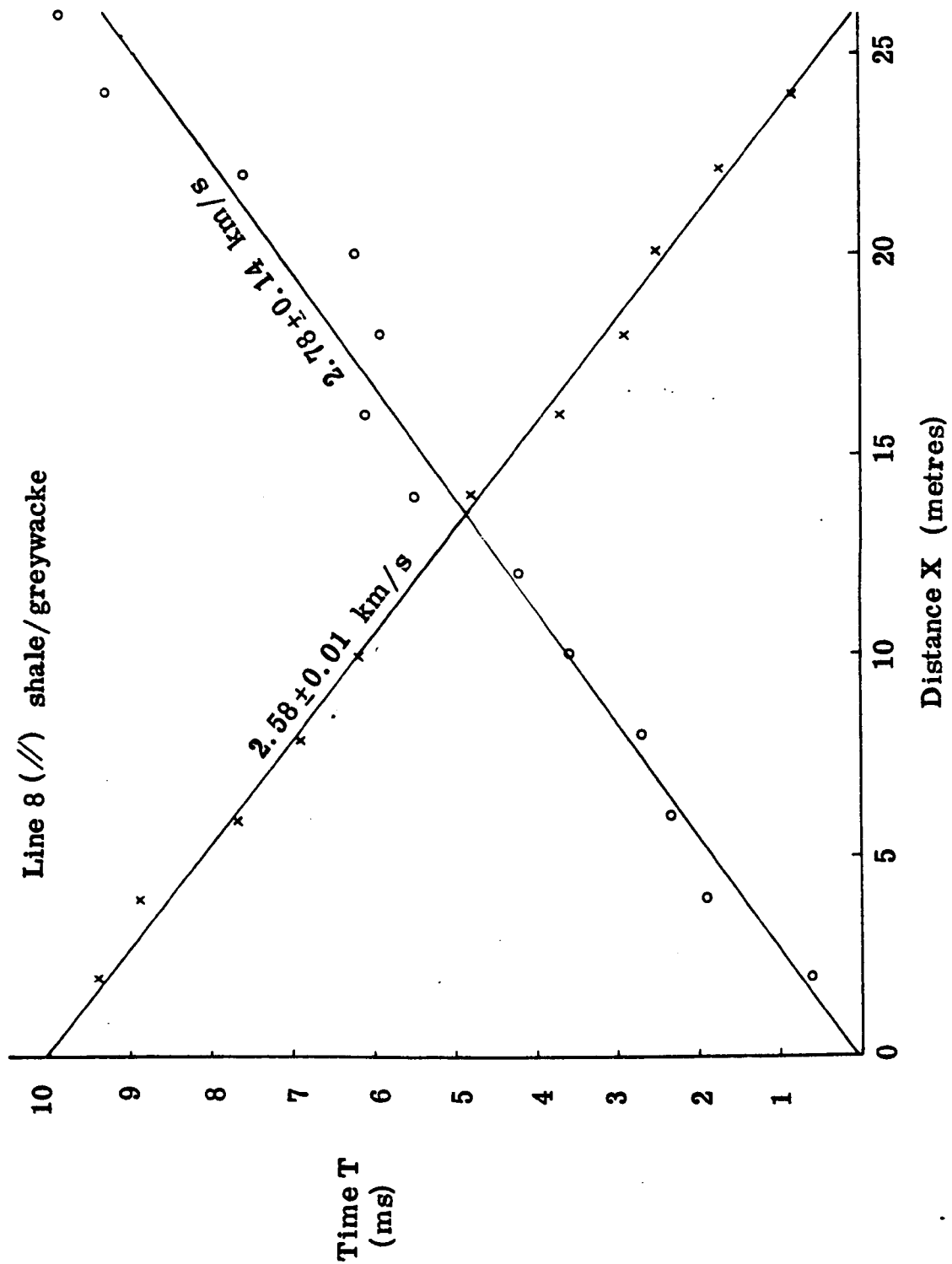
P(N)	VP(N)	VS(N)
0.001	4.501	2.892
0.054	4.542	2.907
0.109	4.582	2.925
0.213	4.650	2.957
0.436	4.770	3.015
0.872	4.948	3.094
1.743	5.154	3.170
3.486	5.280	3.208

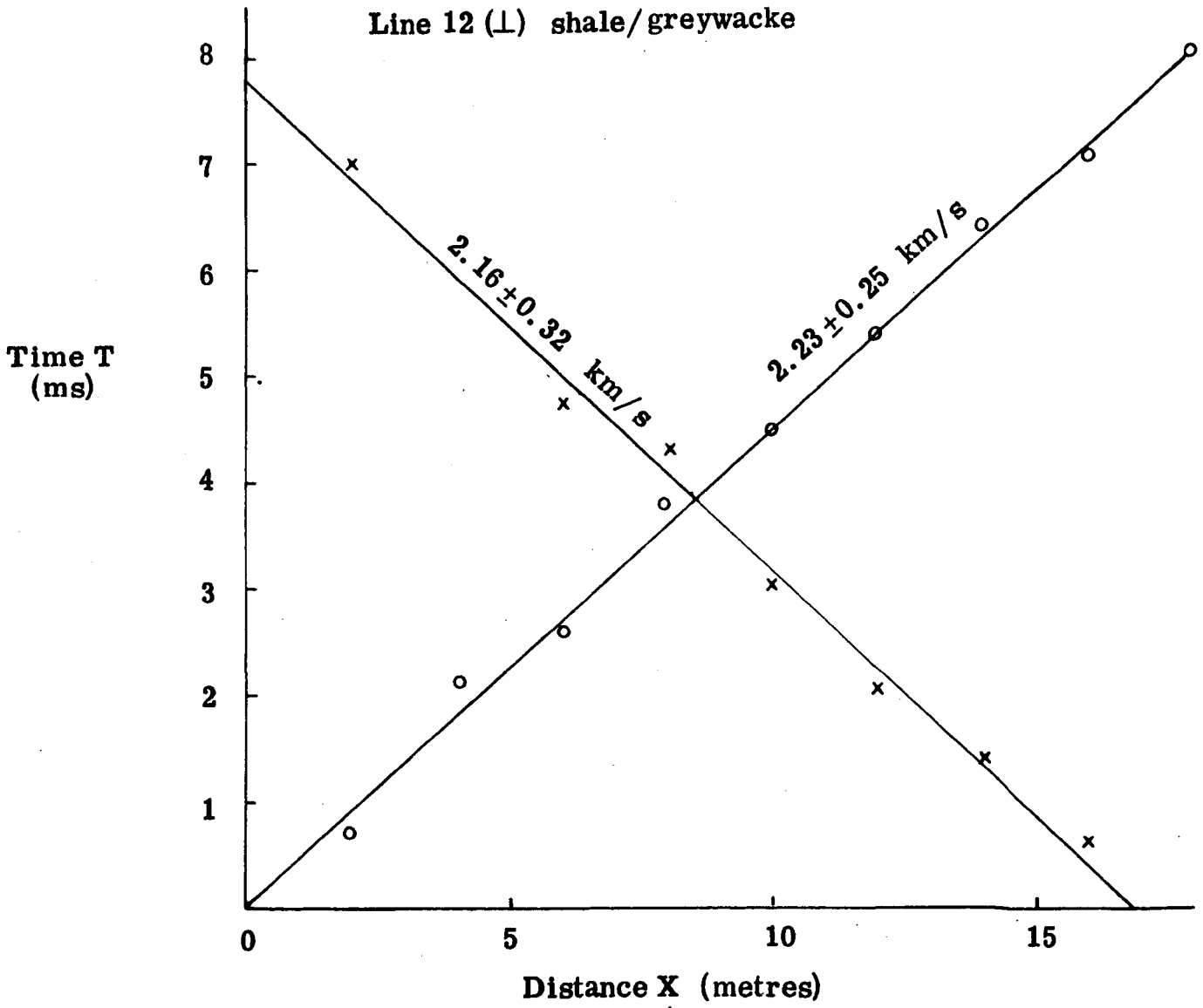
EMOD(N)	EMU(N)
0.242	0.222
0.246	0.224
0.254	0.227
0.264	0.232
0.282	0.241
0.311	0.254
0.349	0.266
0.375	0.273

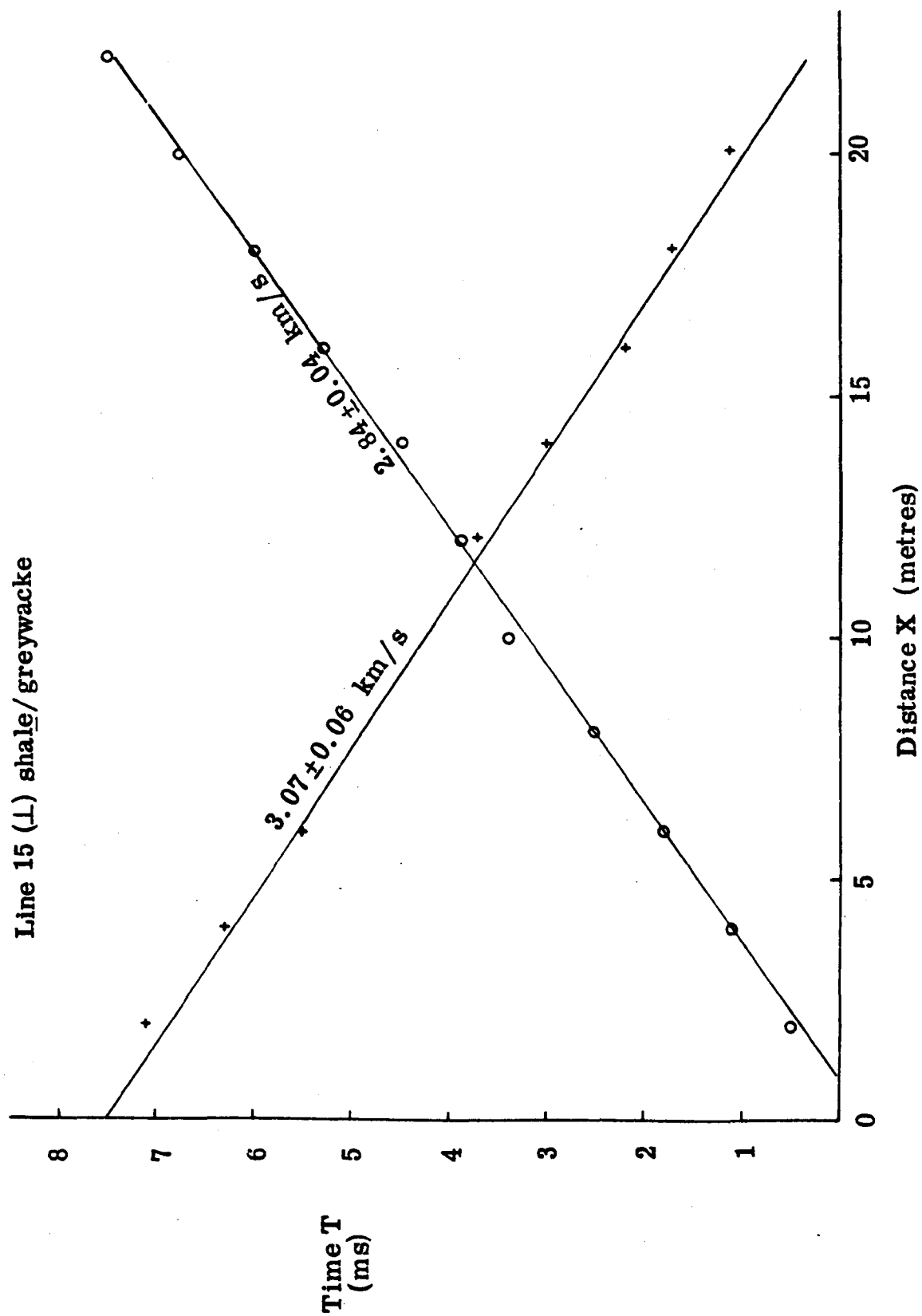
ALPHA(K)	V(K)
0.100-03	0.1220-04
0.200-03	0.9140-04
0.400-03	0.1260-03
0.800-03	0.6110-04
0.160-02	0.1000-02
0.320-02	0.3490-02
0.640-02	0.2510-02
0.130-01	0.5240-03

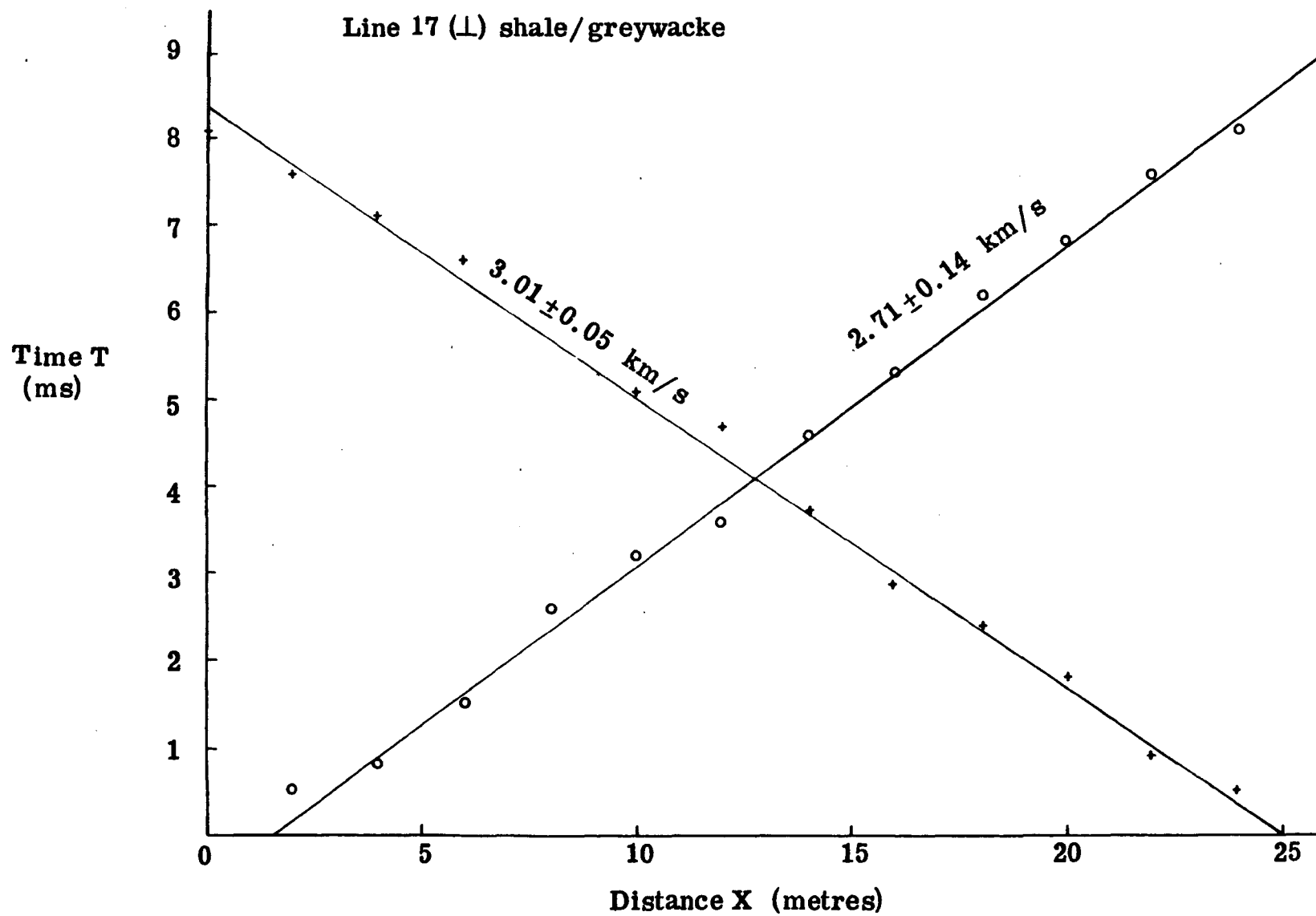
APPENDIX 5

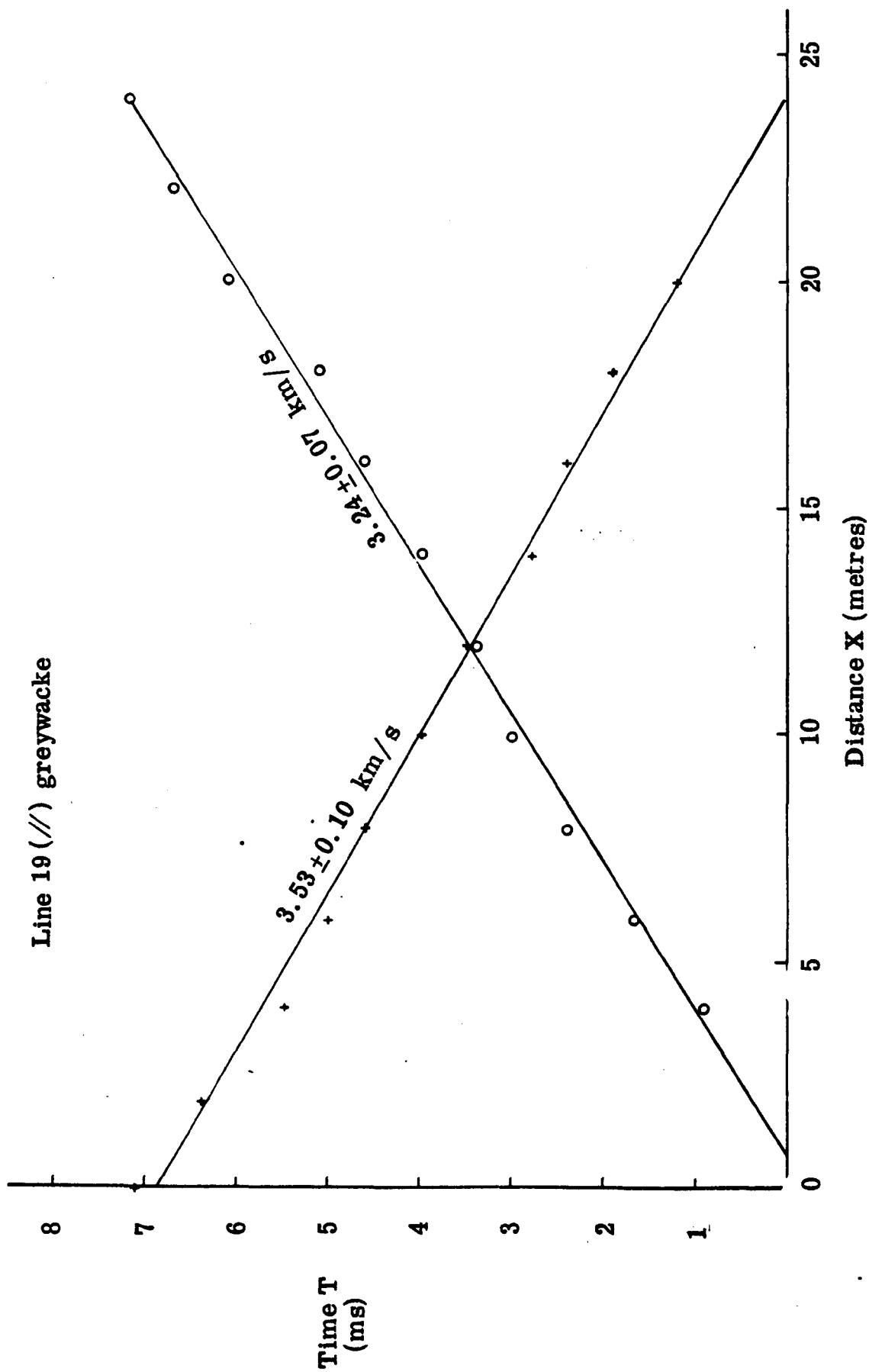
Time-distance (T - X) graphs from hammer lines.

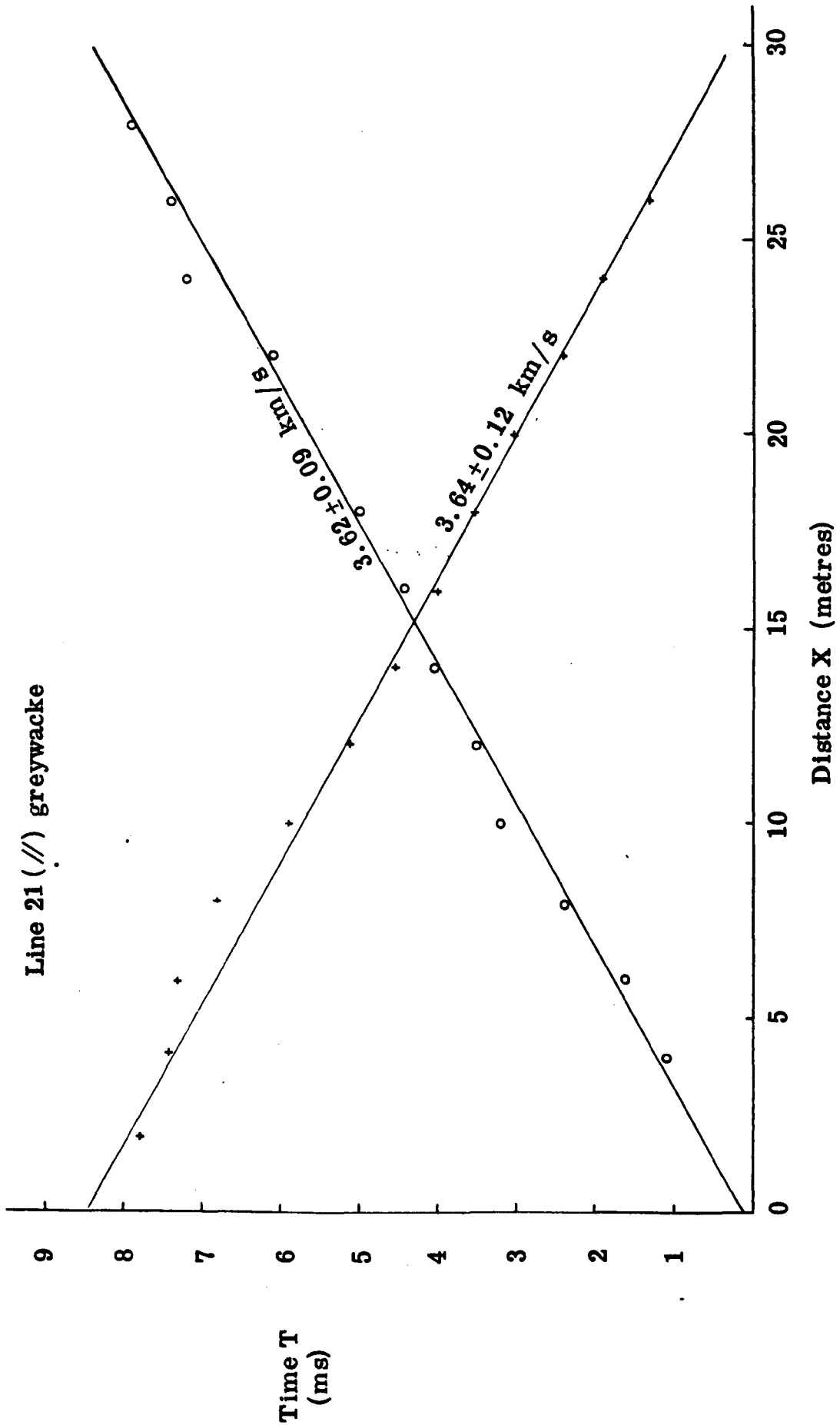


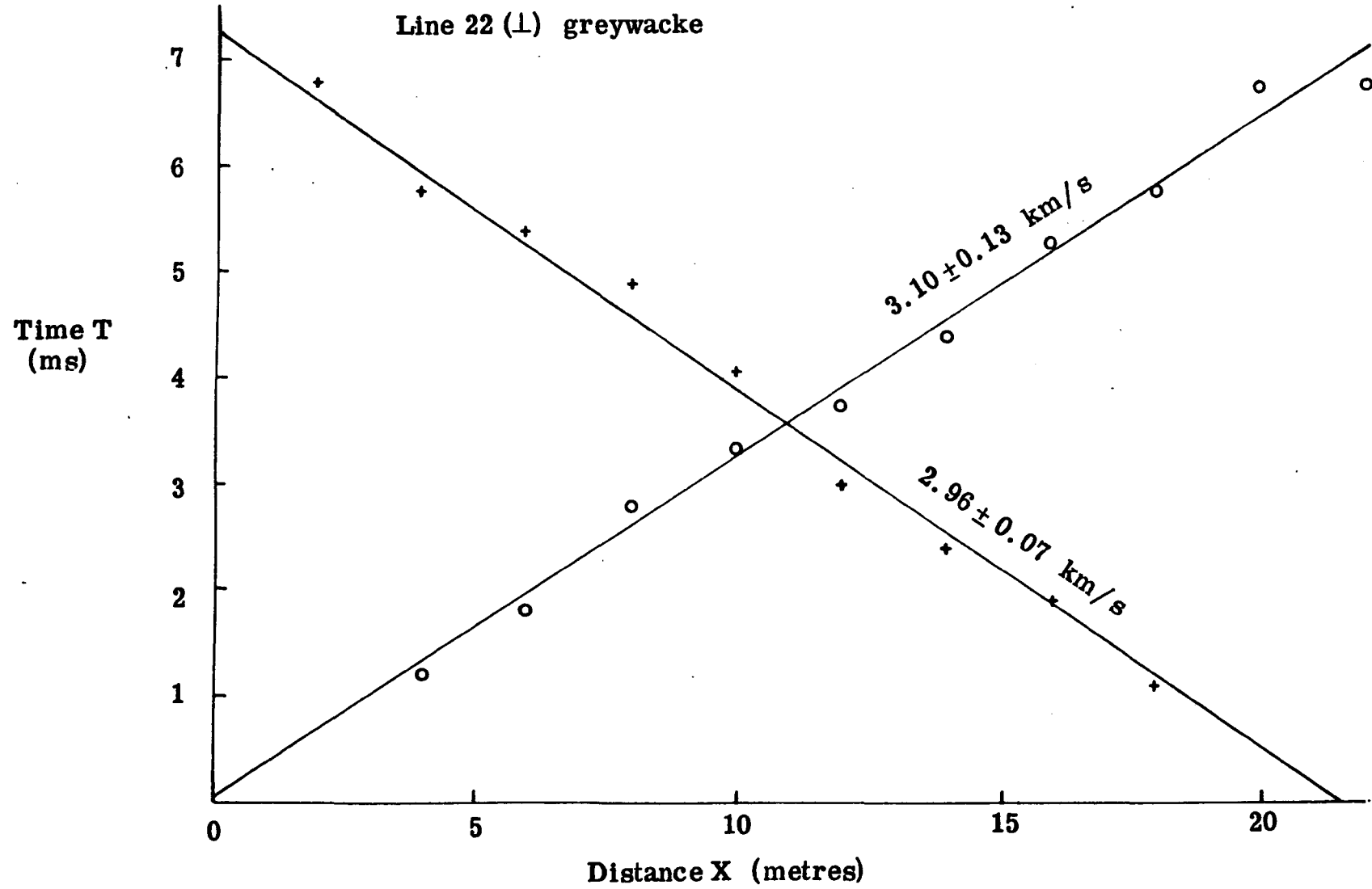




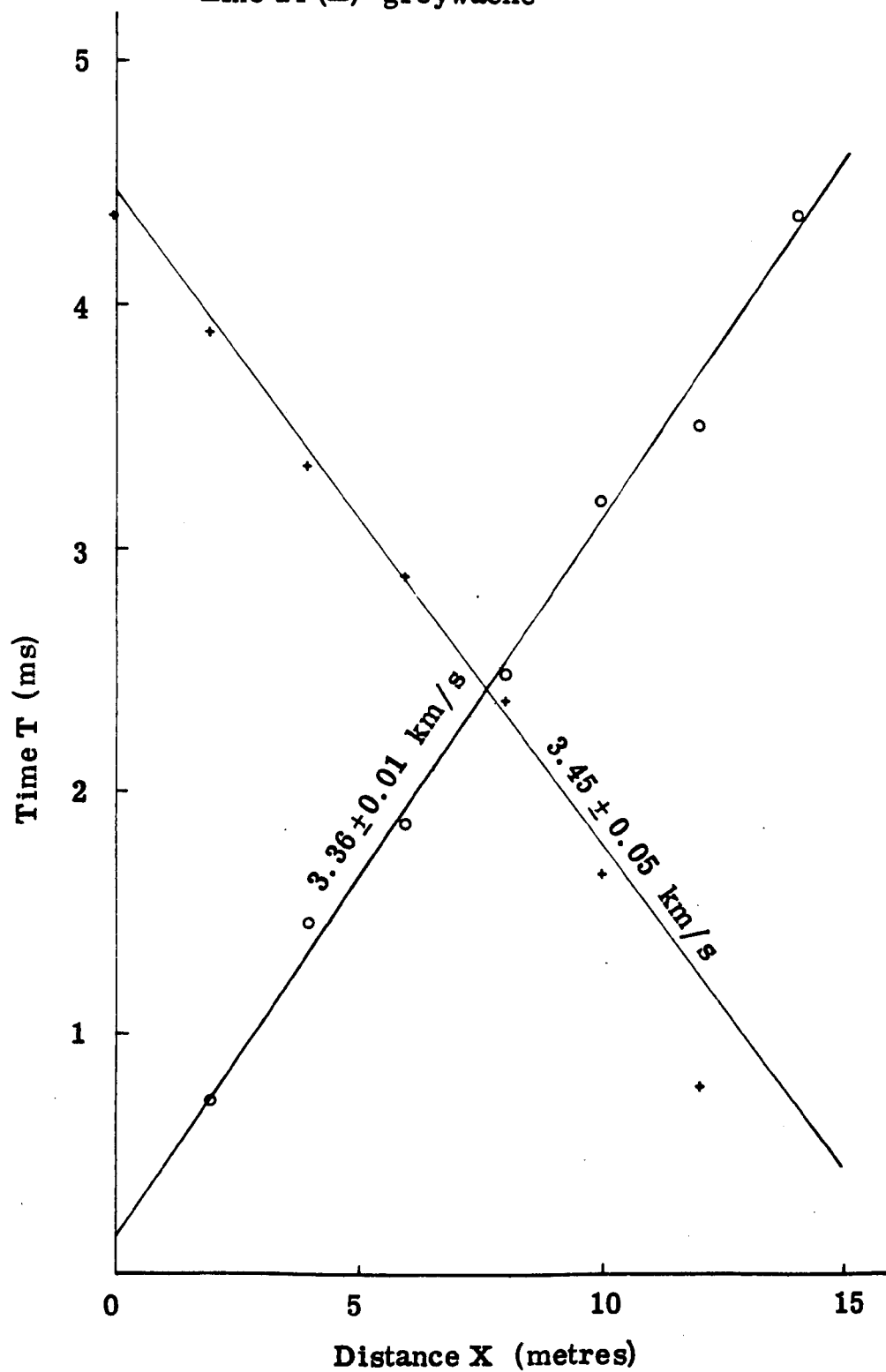


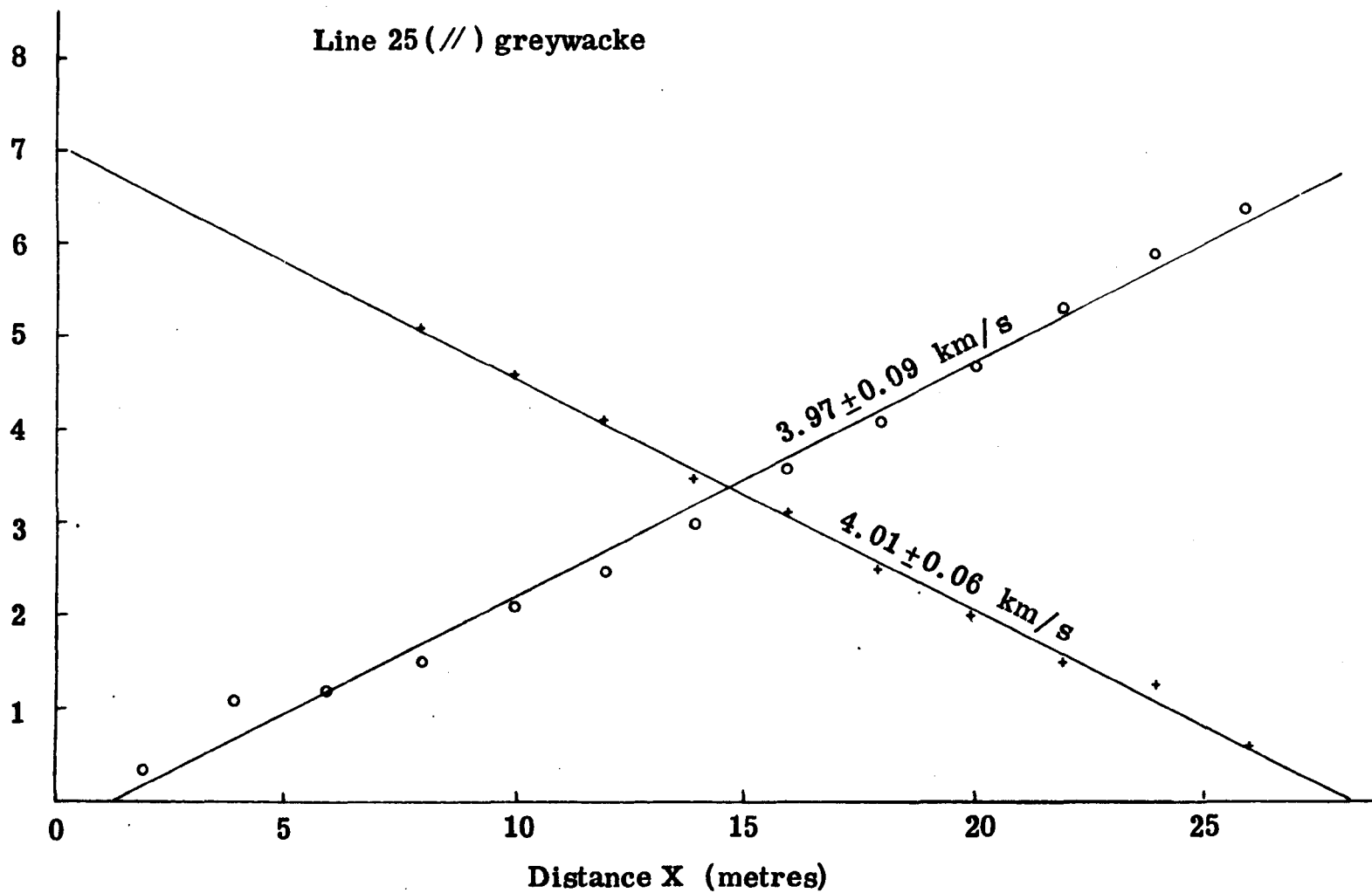


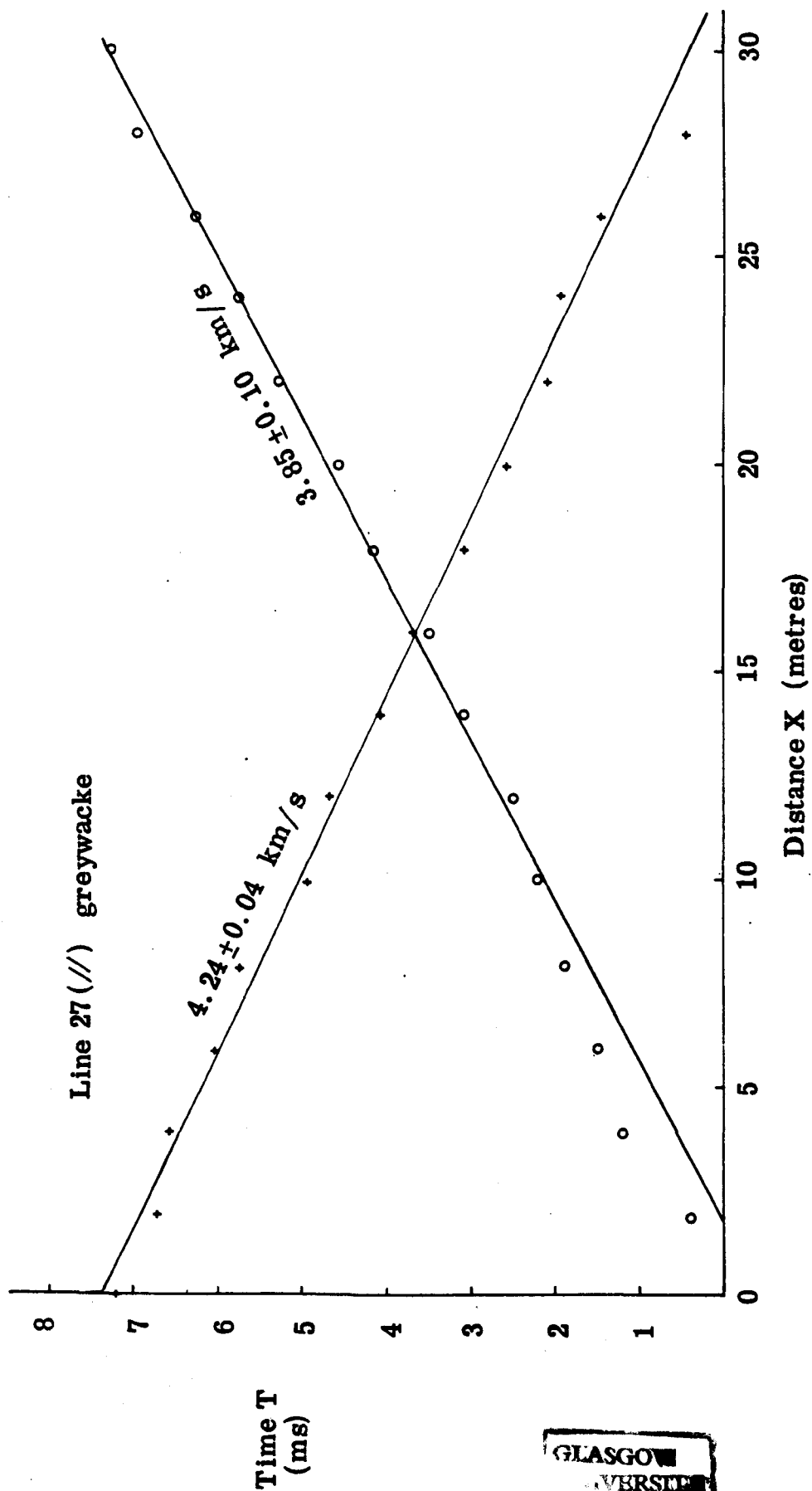




Line 24 (⊥) greywacke







GLASGOW
UNIVERSITY
LIBRARY